INTERNATIONAL DOCTORAL
SCHOOL OF THE USC

Axel Kattar

Doctoral Thesis

DESIGN AND FORMULATION OF NANOCARRIERS FOR THE TREATMENT OF DIABETIC EYE DISEASES

Santiago de Compostela, 2023

Doctoral Program in Drug Research and Development

ESCOLA DE DOUTORAMENTO
INTERNACIONAL DA USC

DOCTORAL THESIS

DESIGN AND FORMULATION OF NANOCARRIERS FOR THE TREATMENT OF DIABETIC EYE DISEASES

Author

Axel KATTAR

Supervisor: Carmen Alvarez-Lorenzo

Tutor: Carmen Alvarez-Lorenzo

DOCTORAL PROGRAM IN DRUG RESEARCH AND DEVELOPMENT

SANTIAGO DE COMPOSTELA

Acknowledgements

First and foremost I would like to thank my thesis director, Carmen Alvarez-Lorenzo for giving me the opportunity to work in her research group and to have always been vigilant to make sure that my work was of the highest standard. Thank you for always being available, week in and week out, in Santiago or during the secondments, to correct manuscripts or provide feedback on experimental ideas.

Secondly I would like to thank my supervision team, Professor Angel Concheiro, Professor Anuj Chauhan, Professor Hákon Hrafn Sigurðsson, and Dr. Paolo Gasco for the effort put in to advise the course of my thesis and their hospitality during secondments. I would like to extend a special thanks to the Chauhan cluster, with Anuj, Zach, Raj, and Bikram who have made my secondment in Colorado that much more fun.

I would like to acknowledge the European Union's Horizon 2020 research and innovation program for the financial support through the Marie Skłodowska-Curie Actions grant agreement Nº 813440 (ORBITAL – Ocular Research by Integrated Training and Learning). Thank you to Tess and Larry for being an anchor point with anything related to the training program, and all the ESRs for the support over the years.

I would like to thank all the people that have made my labwork possible, Ana Filipa, Iago, Diana, Nicola, Maria, Mariana, Paola, Lucia, Xian, Patri, Carol, Alex, Emilio without whom the days would have seemed a lot longer.

I would like to extend my thanks to Bebert, Chen, Sami, Lluis, Tici, Ashraf and all the friend I have made in Santiago that have made the town my home.

J'aimerais remercier mon père qui a toujours été un modèle pour moi, et qui m'a toujours soutenu dans mon projet de faire des études poussées. Mon frère et ma sœur qui m'ont montré des styles de vie différents et qui continuent de m'apprendre et de me conseiller au quotidien.

Ik wil mijn moeder bedanken om zo vaak mij te hebben bezocht hier in het zuiden, en altijd positief is gebleven ondanks de omstandigheden die niet altijd makkelijk waren. Bedankt voor je blik die mij heeft laten zien dat ik begrepen kan zijn.

Ook wil ik de Adventure Animals bedanken om mij vanaf mijn vertrek uit Enschede nooit hebben laten valllen, altijd in contact te zijn gebleven, en een vriendengroep voor het leven te zijn.

Finalement j'aimerais remercier Sandra, qui a été à mes côtés et a vécu mes hauts et mes bas avec moi. Merci pour avoir partagé tout ces moments et les avoir rendu tous plus heureux.

INDEX

RESUMO

RESUMO

O ollo é o órgano no noso corpo que permite percibir visualmente a contorna que nos rodea. Desde movemento a diversión, a nosa sociedade é construída ao redor da habilidade de humanos para ver. Fronte a pregunta de qué sentiría mais unha persoa perder, a gran maioría das persoas responde que a visión. Con todo, cando co resto do corpo, o ollo é suxeito a enfermidades ou accidentes que comprometen a calidade da visión e teñen un impacto moi relevante na calidade de vida. A gama de riscos aos que ten que enfrontarse o ollo inclúe desde infeccións locais temporais a enfermidades crónicas cunha orixe moi variada, como pode ser xenética ou patoloxías sistémicas como a diabetes.

A diabetes mellitus é un trastorno que pode ter unha orixe xenética ou ser causada por factores asociados ao estilo de vida. A crenza actual é que a diabetes tipo I -que afecta o paciente nas etapas máis temperás da súa vida- é causada por un proceso autoimmune que inhibe a produción de insulina no páncreas. A diabetes tipo 2 xurde da resistencia a acción da insulina; o páncreas produce insulina mais o resto do corpo non é capaz de utilizalo correctamente, resultando en niveis de glicosa de sangue sobrantes. En Europa e Norte América a diabetes tipo 2 representa o 90% de tódolos casos de diabetes, e o número dos pacientes que a padecen está aumentando hasta alcanzar proporcións de pandemia.

Os niveis altos de glucosa en sangue en pacientes diabéticos non tratados afecta a todos os órganos. No ollo isto da lugar a que se produzan afeccións coma a retinopatía diabética, edema macular, cataratas, glaucoma, enfermidade de ollo seco e keratopatías que poden afectar ao segmento anterior ou ao segmento posterior do ollo. A

retinopatía diabética, en particular, lidera as causas de perda de visión que poden conducir a cegueira se non se detecta e se trata en estadíos tempranos. Os tratamentos dispoñibles para o tratamento da retinopatía implican inxeccións intraoculares de formulacións anti-VEGF e aplicación de luz láser, e só permiten ralentizar o procesos de dexeneración da retina. Polo tanto, existe unha necesidade de dispor de medidas preventivas e de tratamentos da retinopatía diabética que permitan preservar a visión dos pacientes.

Nos modelos actuais de retinopatía diabética outorgáselle un papel moi relevante á morte das células que ocorre por estrés osmótico e oxidativo. Os niveis altos de glucosa en sangre son o detonante da aparición destes sinais de estrés. Un control deficiente dos niveis de glucosa poden saturar a ruta metabólica convencional pola que se procesa a glucosa nas células, que é a glucolisis, e que converte glucosa a glucosa-6-fosfato. Esta saturación da lugar a que outras rutas paralelas se activen, en particular a ruta do poliol que a través da enzima aldosa reductosa converte a glucosa en sorbitol, que nun segundo paso transfórmase en fructosa. Esta reacción consome NADPH no primeiro paso e NADP+ no segundo. Con todo, a cinética do proceso determina que a primeira reacción sexa a etapa limitante do proceso. Isto da lugar a unha acumulación de sorbitol na célula, que é incapaz de cruzar a membrana celular, e a deplección dos niveis de NADPH. Esta combinación de factores é o que crea o estrés osmótico e oxidativo.

Un dos fármacos máis prometedores neste eido é o epalrestat, xa utilizado en casos de neuropatía diabética en Xapón. Este fármaco tamén podería ser utilizado no caso da retinopatía diabética para bloquear a ruta do poliol xa que é un inhibidor da enzima aldosa reductasa. O epalrestat é unha molécula pequena altamente hidrofóbica (solubilidade en agua 47.9 μg/mL) que se une de maneira

non competitiva a aldosa reductasa. Dado que o lugar de acción é no segmento posterior do ollo, é importante que o fármaco poida superar as barreiras que o separan do lugar de acción.

A administración de fármacos para tratamento ocular pódese facer por tres rutas: oral, tópica e intraocular. A administración oral e tópica non requiren a intervención de persoal especializado, pero conducen a valores de biodisponilidade ocular moi baixos. A administración intraocular proporciona alta biodisponibilidade pero conleva riscos para os pacientes asociados ao uso de agullas de inxección (danos nos tecidos, risco de infeccións,…). O tratamento ideal de enfermidades crónicas debera ser a través de tratamentos tópicos cómodos para os pacientes pero iso só será posible cando as formulacións permitan acadar niveles terapéuticos de fármaco nas estruturas oculares de interese. No caso dos fármacos hidrofóbicos, coma o epalrestat, o deseño dunha formulación tópica enfróntase a un primeiro reto de conseguir solubilizar a cantidade necesaria de fármaco.

Para incrementar a solubilidade aparente dos fármacos e tamén a súa capacidade de penetrar nos tecidos oculares, pódese acudir ao uso de nanotransportadores. A finalidade do uso de transportador é facer chegar o fármaco dun xeito selectivo e a unha velocidade constante ao lugar de acción. O tamaño e as características superficiais do nanotransportador determina o seu tempo de retención na superficie ocular, que barreiras pode cruzar, e o xeito de liberar o fármaco. Os nanotransportadores que se forman por autoemsamblado o autoasociación poden acadar tamaños comprendidos entre poucos nanómetros ata varias micras e son capaces de encapsular unha ampla variedade de substancias activas. Ademais, son moi flexibles en canto a composición e estabilidade. Entre eles cabe destacar as micelas poliméricas, os liposomas e os niosomas, que xa teñen demostrado

posuir unhas características adecuadas para actuar como nanotransportadores de fármacos para administración ocular en estudios preclínicos e clínicos. Outras formas farmacéuticas de uso tópico ocular coma os hidroxeles e os oleoxeles permiten incrementar o tempo de retención sobre a superficie ocular, o que facilita que as moléculas de fármaco poidan penetrar.

O obxectivo principal desde Tese de Doutoramente é desenrolar formulacións tópicas oculares de epalrestat que poidan ser útiles para a prevención ou tratamento da retinopatía diabética. O traballo centróuse principalmente en niosomas e oleoxeles. Para o seu deseño se tiveron en conta as características dos epalrestat de baixa solubilidade e limitada estabilidade, e a necesidade de acadar cantidades terapéuticas coa formulación, facilitando que se acaden os niveis oculares requeridos sen causar problemas de irritación.

O primeiro sistema investigado foron os niosomas, que son nanotransportadores formados por unha bicapa de tensoactivos anfifílicos no iónicos. Os niosomas foron descubertos na década de 1970 por investigadores de L'Oréal e se empregan en aplicacións comerciais desde 1986 principalmente en produtos cosméticos, máis especificamente en cremas de tratamento anti-envellecendo da liña Niosôme de Lancôme. Son a miúdo comparados os liposomas, cando son ambos os dous vesículas bi-capa, coa diferenza principal de que os liposomas están formados por fosfolípidos mentras que os niosomas teñen tensoactivos. O uso de tensoactivos como compoñente principal das vesículas dá os niosomas as vantaxes de ser máis estables, menos caros, máis fáciles de almacenar e cunha capacidade maior de encapsulación de moléculas hidrofóbicas debido ás cantidades máis baixas de lípidos auxiliares requeridos para estabilizar a estrutura bi-capa.

O segundo sistema investigado foron os oleoxeles. Para a súa preparación, o epalrestat ten que ser disolto na fase de aceite do xel, o que debe permitir unha incorporación significativamente maior que no caso de hidroxeles preparados en auga. O oleoxel é un sistema relativamente fácil de preparar a partir de mezclas dun aceite e un axente xelificante que permite unha regulación precisa da súa viscosidade.

Para cumprir estes obxectivos o traballo da Tese de Doutoramento articulouse en catro etapas:

1. **O deseño e caracterización de niosomas capaces de encapsular e liberar epalrestat ao segmento posterior do ollo**

O epalrestat é actualmente utilizado para o tratamento da neuropatía diabética en Xapón, e a súa actividade como inhibidor da aldosa reductasa sitúao en posición de ser empregado por vía tópica ocular para o tratamento da retinopatía diabética. Con todo debido á súa baixa solubilidade en agua, a preparación dun colirio de epalrestat require o desenrolo de nanotransportadores que o poidan encapsular ou o emprego de fases non acuosas. A administración tópica é por lonxe a opción máis atractiva para os pacientes con enfermidades crónicas que necesitan tratamentos de por vida cunha aplicación frecuente do fármaco.

O obxectivo desta etapa de Tese foi por a punto un protocolo robusto para a preparación reproducible de niosomas catiónicos capaces de encapsular cantidades suficientes de epalrestat e que cumpran os requisitos fisicoquímicos requiridos para a administración ocular efectiva. Para cumprir estes requisitos escolléronse polisorbato 60 (Tween 60), colesterol e 1,2-di-O-octadecenil-3- trimetilammonio

propano (DOTMA) para preparar niosomas capaces de encapsular epalrestat na súa bicapa.

A caracterización do niosomas levouse a cabo utilizando dispersión de luz láser, medidas de potencial zeta e microscopía electrónica de transmisión para determinar o seu radio hidrodinámico, a carga e a forma, respectivamente. Ademais, empregouse unha técnica de diálisis para medir a eficacia de encapsulación e rexistrar a cesión do epalrestat ao longo do tempo. Os niosomas caracterizáronse tamén en canto a compatibilidad ocular e capacidade para modificar niveis de glucosa en sangue usando modelos in ovo fecundado baseados no uso de membrana corioalantoidea. A biocompatibilidade foi avaliada tamén nun modelo de embrión de peixe cebra en colaboración con grupo da Profesora Laura Sánchez do Departamento de Zooloxía, Xenética e Antropoloxía Física na Universidade de Santiago de Compostela no Campus de Lugo. Finalmente, rexistrouse a permeabilidade do epalrestat encapsulado a través da córnea e a esclera utilizando células de difusión verticales tipo Franz e análisis de espectroscopía Raman.

Os resultados desta parte da Tese puxeron de manifesto que era posible preparar niosomas cunha ampla variedade de densidade de cargas catiónicas cun tamaño próximo ós 80 nm e cun índice de polidispersión que varía desde 0.3 a 0.5. Os niosomas amosaron forma esférica e foron capaces de encapsular o 99% do epalrestat presente na formulación. Os niosomas amosaron perfís de cesión sostida ao longo de varios días. Os ensaios in ovo revelaron que a encapsulación atenúa o efecto irritante que ten o fármaco libre, protexendo eficazmente ós vasos cos que entra en contacto. Ademais non provocan aumento do nivel de glucosa en sangue. Os niosomas contendo epalrestat encapsulado superaron con éxito o ensaio de biocompatibilidade co peixe zebra. Os niosomas permitiron a paso do fármaco a través da

esclera máis rápidamente que cando se aplicou o fármaco no encapsulado. A acumulación de fármaco en ambos os dous córnea e esclera foi confirmada mediante microscopía Raman.

Os resultados da primeira parte da Tese foron publicados na revista Pharmaceutics (DOI: 10.3390/pharmaceutics15041247)

2. Estudio da estabilidade dos niosomas mediante monocapas de Langmuir dos compoñentes

O estudio do comportamento na interfase aire-auga de cada compoñente por separado e as súas mezclas permite coñecer cómo ten lugar o proceso de ensamblaxe e en qué medida os compoñentes do niosoma interaccionan entre sí. O rexistro e análise das monocapas de Langmuir leváronse a cabo en colaboración co laboratorio Biomembranas da Profesora Matilde Casas Parada na Universidade de Santiago de Compostela no Campus de Santiago de Compostela. As monocapas permiten modelizar o comportamento das moléculas baixo restriccións espaciais. O obxectivo desta parte da Tese foi entender os cambios en comportamento que teñen lugar nas monocapas do componente principal dos niosomas, o polysorbate 60 (Tween 60), a medida que se engaden colesterol e DOTMA, así como availar en qué medida pequenos cambios de temperatura e forza iónica na subfase acuosa afectan o proceso de ensamblado.

No contexto de entrega de fármaco, a comprensión do efecto que estes factores poden ter nunha monocapa debe permitir aplicar criterios racionais no deseño das vesículas. A información recopilada durante os cambios dinámicos ós que se someten monocapas preparadas con

mezclas de distintas composicións permite predecir os efectos dos cambio no entorno e da composición das vesículas.

En primeiro lugar, avaliáronse os efectos do colesterol e do DOTMA, por separado, sobre monocapas de Tween 60. A incorporación do colesterol non alterou significativamente o módulo de compresibilidade das monocapas de Tween 60 mentres que a incorporación de DOTMA incrementou a o módulo de compresibilidade dun xeito proporcional a súa concentración. As monocapas preparadas con máis DOTMA amosaron os valores de módulo de compresibilidade maiores. Estes resultados indicaron que cando Tween 60 é o compoñente principal da monocapa, a incorporación de DOTMA inflúe na súa rixidez máis que o colesterol.

En segundo lugar, avaliouse o efecto do colesterol nun sistema de terciario constituído por monocapas de Tween 60/DOTMA as que se foi adicionando colesterol. A incorporación de colesterol deu lugar a un descenso do módulo de compresibilidade.

Finalmente o efecto de temperatura e a forza iónica da subfase foi investigada. A temperatura alterou o módulo de compresibilidade de xeito máis marcado que a forza iónica da subfase. As temperaturas máis altas (dentro de intervalos fisiolóxicos) xeralmente baixan o módulo de compresibilidade, especialmente no caso das monocapas preparadas con fraccións de DOTMA máis altas.

En conxunto, os experimentos en monocapa de Langmuir e a análise das propiedades mecánicas das monocapas preparadas cun contido fixo en colesterol (0.286 ± 0.01 mg/mL) indicaron que o módulo de compresibilidade aumenta de xeito lineal a medida que aumenta o contido de DOTMA na monocapa. Isto indica que o DOTMA evita que a monocapa teña unha estrutura moi pechada, o que

debe facilitar a encapsulación de fármaco e o posterior proceso de cesión na bicapa dos niosomas.

Ademais, o cambio dos niosomas desde condicións de almacenamento (formulación de auga, 20ºC) a condicións de administración no ollo (medio con electrolitos, máis próximo a 30ºC) en termos de temperatura e forza iónica suxiren que a adición de DOTMA a monocapa binaria de Tween 60/ colesterol aumenta o módulo de compresión a 30 °C cando a subfase é PBS.

3. Formulación e caracterización de oleoxeles para administración tópica de epalrestat

Logo dos colirios, as formas semisólidas ocupan unha posición destacada no abano de tratamentos oculares. Os oleoxeles son formas farmacéuticas compostas por un aceite no que se dispersa un axente xelificante que regula a viscosidade. O obxectivo desta parte da Tese de Doutoramente foi deseñar, formular e caracterizar oleoxeles capaces de incorporar cantidades terapéuticamente significativas de epalrestat para administración tópica ocular. A preparación e caracterización dos oleoxeles abordouse nunha estadia co Profesor Anuj Chauhan na Universidade Colorado School of Mines en Golden, Colorado.

Para preparar o oleoxeles escolleuse unha base de aceite de soia, e avaliáronse tres axentes xelificantes: cera de abella, manteiga de coco, e etilcelulosa. Preparáronse oleoxeles con cada axente xelificante por separado e tamén con mezclas binarias para cubrir un amplo intervalo de valores de viscosidade, tal como se verificou a partir de medidas reolóxicas. Os oleoxeles preparados con mezclas de dous axentes xelificantes foron extruídos en forma de pequenos cilindros a partir dos

cales avaliouse a cesión de epalrestat en medios de cesión de distinta composición e temperatura. A permeabilidade do fármaco formulado nos oleoxeles rexistrouse en córnea e esclera nun modelo ex vivo de ollo porcino. A penetración do fármaco nos tecidos oculares confirmouse mediante espectroscopía Raman. Os ensaios de compatibilidade ocular leváronse a cabo nun modelo in ovo (HET-CAM).

A visualización das formulacións baixo microscopio amosou unha dispersión homoxénea do epalrestat cando se incorporaba en proporcións do 5% e 10% w/w ós xeles. A incorporación de proporcións máis altas de epalrestat evidenciou a presencia de cristais de fármaco, o que foi indicativo da saturación do oleoxel. A avaliación reolóxica dos oleoxeles preparados cun contido fixo de axente xelificante do 5% permitiu comparar o efecto de cada axente xelificante. O oleoxel preparado con manteiga de coco presentou un comportamento reolóxico próximo o do aceite de soia puro, con características Newtonianas. A viscosidade dos oleoxeles preparados con 10% de axente xelificante foi maior ca dos oleoxeles preparados con 5% de axentes xelificante.

Os estudios de cesión de epalrestat evidenciaron unha velocidade de cesión moito máis rápida a 37ºC que a 20 ºC. A pesar da cesión rápida de epalrestat, todas as composicións resultaron ter boa compatibilidade nos ensaios in ovo.

Os ensaios ex vivo de permeabilidade en células de difusión verticais tipo Franz revelaron que o paso a través da esclera é máis rápido que a través da córnea, como se confirmou por espectroscopía Raman.

4. Comparación *in vivo* da cesión e distribución ocular de epalrestat cando se aplica como niosomas, micelas e oleoxeles

Dado que non existen ensaios alternativos á experimentación animal que poidan aportar información sobre o comportamento das formulacións cando se administran de forma tópica ocular, na última etapa da Tese de Doutoramento levouse a cabo un estudio nun modelo animal de coellos (coello branco de Nova Zelandia). Comparouse o comportamento de tres tipos de formulacións preparadas co mesmo contido en epalrestat: niosomas TCD5 e oleoxeles con 5% de manteiga de coco desenrolados nesta Tese, e micelas poliméricas adaptadas dun estudio previo levado a cabo no noso grupo para encapsular epalrestat. Os estudios in vivo foron levados a cabo coa axuda de persoal acreditado do CEBEGA e do noso grupo de investigación, en especial a Dra. María Vivero López.

Nos niosomas de Tween 60, colesterol e DOTMA, e nas micelas poliméricas de Pluronic F127, o epalrestat atópase encapsulado nos nanotransportadores, que a súa vez están dispersos en medio acuoso. Pola contra no oleoxel, o epalrestat atópase disolto na matriz do xel. En todos os casos, o contido en eplarestat fixouse en 0.2 mg/mL. Os ensaios in vivo leváronse a cabo de acordo cos principios 3R (substitución, redución e refinamento), previa aprobación polo comité de bioética da Universidade de Santiago de Compostela e o comité de ética de experimentación animal (CEEA) (número de inscrición: ES150780292901).

As tres formulacións amosaron unha adecuada compatibilidade coa superficie ocular e proporcionaron perfís de cesión rápidos de epalrestat. A análise dos tecidos revelou que o eplarestat pode

atravesar córnea e esclera, pero o acceso ó segmento posterior parece máis factible a través da ruta transescleral.

En conxunto, o traballo desenvolvido nesta Tese de Doutoramento permite ampliar as posibilidades de administración tópica de epalrestat para o tratamento de patoloxías do ollo derivadas da diabetes. Na Tese abordouse o desenvolvemento de dúas formas farmacéuticas, niosomas e oleoxeles, dende o seu deseño ata a caracterización in vitro, in ovo, ex vivo e in vivo. Tamén se adaptou outro tipo de forma farmacéutica, as micelas poliméricas, para a administración ocular de epalrestat. Os resultados obtidos durante esta investigación poden achandar o camiño cara a formas de administración menos invasivas para os pacientes que padecen retinopatía diabética.

INTRODUCTION

The work described in this chapter was published in **Diabetic eye: associated diseases, drugs in clinic, and role of self-assembled carriers in topical treatment**, *Expert Opinion on Drug Delivery*, 18(11), 2021, 1589-1607, authored by

Axel Kattar[a], Angel Concheiro[a], and Carmen Alvarez-Lorenzo[a]

[a]Departamento de Farmacología, Farmacia y Tecnología Farmacéutica, I+D Farma Group (GI-1645), Facultad de Farmacia, Instituto de Materiales (iMATUS) and Health Research Institute of Santiago de Compostela (IDIS), Universidade de Santiago de Compostela, 15782 Santiago de Compostela, Spain.

1. INTRODUCTION

Diabetes mellitus currently affects 8.5% people worldwide, and it is expected to impact on the lives of 570 million people in 2025 [1]. There are five different forms of diabetes, with diabetes type 1 (failure in the production of insulin) and type 2 (deficient insulin sensitivity) being the most common. The other three forms are monogenic diabetes, which is hereditary due to a single gene mutation; gestational diabetes, related to pregnancy; and cystic fibrosis-related diabetes, which is linked to scarring of the pancreas that leads to insulin abnormalities. For people with type 1 diabetes, the immune system attacks pancreatic cells responsible for the production of insulin, disrupting their normal function. Both genetic and environmental factors have been identified as causal agents. Type 2 diabetes is indicative of insulin resistance, which may be caused by excess body weight.

Diabetes is considered a pandemic disease with an increasing morbidity and the highest rate in years of life lost due to disability in both high-income and lower-middle-income countries [2]. Such a high incidence results in an increase in diseases secondary to diabetes. Diabetes-associated diseases range from cardiovascular problems to diabetic neuropathy including kidney failures and ocular diseases. Indeed, the term diabetic eye disease has a broad meaning as it may encompass multiple illnesses in different parts of the eye, mainly diabetic retinopathy, macular edema, cataracts, glaucoma, and keratopathy [3–6].

Control of hyperglycemia is a critical main measure to avoid a fast progression of damage in ocular structures. Depending on the time lag between the first symptoms of diabetes and effective regulation of glycemia levels, the eyes may already be affected when therapeutic measurements are taken. Therefore, early diagnosis may prevent the apparition of diabetes-associated diseases. Nevertheless, continuous high basal glucose levels over time inevitably cause damage to a wide variety of tissues, especially those where glucose is freely accessible [7].

Since diabetes is a chronic disease, ocular treatments may have to be applied for years. Therefore, finding drug delivery systems that combine the patient-friendly administration of topical formulations with the high ocular bioavailability of intraocular injections is an unmet clinical need. In the last decades, eye drops in which the drug molecules are encapsulated in nanocarriers have demonstrated notable enhancements in drug levels in both anterior and posterior eye segments [8,9]. Nanomicelles, liposomes, lipid nanoparticles, and polymer nanospheres provide protection against premature degradation, enhanced retention on eye surface, and novel pathways of penetration through corneal and transscleral routes [10,11]. Carriers that are spontaneously formed by self-assembly of their components in water are advantageous in terms of preparation and scale up because only few steps and energy are required. Polymeric micelles have outstanding capability to encapsulate hydrophobic drugs increasing apparent drug solubility, although concerns about premature disassembly may arise [12]. Lipid-based vesicles, such as liposomes, may host both hydrophobic and hydrophilic active substances [13], but the constituent lipids may be prone to chemical degradation [14,15]. In this context, niosomes as vesicles made of self-assembled nonionic surfactants may gather the advantages of both micelles and liposomes while providing

improved physical and chemical stability. The development of niosomes as eye drops components is still incipient, but preliminary results have evidenced their potential [16]. Other supramolecular structures such as self-assembling polypeptides have shown to be excellent drug carriers for other administration routes and may offer new avenues in the treatment of eye diseases not only as carriers but also as therapeutic agents [17–19]. The aim of this chapter is to revisit first the role of diabetes in the development of eye diseases. Then, the pros and cons of different drug administration routes for diabetic eye treatments are considered. Commercially available drugs as well as those in clinical trials are analyzed in detail. Subsequent sections in this chapter deal with the main self-assembled nano- and micro- carriers suitable for topical eye administration, namely, polymeric micelles, liposomes, and niosomes. Nanocarriers for treatment of diabetes-associated diseases using other administration routes have been tackled elsewhere [20]. Finally, recent advances in the design of self-assembled carriers for topical diabetic eye drug administration are presented. Publications containing ex vivo or in vivo results or reporting on clinical trials have been prioritized.

1.1 DIABETIC EYE DISEASES

Diabetes may affect the anterior segment triggering the development of cataracts, dry eye syndrome, corneal ulcers, warts, tortuous conjunctival vessels, and keratopathy [4,21]. In the posterior segment, diabetes may contribute to glaucoma, retinopathy, and macular edema [22]. Diabetic patients can also suffer from ocular neuropathy, difficulties in healing ocular wounds, and increased infection probabilities [4].

Cataracts are described as the clouding of the lens. Three pathogenesis routes have been described [23]: the polyol pathway where an accumulation of sorbitol induces hydropic lens fiber degeneration, the oxidative and osmotic stress leading to apoptosis of epithelial cells of the lens, and the autoimmunity. The polyol pathway is the one referred to most often and the most researched [24]. Sugars (e.g. glucose and galactose) at elevated concentrations are favorable substrates for aldose reductase and generate intense osmotic stress (as explained in Section 3.1). Also, reducing sugars promote glycation (i.e. non-enzymatic glycosylation) of lens proteins, triggering cataract formation [25].

Dry eye syndrome, which is characterized by an abnormal tear film, can be classified as either aqueous tear-deficient or evaporative (associated to a deficient tear film lipid layer) [26]. Direct correlations have been found between prevalence of the syndrome and glycated hemoglobin and duration of diabetes. In vivo studies suggest that lachrymal glands undergo histological changes in diabetic patients and that oxidative stress derived from hyperglycemia might be involved in dry eye syndrome [27].

Corneal ulcers are sores on the cornea that can alter the vision [28]. The primary cause of corneal ulcers may be unrelated to diabetes (eye surgery, accidents), but the lengthier wound healing process makes ulcers a heavier burden for diabetic patients [29,30]. Therapeutic approaches to deal with diabetic keratopathy have been reviewed elsewhere [31].

Glaucoma is the leading cause of blindness worldwide and is defined by damage of the retinal ganglion cells, leading to irreversible damage of the optic nerve [32]. This is often accompanied by a rise of the intraocular pressure (IOP) triggered through different mechanisms.

Open-angle glaucoma is caused by blocking of the trabecular meshwork, which in turn hinders fluid drainage and increases pressure. This is the most common form of glaucoma and happens at slow pace. Angle closure glaucoma is provoked by the iris coming forward and blocking the drainage angle between the iris and the cornea. It can happen over time or suddenly. Secondary angle closure glaucoma, in which the angle can be opened or closed, is caused by a secondary factor that leads to drainage hindrance, for example excessive pigment release blocking the trabecular meshwork (pigmentary glaucoma). Although the role of diabetes is unclear, direct correlations were found between diabetes duration and fasting glucose levels and the increase in IOP [33].

Diabetic retinopathy involves damage to the retinal blood vessels, which has disastrous effects on the retina [34]. In nonproliferative diabetic retinopathy, the retinal blood vessels are damaged and start leaking, which increases the pressure in the tissue. This condition can progress from microaneurysms to severe macular edema. In the proliferative diabetic retinopathy, the damaged blood vessels close and new blood vessels start to grow abnormally. The consequences may include increased IOP, accumulation of scar tissue, and ultimately nerve damage. Diabetic retinopathy affects one out of two persons with type 1 diabetes [35]. The duration of diabetes is a risk factor, and the prevalence of diabetic retinopathy increases from 8% after 3 years of diabetes to 80% after 15 years [36].

Diabetic macular edema may be a consequence of diabetic retinopathy, where leaking blood vessels increase the fluid volume in the macula, resulting in vision loss [37]. Two types of diabetic macular edema can be clinically differentiated: focal macular edema, which is characterized by microaneurysms on the retinal capillaries, and diffuse

macular edema, which shows leakage from the blood-retinal barrier due to generalized damage [38].

1.2 DELIVERY OF DRUGS TO DIABETIC EYE

1.2.1 Main drug classes and current administration routes

As described earlier, diabetes-related eye diseases are varied and evolve along time to become chronic. This means that their treatment should be designed according to the prolonged time the drug should be administered. In this regard, three main strategies are so far the most investigated and used ones: (i) topical administration, mostly for the treatment of anterior segment diseases, with the limitation of poor ocular bioavailability; (ii) intraocular administration, which is more efficient in terms of ocular bioavailability but entails relevant risks for the patient; and (iii) oral administration, which is the most patient friendly route, but the ocular bioavailability is quite low even when large doses are administered. Pros and cons of the different administration routes are explained in **Table 1.1**.

Table 1.1. Administration routes for delivery of drugs to the eye

Administration route	Advantages	Disadvantages
Topical	Noninvasive approach, well accepted by the patient	All barriers except the blood-eye barriers must be overcome Self-administration may be not feasible in all cases
Oral	High patient compliance, no corneal or anterior segment barriers	Systemic untoward effects, blood-retinal barrier, low on-site concentration
Intracameral	High drug concentration in the anterior chamber	Clinical injection
Subconjunctival	Scleral route to the retina, suitable for depot formulations	Clinical injection
Intravitreal	High drug concentration in the posterior segment, hydraulic pressure gradient	Clinical injection (more invasive than subconjunctival), dependent on vitreous diffusion, the visual axis can be obscured if the formulation is opaque
Retrobulbar	Low risk for intraorbital injury, low influence on IOP	Clinical injection, risk of optic nerve damage
Peribulbar	Low risk for intraorbital injury	Clinical injection
Posterior juxta scleral	Available for inserts	Retinal pigment epithelium is still a barrier

Efficient ocular drug delivery is a difficult goal to reach in any case. Depending on the administration procedure and the dosage form, ocular barriers can be either physiological or anatomical, and either static or dynamic [39]. Different barriers located in the anterior and the posterior segments protect the eye against foreign substances coming from outside or inside the body (e.g. the bloodstream). Also, the goal of drug delivery can be different depending on the target cells. If the drug must reach a tissue protected by many barriers, drug permeation through these barriers is critical; prodrugs, penetration enhancers, and encapsulation in nanocarriers may be helpful tools [40,41]. If the aim is to continuously supply the drug to an area with important dynamic turnover of fluids, sustained drug delivery systems may be required [42].

Regarding topical administration, the eye is dynamically protected by the blinking reflex, the tear clearance rate, andthe nasolacrimal drainage. Adhesion to the corneal surface and promotion of the penetration might overcome these barriers. Drugs can follow three routes: corneal, scleral, and conjunctival [43–47]. Major static corneal barriers are the corneal epithelium, which limits the absorption of macromolecules and hydrophilic drugs through tight junctions, and the corneal stroma, which limits the penetration of lipophilic molecules due to its high aqueous content [44]. Thus, mid- lipophilic drugs are the most suitable candidates for corneal penetration and subsequent diffusion through aqueous humor for intraocular distribution. The iris and the nonpigmented ciliary epithelium further block drugs from passing to the aqueous humor, making make up the blood–aqueous barrier [47]. Furthermore, the aqueous humor flow from the ciliary body to the cornea counteracts the diffusion of hydrophilic molecules trying to enter further in the eye. On this blood–aqueous barrier and also

on the corneal epithelium, there are efflux pumps that expel the drugs back to the front of the eye [48].

The conjunctiva opposes to drug entry in the eye tissues mainly due to the presence of conjunctival blood capillaries and lymph vessels, which reroute a major fraction of the drug dose to the blood stream. Drug access through the conjunctiva to the posterior segment may occur via passive or active transport [45]. Although there are tight junctions among conjunctival epithelium cells, polar solutes up to 20 kDa can enter through paracellular diffusion across 5-nm pores [49]. Peptides and proteins may find the additional barrier of enzymatic degradation and require co-administration with a protease inhibitor [50]. Lipophilic drugs can still penetrate better via the transcellular route; the surface area is larger than for paracellular pathway, although efflux pumps pose a relevant challenge. Intense active carrier-mediated transport occurs at conjunctiva for some ions and nutrients, which may be exploited for drug and prodrug absorption [46]. Drugs encapsulated in nanocarriers take benefit of the additional pathway of endocytosis, which is feasible both in cornea and conjunctiva [51–53].

Once conjunctiva is crossed, the drug can move through sclera into the uvea and the retinal pigmented epithelium, and then move forward to neural retina and vitreous humor. The sclera performs as a size exclusion barrier, with the permeability decreasing exponentially with molecular radius and lipophilicity [54]. The sclera is negatively charged at physiological pH and therefore electrostatic interactions must be considered too. Bruch's–choroid complex traps positively charged lipophilic drugs [55], and since Bruch's membrane becomes less elastic with age (due to calcification of elastin and cross- linking of collagen) drug diffusion is hindered in elderly patients.

Systemic administration of ocular drugs is compromised by the blood-retinal barrier. The inner limiting membrane of the retinal pigment epithelium prevents passage of high- molecular-weight molecules from blood to vitreous and vice versa [56]. Müller cells and astrocytes form tight junctions to regulate the passage of molecules between the outer choroid and the inner retina. Although the information on ocular bioavailability after drug systemic administration in humans is limited, some reports evidenced that for small drugs, such as ciprofloxacin, similar drug levels can be obtained in aqueous humor after topical instillation of the free drug or oral administration. The levels in vitreous humor are commonly higher after oral administration, but at expenses of exposing the whole organism to high drug dose [57]. Also, interestingly, the drug can be found in tear fluid after oral administration but not because of distribution through the eye, as reported for cyclosporine A [58]. The blood-retinal barrier efficiently prevents cyclosporine A diffusion from blood to the anterior segment, except during concomitance of inflammatory processes [59].

Pharmacological treatments intended to stop ocular damage caused by hyperglycemia or at least delay the process rely on (i) reducing IOP (**Table 1.2**), (ii) blocking the abnormal growth of blood vessels, or (iii) inhibiting negative chemical pathways. Drugs like prostaglandins [60], rho kinase inhibitors [61], nitric oxides [62], or miotic/cholinergic agents [63] drain ocular fluids. Alpha-adrenergic agonists, β-blockers, and carbonic anhydrase inhibitors lower the amount of fluid produced in the eye [64]. Both strategies result in a lowering of the IOP and are usually addressed using eye drops (**Table 1.2**). Additionally, new drug candidates are intended to act on the heme oxygenase 1 (HO-1)/carbon monoxide (CO) physiological pathway that regulates the IOP. The HO-1 produces protection against ischemic insult by producing CO, which has anti-inflammatory properties. Incidentally, CO protects retinal

ganglion cells from ischemic/reperfusion injury. Decreased CO levels have been related to increased IOP and, therefore, drugs that release CO may be useful in glaucoma treatment [65].

Table 1.2. Some active substances of medicines used to reduce the IOP. Data from the European Medicines Agency, https://www.ema.europa.eu/en/medicines

Drug class	Drug	Dosage form
Prostaglandin or analog	Travoprost	Eye drop
	Bimatoprost	Eye drop
	Latanoprost	Eye drop
	Unoprostone	Eye drop
Prostaglandin analog nitric oxide	Latanoprostene bunod	Eye drop
Rho kinase inhibitor	Netarsudil	Eye drop
	Ripasudil	Eye drop
Miotic agent	Pilocarpine	Eye drop
Cholinergic agonist	Carbachol	Eye drop or intraocular injection
Alpha-adrenergic agonist	Brimonidine	Eye drop
	Apraclonidine	Eye drop
Beta blocker	Betaxolol	Eye drop or oral tablet
	Timolol	Eye drop
	Carteolol	Eye drop
Carbonic anhydrase inhibitor	Methazolamide	Oral tablet
	Acetazolamide	Eye drop
	Brinzolamide	Eye drop
	Dorzolamide	Eye drop

The growth of abnormal ocular blood vessels can be handled with anti-vascular endothelial growth factor (anti-VEGF) drugs [66].

Bevacizumab and ranibizumab, which are respectively full antibody and antibody fragment that bind VEGF-A, and aflibercept, a recombinant protein that traps VEGF-A and VEGF-B, are the cornerstones for the therapy of diabetes-related macular edema and retinopathy [67]. They require intravitreal injection, which is not absent of complications [68]. Intraocular injections should be used as infrequently as possible, according to pro re nata or treat-and-extend protocols [69]. Biodegradable delivery systems that sustain intraocular release avoiding multiple treatment and maintaining drug stability are under investigation [70,71]. Since each available anti-VEGF agent interacts quite differently with VEGF, characterization of the molecular interactions can improve the design of novel biological drugs potentially useful in clinical practice [72].

Hyperglycemia is also responsible for triggering the polyol pathway. Under normoglycemic conditions, the Embden– Meyerhof–Parnas catabolism route that transforms glucose into pyruvate, NADH, and ATP becomes saturated. Consequently, the polyol pathway, which commonly transforms 3% glucose, enters into action with the participation of two enzymes: (i) aldose reductase that transforms glucose into sorbitol with the consumption of NADPH and (ii) sorbitol dehydrogenase that slowly converts sorbitol into fructose while consuming NAD+. The polyol pathway, which is very active in retina and lens, metabolizes more than 30% glucose under diabetic conditions [73]. Accumulation of sorbitol causes osmotic stress, triggers leukocyte accumulation, disrupts blood-retinal barrier, favors cells apoptosis, and starts a cascade of oxidative stress-mediated reactions [74]. The excess of fructose acts as precursor of advanced glycation-end products (AGEs). In this context, aldose reductase inhibitors are gaining increased attention, and epalrestat is approved in some countries for oral administration. As an alternative, drugs that accelerate the metabolic

rate of sorbitol dehydrogenase and, thus, decrease the levels of sorbitol are being tested [73].

In the later stages of the disease, laser treatment (mainly for photocoagulation) or surgery (when blood vessel leakage becomes excessive or there is scar tissue) can be proposed [75,76]. Vitreoretinal surgery, for example, involves the removal of part of the vitreous and scar tissue in order to ameliorate the patient's vision [77].

1.2.2 Drugs, biologics, and gene therapy in clinical trials

Relevance of the morbidity caused by diabetes on eye structures is exemplified by the 868 clinical studies in phases 1 to 4 in February 2021 when searching for 'diabetic eye' in the ClinicalTrials.gov database. Refinement of the information to select recruiting, enrolling, active, terminated, or completed trails rendered an outcome of 657 studies, with an ample distribution worldwide (**Figure 1.1**). Most clinical trials are focused on the efficacy and safety of new molecules or novel administration routes, drug combinations, or delivery systems such as implants, microparticle depot formulations, or biopolymer–antibody conjugates. Microneedle patches that can be applied onto cornea or sclera for direct drug delivery in the aqueous or vitreous humor, respectively, are gaining increasing interest, although still in the preclinical phase [78–80].

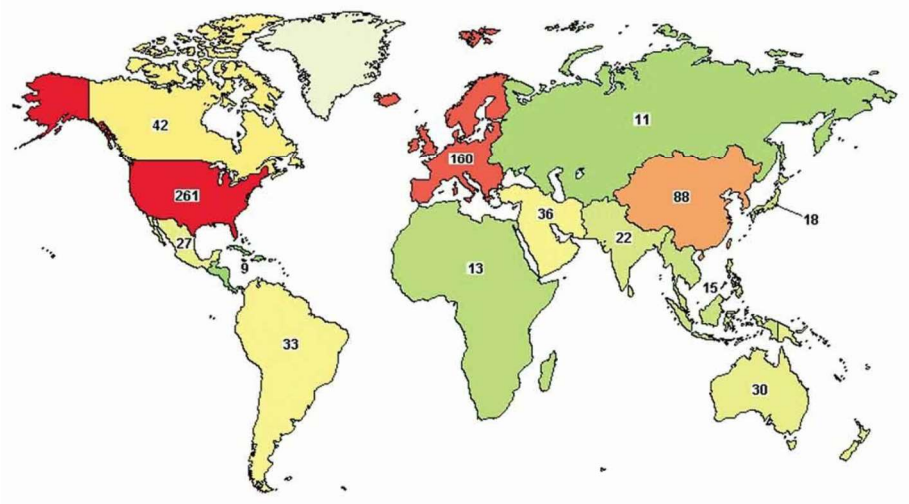

Figure 1.1. Regional distribution of clinical trials related to diabetic eye. Data source: ClinicalTrials.gov. There were 657 outcomes for 'diabetic eye' on February 2021. Applied filters were Recruiting, Active not recruiting, Completed, Enrolling by invitation, and Terminated. Made by the author of this Thesis.

Most clinical trials related to diabetic eye refer to the conditions macular edema (**Table 1.3**) and retinopathy (**Table 1.4**), and most interventions deal with drugs or biologics, particularly intravitreal injection of antibodies. However, the interest for oral administration as well as topical formulations does not decrease but is gaining attention, spearheaded by the search for novel active substances with improved ocular bioavailability and new therapeutic targets. Intense research on small molecules that perform as anti-inflammatory (e.g. nepafemac, loteprednol etabonate) or as anti-angiogenic/angiolytic (e.g. EXN407, OC-10X) is being carried out.

Table 1.3. Pharmacological treatments in clinical trials for diabetes-related macular edema classified as a function of the administration route, drug/biologic active substance, and number of clinical studies

Administration route	Drug/Biologic class	Active substance	Number of clinical trials
Intravitreal	Antibodies or blockers	Aflibercept and biosimilars	42
		Anti-angiopoietin-2 antibody REGN910	1
		REGN910-3 (co-formulation of REGN910 and aflibercept)	1
		Anti-erythropoietin LKA651	1
		Anti-PlGF recombinant monoclonal antibody	1
		Anti-$ROBO_4$ antibody DS-7080a	1
		Bevacizumab	16
		Bevasiranib	1
		Tofacitinib (BI 764,524)	1
		Conbercept (KH902)	1
		Faricimab	1
		Infliximab, anti-TNFα	1
		OPT-302, anti-VEGF-C and anti-VEGF-D	1
		Pegaptanib	7
		Ranibizumab	40
		Teprotumumab	1
	Small molecules	Dexamethasone	31
		Fluocinolone acetonide	9
		Triamcinolone acetonide	11
		Anti-VEGF drugs	7
		KVD001 plasma kallikrein inhibitor	2

		AR-13,503, small-molecule inhibitor of both Rho kinase and protein kinase C	1
		UBX1325, inhibitor of Bcl-xL (anti-apoptotic regulatory protein)	1
	Peptides	AXT107, tyrosine kinase blocking collagen IV-derived peptide	1
		Luminate (Alg-1001) integrin inhibitor	1
	Proteases	Ocriplasmin	1
	Gene therapy	ADVM-022 gene therapy (AAV.7m8-aflibercept)	1
		iCo-007, a single-stranded antisense that degrades messenger RNA (mRNA)	1
		PF-04523655, small-interfering RNA (siRNA)	1
Oral	Small molecules	GSK2798745, transient receptor potential vanilloid 4 (TRPV4) channel blocker	1
		Aliskiren	1
		Danazol	1
		Fenofibrate/pemafibrate	2
		Imatinib mesylate (YD312)	1
		Levosulpiride	1
		Minocycline	1
		MS-533 protein kinase inhibitor	1
		Ruboxistaurin	1
		Semaglutide	1
	Dietary supplements	Alzer®, Diamel®, others	2
Topical eyedrops	Small molecules	Bromfenac	1
		Dexamethasone	2
		Diclofenac	1

		EXN407, specific serine/threonine-protein kinase 1 (SRPK1) inhibitor	1
		FOV2304, inhibitor of bradykinin B1 receptor	1
		Fluocinolone acetonide	1
		Ketorolac	3
		Nepafenac	5
		OC-10X tubulin inhibitor	1
		Loteprednol etabonate	1
		Mecamylamine nonspecific nACh receptor blocker	1
		SF0166 small-molecule αvβ3 antagonist	1
		Vitamin E	2
	Peptides	Elamipretide (MTP-131), mitochondria-targeting peptide	1
Intravenous	Small molecules	Methotrexate	1
Intramuscular	Peptides	Octreotide acetate in microspheres	1
Episcleral	Small molecules	Dexamethasone implant	1
Subconjunctival	Antibody	Bevacizumab	1
	Small molecule	Rapamycin	2
Subcutaneous	Small molecule	Razuprotafib (AKB-9778), inhibitor of VE-PTP (vascular endothelial protein tyrosine phosphatase)	2
Sub-macular	Antibodies	Ranibizumab	1
Suprachoroidal	Gene therapy	RGX-314 (AAV8 vector containing a transgene for anti-VEGF fab)	1

Table 1.4. Pharmacological treatments in clinical trials for diabetes-related retinopathy classified as a function of the administration route, drug/biologic active substance, and number of clinical studies

Administration route	Drug/Biologic class	Active substance	Number of clinical trials
Intravitreal	Antibodies or blockers	Aflibercept and biosimilars	14
		Anti-PlGF recombinant monoclonal antibody	1
		Bevacizumab	14
		Tofacitinib (BI 764,524)	1
		Conbercept (KH902)	2
		Pegaptanib	2
		Ranibizumab	20
	Small molecules	Dexamethasone	3
		Triamcinolone acetonide	5
		Anti-VEGF Drugs	1
	Gene therapy	PF-04523655, small-interfering RNA (siRNA)	1
Oral	Small molecules	Acetazolamide	1
		Alpha-lipoic acid	1
		Aminoguanidine	1
		Brimonidine	1
		Darapladib	1
		Doxycycline	1
		Emixustat hydrochloride	1
		Empaglifozin	1
		Fenofibrate/pemafibrate	3
		Finerenone	1
		Melatonin	1

		RG7774	1
		Ruboxistaurin	2
		Semaglutide	1
		Sinemet	1
		Sulodexide	1
		Tientine	1
		Ubiquinone	1
	Dietary supplements	Alpha-lipoic acid, carotenoid vitamins, omega 3, multi-component nutritional supplement (vitamin C, mixed tocopherols/tocotrienols, vitamin D, fish oil, lutein, zeaxanthin, pine bark extract, benfotiamine, green tea extract, curcumin), Ocufolin®	5
Topical eyedrops	Small molecules	Anecortave acetate	1
		Citicoline	1
		Curcumin, homotaurine, and vitamin D3	1
		Dexamethasone	1
		Diclofenac	1
		Dorzolamide	1
		Ketorolac	3
		Latanoprost	2
		Napafenac	3
		OC-10X tubulin inhibitor	2
		Prednisolone acetate	2
		Squalamine lactate	1
		TG100801 multikinases inhibitor	1
	Peptides	Somatostatin (with brimonidine)	1
Intravenous	Protein	Pulsatile insulin	2

Intramuscular	Peptides	Octreotide acetate in microspheres	4
Subconjunctival	Small molecule	Rapamycin	1
Subcutaneous	Small molecule	Razuprotafib (AKB-9778), inhibitor of VE-PTP (vascular endothelial protein tyrosine phosphatase)	1
Suprachoroidal	Gene therapy	RGX-314 (AAV8 vector containing a transgene for anti-VEGF fab)	1

For corneal epithelial defects, clinical trials deal with combinations of anti-inflammatory and antimicrobial drugs or autologous serum [81]. Fonadelpar (SJP 0035), a peroxisome proliferator-activated receptor delta agonist, is in Phase III for dry eyes and Phase II for corneal disorders [82]. Topical insulin and naltrexone eye drops have been shown to accelerate corneal epithelial healing and ameliorate dry eye symptoms in a variety of animal models [83,84]. Results of topical insulin and naltrexone clinical trials have not been posted yet [85,86].

Gene therapy of diabetic eye diseases is also an active field of research and clinical translation. The approval of Luxturna®, a virus-based gene delivery system for inherited retinal dystrophy, paved the road for other developments [87–89]. There are currently 492 recruiting or active clinical trials on ocular gene therapy, most of which use adeno-associated viruses as carriers, according to ClinicalTrials.gov, clinicaltrialsregister.eu and rctportal.niph.go.jp. Differently to the repeated administration of drugs and biologics, gene therapy approaches pursue potential one-time treatment, namely the cells are instructed once to produce the needed therapeutic substance or to not produce the harmful substance. In the case of diabetes-related macular edema, three clinical trials with intra- vitreal formulations and one clinical trial with a suprachoroidal formulation for gene therapy are ongoing (**Table 1.3**). ADVM-022 (AAV.7m8-aflibercept) and RGX-314 (AAV8 vector containing a transgene for anti-VEGF fab) are intended to provide durable expression of an anti-VEFG antibody [90,91]. RGX-314 is also being tested for diabetic retinopathy [92].

RNA interference therapy is in clinical trials too, although it may require repeated injections [93]. For example, iCo-007 is a single-stranded antisense that degrades messenger RNA intended to target c-Raf kinase for diabetic macular edema treatment. Phase II results using

intravitreal injections were not conclusive about safety and efficacy [94]. PF-04523655 (RTP801I-14), a small-interfering RNA (siRNA) that may inhibit RTP801 gene transcription, is under evaluation as direct intravitreal injection. RTP801 is strongly upregulated in diabetic eyes and is associated with hypoxia and stress-related damage to retina cells [95]. Gene therapy also offers excel- lent opportunities to address ocular inflammation triggered by sorbitol accumulation and AGEs [74,96,97]. Gene therapy may allow for regulation of pro- and anti-inflammatory cytokines and neovascularization in keratitis, as reviewed elsewhere [98].

1.3 SELF-ASSEMBLED NANOCARRIERS FOR TOPICAL DIABETIC EYE DRUGS

Most of drugs and new drug candidates in clinical trials for diabetic eye therapy, as referred in **Tables 1.3** and **Table 1.4**, are quite hydrophobic and must be formulated as suspensions or ointments, showing limited ocular bioavailability after instillation. Thus, noninvasive topical therapeutic approaches may be notably improved if the drugs are formulated into delivery systems that could enhance their solubility and ocular permanence. In preclinical tests, micelles and cyclodextrin aggregates have been shown to enhance cornea and sclera accumulation and permeation of various hydrophobic diabetic eye drugs [99–101]. Even in the search for novel delivery strategies, contact lenses have been designed specifically to deliver epalrestat [102] and naltrexone [103] and viral-based gene vectors [104]. Regarding intravitreal gene therapy, siRNAs are extremely labile and rapidly cleared, and thus demand adequate nanocarriers. However, most non-viral vectors are strongly cationic polymers or lipids that may interact with negatively charged glycosaminoglycans in the vitreous humor.

Such an interaction may prematurely break the poly/ lipoplexes or alter the cell transfection and, thus, a very fine equilibrium in surface charge or a shell able to minimize retention in vitreous is required [105,106].

Self-assembled drug carriers that can be prepared in few steps and can encapsulate both small and large active sub- stances, while providing a highly biocompatible, stealth inter- face are gaining increasing attention for ocular delivery. Although a plethora of novel self-assembled carriers are being tested, polymeric micelles, liposomes, and niosomes have already demonstrated in vivo promising performances [13,16,99,107]. Below, first the variables that drive the formation of these carriers and the main preparation protocols are revisited. Then, specific applications for management of diabetic eye diseases are analyzed.

1.3.1 The self-assembly process

Self-assembled carriers rely on amphiphilic components that bear regions of different affinity for water [108]. The simplest self-assembled structure is that of common surfactant micelles. In contact with water, small surfactants move to the air–water interface with the polar head immersed in water while the apolar tail is prone to the air. Above a certain con- centration, designed as critical micelle concentration (CMC), the air–water interface is saturated, and the surfactant molecules inside the aqueous medium associate to minimize the thermodynamically unfavorable exposure of the apolar tails to the aqueous environment. Thus, the apolar tails become the core (nucleus) of a supramolecular structure in which the polar heads remain exposed to the aqueous environment. The cap- ability of surfactant micelles to encapsulate hydrophobic drugs is well known, but toxicity and physical

instability limit their practical use as drug carriers [109]. Micelles may extract relevant components from cells and, if they are made of ionic surfactants, may alter vital cell pathways, compromising the safety of the formulation [110]. Moreover, the self-assembly is a reversible process, and assembled and non-assembled com- ponents are in a fragile equilibrium that can be displaced in any direction quite rapidly. Although the volume of liquid at the eye surface is less than in other administration routes, all topically instilled formulations are exposed to relevant tear turnover [111]. Thus, one drop of common micelle formulation in contact with the lachrymal fluid undergoes a rapid decrease in surfactant concentration, and below the CMC, the micelle rapidly disassembles into their individual components [112]. Consequently, few improvements (if any) compared to the instillation of the drug solely solution can be noticed, with the aggravating toxic effects that surfactant molecules may have on eye surface.

When searching for more biocompatible and stable self- assembled nanocarriers, two different strategies came up: core-shell polymeric micelles and bioinspired bilayered vesicles. This classification relies on the arrangement of the com- ponents, but as explained below, the same component can lead to micelles exhibiting a variety of shapes or to bilayered vesicles depending on its concentration and the presence of certain additives [113]. For the sake of clarity, polymeric micelles are considered here as supramolecular assemblies of amphiphilic polymers (unimers) that have a core formed by apolar segments and a shell formed by polar segments [112]. Thus, a gradient in polarity is observed from inside to outside [113]. Differently, bilayered vesicles are defined as quasi- spherical structures in which the amphiphilic components are assembled in cell membrane-like bilayers (**Figure 1.2**). Two or more bilayers can be arranged concentrically being separated from each other by an aqueous compartment. Therefore, bilayered vesicles do not

exhibit progressive gradients in polarity, but stepped apolar-polar regions that can respectively encapsulate hydrophobic and hydrophilic compounds [114,115].

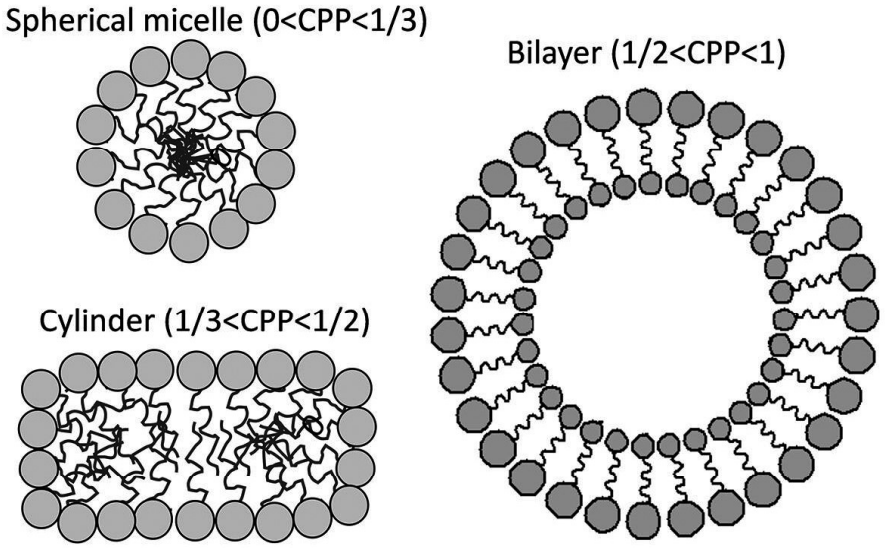

Figure 1.2. Dependence of the architecture of the self-assembled nanocarrier on the critical packing parameter (CPP). Made by the author of this Thesis.

The amphiphilic component determines the physicochemical and biological properties of the self-assembled nanocarrier. The self-assembly process is regulated by hydrophobic interactions in aqueous environment, and thus the critical packing parameter (CPP) and the hydrophilic/lipophilic balance (HLB) of the amphiphilic component become decisive [116,117]. The hydrophilic heads maximize the contact surface with water, while the hydrophobic tails cluster together to minimize the contact with water. The formed structure arranges into the lower energy configuration, which is spherical or cylindrical depending on the CPP.

The volume of the head group, the volume of the hydrophobic tail (V), the equilibrium area per molecule at the inter- face surface (A), and the length of the hydrophobic tail (l) are the primary physical characteristics that determine the *CPP*, as follows [116]:

$$CPP = \frac{V}{A * l}$$

The resulting value, which is unitless, determines the shape of the self-assembled structure. If the CPP is between 0 and 0.33, the self-assembled structure looks like a spherical micelle; between 0.33 and 0.5, the structure has rod-like shape; and only above 0.5 the structure becomes a bilayer, which can form vesicles (**Figure 1.2**) [118]. The HBL, which is a measure of the balance of the size and strength of hydrophilic to hydrophobic regions, is calculated differently for different classes of amphiphilic substances. The HLB of polyoxyethylene alkyl ethers and polyoxyethylene esters is roughly estimated as the mass percentage of oxy- ethylene divided by five [119]. The ideal HLB values for vesicle bilayer formation lies between 3 and 8, namely they fall in the range of 'hydrophobic' surfactants [120]. Another relevant physical property is the gel–liquid transition temperature, which is the temperature at which the amphiphilic components go from closely packed in a gel state to a liquid state where they flow more freely. The aforementioned parameters come into play once the concentration of the amphiphilic component is appropriate for the structure desired, as it is possible to saturate the dispersions and create different aggregates based on the concentration of the surfactant. As an example, in the case of amphiphilic block copolymers, an increase in concentration may drive different unimers and micelles packaging leading to hydrogels and lyotropic liquid crystals [121].

The physical stability of a self-assembled structure depends on thermodynamic and kinetic contributions [112]. Self- assembly is a spontaneous phenomenon and, a priori, does not require solvent exchanges and purification, but it does not mean that occurs quickly and in many cases energy or multistep pro- cesses are required to obtain the desired structure. Moreover, an equilibrium between assembled and non-assembled components should be considered. The lower the CMC or the critical aggregation concentration (CAC), the less the ratio of free non- assembled components (unimers). The self-assembled structure is more thermodynamically stable when CMC or CAC are low and, therefore, less prone to disassembly once diluted. The strength of the interactions among the hydrophobic tails also determines the kinetics of the disassembly process. Closely packed components require more time for separation once the formulation is strongly diluted and, in turn, the integrity of the nanocarrier can be maintained for prolonged time [12]. Indeed, physical stability under dilution is an index of the time that the unimers remain aggregate when the concentration is below the CMC and of the capability of the self-assembled carriers to retain the drug inside [91,122]. Strong changes in temperature as those that occur when steam heat sterilization is applied to prepare ophthalmic eye drops may trigger the aggregation or fusion of the self-assembled structure, or an increase in the permeability of the bilayer, which is quite common in the case of liposomes [123].

1.3.2 Applications to diabetic eye

1.3.2.a Polymeric micelles

Polymeric micelles can host a wide variety of low- and mid-polarity drugs and provide passive and active targeting [99,124].

Nevertheless, only a few papers have focused on the design of polymeric micelles for diabetes-related ocular diseases (**Table 1.5**). Soluplus® (polyvinyl caprolactam-polyvinyl acetate- polyethylene glycol copolymer) micelles (70–80 nm) have shown outstanding capability to solubilize alpha-lipoic acid and to withstand dilution in lachrymal fluid [99]. Alpha-lipoic acid has beneficial effects in dry eye disease and diabetic retinopathy [125], but its solubility and stability in aqueous medium are low. Drug-loaded Soluplus polymeric micelles could be sterilized through membrane filtration, freeze-dried, and reconstituted while maintaining their size and encapsulation efficiency. Corneal permeability (bovine) studies revealed that the micelles facilitate drug accumulation and pass across the tissue, providing alpha-lipoic acid levels well above those recorded for the commercially available eye drops [125]. Moreover, the in situ gelling performance of Soluplus micelle formulations may provide prolonged retention time on the eye surface. Soluplus micelles also encapsulate progesterone, which has therapeutic potential against retinal degeneration, more efficiently than Pluronic micelles [126]. The hydrophobic core of Soluplus facilitates the assembly at much lower CMC and the micelles are more stable. Studies carried out with cornea and sclera ex vivo from different animal sources (rabbit, pig, cow) revealed the strong influence of the interspecies anatomic differences on the drug permeability results, which may have an impact on the predictions of the performance on human eyes (**Figure 1.3**) [126].

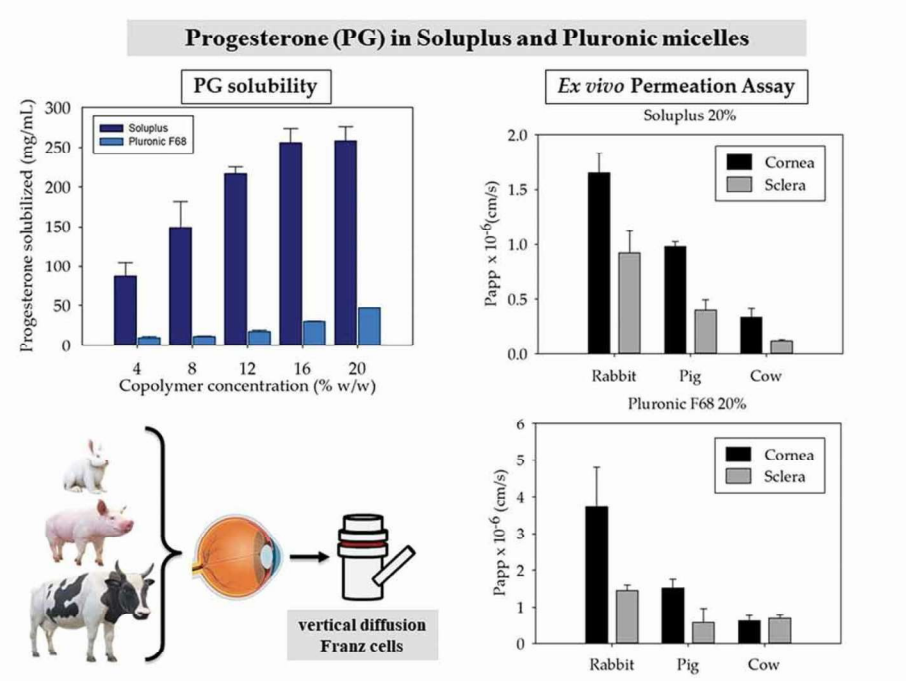

Figure 1.3. Progesterone (PG) apparent solubility in Soluplus and Pluronic F68 micelles, and permeability coefficients of cornea and sclera recorded for PG encapsulated in Soluplus 20% micelles or Pluronic F68 20% micelles. Reproduced from Alambiaga-Caravaca et al. [126] (Creative Commons Attribution License).

Table 1.5. Recent examples of self-assembled nanocarriers proposed for the topical ocular treatment of diabetic eye

Nanocarrier	Drug	Disease/Outcome	Reference
Polymeric micelles	Alpha-lipoic acid	Dry eye and diabetic retinopathy (bovine cornea). Soluplus micelles facilitated alpha-lipoic acid accumulation and pass across the tissue.	[99]
	Progesterone	Retina degeneration (rabbit, pig, cow). Soluplus and Pluronic micelles enhanced drug permeability through cornea with respect to sclera. Important interspecies differences.	[128]
	Dexamethasone, triamcinolone and triamcinolone acetonide	Macular edema (cell cultures). Micelles of copolymer of inulin derivatized with ethylenediamine and retinoic acid efficiently encapsulated the drugs, were internalized by different cell lines, and favored transcorneal permeation.	[130]
	Dexamethasone	Posterior uveitis (rabbit). Mixed micelles of polyoxyl 40 stearate and polysorbate 80 provided therapeutic levels in retina and choroid after one single instillation.	[132]
	Anti-angiogenic peptide aANGP	Diabetic retinopathy and macular edema (cell cultures). aANGP-micelles inhibited tube formation at 1000-fold lower concentration than free peptide.	[133]
	Glycyrrhizin and genistein	Wound healing in diabetic eye model (mice). Genipin-loaded glycyrrhizinate micelles down-regulated high mobility group box protein-1 (HMGB1) and its receptors for advanced glycation-end products (RAGEs) and toll-like receptors (TLRs), as well as inflammatory factor interleukin (IL)-6 and IL-1β, which favored diabetic corneal and nerve wound healing.	[134]
Liposomes	Citicoline	Diabetic retinopathy (mouse). Topical administration twice a day, for 15 days, prevented glial activation and neural apoptosis.	[138]
	Triamcinolone acetonide	Macular edema (patients). Drug-loaded QuSomes® instilled every 2 h decreased the central foveal thickness and increased the best-corrected visual acuity.	[141]

	Triamcinolone acetonide	Macular edema (rabbit). Chitosan-coated liposomes instilled five times a day provided efficient delivery to anterior and posterior segments due to enhanced cell uptake.	[142]
	Berberine hydrochloride	Macular edema (rabbit). PAMAM G3.0-coated liposomes promoted transcorneal permeability.	[143]
	Bevacizumab	Macular degeneration (rat and rabbit). Unilamellar vesicles with annexin A5 enhanced uptake and transcytosis through cornea, supplying therapeutic concentrations to the back of the eye.	[144]
	Transforming growth factor-ß1 (TGF-ß1)	Macular degeneration (rabbit). Unilamellar vesicles with annexin A5 provided therapeutic levels to the back of the eye.	[148]
	Thrombospondin (TSP)-1-derived peptide	Chronic ocular surface inflammation and tear film instability (ex vivo porcine cornea). Liposomes enhanced cornea permeation.	[149]
	Plasmid DNA	Gene therapy at retinal pigment epithelium (rat). Transferrin-modified small liposomes (<80 nm) selectively distributed to the retinal pigment epithelium. Larger liposomes could be targeted to choroidal endothelial cells.	[151]
Niosomes	Naltrexone·HCl	Diabetic keratopathy (bovine). Span 60 and cholesterol (30 mol%) niosomes sustainedly release the drug while still allowed for high cornea permeability.	[167]
	Flurbiprofen	Keratitis (rabbit). Span 60 and cholesterol (50 mol%) niosomes solely or dispersed in Carbopol gel enhanced drug ocular bioavailability.	[168]
	Latanoprost	Glaucoma (rabbit). One instillation of Span 60 and cholesterol (50:50 weight ratio) niosomes dispersed in Pluronic F127 gel decreased IOP for more than 48 h.	[169]

Poly(ethylene glycol)-b-poly(lactic acid) micelles increased 10-fold triamcinolone acetonide apparent solubility using a copolymer concentration as low as 0.5 mg/mL. Drug-loaded micelles formulated in chitosan dispersion prolonged drug release for more than 1 week. In vivo (rabbit) evaluation in an inflammatory disease model revealed that twice a day instillation of the micelle solution with or without chitosan was able to recover the normal corneal epithelium [127]. Inulin-based mucoadhesive micelles have been shown suitable for encapsulation of anti-inflammatory drugs adequate for macular edema treatment, such as dexamethasone, triamcinolone, and triamcinolone acetonide, enhancing drug permeability through corneal cells, which could be an alternative to intraocular injections [128]. Also intended for macular degeneration, tacrolimus delivery may benefit from encapsulation in micelles made of PEG-hydrogenated castor oil-40 and octyx-onyl-40, which have low CMC and provide slow drug release. Tacrolimus-loaded micelles showed faster cell internalization than the free drug [129]. Mixed micelles of polyoxyl 40 stearate and polysorbate 80 successfully delivered dexamethasone (0.1%) to the back of the eye, providing therapeutic drug levels in retina and choroid after eye drop instillation [130].

Prevention of abnormal growth of blood vessels in retina can be achieved by means of poly(ethylene glycol)-b-poly (propylene sulfide) micelles decorated with the anti- angiogenic peptide aANGP. The aANGP-micelles showed potent angiogenic inhibitory effect at 1000-fold lower concentration than the free peptide in cell cultures [131].

Treatment of diabetic keratopathy may notably benefit from the encapsulation of genipin in dipotassium glycyrrhizinate micelles (29.5 nm) [132]. Genipin and glycyrrhizin were shown to synergically block the high mobility group box 1 signaling and, in turn, attenuate the

inflammation cascade overexpressed in diabetic eyes. These micelles showed good corneal permeability and favored corneal re-epithelialization and nerve regeneration in diabetic mice.

1.3.2.b Liposomes

Liposomes are uni- or multi-bilayer vesicles composed of mainly amphiphilic lipids (phospholipids) and cholesterol. Each bilayer (also known as lamella) resembles the cell mem- brane, which endows liposomes with high biocompatibility. According to the number of bilayers and the overall size, liposome size may range from 10 to 100 nm (small unilamellar vesicles, SUV) to few microns (large unilamellar vesicles, LUV, and large multilamellar vesicles, LMV). General description of liposomes composition and preparation can be found else- where [133]. Liposomes have been widely used as carriers since several decades ago because of their dual capability to simultaneously host hydrophilic and hydrophobic drugs plus the general advantages of passive and active targeting [134,135]. Usefulness of liposomes for topical ophthalmic drug delivery, and especially management of ocular surface diseases, has been recently reviewed [13]. Importantly, the bioinspired structure and composition of liposomes facilitate the fusion with cell membrane at the cornea and conjunctiva surface and drug transfer to cell cytoplasm. Examples related to diabetic eye diseases are summarized in **Table 1.5**.

Regarding diabetic retinopathy, liposomes loaded with citicoline exhibited anti-inflammatory properties [136]. Citicoline or cytidine 5′-diphosphocoline is an endogenous compound involved in the biosynthesis of phospholipids, showing neuro- protective activity. Citicoline oral solution is registered as Food for Special Medical

purposed for patients suffering glaucoma, and an eye drop solution of a combination with vitamin B12 and sodium hyaluronate has been shown able to delay retinal changes in type 1 diabetic patients [137]. The liposomal formulation has the advantage of avoiding the use of the benzalkonium chloride included in the eye drop solution. In a db/db mouse model, citicoline-loaded liposomes (instilled twice a day for 15 days) prevented the downregulation of synaptophysin in the retina and the upregulation of NF-κB and TNF-α induced by diabetes, which may be useful for the treatment in the early stages of the disease [136].

Liposomes were also tested for the delivery of triamcinolone acetonide to the posterior segment to prevent macular edema [138]. Preclinical studies revealed that 12 h after instillation (rabbits) of drug-loaded liposomes, a peak of triamcinolone acetonide concentration is reached in vitreous and retina, without triggering adverse events. The optimized formulation (QuSomes®) was formed spontaneously by adding Kolliphor HS15 and PEG-12 glyceryl dimyristate to an aqueous medium containing the drug (final concentration 2 mg/mL; i.e. 0.2%). In a clinical study with patients suffering from refractory pseudo-phakic cystoid macular edema, the triamcinolone acetonide- loaded liposomes (applied every 2 h for 90 days) improved the central foveal thickness and best-corrected visual acuity (BCVA) (**Figure 1.4**) [139]. The formulation was well tolerated in both vitrectomized and nonvitrectomized eyes, being an alternative to the intraocular injections.

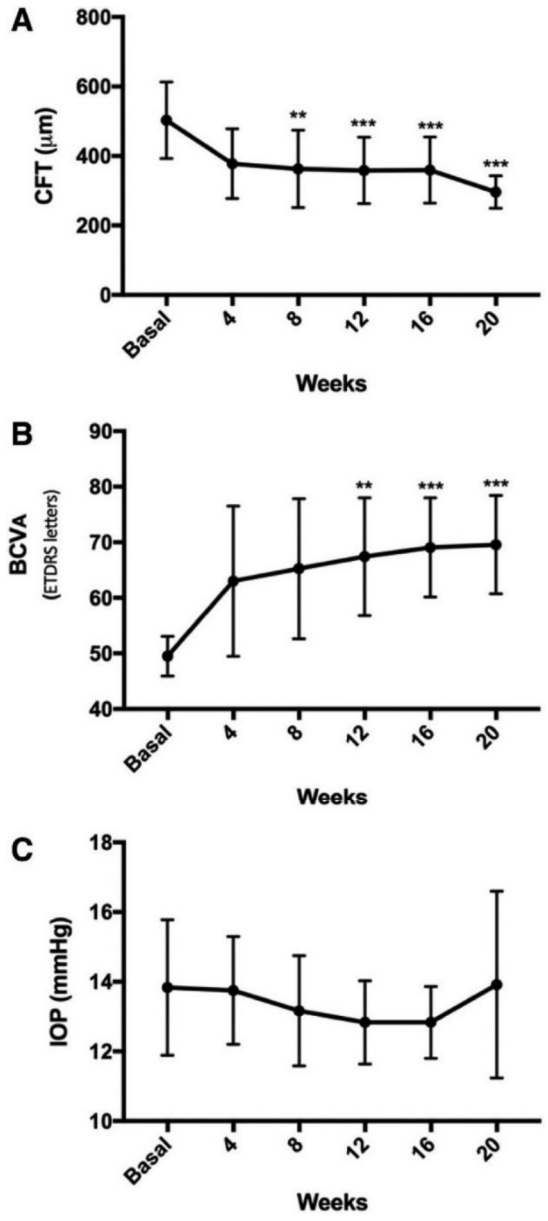

Figure 1.4. (a) Central foveal thickness (CFT), (b) best-corrected visual acuity (BCVA), and (c) intraocular pressure (IOP) recorded for patients with refractory pseudophakic cystoid macular edema during treatment with triamcinolone-loaded liposomes (one drop every 2 h for 90 days). Reproduced from Gonzalez-De la Rosa et al. [139] (Creative Commons License).

Coating of liposomes with chitosan may improve the encapsulation efficiency and accelerate the release of triamcinolone acetonide [139]. After ocular instillation (rabbit) of coumarin-6 encapsulated in the chitosan-coated liposomes, OCT images of anterior and posterior segment evidenced an increase in fluorescence from the first 10 min up to 6 h and then the fluorescence slowly vanished. Differently, non-coated liposomes disappeared faster. As a control, free coumarin-6 solution did not significantly increase the fluorescence in the eye structures. These findings were attributed to the remark- ably higher uptake of the chitosan-coated liposomes by corneal epithelial human colonic epithelial cells (HCECs) and retinal pigment epithelial (ARPE-19) [140]. Similarly, polyamidoamine dendrimer (PAMAM G3.0)-coated liposomes have shown enhanced permeability in HCECs and in vivo (rabbit) transcorneal permeability of berberine hydrochloride [141].

Interestingly, large molecules such as bevacizumab (avastin) may overcome the corneal barrier when encapsulated in liposomes that bind to the calcium-dependent phospholipid- binding protein annexin A5 [142]. Annexin A5 can trigger the formation of endocytic vesicles and is quite abundant in the corneal epithelium [143]. Liposomes (100 nm) formed by phospholipids, such as phosphatidylserine (PS) or phosphatidylethanolamine (PE), and annexin A5 (500:1 mol ratio) remarkably enhanced the transport through cornea compared to the same formulation without annexin A5. Instillation of one drop per day for 5 days (to rabbits) of bevacizumab- loaded liposomes resulted in levels 3-times higher in vitreous and 15-times higher in retina/choroid compared to a solution of free bevacizumab [142]. Although these results are promising, the obtained levels of bevacizumab are still quite below those provided by intravitreal injection [144]. Thus, intense research is devoted to improve the encapsulation yield of liposomes

[145]. Annexin A5-based unilaminar vesicles are also useful for the delivery of transforming growth factor-β1 (TGF-β1) for the treatment of macular degeneration. One hour after topical instillation (rabbit), therapeutical levels of TGF-β1 were quantified in the vitreous without signs of ocular irritation, which may help avoiding intraocular injections [146].

Capability of liposomes to enhance corneal penetration has also been demonstrated for other therapeutic peptides. For example, vitamin E-based liposomes efficiently encapsulated a thrombospondin (TSP)-1-derived peptide for the handling of chronic ocular surface inflammation and tear film instability. Ex vivo studies revealed that the permeation through corneal tissue was remarkably improved for the encapsulated peptide [147].

Improved gene delivery may be achieved with lipoplexes prepared with PEG-ceramide that enhances the transfection efficiency to the retinal pigment epithelium. PEG prevents lipoplexes aggregation in the vitreous, but hinders the trans- fection efficiency. Differently, PEG-ceramide detaches from the lipoplexes once in contact with the cell membranes, and the de-pegylated liposomes may escape from the endosome [148]. Lipoplexes able to reach the posterior segment were produced using a microfluidizer and combining hydrogenated soy L-a-phosphatidylcholine, 1,2-distearoyl-sn-glycero-3-phosphoethanolamine -N-[amino(polyethylene glycol)-2000] and cholesterol. After one drop instillation (rat), small liposomes (<80 nm) decorated with transferrin permeated to the retinal pigment epithelium and were selectively retained in this tissue. Differently, larger liposomes lacking transferrin moved to the choroidal epithelium [149].

1.3.2.c Niosomes

Niosomes are gaining increasing interest due to the feasibility of combining the advantages of micelles (spontaneous self-assembly in water) and liposomes (encapsulation of both hydrophilic and lipophilic drugs) in unique polymeric multilayered vesicles while minimizing physical and chemical instability concerns.

Niosomes are defined as a uni- or multi-bilayer vesicles composed of mainly nonionic surfactants. This name was given by researchers at the L'Oréal laboratories in 1979 [150], but niosomes have attracted interest as drug carriers only recently [120]. Scientific research has been steadily increasing over the years from 4 articles about 'niosomes AND drug' in 2002 to 49 articles in 2020, and 1 article about 'niosomes AND gene' in 2005 to 14 articles in 2020 according to Web of Science database. The use of nonionic surfactants as primary building blocks grants niosomes high stability and long shelf life. Like liposomes, niosomes size may range from 10 to 100 nm (SUV) to few microns (LUV and LMV) [120]. Tuning the affinity of the components for the drug as well as the permeability of the layer may allow for precise regulation of drug release [151,152]. These attributes make niosomes very attractive as drug nanocarriers.

To improve the performance of niosomes for specific applications multiple other molecules can be added. Examples are cholesterol and squalene, which increase the stiffness of the vesicle to enhance the stability [153], dicetyl phosphate, or stearylamine that add charged groups to the vesicle to improve its drug delivery capabilities, or PEG that provides a stealth layer to increase blood residence time. Also, niosomes responsive to changes in pH or even to glucose have been designed [154,155].

Most techniques to prepare niosomes are derived from liposome formation and adapted to the needs of nonionic surfactants (**Figure 1.5**). The drugs are dissolved either in an organic solvent or in the aqueous phase depending on their affinity for water. The preparation method may have a major impact on the size, structure and, therefore, properties of the niosomes [120,152,156]. The methods of thin-film hydration, reverse-phase evaporation, and emulsification/sonication are quite similar as they use mechanical disruption to form the niosomes in a hydration step. Organic phase injection and microfluidics are positioning as suitable techniques for precise control of niosomes size and polydispersity and preliminary scale-up [157]. On the other hand, proniosome appeared as a tool to extend shelf-life avoiding any premature leakage of the drug. Proniosomes can be presented as either anhydrous free-flowing powders or as gel-like mixtures of the niosome components in a liquid medium without water or with a minor content in water. Thus, proniosomes are intended for rapid reconstitution with water before administration or once in contact with the physiological fluids [158].

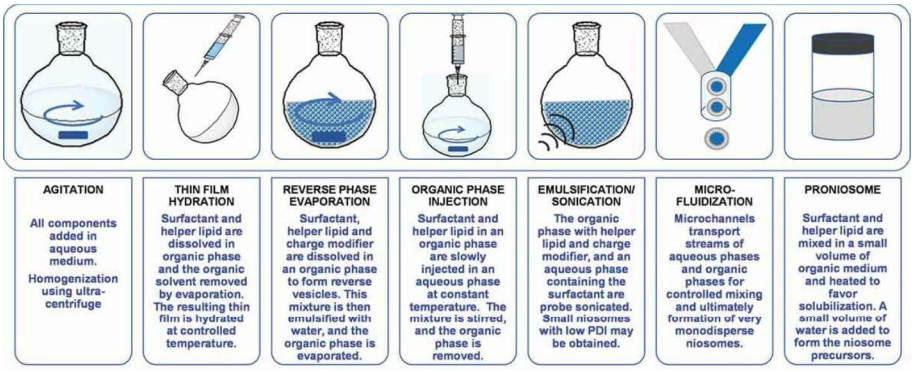

Figure 1.5. Main techniques used to prepare drug-loaded niosomes. Made by the author of this Thesis.

Niosomes have been shown able to improve oral bioavailability of a variety of treatments for diabetes, including insulin [159], metformin hydrochloride solely or combined with glipizide [160,161], and plant extracts [162]. Niosomes also attract great attention as ocular drug carriers due to their excellent tolerability, prolonged precorneal residence, and enhanced ocular bioavailability [16,151]. Nevertheless, examples of their performance as delivery systems of diabetic eye drugs are still incipient (**Table 1.5**). Multilayered niosomes (7–14 μm) have been designed to encapsulate naltrexone hydrochloride, which is a potent opioid antagonist that markedly accelerates cornea healing and repairs the signs of diabetic keratopathy. The niosomes prepared with Span 60 and cholesterol using the thin-film hydration method showed high encapsulation efficiency [163]. These niosomes had a gel–liquid transition of few degrees above physiological temperature, which is considered as an advantage to avoid dragging by blinking and to control drug release [164]. Ex vivo tests in bovine cornea evidenced that niosomes sustainedly released the drug for several hours and allowed for high permeability [165].

Span 60-based niosomes (2.8 μm) dispersed in 1% Carbopol 934 gel were shown suitable for delivery of the anti- inflammatory drug flurbiprofen in the aqueous humor [166]. Once applied onto the cornea (rabbits), flurbiprofen-loaded niosomes either solely or in the Carbopol gel provided drug levels in aqueous humor one order of magnitude above those achieved using a free drug solution. Relative drug bioavailability from the niosome and the niosome-gel formulations was 3.6- and 6.2-fold that of the flurbiprofen solution because the gel notably extended the permanence time on the eye sur- face. The niosome formulations also demonstrated to be therapeutically efficient against keratitis (carrageenan-induced inflammation). The obtained

results suggest that once a day instillation may be sufficient to manage ocular inflammatory diseases.

Feasibility of using niosomes for glaucoma therapy has been evidenced recently. Niosomes prepared by the reverse-phase evaporation technique covering wide ratios of cholesterol and Span 40 or Span 60 could host latanoprost with an encapsulation efficiency of ~98%. Latanoprost-loaded niosomes (8–10 μm size) were dispersed in Pluronic F127 gel (drug concentration 0.005%) and the effects on IOP were monitored after instillation (50 μL) in the cul-de-sac of rabbit eyes. Latanoprost-loaded niosomes reduced IOP for 3 days, which was remarkably longer than the outcome achieved with the standard latanoprost eye drops (Xalatan®; 0.005%) (**Figure 1.6**) [167]. Proniosomal gel formulations are promising also for other anti-glaucoma agents, including dorzolamide hydrochloride and brimonidine tartrate [168,169].

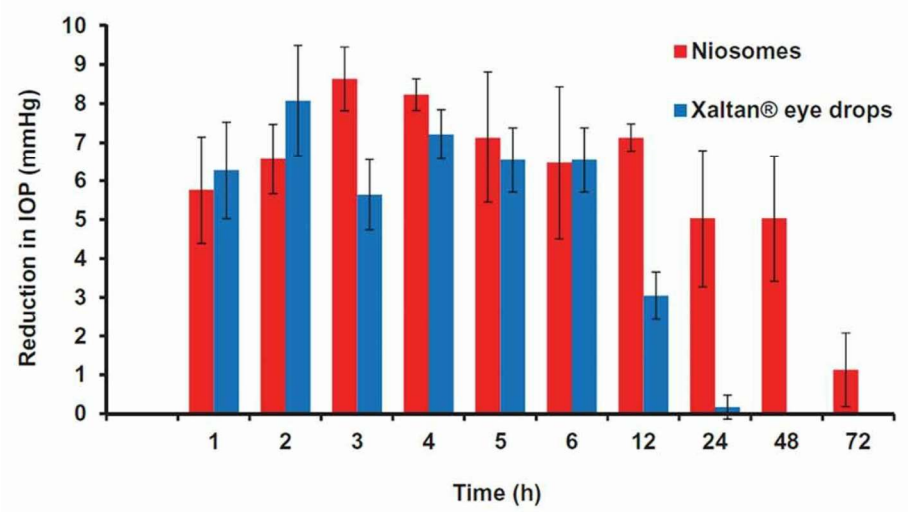

Figure 1.6. Reduction in the intraocular pressure (IOP) observed after topical administration to normotensive rabbits of latanoprost-loaded niosome gel or conventional latanoprost eye drops. Error bars represent standard deviation of six replicates. Reproduced from Fathalla et al. [167] with permission from Taylor & Francis.

Interestingly, in the last few years, most publications on niosomes refer to the feasibility of forming nioplexes for a variety of therapeutic applications, including gene therapy to the back of the eye [170]. Nevertheless, most reports rely on subretinal or intravitreal injections [171,172]. To the best of our knowledge, the suitability of nioplexes for topical ocular administration is still to be explored.

1.4 CONCLUSION

With the upward trend in obesity worldwide, the number of cases of diabetic eye diseases is also bound to increase, making research on the delivery of ocular drugs an active field. This is reflected in the large number of ongoing clinical trials for diabetic eye diseases. The trials are primarily focused on macular edema and retinopathy, with a

plethora of active substances to be administered through multiple routes. Although the eye presents challenging anatomical barriers, different self-assembled carriers have been proven to be capable of overcoming them and offer a promising future for drug delivery to the ocular therapeutic sites. Micelles, liposomes, and niosomes offer diverse advantages covering from the increase in drug solubility to the use of additional path- ways of penetration into tissues. Preclinical and clinical studies have confirmed their ability to protect the cargo from degradation, target specific areas, enhance permeation through different ocular barriers, and sustain the release, which in turn improves the therapeutic effects both in intensity and in duration. Niosomes made of nonionic surfactants are particularly interesting, and scientific research has grown steadily in the last few years, as an alternative to liposomes in terms of higher stability and lower production costs. Advances in right choosing of the composition and size of the self-assembled carriers may result in more successful management of both anterior and posterior segment eye diseases.

1.5 EXPERT OPINION

The diabetic eye is one of the clearest examples of the need to develop adequate drug delivery systems that can improve or reverse the effects of a very relevant chronic disease. Given the pandemic character of diabetes, developing formulations that alleviate or reverse the deleterious effects at ocular level and the subsequent consequences on the quality of life of patients is an unsatisfied clinical demand. Most drugs currently approved or under evaluation in clinical trials require nonviable frequent instillation or intraocular administration using invasive procedures. Since diabetic-eye diseases need chronic

treatments, an adequate balance between patient acceptability and drug ocular bioavailability should be reached.

Most clinical trials related to diabetic eye refer to macular edema and retinopathy, although affectation of anterior segment is also considered. Strong research efforts are being made at two levels: (I) to find new drug candidates and to test the therapeutic efficiency of drugs already approved for systemic administration when they are directly administered to the ocular tissues and (II) to find suitable delivery vehicles that can overcome eye barriers and help the drug to get access to the damaged tissue and to remain in it for prolonged time. At the pharmacological level, a myriad of drugs and biologics are being tested, mostly searching for anti-inflammatory and anti-angiogenic activities. Although long sought, the recent approval of gene therapy treatments for inherited eye diseases is undoubtedly driving the development of appropriate approaches for acquired diseases. The feasibility of transforming the patient's eye cells into factories of the necessary drug is closer than ever. Gene therapy relies on a single administration or administrations widely separated in time. One-time treatment may be compatible with invasive maneuvers as the benefit may counteract the risks. Nevertheless, drugs, biologics, and genes may strongly benefit from more patient-friendly approaches.

From a pharmaceutical technology level, most therapeutic agents for diabetic eye have poor biopharmaceutic properties because they are poorly soluble or the size is quite large. Thus, self-assembled carriers (polymeric micelles, liposomes, and niosomes) that can facilitate the penetration of small and large molecules deep in the ocular tissues may become valuable tools. Topical management of eye surface and anterior segment diseases has already been shown to improve with self-assembled carriers that show prolonged permanence on ocular surface,

facilitate drug permeation through cornea, and diffusion into the aqueous humor. Moreover, the feasibility of the carriers to encapsulate large molecules (including antibodies and genes) pass through sclera while minimizing systemic clearance, and modulate diffusion through vitreous may make topical administration a realistic alternative to intraocular injection. Remarkably, the gain in knowledge about transporters present in each ocular tissue and about the biomarkers that can be found altered due to diabetes may provide interesting clues for the design of drug carriers with greater penetration capacity and targeting ability. This field is still in its infancy, but the intense quest to provide the patients with efficient yet friendly formulations for long-term use will pave the way to clinic of novel topical formulations.

1.6 REFERENCES

Papers of special note have been highlighted as either of interest (•) or of considerable interest (••) to readers.

1. Lin X, Xu Y, Pan X, et al. Global, regional, and national burden and trend of diabetes in 195 countries and territories: an analysis from 1990 to 2025. *Sci Rep*. **2020**;10:14790.

2. Greiner W, Patel K, Crossman-Barnes CJ, et al. High-expenditure dis- ease in the EU-28: does drug spend correspond to clinical and eco- nomic burden in oncology, autoimmune disease and diabetes? *Pharmacoecon Open*. **2021**. DOI:10.1007/s41669-020-00253-4

3. National Institute of Diabetes and Digestive and Kidney Diseases. Diabetic Eye Disease. [cited Feb 2021]. https://www.niddk.nih.gov/ health-information/diabetes/overview/preventing-problems/diabetic-eye-disease

4. Zhu L, Titone R, Robertson DM. The impact of hyperglycemia on the corneal epithelium: molecular mechanisms and insight. *Ocul Surf.* **2019**;17:644–654.

5. Sayin N. Ocular complications of diabetes mellitus. *World J Diabetes*. **2015**;6:92.

6. Han SB, Yang HK, Hyon JY. Influence of diabetes mellitus on anterior segment of the eye. *Clin Interv Aging*. **2019**;14:53–63.

7. Giri B, Dey S, Das T, et al. Chronic hyperglycemia mediated physiological alteration and metabolic distortion leads to

organ dysfunction, infection, cancer progression and other pathophysiological consequences: an update on glucose toxicity. *Biomed Pharmacother*. **2018**;107:306–328.

8. Madni A, Rahem MA, Tahir N, et al. Non-invasive strategies for targeting the posterior segment of eye. *Int J Pharm*. **2017**;530:326–345.

9. Jumelle C, Gholizadeh S, Annabi N, et al. Advances and limitations of drug delivery systems formulated as eye drops. *J Control Release*. **2020**;321:1–22.

   • Recent review on the most recent advances in delivery systems for topical eye administration and the challenges to reach the market.

10. Liu S, Jones L, Gu FX. Nanomaterials for ocular drug delivery. *Macromol Biosci*. **2012**;12:608–620.

11. Mazureki Campos P, Petrilli R, Lopez RFV. The prominence of the dosage form design to treat ocular diseases. *Int J Pharm*. **2020**;586:119577.

12. Polat H, Kutluay G, Polat M. Analysis of dilution induced disintegration of micellar drug carriers in the presence of inter and intra micellar species. *Colloid Surf A-Physicochem Eng Asp*. **2020**;601:124989.

13. López-Cano JJ, González-Cela-Casamayor MA, Andrés-Guerrero V, et al. Liposomes as vehicles for topical ophthalmic drug delivery and ocular surface protection. *Expert Opin Drug Deliv*. **2021**;18 (7):819–847.

• Recent review on the design of liposomes for ocular drug delivery.

14. FDA. Liposome Drug Products. Guidance for Industry. April 2018. [cited Feb 2021]. https://www.fda.gov/media/70837/download

15. Delma KL, Lechanteur A, Evrard B, et al. Sterilization methods of liposomes: drawbacks of conventional methods and perspectives. *Int J Pharm*. **2021**;597:120271.

16. Durak S, Rad ME, Yetisgin AA, et al. Niosomal drug delivery systems for ocular disease—recent advances and future prospects. *Nanomaterials*. **2020**;10:1191.

• Recent review on the design of niosomes for ocular drug delivery.

17. MacEwan SR, Chilkoti A. Applications of elastin-like polypeptides in drug delivery. *J Control Release*. **2014**;190:314–330.

18. Castillo-Díaz LA, Ruiz-Pacheco JA, Elsawy MA, et al. Self-assembling peptides as an emerging platform for the treatment of metabolic syndrome. *Int J Nanomed*. **2020**;15:10349–10370.

19. Sreekumar PG, Kannan R. Mechanisms of protection of retinal pigment epithelial cells from oxidant injury by humanin and other mitochondrial-derived peptides: implications for age-related macular degeneration. *Redox Biol*. **2020**;37:101663.

20. Kesharwani P, Gorain B, Low SY, et al. Nanotechnology based approaches for anti-diabetic drugs delivery. *Diabetes Res Clin Pract*. **2018**;136:52–77.

21. Adeoti CO, Isawumi MA, Ashaye AO, et al. The anterior segment of the eye in diabetes. *Clin Ophthalmol*. **2012**;6:667–671.

22. Lutty GA. Effects of diabetes on the eye. *Investig Ophthalmol Vis Sci*. **2013**;54:81–87.

23. Kiziltoprak H, Tekin K, Inanc M, et al. Cataract in diabetes mellitus. *World J Diabetes*. **2019**;10:140–153.

24. Pollreisz A, Schmidt-Erfurth U. Diabetic cataract—pathogenesis, epidemiology and treatment. *J Ophthalmol*. **2010**;2010:1–8.

25. Abdelkader H, Alany RG, Pierscionek B. Age-related cataract and drug therapy: opportunities and challenges for topical antioxidant delivery to the lens. *J Pharm Pharmacol*. **2015**;67:537–550.

26. Zhang X, Zhao L, Deng S, et al. Dry eye syndrome in patients with diabetes mellitus: prevalence, etiology, and clinical characteristics. *J Ophthalmol*. **2016**;2016:8201053.

27. Módulo CM, Jorge AG, Dias AC, et al. Influence of insulin treatment on the lacrimal gland and ocular surface of diabetic rats. *Endocrine*. **2009**;36:161–168.

28. Hyndiuk RA, Kazarian EL, Schultz RO, et al. Neurotrophic corneal ulcers in diabetes mellitus. *Arch Ophthalmol*. **1977**;95:2193–2196.

29. Ioannidis AS, Zagora SL, Wechsler AW. A non-healing corneal ulcer as the presenting feature of type 1 diabetes mellitus: a case report. *J Med Case Rep*. **2011**;5:539.

30. Xu KP, Li Y, Ljubimov AV, et al. High glucose suppresses epidermal growth factor receptor/ phosphatidylinositol 3-kinase/akt signaling pathway and attenuates corneal epithelial wound healing. *Diabetes*. **2009**;58:1077–1085.

31. Abdelkader H, Patel DV, McGhee CN, et al. New therapeutic approaches in the treatment of diabetic keratopathy: a review. *Clin Exp Ophthalmol*. **2011**;39:259–270.

32. Weinreb RN, Aung T, Medeiros FA. The pathophysiology and treatment of glaucoma. *JAMA*. **2014**;311:1901.

33. Zhao D, Cho J, Kim MH, et al. Diabetes, fasting glucose, and the risk of glaucoma: a meta-analysis. *Ophthalmology*. **2015**;122:72–78.

34. Rübsam A, Parikh S, Fort PE. Role of inflammation in diabetic retinopathy. *Int J Mol Sci*. **2018**;19:1–31.

35. Mathur R, Douglas I, Bhaskaran K, et al. Diabetic eye disease: a UK Incidence and Prevalence Study; 2017. [cited Feb 2021]. https:// www.rnib.org.uk/sites/default/files/Diabetic%20eye%20disease.% 20A%20UK%20Incidence%20and%20Prevalence%20Study %20-% 20Full%20report.pdf

36. Fong DS, Aiello L, Gardner TW, et al. Retinopathy in diabetes. *Diabetes Care*. **2004**;27:S84–87.

37. Bandello F, Pognuz R, Polito A, et al. Diabetic macular edema: classification, medical and laser therapy. *Semin Ophthalmol.* **2003**;18:251–258.

38. 38. Browning DJ, Altaweel MM, Bressler NM, et al. Diabetic retinopathy clinical research network. Diabetic macular edema: what is focal and what is diffuse? *Am J Ophthalmol.* **2008**;146:649–655.

39. Agrahari VV, Mandal A, Agrahari VV, et al. A comprehensive insight on ocular pharmacokinetics. *Drug Deliv Transl Res*. **2016**;6:735–754.

40. Gote V, Ansong M, Pal D. Prodrugs and nanomicelles to overcome ocular barriers for drug penetration. *Expert Opin Drug Metab Toxicol*. **2020**;16:885–906.

• Recent review on the performance of micelles for ocular drug delivery.

41. Thareja A, Hughes H, Alvarez-Lorenzo C, et al. Penetration enhancers for topical drug delivery to the ocular posterior segment – a systematic review. *Pharmaceutics*. **2021**;13:276.

42. Subrizi A, del Amo EM, Korzhikov-Vlakh V, et al. Design principles of ocular drug delivery systems: importance of drug payload, release rate, and material properties. *Drug Discov Today*.**2019**;24:1446–1457.

43. Mari K, Kirsi H, Seppo K, et al. Characterization of paracellular and aqueous penetration routes in cornea, conjunctiva, and sclera. *Invest Ophthalmol Vis Sci.* **1997**;38:627–634.

44. Gaudana R, Ananthula HK, Parenky A, et al. Ocular drug delivery. *AAPS J*. **2010**;12:348–360.

45. Lee SJ, He W, Robinson SB, et al. Evaluation of clearance mechanisms with transscleral drug delivery. *Invest Ophthalmol Vis Sci*. **2010**;51:5205–5212.

46. Hosoya K, Lee VHL, Kim KJ. Roles of the conjunctiva in ocular drug delivery: a review of conjunctival transport mechanisms and their regulation. *Eur J Pharm Biopharm.* **2005**;60:227–240.

47. Delamare NA. Ciliary body and ciliary epithelium. *Adv Organ Biol.* **2005**;10:127–148.

48. Dahlin A, Geier E, Stocker SL, et al. Gene expression profiling of transporters in the solute carrier and ATP-binding cassette super-families in human eye substructures. *Mol Pharm*. **2013**;10:650–663.

49. Horibe Y, Hosoya K, Kim KJ, et al. Polar solute transport across the pigmented rabbit conjunctiva: size dependent and the influence of 8-bromo cyclic adenosine monophosphate. *Pharm Res.* **1997**;14:1246–1251.

50. Sun L, Basu SK, Kim KJ, et al. Arginine vasopressin transport and metabolism in the pigmented rabbit conjunctiva. *Eur J Pharm Sci*. **1998**;6:47–52.

51. Liu D, Lian Y, Fang Q, et al. Hyaluronic-acid-modified lipid-polymer hybrid nanoparticles as an efficient ocular delivery platform for moxifloxacin hydrochloride. *Int J Biol Macromol*. **2018**;116:1026–1036.

52. Qaddoumi MG, Gukasyan HJ, Davda J, et al. Clathrin and caveolin-1 expression in primary pigmented rabbit conjunctival epithelial cells: role in PLGA nanoparticle endocytosis. *Mol Vis.* **2003**;9:559–568.

53. Müller-Lierheim WGK. Why chain length of hyaluronan in eye drops matters. *Diagnostics.* **2020**;10:511.

54. Ambati J, Adamis AP. Transscleral drug delivery to the retina and choroid. *Prog Retin Eye Res*. **2002**;21:145–151.

55. Cheruvu NPS, Kompella UB. Bovine and porcine transscleral solute transport: influence of lipophilicity and the choroid-Bruch's layer. *Invest Ophthalmol Vis Sci.* **2006**;47:4513–4522.

56. Ramsay E, Hagström M, Vellonen KS, et al. Role of retinal pigment epithelium permeability in drug transfer between posterior eye segment and systemic blood circulation. *Eur J Pharm Biopharm*. **2019**;143:18–23.

57. Çekiç O, Batman C, Yasar U, et al. Human aqueous and vitreous humour levels of ciprofloxacin following oral and topical administration. *Eye*. **1999**;13:555–558.

58. Mora P, Ceglarek U, Manzotti F, et al. Cyclosporin A in the ocular fluids of uveitis patients following long-term systemic administration *Graefe's Arch. Clin Exp Ophthalmol.* **2008**;246:1047–1052.

59. BenEzra D, Maftzir G, De Courten C, et al. Ocular penetration of cyclosporine A. III: the human eye. *Br J Ophthalmol*. **1990**;74:350–352.

60. Toris CB, Gabelt BT, Kaufman PL. Update on the mechanism of action of topical prostaglandins for intraocular pressure reduction. *Surv Ophthalmol*. **2008**;53:107–120.

61. Moshirfar M, Parker L, Birdsong OC, et al. Use of rho kinase inhibi- tors in ophthalmology: a review of the literature. *Med Hypothesis Discov Innov Ophthalmol J*. **2018**;7:101–111.

62. Muenster S, Lieb WS, Fabry G, et al. The ability of nitric oxide to lower intraocular pressure is dependent on guanylyl cyclase. *Invest Ophthalmol Vis Sci.* **2017**;58:4826–4835.

63. Faiq MA, Wollstein G, Schuman JS, et al. Cholinergic nervous system and glaucoma: from basic science to clinical applications. *Prog Retin Eye Res*. **2019**;72:100767.

64. Schmidl D, Schmetterer L, Garhöfer G, et al. Pharmacotherapy of glaucoma. *J Ocul Pharmacol Ther*. **2015**;31:63–77.

65. Bucolo C, Drago F. Carbon monoxide and the eye: implications for glaucoma therapy. *Pharmacol Ther*. **2011**;130:191–201.

66. Akiyode O, Tran C. Overview of ocular anti-vascular endothelial growth factor therapy in the management of diabetic eye complications. *Diabetes Spectr.* **2016**;29:44–49.

67. Gale MJ, Scruggs BA, Flaxel CJ. Diabetic eye disease: a review of screening and management recommendations. *Clin Exp Ophthalmol*. **2021**;49:128–145.

68. Smith SJ, Smith BD, Mohney BG. Ocular side effects following intravitreal injection therapy for retinoblastoma: a systematic review. *Br J Ophthalmol*. **2014**;98:292–297.

69. Augsburger M, Sarra GM, Imesch P. Treat and extend versus pro re nata regimens of ranibizumab and aflibercept in neovascular age- related macular degeneration: a comparative study *Graefe's. Arch Clin Exp Ophthalmol*. **2019**;257:1889–1895.

70. Radhakrishnan K, Sonali N, Moreno M, et al. Protein delivery to the back of the eye: barriers, carriers and stability of anti-VEGF proteins. *Drug Discov Today*. **2017**;22:416–423.

71. Conti B, Bucolo C, Giannavola C, et al. Biodegradable microspheres for the intravitreal administration of acyclovir: in vitro/in vivo evaluation. *Eur J Pharm Sci.* **1997**;5:287–293.

72. Platania CB, Di Paola L, Leggio GM, et al. Molecular features of interaction between VEGFA and anti-angiogenic drugs used in retinal diseases: a computational approach. *Front Pharmacol.* **2015**;6:248.

73. Patil KK, Gacche RN. The fate of aldose reductase inhibition and sorbitol dehydrogenase activation. *Austin J Endocrinol Diabetes.* **2019**;6:1064.

74. Obrosova IG, Kador PF. Aldose reductase/polyol inhibitors for diabetic retinopathy. *Curr Pharm Biotechnol.* **2011**;12:373–385.

75. Evans JR, Michelessi M, Virgili G. Laser photocoagulation for proliferative diabetic retinopathy. Cochrane Database Syst Rev.;**2014**:CD011234.

76. Crosson JN, Mason L, Mason JO. The role of focal laser in the anti-vascular endothelial growth factor era. *Ophthalmol Eye Dis.* **2017**;9.

77. Papastefanou VP, Dooley I, Zambarakji H. Management of macular edema in vitrectomized patients with diabetes. *Expert Rev Ophthalmol.* **2018**;13:87–103.

78. Thakur RRS, Tekko IA, Al-Shammari F, et al. Rapidly dissolving polymeric microneedles for minimally invasive intraocular drug delivery. *Drug Deliv Transl Res*. **2016**;6:800–815.

79. Roy G, Galigama RD, Thorat VS, et al. Microneedle ocular patch: fabrication, characterization, and ex-vivo evaluation using pilocarpine as model drug. *Drug Dev Ind Pharm.* **2020**;46:1114–1122.

80. Amer M, Chen RK. Self-adhesive microneedles with interlocking features for sustained ocular drug delivery. *Macromol Biosci.* **2020**;20:2000089.

81. Chen YM, Hu FR, Huang JY, et al. The effect of topical autologous serum on graft re-epithelialization after penetrating keratoplasty. *Am J Ophthalmol*. **2010**;150:352–359.e2.

82. A study to assess the safety and effectiveness of sjp-0035 for the treatment of patients with dry eye disease. https://clinicaltrials.gov/ ct2/show/NCT03527212

83. Klocek MS, Sassani JW, McLaughlin PJ, et al. Naltrexone and insulin are independently effective but not additive in accelerating corneal epithelial healing in type I diabetic rats. *Exp Eye Res*. **2009**;89:686–692.

84. Ionascu I, Argaseala A, Uzun S, et al. A new eye drop formulation used in the management of corneal ulcers in dogs and cats. *Agrolife Sci J.* **2020**;9:164–171.

85. Topical Autologous Insulin Application for the Treatment of Corneal Epithelium Defect After Ocular Surgeries. https://clinical trials.gov/ct2/show/study/NCT01031888?term=topical+insulin& draw=2&rank=2

86. Effect of Topical Naltrexone Ophthalmic Solution on the Signs and Symptoms of Dry Eye in Diabetic Subjects. https://ClinicalTrials. gov/show/NCT03660475

87. Keeler AM, Flotte TR. Recombinant adeno-associated virus gene therapy in light of Luxturna (and Zolgensma and Glybera): where are we, and how did we get here? *Annu. Rev Virol.* **2019**;6:601–621.

88. Auricchio A, Smith AJ, Ali RR. The future looks brighter after 25 years of retinal gene therapy. *Hum Gene Ther.* **2017**;28:982–987.

89. Bastola P, Song LJ, Gilger BC, et al. Adeno-associated virus mediated gene therapy for corneal diseases. *Pharmaceutics*. **2020**;12:767.

90. ADVM-022 Intravitreal Gene Therapy for DME (INFINITY). https:// ClinicalTrials.gov/show/NCT04418427

91. Liu Y, Fortmann SD, Shen J, et al. AAV8-antiVEGFfab ocular gene transfer for neovascular age-related macular degeneration. *Mol Ther*. **2018**;26:542–549.

92. RGX-314 Gene Therapy Administered in the Suprachoroidal Space for Participants With Diabetic Retinopathy (DR) Without Center Involved-Diabetic Macular Edema (CI-DME) (ALTITUDE). https://clinicaltrials.gov/ct2/show/record/NCT04567550

93. Jiang J, Zhang X, Tang Y, et al. Progress on ocular siRNA gene-silencing therapy and drug delivery systems. *Fundam Clin Pharmacol*. **2021**;35:4–24.

94. A randomized, multi-center, phase ii study of the safety, tolerability and bioactivity of repeated intravitreal injections of iCo-007 as monotherapy or in combination with ranibizumab or laser photocoagulation in the treatment of diabetic macular edema (the iDEAL Study) (iDEAL). https://ClinicalTrials.gov/show/ NCT01565148

95. Rittenhouse KD, Johnson TR, Vicini P, et al. RTP801 gene expression is differentially upregulated in retinopathy and is silenced by PF-04523655, a 19-Mer siRNA directed against RTP801. *Invest Ophthalmol Vis Sci*. **2014**;55:1232–1240.

96. Kallinikou D, Soldatou A, Tsentidis C, et al. Diabetic neuropathy in children and adolescents with type 1 diabetes mellitus: diagnosis, pathogenesis, and associated genetic markers. *Diabetes Metab Res Rev*. **2019**;35:e3178.

97. Papachristoforou E, Lambadiari V, Maratou E, et al. Association of glycemic indices (hyperglycemia, glucose variability, and hypoglycemia) with oxidative stress and diabetic complications. *J Diabetes Res*. **2020**;2020:7489795.

98. Torrecilla J, del Pozo-Rodríguez A, Vicente-Pascual M, et al. Targeting corneal inflammation by gene therapy: emerging strategies for keratitis. *Exp Eye Res*. **2018**;176:130–140.

99. Mandal A, Bisht R, Rupenthal ID, et al. Polymeric micelles for ocular drug delivery: from structural frameworks to recent preclinical studies. *J Control Release*. **2017**;248:96–116.

100. Alvarez-Rivera F, Fernandez-Villanueva D, Concheiro A, et al. α- Lipoic acid in Soluplus® polymeric nanomicelles for ocular treatment of diabetes-associated corneal diseases. *J Pharm Sci*. **2016**;105:2855–2863.

101. Loftsson T, Stefansson E. Cyclodextrins and topical drug delivery to the anterior and posterior segments of the eye. *Int J Pharm*. **2017**;531:413–423.

102. Alvarez-Rivera F, Concheiro A, Alvarez-Lorenzo C. Epalrestat-loaded silicone hydrogels as contact lenses to address diabetic-eye complications. *Eur J Pharm Biopharm*. **2018**;122:126–136.

103. Alvarez-Rivera F, Serro AP, Silva D, et al. Hydrogels for diabetic eyes: naltrexone loading, release profiles and cornea penetration. *Mater Sci Eng C*. **2019**;105:110092.

104. Alvarez-Rivera F, Rey-Rico A, Venkatesan JK, et al. Controlled release of rAAV vectors from APMA-

functionalized contact lenses for corneal gene therapy. *Pharmaceutics*. **2020**;12:335.

105. Huang X, Chau Y. Investigating impacts of surface charge on intraocular distribution of intravitreal lipid nanoparticles. *Exp Eye Res*. **2019**;186:107711.

106. Ryoo NK, Lee J, Lee H, et al. Therapeutic effects of a novel siRNA-based anti-VEGF (siVEGF) nanoball for the treatment of choroidal neovascularization. *Nanoscale*. **2017**;9:15461–15469.

107. Lai S, Wei Y, Wu Q, et al. Liposomes for effective drug delivery to the ocular posterior chamber. *J Nanobiotechnol*. **2019**;17:64.

108. Akter N, Radiman S, Mohamed F, et al. Self-assembled potential bio nanocarriers for drug delivery. *Mini Rev Med Chem*. **2013**;13:1327–1339.

109. Lu Y, Yue Z, Xie J, et al. Micelles with ultralow critical micelle concentration as carriers for drug delivery. *Nat Biomed Eng*. **2018**;2:318–325.

110. Kapoor Y, Howell BA, Chauhan A. Liposome assay for evaluating ocular toxicity of surfactants. *Invest Ophthalmol Vis Sci*. **2009**;50:2727–2735.

111. Garaszczuk IK, Montes Mico R, Iskander DR, et al. The tear turnover and tear clearance tests – a review. *Expert Rev Med Dev*. **2018**;15:219–229. .

112. Owen SC, Chan DPY, Shoichet MS. Polymeric micelle stability. *Nano Today*. **2012**;7:53–65.

113. Söderman O, Herrington KL, Kaler EW, et al. Transition from micelles to vesicles in aqueous mixtures of anionic and cationic surfactants. *Langmuir*. **1997**;13:5531–5538.

114. Dutta R, Ghosh S, Banerjee P, et al. Micelle-vesicle-micelle transition in aqueous solution of anionic surfactant and cationic imidazolium surfactants: alteration of the location of different fluorophores. *J Colloid Interf Sci*. **2017**;490:763–773.

115. Afri M, Alexenberg C, Bodner E, et al. NMR-based molecular ruler for determining the depth of intercalants within the lipid bilayer. Part V: a comparison of liposomes, bioliposomes and erythrocyte ghosts. *Chem Phys Lipids*. **2014**;184:52–60.

116. Israelachvili JN, Mitchell DJ, Ninham BW. Theory of self-assembly of lipid bilayers and vesicles. *BBA - Biomembr*. **1977**;470:185–201.

117. Segota S, Tezak D. Spontaneous formation of vesicles. *Adv Colloid Interface Sci*. **2006**;121:51–75.

118. Nagarajan R. Molecular packing parameter and surfactant self-assembly: the neglected role of the surfactant tail. *Langmuir*. **2002**;18:31–38.

119. Pasquali RC, Taurozzi MP, Bregni C. Some considerations about the hydrophilic – lipophilic balance system. *IntJ Pharm.* **2008**;356:44–51.

120. Moghassemi S, Hadjizadeh A. Nano-niosomes as nanoscale drug delivery systems: an illustrated review. *J Control Release*. **2014**;185:22–36.

121. Bodratti AM, Alexandridis P. Amphiphilic block copolymers in drug delivery: advances in formulation structure and performance. *Expert Opin Drug Deliv*. **2018**;15:1085–1104.

122. Polat H, Kutluay G, Polat M. Analysis of dilution induced disintegration of micellar drug carriers in the presence of inter and intra micellar species. *Colloid Surf A*. **2020**;301:124989.

123. Kikuchi H, Carlsson A, Yachi K, et al. Possibility of heat sterilization of liposomes. *Chem Pharm Bull*. **1991**;39:1018–1022.

124. Hwang D, Ramsey JD, Kabanov AV. Polymeric micelles for the delivery of poorly soluble drugs: from nanoformulation to clinical approval. *Adv Drug Deliv Rev*. **2020**;156:80–118.

125. Ajith TA. Alpha-lipoic acid: a possible pharmacological agent for treating dry eye disease and retinopathy in diabetes. *Clin Exp Pharmacol Physiol*. **2020**;47:1883–1890.

126. Alambiaga-Caravaca AM, Calatayud-Pascual MA, Rodilla V, et al. Micelles of progesterone for topical eye administration: interspecies and intertissues differences in ex vivo ocular permeability. *Pharmaceutics*. **2020**;12:702.

    • Experimental evidence of interspecies differences regarding drug penetration through cornea and sclera.

127. Safwat MA, Mansour HF, Hussein AK, et al. Polymeric micelles for the ocular delivery of triamcinolone acetonide: preparation and in vivo evaluation in a rabbit ocular inflammatory model. *Drug Deliv*. **2020**;27:1115–1124.

128. Di Prima G, Saladino S, Bongiovi F, et al. Novel inulin-based mucoadhesive micelles loaded with corticosteroids as potential transcorneal permeation enhancers. *Eur J Pharm Biopharm*. **2017**;117:385–399.

129. Gote V, Mandal A, Alshamrani M, et al. Self-assembling tacrolimus nanomicelles for retinal drug delivery. *Pharmaceutics*. **2020**;12:1072.

130. Patel S, Garapati C, Chowdhury P, et al. Development and evaluation of dexamethasone nanomicelles with potential for treating posterior uveitis after topical application. *J Ocul Pharmacol Ther.* **2015**;31:215–227.

131. Nagaraj R, Stack T, Yi SJ, et al. High density display of an anti- angiogenic peptide on micelle surfaces enhances their inhibition of αvβ3 integrin-mediated neovascularization in vitro. *Nanomaterials*. **2020**;10:581.

132. Hou Y, Xin M, Li Q, et al. Glycyrrhizin micelle as a genistein nano- carrier: synergistically promoting corneal epithelial wound healing through blockage of the HMGB1 signaling pathway in diabetic mice. *Exp Eye Res*. **2021**;204:108454.

133. Ahmed KS, Hussein SA, Ali AH, et al. Liposome: composition, char- acterisation, preparation, and recent innovation in clinical applications. *J Drug Target*. **2019**;27:742–761.

134. Torchilin VP. Recent advances with liposomes as pharmaceutical carriers. *Nat Rev Drug Discov*. **2005**;4:145–160.

135. Khan AA, Allemailem KS, Almatroodi SA, et al. Recent strategies towards the surface modification of liposomes: an innovative approach for different clinical applications. *3 Biotech*. **2020**;10:163.

136. Bogdanov P, Sampedro J, Solà-Adell C, et al. Effects of liposomal formulation of citicoline in experimental diabetes-induced retinal neurodegeneration. *Int J Mol Sci.* **2018**;19:2458.

137. Parravano M, Scarinci F, Parisi V, et al. Citicoline and vitamin B12 eye drops in type 1 diabetes: results of a 3-year pilot study evaluating morpho-functional retinal changes. *Adv Ther.* **2020**;37:1646–1663.

138. Altamirano-Vallejo JC, Navarro-Partida J, Gonzalez-de La Rosa A, et al. Characterization and pharmacokinetics of triamcinolone acetonide-loaded liposomes topical formulations for vitreoretinal drug delivery. *J Ocul Pharmacol Ther*. **2018**;34:416–425.

139. Gonzalez-de La Rosa A, Navarro-Partida J, Altamirano-Vallejo JC, et al. Novel triamcinolone acetonide-loaded liposomes topical formulation for the treatment of cystoid macular edema after cataract surgery: a pilot study. *J Ocul Pharmacol Ther*. **2019**;35:106–115.

• Clinical study that evidenced the capability of liposomes to provide triamcinolone acetonide therapeutic levels in vitreous and retina.

140. Li J, Cheng T, Tian Q, et al. A more efficient ocular delivery system of triamcinolone acetonide as eye drop to the posterior segment of the eye. *Drug Deliv*. **2019**;26:188–198.

141. Lai S, Wei Y, Wu Q, et al. Liposomes for effective drug delivery to the ocular posterior chamber. *J Nanobiotechnol*. **2019**;17:64.

142. Davis BM, Normando EM, Guo L, et al. Topical delivery of avastin to the posterior segment of the eye in vivo using annexin A5-associated liposomes. *Small*. **2014**;10:1575–1584.

143. Giambanco I, Pula G, Ceccarelli P, et al. Immunohistochemical localization of annexin V (CaBP33) in rat organs. *J Histochem Cytochem*. **1991**;39:1189–1198.

• Liposomes that can bind to the calcium-dependent phospholi- pid binding protein annexin A5 facilitate the penetration of bevacizumab (avastin) towards vitreous and retina/choroid.

144. Urtti A. Comment on "Topical Delivery of Avastin to the Posterior Segment of the Eye In Vivo Using Annexin A5-Associated Liposomes": topical Liposomal Bevacizumab Results in Negligible Retinal Concentrations. *Small*. **2019**;15:1805199.

145. Malakouti-Nejad M, Bardania H, Aliakbari F, et al. Formulation of nanoliposome-encapsulated bevacizumab (Avastin): statisticaloptimization for enhanced drug encapsulation and properties evaluation. *Int J Pharm*. **2020**;590:119895.

146. Platania CBM, Fisichella V, Fidilio A, et al. Topical ocular delivery of TGF-β1 to the back of the eye: implications in age-related neuro- degenerative diseases. *Int J Mol Sci*. **2017**;18:2076.

• In vivo demonstration that ocular instillation of annexin A5-based unilaminar vesicles may provide therapeutical levels of TGF-β1 in the vitreous.

147. Soriano-Romaní L, Alvarez-Trabado J, López-García A, et al. Improved in vitro corneal delivery of a thrombospondin-1-derived peptide using a liposomal formulation. *Exp Eye Res*. **2018**;167:118–121.

148. Peeters L, Sanders NN, Jones A, et al. Post-pegylated lipoplexes are promising vehicles for gene delivery in RPE cells. *J Control Release*. **2007**;121:208–217.

149. Lajunen T, Hisazumi K, Kanazawa T, et al. Topical drug delivery to retinal pigment epithelium with microfluidizer produced small liposomes. *Eur J Pharm Sci*. **2014**;62:23–32.

150. Hanjdani-Vila RM, Ribier A, Rondot B, et al. Dispersions of lamellar phases of non-ionic lipids in cosmetic products. *Int J Cosmet Sci*. **1979**;1:303–314.

151. Biswas GR, Majee S. Niosomes in ocular drug delivery. *Eur J Pharm Med Res*. **2018**;4:813–819.

152. Marianecci C, Di Marzio L, Rinaldi F, et al. Niosomes from 80s to present: the state of the art. *Adv Colloid Interface Sci*. **2014**;205:187–206.

153. Ritwiset A, Krongsuk S, Roy J. Molecular structure and dynamical properties of niosome bilayers with and without cholesterol incorporation: a molecular dynamics simulation study. *Appl Surf Sci*. **2016**;380:23–31.

154. Marianecci C, Di Marzio L, Del Favero E, et al. Niosomes as drug nanovectors: multiscale pH-dependent structural response. *Langmuir.* **2016**;32:1241–1249.

155. Mandal D, Das S. Glucose-triggered dissolution of phenylboronic acid-functionalized cholesterol-based niosomal self-assembly for tuneable drug release. *New. J. Chem.* **2019**;43:7855–7865.

156. Baillie AJ, Florence AT, Hume LR, et al. The preparation and proper- ties of niosomes—non-ionic surfactant vesicles. *J Pharm Pharmacol.* **1985**;37(12):863–868.

157. Machado ND, Garcia-Manrique P, Fernandez MA, et al. Cholesterol free niosome production by microfluidics: comparative with other conventional methods. *Chem Eng Res Des*. **2020**;162:162–171.

158. Khatoon M, Shah KU, Din FU, et al. Proniosomes derived niosomes: recent advancements in drug delivery and targeting. *Drug Deliv*. **2017**;24:56–69.

159. Pardakhty A, Moazeni E, Varshosaz J, et al. Pharmacokinetic study of niosome-loaded insulin in diabetic rats. *DARU*. **2011**;19:404–411.

160. Hasan AA, Madkor H, Wageh S. Formulation and evaluation of metformin hydrochloride-loaded niosomes as controlled release drug delivery system. *Drug Deliv*. **2013**;20:120–126.

161. Samed N, Sharma V, Sundaramurthy A. Hydrogen bonded niosomes for encapsulation and release of hydrophilic and hydrophobic anti-diabetic drugs: an efficient system for oral anti-diabetic formulation. *Appl Surf Sci*. **2018**;449:567–573.

162. Kamble B, Talreja S, Gupta A, et al. Development and biological evaluation of Gymnema sylvestre extract-loaded nonionic surfactant-based niosomes. *Nanomedicine*. **2013**;8:1295–1305.

163. Abdelkader H, Ismail S, Kamal A, et al. Preparation of niosomes as an ocular delivery system for naltrexone hydrochloride: physicochemical characterization. *Pharmazie*. **2010**;65:811–817.

164. Uchegbu IF, Vyas SP. Non-ionic surfactant based vesicles (niosomes) in drug delivery. *Int J Pharm*. **1998**;172:33–70.

165. Abdelkader H, Ismail S, Kamal A, et al. Design and evaluation of controlled-release niosomes and discomes for naltrexone hydro- chloride ocular delivery. *J Pharmaceutical Sci.* **2011**;100 (5):1833–1846.

166. El-Sayed MM, Hussein AK, Sarhan HA, et al. Flurbiprofen-loaded niosomes-in-gel system improves the ocular bioavailability of flurbiprofen in the aqueous humor. *Drug Dev Ind Pharm*. **2017**;43:902–910.

167. Fathalla D, Fouad EA, Soliman GM. Latanoprost niosomes as a sustained release ocular delivery system for the management of glaucoma. *Drug Dev Ind Pharm*. **2020**;46:806–813.

•Topical administration to normotensive rabbits of latanoprost-loaded niosome gel caused sustained decrease in intraocular pressure.

168. Fouda NH, Abdelrehim RT, Hegazy DA, et al. Sustained ocular delivery of dorzolamide-HCl via proniosomal gel formulation: in-vitro characterization, statistical optimization, and in-vivo pharmacodynamic evaluation in rabbits. *Drug Deliv*. **2018**;25:1340–1349.

169. Emad Eldeeb A, Salah S, Ghorab M. Proniosomal gel-derived niosomes: an approach to sustain and improve the ocular delivery of brimonidine tartrate; formulation, in-vitro characterization, and in-vivo pharmacodynamic study. *Drug Deliv*. **2019**;26:509–521.

170. Al Qtaish N, Gallego I, Villate-Beitia I, et al. Niosome-based approach for in situ gene delivery to retina and brain cortex as immune-privileged tissues. *Pharmaceutics*. **2020**;12:198.

171. Villate-Beitia I, Gallego I, Martinez-Navarrete G, et al. Polysorbate 20 non-ionic surfactant enhances retinal gene delivery efficiency of cationic niosomes after intravitreal and subretinal administration. *Int J Pharm*. **2018**;550:388–397.

172. Qin Y, Tian Y, Liu Y, et al. Hyaluronic acid-modified cationic niosomes for ocular gene delivery: improving transfection efficiency in retinal pigment epithelium. *J Pharm Pharmacol*. **2018**;70:1139–1151.

AIMS

2. AIMS

Diabetic ocular diseases are a challenge in terms of successful drug delivery, as the static and dynamic barriers of the eye form a great obstacle to any formulation trying to reach a therapeutic site in the anterior and posterior segment. While different macro sized systems have been explored, the relatively new world of nanometer scale carriers is advancing the field of controlled, targeted and sustained drug delivery at a fast pace. In the context of diabetic eye diseases, and in particular diabetic retinopathy, epalrestat is a drug that has the potential to treat patients with chronic high blood glucose levels, and prevent their loss of vision. However, this molecule is poorly soluble in water.

To overcome the hydrophobicity of the epalrestat molecule, different formulations have been investigated. The use of niosomes, micelles and oleogels were explored to encapsulate or solubilize epalrestat with the objective of topical administration. Niosomes and micelles have the advantage of being self-assembled, stable and highly tunable. While micelles encapsulate the drug in their hydrophobic core, niosomes encapsulate the drug in their hydrophobic bilayer. Oleogel for its part dissolves the drug in its midst. All three formulations are then delivered into the eye topically.

The main objective of this Thesis was to design reproducible, stable and safe formulations and characterize them in order to validate their potential for topical administration of epalrestat for diabetic eye diseases. This objective was split into four parts that are exposed as follows.

1. The design, formulation and characterization of niosomes for ocular delivery of epalrestat

Diabetic patients with elevated levels of blood glucose have a metabolic pathway, the polyol pathway, that becomes available which is not active under normal glycemic conditions. The polyol pathway, turns glucose into sorbitol and subsequently sorbitol into fructose. This first step is the rate limiting step, meaning that sorbitol accumulates with time. Sorbitol not being permeable to cell membranes and this first step consuming NADPH, the environment where this reaction takes place is prone to oxidative and osmotic stress, resulting in tissue degradation. The glucose to sorbitol conversion step is catalyzed by aldose reductase, an enzyme present in the retina.

Epalrestat is a non-competitive and reversible aldose reductase inhibitor that is used for the treatment of diabetic neuropathy in Japan as an oral formulation. Clinical trials confirmed the efficacy of orally administered epalrestat in the treatment of diabetic retinopathy. However, epalrestat being poorly soluble in water, it needs to be encapsulated to cross the different ocular barriers.

Niosomes are self-assembled vesicles that are composed of amphiphilic molecules creating a hydrophobic bilayer capable of accommodating small molecules. They are made by bringing together a non-ionic surfactant and a helper lipid at set ratios in water and use different techniques to tune the size, polydispersity and surface potential of the particle.

The first part of the Thesis aimed to elaborate a robust protocol for the preparation of nanometer scale niosomes that are able to encapsulate epalrestat and permeate different ocular tissues. The aim of this section of the Thesis is to assess the reproducibility, stability, safety and

compliance with the requirements of ocular drug transport of the niosomes designed and prepared. This allowed for the selection of the best niosomal formulation to be tested *in vivo*.

The zebrafish embryotoxicity experiments for safety characterization of the niosomes were done in collaboration with the laboratory of Professor Laura Sánchez from the Departamento de Zooloxía, Xenética y Antropoloxía Física at the Universidade de Santiago de Compostela in Lugo.

2. **The understanding of the underlying physical forces governing molecular interactions of the components of the niosomes**

Niosomes are self-assembled particles that are composed of a bilayer. The forces governing the molecular arrangement in the bilayer are the ones determining the physical characteristics of the niosomes such as their size or stability. Using a Langmuir-Blodgett through, monolayers made from the molecules present in the niosomal bilayer can be studied under different pressures. This part of the Thesis relies on the hypothesis that the molecular arrangement of a monolayer made from Tween 60, cholesterol and DOTMA in the ratios leading to niosome formation is mainly governed by the Tween 60, is also influenced by interactions with cholesterol and DOTMA and by the temperature and ionic strength of the subphase.

The aim of the second chapter of this Thesis was to understand which variables had an influence on the monolayer behavior and to quantify the effects of these variables to ascertain an understanding of the stability of the self-assembly in storage and administration conditions. This was achieved through the study of four effects: (I) the effect of cholesterol on a Tween 60 monolayer, (II) the effect of

DOTMA on a Tween 60 monolayer, (III) the effect of cholesterol on a Tween 60/DOTMA binary monolayer, and (IV) the effect of temperature and ionic strength of the subphase on a Tween 60/DOTMA/cholesterol tertiary monolayer.

The experiments in this section were performed in collaboration with the Biomemebranes Laboratory of Professor Matilde Casas Parada at the Universidade de Santiago de Compostela in Santiago de Compostela.

3. The formulation and characterization of oleogels for topical ocular delivery of epalrestat

Gels are gathering interest in the pharmaceutical industry as a vehicle for drug delivery. They are viscoelastic fluids made of a liquid and a gelator. As the drug to be delivered, epalrestat, is hydrophobic, oleogels were chosen. These oleogels are made up from an oil phase and a gelator, allowing the formulation to tune its viscosity, and homogeneously distribute the drug in the oleogel matrix. The work done in this part of the Thesis was based on the hypothesis that oleogels are suitable carriers to solubilize and release epalrestat, allowing it to permeate through corneal and scleral tissues.

The aim of this part of the Thesis was to assess the reproducibility, safety and efficiency in drug release and permeation of the oleogels designed and prepared. This allowed for the selection of the best oleogel formulation to be tested *in vivo*.

Multiple different oleogels were designed and characterized. Soybean oil was chosen as the base, as it possesses a high smoke point and permits higher temperatures during the melting of the gelators.

Three gelators were used to prepare single and double gelator oleogels: beeswax, cocoa butter and ethyl cellulose.

The oleogel formulation was developed during a research secondment at the Chemical and Biological Engineering Department of the Colorado School of Mines in Golden, Colorado, under the supervision of Professor Anuj Chauhan.

4. The comparison of epalrestat loaded niosomes, micelles and oleogels distribution *in vivo*

Micelles are self-assembled structures that are formed from amphiphilic molecules. These molecules join their hydrophobic moieties to form a core and expose their hydrophilic heads to the aqueous medium. Pluronic® F127 was chosen to prepare micelles as they have already been prepared and characterized in our research group. The best niosomal, micellar and oleogel formulations were selected to be tested in an animal model in the context of in vivo experiments.

The aims of the in vivo study were: (I) to assess the safety of the three formulations for topical ocular delivery of epalrestat, (II) to quantify the epalrestat concentration in the lacrimal fluid of the rabbits during the experiment, and (III) to quantify the epalrestat concentration in the different ocular tissues 6 hours after administration of the formulations.

The experiments were conducted on rabbits within the 3R principles and with the authorization of both the committee of animal experimentation ethics (CEEA) of University of Santiago de Compostela and the Consellería de Medio Rural of Xunta de Galicia.

Chapter 3

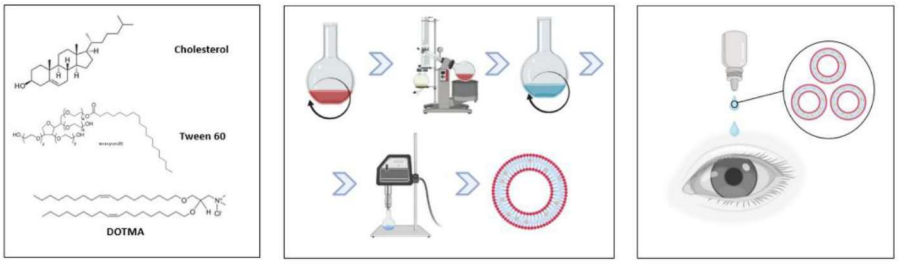

The work described in this chapter was published in **Formulation and Characterization of Epalrestat-Loaded Polysorbate 60 Cationic Niosomes for Ocular Delivery**, *Pharmaceutics* 15(4), 1247, 2023, authored by:

Axel Kattar [a], Ana Quelle-Regaldie [b], Laura Sánchez [b,c], Angel Concheiro [a] and Carmen Alvarez-Lorenzo [a]

[a] Departamento de Farmacología, Farmacia y Tecnología Farmacéutica, I+D Farma (GI-1645), Facultad de Farmacia and Health Research Institute of Santiago de Compostela (IDIS), Universidade de Santiago de Compostela, 15782 Santiago de Compostela, Spain.

[b] Departamento de Zooloxía, Xenética y Antropoloxía Física, Facultade de Veterinaria, Universidade de Santiago de Compostela, 27002 Lugo, Spain

[c] Preclinical Animal Models Group, Health Research Institute of Santiago de Compostela (IDIS), 15706 Santiago de Compostela, Spain

3. FORMULATION AND CHARACTERIZATION OF EPALRESTAT-LOADED POLYSORBATE 60 CATIONIC NIOSOMES FOR OCULAR DELIVERY

3.1 INTRODUCTION

In 2021 the prevalence of diabetes in adults ranging from 20 to 79 years worldwide was 9.8%, representing 536.6 million patients [1]. Diabetic patients have elevated levels of glucose in their blood, which leads to a range of conditions. A subcategory of complications derived from diabetes is diabetic ocular diseases. Examples include diabetic retinopathy, diabetic keratopathy, or cataracts, which have been linked to the polyol pathway [2]. These different illnesses affect the patient with loss of vision, culminating in blindness if left untreated. The current treatments for diabetic ocular diseases involve intravitreal injections [3], laser treatment [4], or even vitrectomy [5].

The polyol pathway transforms glucose into sorbitol when hexokinases active in the Embden-Meyerhof pathway are saturated, and subsequently, glucose is oxidated to sorbitol and further transformed into fructose. It is important to mention that this pathway is rarely used by the body in a healthy state as it is only activated at high intracellular glucose concentrations [6]. However, in the case of diabetes, the blood glucose levels can be high enough for the reaction balance to favor

sorbitol production. Sorbitol is not permeable to cell membranes and accumulates inside the cells, and this excess creates osmotic stress [7]. Moreover, the conversion of glucose to sorbitol consumes NADPH which depletes NADPH stock [8] and competes with glutathione reduction, which in turn adds to oxidative damage [9]. This induces a lack of antioxidants and therefore increases the number of reactive oxygen species (ROS), increasing the oxidative stress in the affected tissue [10].

The polyol pathway can be blocked by inhibiting aldose reductase, an essential enzyme in the reduction of glucose to sorbitol [7,11]. In the case of diabetic retinopathy, the posterior segment of the eye is affected by sorbitol accumulation, and therefore, a carrier able to deliver the aldose reductase inhibitor to the inner eye tissues is needed. The aldose reductase inhibitor epalrestat is approved in Japan for oral administration thrice a day in 50 mg doses [12] to treat diabetic neuropathy. Its IC90 as an aldose reductase inhibitor was found to be 2.5×10^{-2} mg/mL [13] and an IC50 of 1.41×10^{-6} mg/mL in rat lens [14]. Epalrestat was shown to reduce aldose reductase expression and vascular endothelial growth factor (VEGF) secretion in retinal pigment epithelial cells [15]. Compared to methylcobalamine, epalrestat taken orally thrice daily for twelve weeks is better tolerated by patients and showed fewer adverse effects [16].

Although the information on ocular delivery systems of aldose reductase inhibitors is limited, topical instillation of tolrestat in rats was successful in preventing cataract development [17]. Biodegradable injectable implants for sustained delivery of N-4-(benzoylaminophenylsulfonyl glycine) also demonstrated inhibition of aldose reductase activity and VEGF expression in ARPE cells, as well as in galactose-fed rats [18]. Similarly, 2-methylsorbinil suspensions

were shown to be successful in inhibiting cataracts in galactose-fed rats [19]. The only previous work attempting to deliver epalrestat to the posterior segment of the eye made use of contact lenses either through direct loading [20] or previous encapsulation in PEGylated solid lipid nanoparticles [21]. This work aims to show the viability of a nanoparticle system as a topical delivery system for epalrestat without the need for a contact lens.

In order to deliver epalrestat to the therapeutic site topically, it has to be encapsulated to cross different ocular barriers due to the high hydrophobicity of the molecule. Therefore, niosomes were prepared to encapsulate the drug and carry it to the posterior segment for it to reach the therapeutic site [22]. Niosomes are vesicles of small size with a bilayer made of surfactants and supplementary molecules that self-assemble through hydrophobic interactions as the involved molecules are amphiphilic. The shape, size, and surface charge can be modified by adjusting the concentration and molar ratios of different reagents [23,24]. They are being investigated for topical administration in ocular and skin tissue [25,26,27].

This work aims to formulate a niosomal carrier that fits the requirements to deliver epalrestat to the posterior segment of the eye through the scleral route. This was done by selecting polysorbate 60 (Tween 60), cholesterol, and 1,2-di-O-octadecenyl-3-trimethylammonium propane (DOTMA) and preparing niosomes with specific size, polydispersity, and surface charge. The obtained systems loaded with epalrestat were characterized in depth using various methods testing its physicochemical properties, encapsulation efficiency, release profile, permeation profile through the porcine cornea and sclera, ocular irritability potential, impact on blood glucose levels, and toxicity. Alternatives to animal testing were used according

to the 3Rs principles: the HET-CAM [28] model for the ocular irritability potential, an extension of this model (Gluc-HET) to monitor the effect of the loaded niosome on the blood glucose levels [29], a zebrafish embryo model was used to assess the toxicity of the loaded niosomes [30,31,32], and porcine eye tissues from the slaughterhouse for ex vivo permeability tests.

3.2 MATERIALS AND METHODS

Materials. Polysorbate 60 MW 1311.7 g/mol (Tween 60, HLB 14.9, Sigma Aldrich, Buchs, Switzerland), polysorbate 80 MW 1310 g/mol (Tween 80, HLB 15, Sigma Aldrich, Switzerland), 1,2-di-O-octadecenyl-3-trimethylammonium propane (chloride salt) (DOTMA, 670.58 g/mol) (Avanti, Alabaster, AL, USA), epalrestat (319.4 g/mol) (TCI, Tokyo, Japan), cholesterol (386.7 g/mol) (Chemtrec, Madrid, Spain), ethanol (VWR Chemicals, Briare, France), dichloromethane (Fischer Scientific, Waltham, MA USA), chloroform (Cienytech, Santiago de Compostela, Spain), phosphate-buffered saline (Life Tecnologies Co., Carlsbad, CA, USA), sodium chloride (Labkem, Barcelona, Spain), potassium chloride (Panreac, Castellar del Vallès, Spain), sodium bicarbonate (Merck, St Louis, MO, USA), calcium dihydrochloride (Merck, Darmstadt, Germany), potassium dihydrogen phosphate 1-basic (Panreac, Castellar del Vallès, Spain), disodium hydrogen phosphate dihydrate (VWR Chemicals, Briare, France), phosphate-buffered saline solution (Sigma-Aldrich, Lyon, France), Hanks' Balanced Salt Solution (HBSS) (Paisley, Scotland, UK), glibenclamide (Roche, Basel, Switzerland). Ultrapure water (resistivity > 18.2 MΩ cm) was obtained by reverse osmosis (Milli-Q®, Millipore Ibérica, Madrid, Spain).

Niosome formulation. The protocol was adapted from previous reports [33,34,35]. Briefly, polysorbate 60 and cholesterol were dissolved in 2 mL ethanol in the presence or absence of DOTMA (at 1/0.42/0, 1/0.42/0.075 and 1/0.42/0.158 molar ratios of Tween 60/cholesterol/DOTMA as shown in **Table 3.1**). The combined total amount was kept at 76.38 µmol. Epalrestat (2 mg) was dissolved in 500 µL ethanol and added to the flask. The organic solvent was evaporated in a round bottom flask with a rotary evaporator at 70 °C under 50 mbar pressure to create a film. The film was subsequently desiccated for 30 min. 10 mL of ultrapure water was added to the flask. The film was removed from the walls of the flask by ultrasonication for 30 min. In order to form the niosomes, the solution was sonified for 90 s at 20% amplitude on a Branson Digital Sonifier 450 (Marshall Scientific, Hampton, NH, USA). This yielded epalrestat-loaded niosomes in water. In order to remove the unencapsulated drug, dialysis was performed for 30 min in 500 mL ultrapure water with 1 vol% Tween 80 with a 14,000 Da dialysis tubing (Sigma-Aldrich, Milwaukee, WI, USA).

Table 3.1. Mol fractions of the surfactant, helper lipid, and cationic lipid are used to prepare the niosomes.

Formulation	Tween 60 (mol Fraction)	Cholesterol (mol Fraction)	DOTMA (mol%)
1	1	0.2	0
2	1	0.3	0
3	1	0.4	0
4	1	0.5	0
5	1	0.75	0
6	1	1	0
TCD0	1	0.4	0
TCD5	1	0.4	5
TCD10	1	0.4	10

The formulations were named with a code TCDX based on the included components: T for Tween, C for cholesterol, D for DOTMA, and x for the molar percentage of DOTMA present in the niosome. The

code FD (free drug) was used to refer to a solution of 10% ethanol in water containing epalrestat at the same concentration as the epalrestat in the niosome formulation. For storage, the niosomes were kept in 15 mL Falcon tubes at room temperature in the absence of light.

Niosome characterization. The particle size and zeta potential of the niosomes were measured with DLS using a Zetasizer Nano (Malvern Instruments, Herrenberg, Germany) in ultrapure water at 20 °C with 10 s equilibration time using backscatter. The values taken were measured by intensity. The pH of the formulation solution was measured using a GL22 pH & ion meter (Crison, Barcelona, Spain). Viscosity at 35 °C was recorded between 0.05 and 200 rad/s in a Rheolyst AR-1000N rheometer (TA Instruments, Newcastle, UK) equipped with a Peltier plate and a cone geometry (40 mm diameter, 2 °).

Stability study. The stability of epalrestat-loaded niosomes over 7 days was assessed at 4 °C (fridge) and 25 °C (oven) in the absence of light. The size, polydispersity index, zeta-potential, and content in epalrestat were measured at time points 0 and after 7 days.

TEM. Drops of 5 µL of blank and epalrestat-loaded niosome dispersions were placed on carbon-coated grids, and the excess the solution was removed with filter paper. The samples were dyed with 1% phosphotungstic acid in water. The grid was allowed to dry and observed using a high-resolution JEM-1011 transmission electron microscope (JEOL USA Inc., Peabody, MA, USA).

HPLC. Quantitative analysis of epalrestat was performed on a Waters 717 plus Autosampler with a 4.6 × 250 mm C18 Symmetry column (Waters, Wexford, Ireland) with 5 µm pores. The mobile phase was acetonitrile:elution buffer 45:55 (v/v). The elution buffer was

composed of 25 mM potassium dihydrogen phosphate and 25 mM disodium hydrogen phosphate dihydrate in ultrapure water adjusted to pH 6.5 with phosphoric acid. The flow rate was 0.85 mL/min, the detection wavelength was 295 nm, the temperature was maintained at 25 °C, and the injection volume was 40 µL. The calibration curve was prepared with concentrations ranging from 1 to 10 µg/mL with an increment step of 1 µg/mL. The retention time of epalrestat was 4.5 min. The HPLC quantification method was validated with regard to specificity, detection and quantitation limits, linearity, accuracy, precision, and range (**Figure 3.1**).

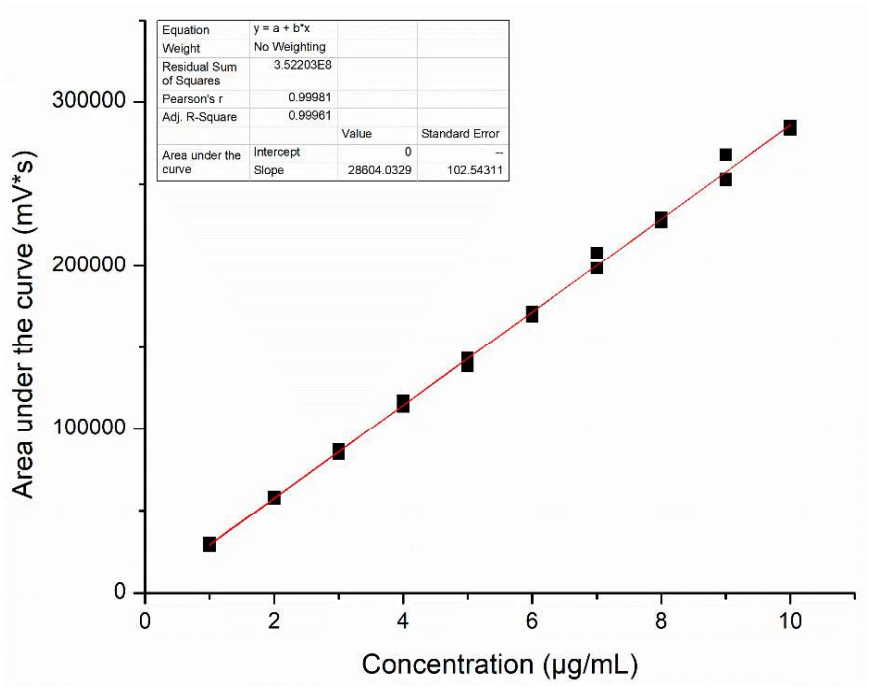

Figure 3.1. HPLC validation curve of epalrestat detection using the experimental conditions described in the HPLC section of the materials and methods.

Encapsulation efficiency. The encapsulation efficiency (EE%) was calculated by dialyzing the niosomes for 30 min in ultrapure water with

1 vol% Tween 80 [36] and analyzing the medium with HPLC. The dialysis membrane had a molecular weight cutoff of 12,000 Da and an effective dialysis area of 4.2 cm^2. The concentration was confirmed by lysing the niosomes with methanol [34] and measuring the concentration of the drug encapsulated by HPLC. The efficiency was then calculated with **Equation 3.1** [35]:

$$EE\% = 1 - \frac{amount\ of\ drug\ out\ of\ the\ dyalisis\ membrane}{total\ amount\ of\ drug} * 100,$$

Equation 3.1. Encapsulation efficiency of epalrestat in niosomes.

Release study. The release was tested by placing 5 mL of niosomes (0.20 ± 0.01 mg epalrestat/mL) in 14,000 MWCO dialysis tubing (Sigma-Aldrich, St Louis, MO, USA) and using 500 mL ultrapure water with 1% Tween 80 as receptor medium [36]. The medium was left at 20 °C for 20 days or 37 °C for 24 h stirring at 400 rpm with a magnetic stirrer. 1 mL of the medium was taken and replaced with 1 mL of fresh medium every day for 8 days and then every two days until day 21. The concentration of epalrestat in the release medium was quantified with HPLC. The niosomes left in the dialysis bag were lysed, and the remaining epalrestat was quantified with HPLC.

HET-CAM. For the Hen's Egg Test on Chorioallantoic Membrane (HET-CAM) assay [28], fertilized eggs (15) were supplied by Coren (Ourense, Spain) and cleaned before incubation in a CCRS 0150 incubator (Ineltec, Tona, Spain) for 9 days at 37 °C and 60% relative humidity. On the day of the experiment, the shell of the eggs was pared off with a circular saw at the location of the air cell. The untouched inner membrane was moistened with a 0.9% NaCl solution, and the eggs were placed back in the incubator for 30 min. The 0.9% NaCl solution was subsequently removed, as well as the inner membrane, while being careful not to damage the blood vessels of the CAM

underneath. Any non-viable egg was discarded. The positive control was NaOH 0.1M, and the negative control was 0.9% NaCl. The solutions tested were formulation TCD0, TCD5, and TCD10 in water loaded with 0.2 mg/mL epalrestat, unloaded niosomes of the same molar ratios, and epalrestat dissolved in ethanol: water 10/90 v/v mixture. The 300 µL of the testing solution was then added to the eggs, and the effect on the blood vessels regarding hemorrhage, lysis, and coagulation was recorded. The ocular irritability potential score was calculated with **Equation 3.2** [28]:

$$score = \frac{301 - H}{300} * 5 + \frac{301 - L}{300} * 7 + \frac{301 - C}{300} * 9,$$

with H = hemorrhage time (s), L = lysis time (s), C = coagulation time (s).

Equation 3.2. Ocular irritability potential score from the Hen's Egg Test on Chorioallantoic Membrane assay.

Gluc-HET. For the Gluc-HET assay [29], fertilized eggs (15) were supplied by Coren (Ourense, Spain) and cleaned before incubation in a CCRS 0150 incubator (Ineltec, Tona, Spain) for 11 days at 37 °C and 60% relative humidity. On the day of the experiment, the shell of the egg above the air pocket was pierced with a needle, and 300 µL of the testing solution was deposited inside the air compartment. The air compartment of the negative controls was pieced, but no solution was added [29]. The positive control was a solution of 0.002 mg/mL glibenclamide solution in HBSS. The eggshells are then closed off with parafilm. After 2 h incubation, the eggshell above the air compartment was removed, and the chorioallantoic membrane was cut next to a blood vessel with a scalpel. The blood vessel was placed on a flat metal tong and dried with paper. Once no moisture was absorbed anymore by the paper, the vessel was cut, and the blood glucose level was measured

with a glucose meter (Contour next, Ascensia Diabetes Care, Basel, Switzerland).

Zebrafish embryotoxicity test. Epalrestat-loaded niosome toxicity was assessed using zebrafish embryos (Danio rerio) and the Fish Embryo Acute Aquatic Toxicity (FET) Test. Zebrafish embryos were selected around 3 h post-fertilization (hpf). The test was considered valid if the mortality of fish embryos was at least 30% in the positive control (3,4-dichloroaniline) and lower than 10% in the negative control. In our experiment, the mortality of the negative control was 3.3%, and the mortality of the positive control was 100%. The larvae were grown in autoclaved osmosis water. The experiment was carried out by including 5 or 10 µL of formulation in 200 µL of medium (4.9 µg/mL and 9.5 µg/mL, respectively) and quantifying the mortality at 24, 48, 72, and 96 h. The formulations tested were TCD0, TCD5, and TCD10. The experiments were conducted in triplicate.

Corneal permeation. Porcine eyes were supplied by a slaughterhouse and transported to the laboratory in diluted PBS solution at 4 °C in an ice bath. The corneas were dissected with 2–3 mm of surrounding tissue and washed with 0.9% NaCl to remove any attached tissue. The corneas were mounted in Franz diffusion cells with the outer part of the cornea facing up. The area available for permeation was 0.785 cm2. The receiving chamber was filled with 6 mL of Tween 80:water 10:90 v/v solution while making sure no bubbles formed and then agitated with a magnetic stirring rod at 400 rpm. The donor chamber was filled with 2 mL of carbonated buffer (pH 7.2) and closed off with parafilm to prevent evaporation. The system was then left to equilibrate for 1 h at 37 °C. Once the system was balanced, the carbonated buffer in the donor chamber was replaced by 2 mL of either 0.2 mg/mL epalrestat solution in 10 mL of ethanol:water 10:90 v/v or

0.2 mg/mL epalrestat encapsulated in the TCD0, TCD5, and TCD10 formulations. After 30 min, at 1 h and then every hour, 1 mL of the solution in the receiving chamber was removed and replaced with 1 mL of fresh Tween 80:water 10:90 v/v solution. After 6 h, the last sample was taken, and the corneas were incubated in ethanol at 37 °C for 24 h. They were then sonicated at 37 °C in an ultrasonic bath for 90 min. The resulting mixture was centrifuged at 1000 rpm at 25 °C for 5 min, and the supernatant was centrifuged at 14,000 rpm at 25 °C for 20 min. After filtration through 0.22 µm pore syringe filters (Scharlab, Barcelona, Spain), all the samples from the receptor chamber as well as the supernatant from the tissue incubation, were analyzed with HPLC according to the protocol described above. All experiments were carried out in triplicate (**Figure 3.2**)

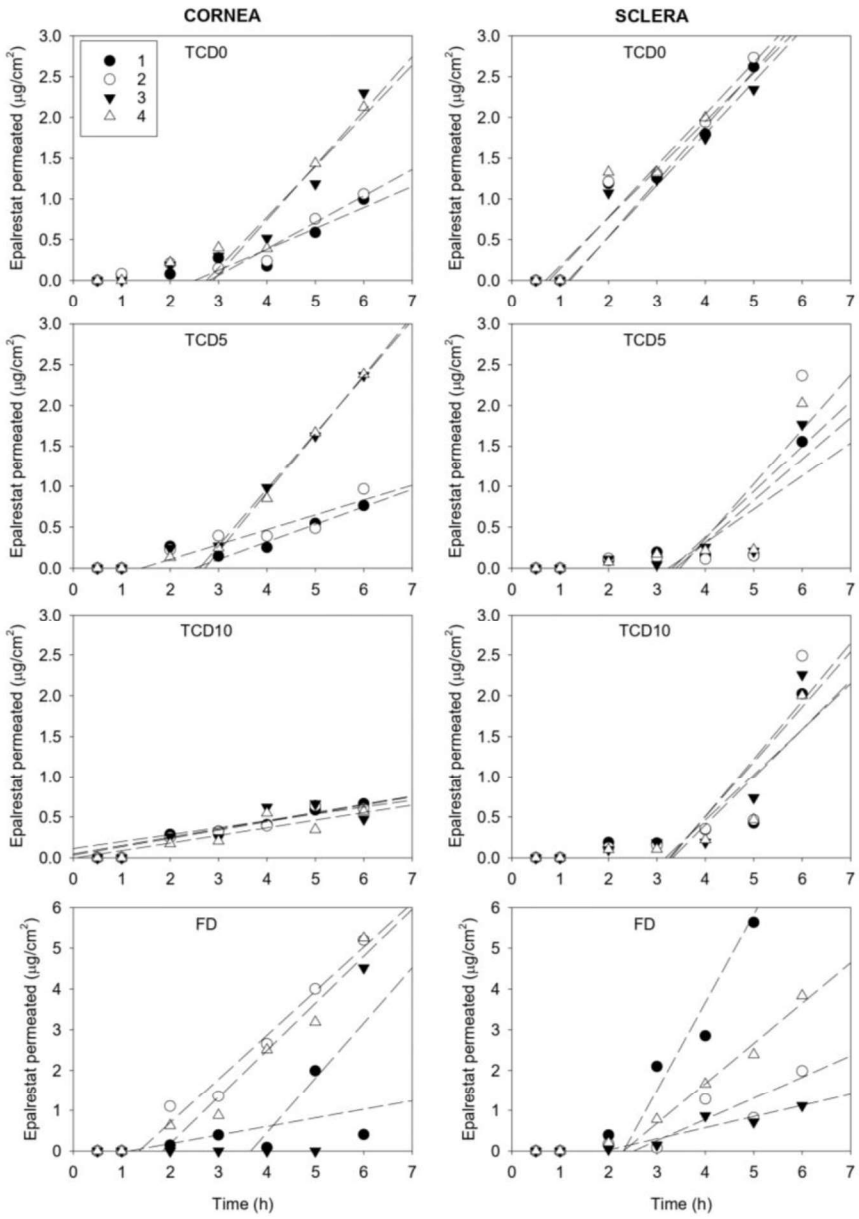

Figure 3.2. Epalrestat permeability data through cornea and sclera recorded for four independent replicates of each niosome formulation (TCD0, TCD5, TCD10) and control epalrestat solution (200 µg/mL).

Scleral permeation. Scleral permeation was performed the same way as corneal permeation, except the tissue used to permeate through was the porcine sclera instead of the porcine cornea.

IR-Raman. Porcine cornea and sclera were permeated with TCD0, TCD5, and TCD10 niosomes for 6 h under the same conditions as the corneal and scleral permeation experiment described above. The IR-Raman study was performed by taking a minimum of 3 points and a maximum of 6 points per cornea and per sclera (**Figures 3.3 and 3.4**) and measuring the Raman scattering of the surface. Furthermore, a line scan was performed in the x-z plane (**Figures 3.5-3.7**). The excitation wavelength was 532.188 nm, the sample was kept at a temperature of 8 °C for the duration of the experiment, the laser power was 3 mW, and each point was measured with 60 accumulations, with an integration time of 0.3 s and an objective of ×50 (Zeiss LD EC Epiplan-Neofluar Dic 50×/0.55). The measurement was done on the top and bottom part of the tissue, and the absolute height of the peak (**Figure 3.8**) (CCD cts) was compared between the top and bottom of each tissue. For the line scan, spectra were accumulated by taking 30 spectra per line and 15 lines per image, each spectrum at a distance of 1 µm from the previous point, both in the x and the z direction.

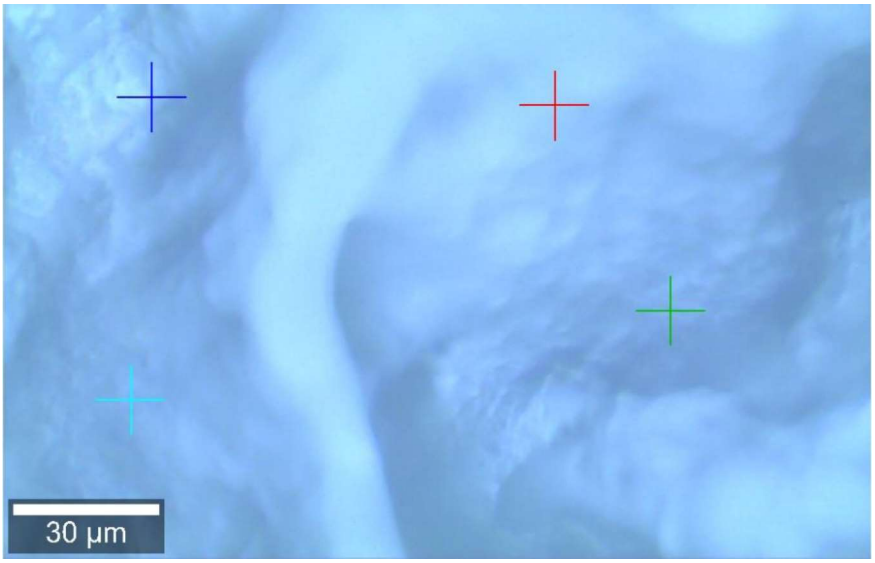

Figure 3.3. Image of the cornea sample free drug cornea top under x50 magnification, with the crosses indicating the locations the RAMAN spectrum was taken.

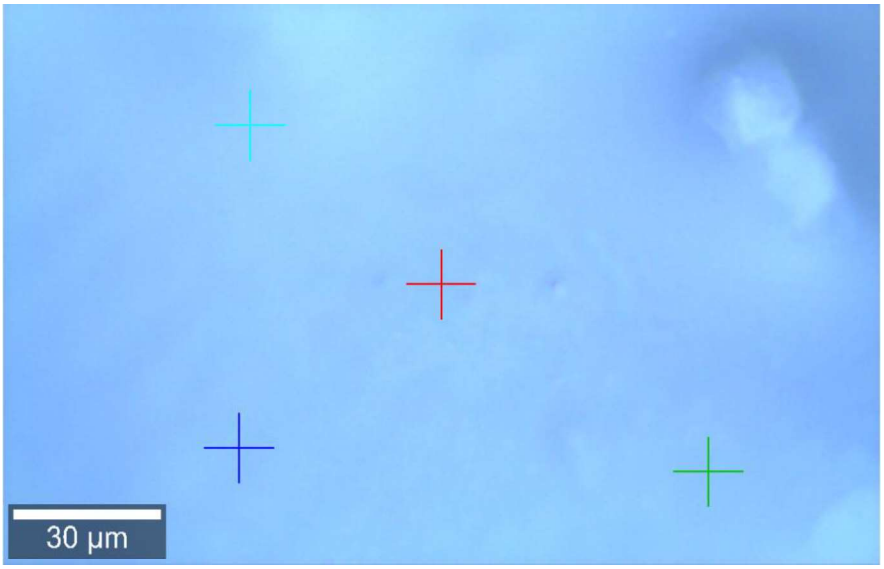

Figure 3.4. Image of the cornea sample free drug cornea bottom under x50 magnification, with the crosses indicating the locations the RAMAN spectrum was taken.

Figure 3.5. Image of the cornea sample TCD0 cornea bottom under x50 magnification, with the line indicating the locations the RAMAN spectra were taken.

Figure 3.6. Image of the cornea sample TCD5 cornea bottom under x50 magnification, with the line indicating the locations the RAMAN spectra were taken.

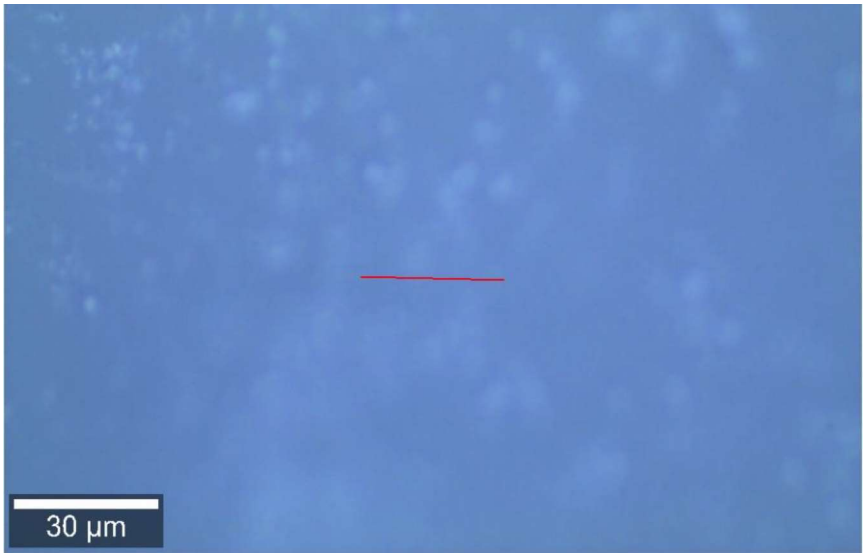

Figure 3.7. Image of the cornea sample TCD10 sclera bottom under x50 magnification, with the line indicating the locations the RAMAN spectra were taken.

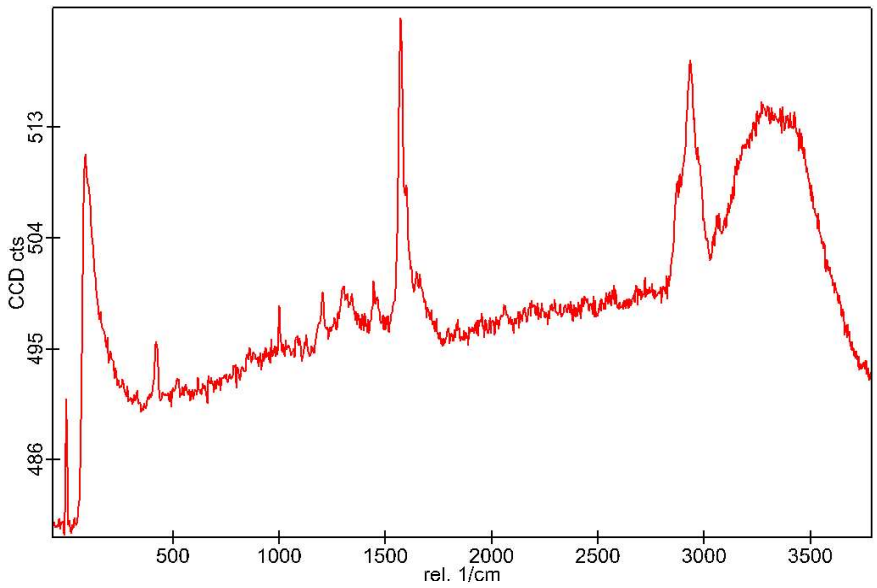

Figure 3.8. Raman spectrum of sample free drug cornea top at the blue cross in **Figure 3.3**.

Statistical analysis. All conditions in the experiments were carried out in triplicate, and the data were shown as an average with a standard deviation when possible. Statistical analysis was carried out in Origin, making use of a one-way analysis of variance (one-way ANOVA) with Tukey's comparison for evaluation. The difference between groups was statistically significant when the p-value was lower than 0.05.

3.3 RESULTS

3.3.1 Niosome Characterization

Cationic niosomes were chosen to allow for efficient encapsulation [37], enhanced stability of the nanoparticles in suspension [38], increased ocular retention time [39], and increased bioavailability [40]. To prepare niosomes, the ratio of surfactant to helper lipids determined the stiffness and curvature of the bilayer. The incorporation of cholesterol changes the assembly of the bilayer as it lodges itself between the hydrophobic tails with the exception of its hydroxyl group [41,42]. In cell membranes, this translates into lowering the membrane permeability to water-soluble molecules, increasing the packing order of the lipids, reducing the bilayer fluidity, and separating the lipid tails to prevent crystallization [43,44,45].

The ratio of cholesterol incorporated in the niosomes affected the physicochemical properties as it intercalated itself within the organic chains of the surfactant in the niosome. The final mol fraction of cholesterol was determined by preparing and characterizing six formulations with different ratios of Tween 60 to cholesterol in terms of size, zeta- potential, and polydispersity index (**Table 3.2**). The short-term stability of the niosomes was assessed by running the same

characterization experiments after 24 h. The size converged towards a similar size between 120 and 170 nm (**Table 3.2**). Formulations 5 and 6, which were outliers and had a hydrodynamic radius of 273.5 and 340.3 nm at t0, showed a decrease in size to 129.3 and 148.5 nm, respectively, after 24 h equilibration. The size of formulations 1 to 3 increased between 10 and 20 nm. Only formulation 4, containing a 0.5 mol fraction of cholesterol, stayed stable at the same size. The PDI remained stable while the zeta-potential rose across all samples. As the PDI of all formulations was similar, the initial greater size of formulations 5 and 6 could be due to the creation of multilamellar vesicles, which then evolved into smaller vesicles [46,47,48]. Due to the acceptable stability of formulation 3 with regards to size (+12 nm) and PDI (−0.03) while having similar zeta-potential stability (+2.84 mV) as all formulations, formulation 3 was chosen. It fitted our desired characteristics the most for cationic niosomes, having a size closest to 100 nm, a zeta-potential high enough to compensate with DOTMA incorporation, and a small size dispersion. The molar fraction of cholesterol was kept at 0.4 for all subsequent niosomal formulations.

Table 3.2. Size, PDI, and zeta-potential of Tween 60/cholesterol niosomes at t = 0 and t = 24 h were used to determine the molar fraction of cholesterol used in subsequent experiments.

Formulation	Time t = 0			Time t = 24 h		
	Size (nm)	PDI	Zeta-Potential (mV)	Size (nm)	PDI	Zeta-Potential (mV)
1	155.0 ± 53.3	0.51 ± 0.02	−14.53 ± 0.32	172.3 ± 52.9	0.55 ± 0.11	−12.11 ± 0.84
2	162.3 ± 63.2	0.54 ± 0.02	−19.83 ± 0.26	174.0 ± 34.2	0.47 ± 0.11	−15.16 ± 0.51
3	108.8 ± 13.4	0.58 ± 0.14	−17.82 ± 0.48	120.8 ± 12.7	0.55 ± 0.13	−14.98 ± 1.29
4	158.6 ± 62.6	0.60 ± 0.14	−24.43 ± 0.38	154.2 ± 30.6	0.54 ± 0.05	−21.79 ± 1.75
5	273.5 ± 59.7	0.57 ± 0.02	−24.04 ± 0.26	129.3 ± 13.8	0.47 ± 0.05	−20.21 ± 0.22
6	340.3 ± 71.8	0.54 ± 0.03	−24.64 ± 0.37	148.5 ± 25.0	0.55 ± 0.08	−23.88 ± 0.70

Niosomes with three different molar ratios of DOTMA were characterized in terms of size, zeta-potential, and PDI (**Table 3.3, Figure 3.9**). Increasing the DOTMA concentration decreased the size and polydispersity index while increasing the zeta potential. The pH of formulations was between 4.26 and 4.35. The encapsulation efficiency was between 99.22% ± 0.24 and 99.76% ± 0.35, and the drug loading was in the range of 25 to 26 mg epalrestat/g niosome for the three formulations.

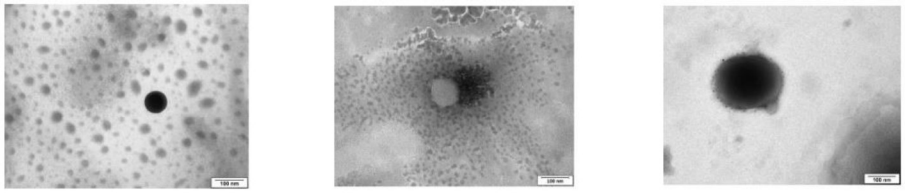

Figure 3.9. TEM images of epalrestat-loaded niosomes were used to assess the morphology of the niosomes (spherical) (from top to bottom: TCD0, TCD5, and TCD10). Scale bar 100 nm.

Niosome dispersions behave as pseudoplastic (**Table 3.3**) with a similar dependence on shear conditions. For a shear rate of 20 s^{-1}, viscosity values of TCD0, TCD5, and TCD10 were 3.62, 4.23, and 3.32 mPa·s. Slightly high viscosity was recorded at very low shear rates, which can be related to the fact that relatively large niosomes offer resistance (although low) to start flowing. The obtained viscosity values were in good agreement with those recorded in previous reports [49,50].

Table 3.3. Viscosity values recorded at 35 ºC for the epalrestat-loaded niosomes under increasing shear stress conditions.

TCD0			TCD5			TCD10		
Shear stress(Pa)	Shear rate (s^{-1})	Viscosity (Pa·s)	Shear stress(Pa)	Shear rate (s^{-1})	Viscosity (Pa·s)	Shear stress(Pa)	Shear rate (s^{-1})	Viscosity (Pa·s)
0.05532	3.667	0.01508	0.06584	3.641	0.01808	0.04964	3.424	0.0145
0.05856	7.664	7.64E-03	0.08584	7.64	0.01124	0.05635	7.422	7.59E-03
0.06467	11.66	5.54E-03	0.05987	11.64	5.14E-03	0.0571	11.42	5.00E-03
0.04693	15.67	3.00E-03	0.04123	15.64	2.64E-03	0.05781	15.42	3.75E-03
0.07116	19.66	3.62E-03	0.08314	19.64	4.23E-03	0.06444	19.42	3.32E-03
0.05301	23.66	2.24E-03	0.05154	23.63	2.18E-03	0.06574	23.42	2.81E-03
0.07594	27.66	2.75E-03	0.0685	27.64	2.48E-03	0.07211	27.42	2.63E-03
0.08408	31.66	2.66E-03	0.09397	31.64	2.97E-03	0.07641	31.42	2.43E-03
0.08446	35.66	2.37E-03	0.09725	35.63	2.73E-03	0.07975	35.42	2.25E-03
0.08825	39.66	2.23E-03	0.1009	39.63	2.55E-03	0.0842	39.42	2.14E-03
0.0951	43.66	2.18E-03	0.1059	43.63	2.43E-03	0.0878	43.41	2.02E-03
0.09892	47.66	2.08E-03	0.09583	47.64	2.01E-03	0.09117	47.41	1.92E-03
0.08522	51.66	1.65E-03	0.07739	51.63	1.50E-03	0.0941	51.41	1.83E-03
0.1034	55.65	1.86E-03	0.1159	55.62	2.08E-03	0.1007	55.41	1.82E-03
0.09611	59.66	1.61E-03	0.08602	59.63	1.44E-03	0.1021	59.41	1.72E-03
0.1154	63.65	1.81E-03	0.1254	63.63	1.97E-03	0.1083	63.41	1.71E-03
0.1069	67.65	1.58E-03	0.1148	67.62	1.70E-03	0.111	67.41	1.65E-03
0.1015	71.65	1.42E-03	0.09972	71.62	1.39E-03	0.1137	71.41	1.59E-03
0.1076	75.65	1.42E-03	0.1007	75.62	1.33E-03	0.1173	75.4	1.56E-03
0.1092	79.65	1.37E-03	0.105	79.62	1.32E-03	0.1214	79.41	1.53E-03
0.1174	83.65	1.40E-03	0.1225	83.62	1.47E-03	0.1258	83.4	1.51E-03
0.1359	87.64	1.55E-03	0.149	87.62	1.70E-03	0.1342	87.4	1.54E-03
0.1323	91.65	1.44E-03	0.1274	91.63	1.39E-03	0.1348	91.4	1.48E-03
0.1328	95.64	1.39E-03	0.1418	95.61	1.48E-03	0.1387	95.4	1.45E-03
0.1377	99.65	1.38E-03	0.1318	99.63	1.32E-03	0.1423	99.41	1.43E-03
0.1522	103.6	1.47E-03	0.1651	103.6	1.59E-03	0.1513	103.4	1.46E-03
0.1454	107.6	1.35E-03	0.1533	107.6	1.43E-03	0.1505	107.4	1.40E-03
0.1419	111.6	1.27E-03	0.1424	111.6	1.28E-03	0.1523	111.4	1.37E-03
0.1448	115.6	1.25E-03	0.144	115.6	1.25E-03	0.1554	115.4	1.35E-03
0.1531	119.6	1.28E-03	0.1575	119.6	1.32E-03	0.1603	119.4	1.34E-03
0.1687	123.6	1.36E-03	0.1819	123.6	1.47E-03	0.1711	123.4	1.39E-03

0.1713	127.6	1.34E-03	0.1753	127.6	1.37E-03	0.1756	127.4	1.38E-03
0.1597	131.6	1.21E-03	0.1567	131.6	1.19E-03	0.1715	131.4	1.31E-03
0.1823	135.6	1.34E-03	0.1924	135.6	1.42E-03	0.1862	135.4	1.38E-03
0.1725	139.6	1.24E-03	0.1766	139.6	1.27E-03	0.1796	139.4	1.29E-03
0.1708	143.6	1.19E-03	0.1654	143.6	1.15E-03	0.1869	143.4	1.30E-03
0.1849	147.6	1.25E-03	0.1875	147.6	1.27E-03	0.1972	147.4	1.34E-03
0.1938	151.6	1.28E-03	0.2019	151.6	1.33E-03	0.2048	151.4	1.35E-03
0.1956	155.6	1.26E-03	0.2028	155.6	1.30E-03	0.2084	155.4	1.34E-03
0.1898	159.6	1.19E-03	0.1882	159.6	1.18E-03	0.2087	159.4	1.31E-03
0.1885	163.6	1.15E-03	0.1863	163.6	1.14E-03	0.2041	163.4	1.25E-03
0.213	167.6	1.27E-03	0.2286	167.6	1.36E-03	0.2169	167.4	1.30E-03
0.1975	171.6	1.15E-03	0.1967	171.6	1.15E-03	0.2212	171.4	1.29E-03
0.2211	175.6	1.26E-03	0.236	175.6	1.34E-03	0.2264	175.4	1.29E-03
0.2039	179.6	1.14E-03	0.2024	179.6	1.13E-03	0.2218	179.4	1.24E-03
0.2104	183.6	1.15E-03	0.2114	183.6	1.15E-03	0.2377	183.4	1.30E-03

The loaded niosomes were kept at 4 °C and 25 °C for 7 days and evidenced a slight increase in size and zeta-potential, while no significant changes were recorded in poly- dispersity index and encapsulation efficiency (**Table 3.5**). The niosomes were characterized again after two months at room temperature (**Table 3.4**). The size of the niosomes increased slightly while the PDI decreased slightly. The small decrease in the size of the niosomes when loaded with epalrestat may be due to the ability of the drug to disrupt the niosomal bilayer structure. Epalrestat is a hydrophobic drug that can partition into the hydrophobic region of the bilayer, causing the surfactants to rearrange themselves around the drug molecules. The rearrangement of the surfactants would lead to a slight reduction in the size of the niosomes [51,52]. The zeta-potential, however, increased except for the 10% DOTMA sample. The pH remained constant.

Table 3.4. Size, PDI, zeta-potential of epalrestat loaded Tween 60/cholesterol niosomes with 0, 5, and 10 mol% DOTMA at time 0 and after 2 months at room temperature.

Formulation	Time t = 0			Time t = 2 Months		
	Size (nm)	PDI	Zeta-Potential (mV)	Size (nm)	PDI	Zeta-Potential (mV
TCD0	84	0.54	−23.34 ± 5.34	91	0.52	+1.75 ± 5.77
TCD5	68	0.46	+17.27 ± 10.29	93	0.36	+31.80 ± 7.58
TCD10	75	0.28	+40.39 ± 10.29	110	0.26	+42.07 ± 8.26

Niosome dispersions behave as pseudoplastic (**Table 3.3**) with a similar dependence on shear conditions. For a shear rate of 20 s^{-1}, viscosity values of TCD0, TCD5, and TCD10 were 3.62, 4.23, and 3.32 mPa·s. Slightly high viscosity was recorded at very low shear rates, which can be related to the fact that relatively large niosomes offer resistance (although low) to start flowing. The obtained viscosity values were in good agreement with those recorded in previous reports [49,50].

The loaded niosomes were kept at 4 °C and 25 °C for 7 days and evidenced a slight increase in size and zeta-potential, while no significant changes were recorded in polydispersity index and encapsulation efficiency (**Table 3.5**). The niosomes were characterized again after two months at room temperature (**Table 3.4**). The size of the niosomes increased slightly while the PDI decreased slightly. The small decrease in the size of the niosomes when loaded with epalrestat may be due to the ability of the drug to disrupt the niosomal bilayer structure. Epalrestat is a hydrophobic drug that can partition into the hydrophobic region of the bilayer, causing the surfactants to rearrange themselves around the drug molecules. The rearrangement of the surfactants would lead to a slight reduction in the size of the niosomes [51,52]. The zeta-potential, however, increased except for the 10% DOTMA sample. The pH remained constant.

Table 3.5. The difference in size, PDI, zeta-potential, and drug content of epalrestat loaded Tween 60/cholesterol niosomes with 0, 5, and 10 mol% DOTMA after 7 days in storage at 4 °C and 25 °C.

Formulation	Δ Size (nm)		Δ Zeta-Potential (mV)		Δ Polydispersity Index		Δ Encapsulation Efficiency (%)	
	4 °C	25 °C	4 °C	25 °C	4 °C	25 °C	4 °C	25 °C
TCD0	22.1	26.3	−2.3	−3.6	−0.14	0.13	−1.2	−0.1
TCD5	33.0	59.1	11.1	7.9	−0.27	0.08	−1.1	−0.2
TCD10	17.9	14.6	21.4	26.3	−0.05	0.01	−0.7	−0.4

3.3.2 Epalrestat Release

The release study was carried out in water containing 1% Tween 80 to ensure sink conditions, as epalrestat has a solubility in water of 0.047 mg/mL. With the results from the encapsulation efficiency, the final concentration of epalrestat was between 0.199 and 0.200 mg/mL in the dialysis bag, meaning that 100% epalrestat release corresponds to 1 mg released. The release profile of the niosomes over time is shown in **Figure 3.10** In the first 8 days, epalrestat released from the niosomes negatively correlated with the DOTMA percentage of the niosome. However, after 10 days, 0% DOTMA niosomes showed a lower release rate, which may be related to its greater stability. These niosomes were the ones that changed their size during storage (**Table 3.4**), which indicates that they are less prone to destabilize.

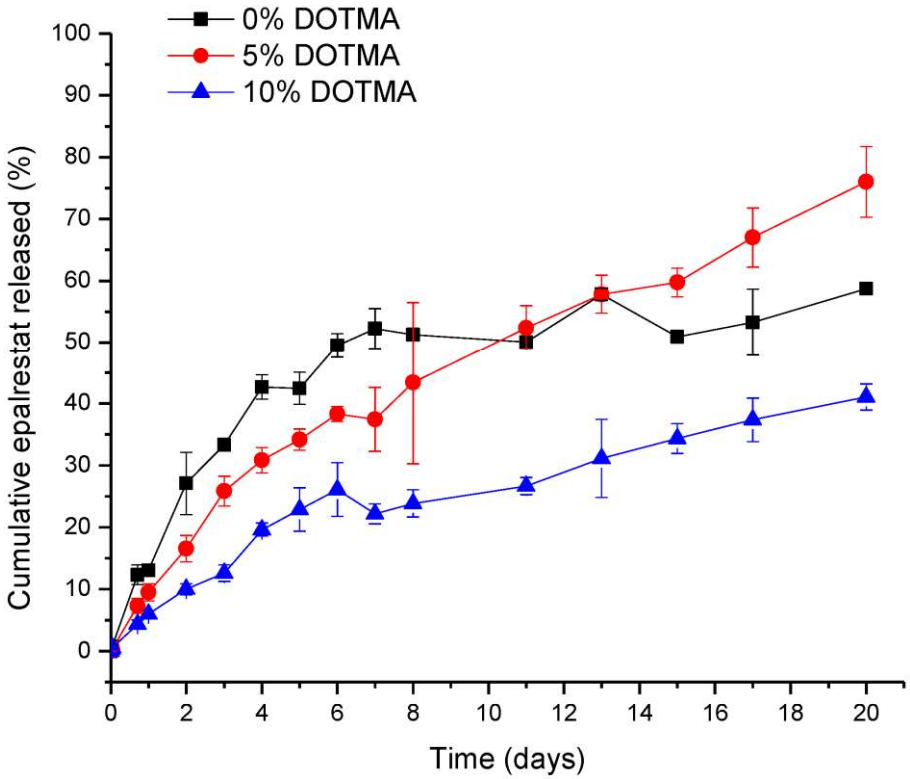

Figure 3.10. The release profile of epalrestat encapsulated in niosomes in Tween 80 1% aqueous medium at 20 °C over 20 days.

Another release experiment was carried out at 37 °C to mimic inside the back of the human eye. The amounts of released epalrestat over 24 h and non-released epalrestat are summarized in **Table 3.6**. The mass balance turned out to be about 96% for the niosomes, including DOTMA in their formulation, and 98.6% for niosomes without DOTMA. This finding indicated that niosomes protect epalrestat from degradation, which contrasts with the degradation of unencapsulated epalrestat in an aqueous medium [48]. This finding also confirms that niosomes are stable in the release medium.

Table 3.6. Amounts of epalrestat released and remaining in the niosomes after 24 h in Tween 80 1% aqueous medium at 37 °C.

Formulation	Epalrestat Released after 24 h (%)	Epalrestat Remaining in the Niosomes (%)	Sum of Released and Non-Released Epalrestat (%)
TCD0	12.9 ± 0.50	85.7 ± 0.82	98.6 ± 0.66
TCD5	11.7 ± 0.33	84.3 ± 1.42	96.0 ± 0.87
TCD10	10.3 ± 0.53	86.2 ± 0.97	96.5 ± 0.75

3.3.3 HET-CAM Assay

The HET-CAM assay was performed using the three epalrestat-loaded niosomal formulations, one unloaded niosome formulation, and epalrestat dissolved in 10/90 v/v ethanol-water solution. The HET-CAM assay is not considered an animal experiment under Directive 2010/63/EU [53] as no nervous system is developed before day 11 of the embryo development. The positive (0.1 M NaOH) and negative controls (0.9% NaCl) had ocular irritability potential scores of 19.04 and 0, respectively. Epalrestat solution (0.2 mg/mL) (**Figure 3.11A**) triggered blood coagulation and had a score of 18.58. Differently, the loaded and unloaded niosomes did not show any noticeable hemorrhage of the blood vessels (**Figure 3.11B–E**) and obtained a score of 0. This indicated that the encapsulation of epalrestat decreases the ocular irritability potential and, therefore, allows for topical administration.

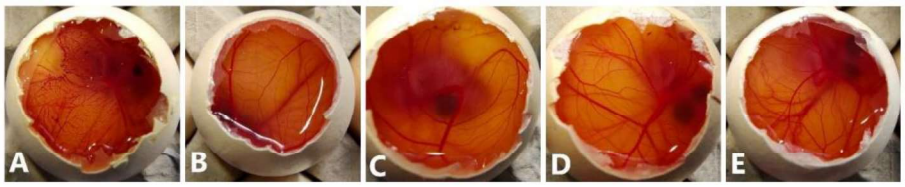

Figure 3.11. Pictures of the chorioallantoic membrane after 300 s (**A**): epalrestat dissolved in 10/90 ethanol/water (0.2 mg/mL), (**B**): unloaded TCD0 niosomes, (**C**–**E**): loaded niosomes (0.2 mg/mL) (**C**): TCD0, (**D**): TCD5, (**E**): TCD10.

3.3.4 Gluc-HET Assay

To measure the effect on the blood glucose level, the gluc-HET [29] test was chosen as it presents a few advantages. It is not considered an animal experiment under Directive 2010/63/EU [53] as no nervous system is developed before day 11 of the embryo development. Furthermore, the embryos exhibit high glucose levels that are susceptible to insulin without interference from naturally produced insulin, which starts on day 12. Both the TCD0 and TCD10 loaded niosomal formulations behaved the same way as the epalrestat in solution (**Figure 3.12**) in that they reduced the blood glucose levels in a similar fashion to the positive control (glibenclamide). Tests carried out on the effect of the developmental stage on assay performance revealed a significant increase in the sensitivity of the embryos to the glucose-reducing compounds for day 10 and day 11 embryos [29]; therefore, day 11 was chosen to perform the experiment. Formulation TCD5 exhibited blood glucose level reduction but in a lower amount than the positive control.

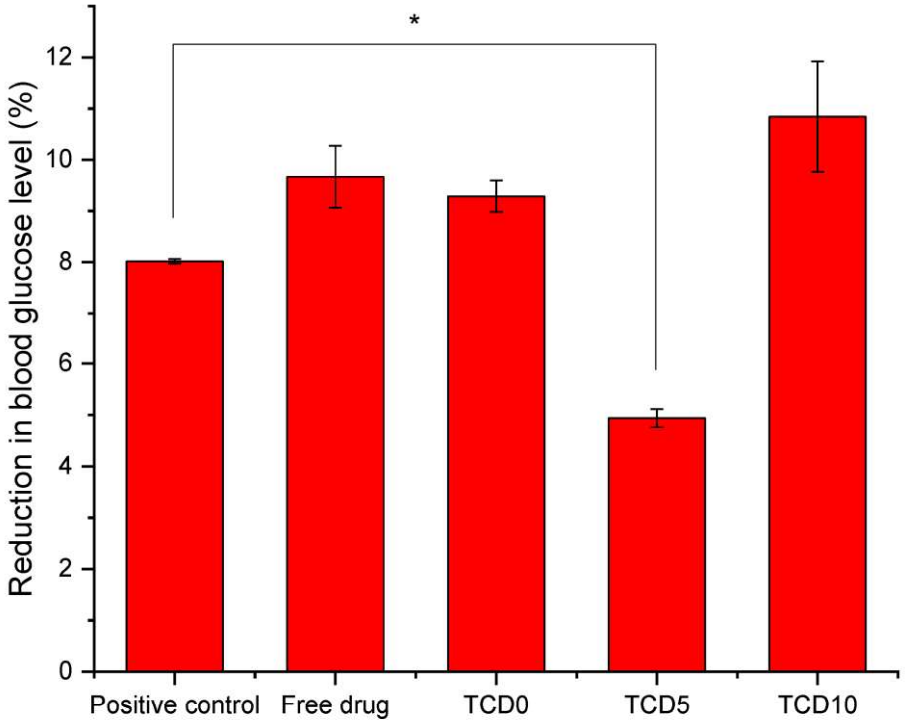

Figure 3.12. Blood glucose level after exposure to glibenclamide, epalrestat in 10/90 ethanol/water solution, TCD0, TCD5, and TCD10 niosomes loaded with epalrestat. * Statistically significant differences ($p < 0.05$).

3.3.5 Zebrafish Embryotoxicity Assay

Zebrafish embryotoxicity tests have been increasing in use for developmental toxicology and ToxCast high-throughput screening of chemicals and nanomaterials [54] due to the high concordance between zebrafish and mammalian studies demonstrating its potential to reduce and refine, if not replace animal studies [30,31,32]. The survival of Danio rerio (zebrafish) embryos was therefore measured after 96 h of exposure to loaded niosomes TCD0, TCD5, and TCD10 (**Table 3.7**).

Table 3.7. Survivability of zebrafish embryos after 96 h of exposure to different loaded niosome formulations.

Tested Formulation	Survival of **Danio rerio** (%)	
	5 µL Solution Exposure	10 µL Solution Exposure
Negative control	98.0	96.7
TCD0	98.0	56.7
TCD5	93.0	60.0
TDC10	96.6	43.3
Epalrestat in solution	57.5	40.0

With 5 µL solution, exposure formulation epalrestat-loaded niosomes were all highly compatible with the zebrafish embryos and demonstrated that the niosome encapsulation reduced the toxicity of epalrestat significantly.

3.3.6 Corneal and Scleral Permeation

Epalrestat from formulations TCD0, TCD5, and TCD10 permeated at different rates through the porcine cornea and sclera (**Figure 3.13**). The steady-state flux and lag time were obtained from the slope and x-intercept of the linear regressions of the curves in **Figure 3.13** (individual plots are shown in **Figure 3.1**) and used to calculate the permeability coefficient (**Table 3.8**) [55]. Encapsulated epalrestat permeation through the cornea was lower compared to epalrestat in solution (ANOVA; $F_{3,12} = 9.32$; $p < 0.05$). Differently, no statistically different results were recorded for permeability through the sclera for epalrestat in niosomes compared to free drug. Compared to the free drug solution, formulation in niosomes provided more reproducible data with less variability, and as expected, permeability coefficients through sclera were greater than through cornea, particularly in the case of the most cationic niosomes (TDC10) (**Table 3.8**).

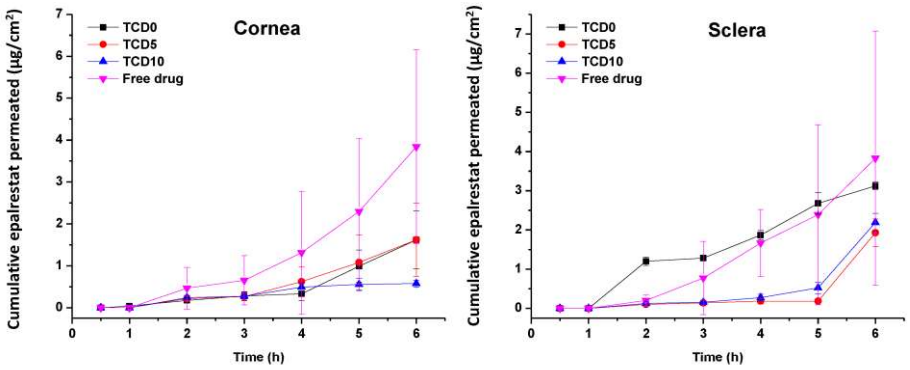

Figure 3.13. Amounts of encapsulated epalrestat permeated through the cornea (**left**) and sclera (**right**) after 6 h permeation experiment in Franz's diffusion cells.

Table 3.8. Steady-state flux, lag time, and permeability coefficient of different tissues and formulations.

Sample		Steady State Flux (µg/cm² × h)	Lag Time (min)	Permeability Coefficient (×10⁶ cm/s)
Cornea	Free drug	1.029 (0.356)	152 (66)	1.43 (0.49)
	TCD0	0.469 (0.204)	163 (12)	0.65 (0.28)
	TDC5	0.453 (0.295)	138 (36)	0.63 (0.40)
	TDC10	0.095 (0.008)	33 (32)	0.13 (0.01)
Sclera	Free drug	0.887 (0.758)	118 (4)	1.23 (1.09)
	TCD0	0.634 (0.035)	57 (16)	0.88 (0.05)
	TDC5	0.538 (0.110)	201 (6)	0.75 (0.15)
	TDC10	0.636 (0.070)	196 (4)	0.88 (0.09)

TCD5 and TCD10 niosomes displayed lower accumulation in corneal tissue than TCD0 niosomes and the epalrestat in solution. The niosomes showed lower drug accumulation than the epalrestat in solution in scleral tissue (**Figure 3.14**).

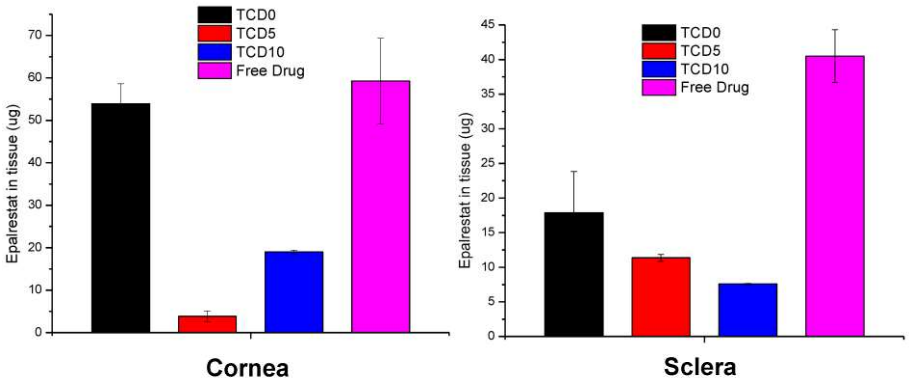

Figure 3.14. Epalrestat retained in corneal (**left**) and scleral (**right**) tissue after 6 h permeation experiment in Franz's diffusion cells.

3.3.7 IR-Raman

To confirm the permeation of epalrestat through the different tissues IR-Raman spectroscopy was performed on corneal and scleral porcine tissues after 6 h permeation experiments in Franz's diffusion cells. The ratio of the Raman spectrum peak for epalrestat from the top part of the tissue (in contact with the donor chamber) to the bottom part of the tissue (in contact with the receiving chamber) was taken as an indication for confirmation of permeation of epalrestat through the tissue (**Figure 3.15**). Furthermore, pictures were assembled using accumulations of Raman spectra in a plane throughout the different tissues. This allowed for the production of heat maps showing the concentration of epalrestat at different levels of the tissue. Samples of TCD0 cornea, TCD10 cornea, and TCD10 sclera were able to produce readable pictures (**Figure 3.16**). This can be difficult due to the focus of the laser on the sample changing as the tissue moves with dehydration and burning. White lines were used to mark the tissue delimitation on the heat maps.

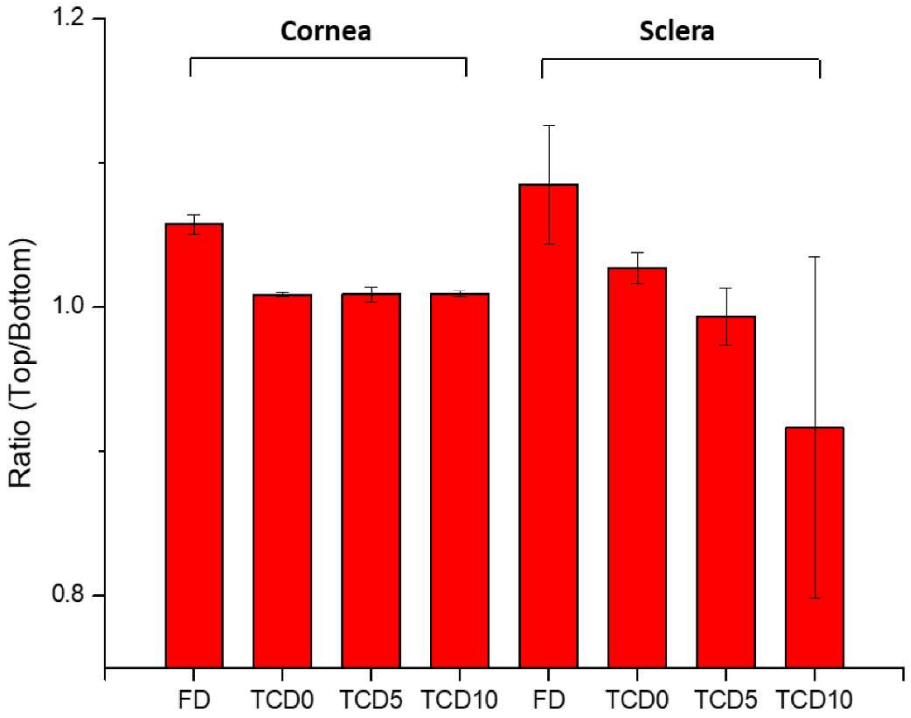

Figure 3.15. The ratio of the top-to-bottom intensity of Raman peaks indicates the presence of epalrestat in the tissue's outside layer.

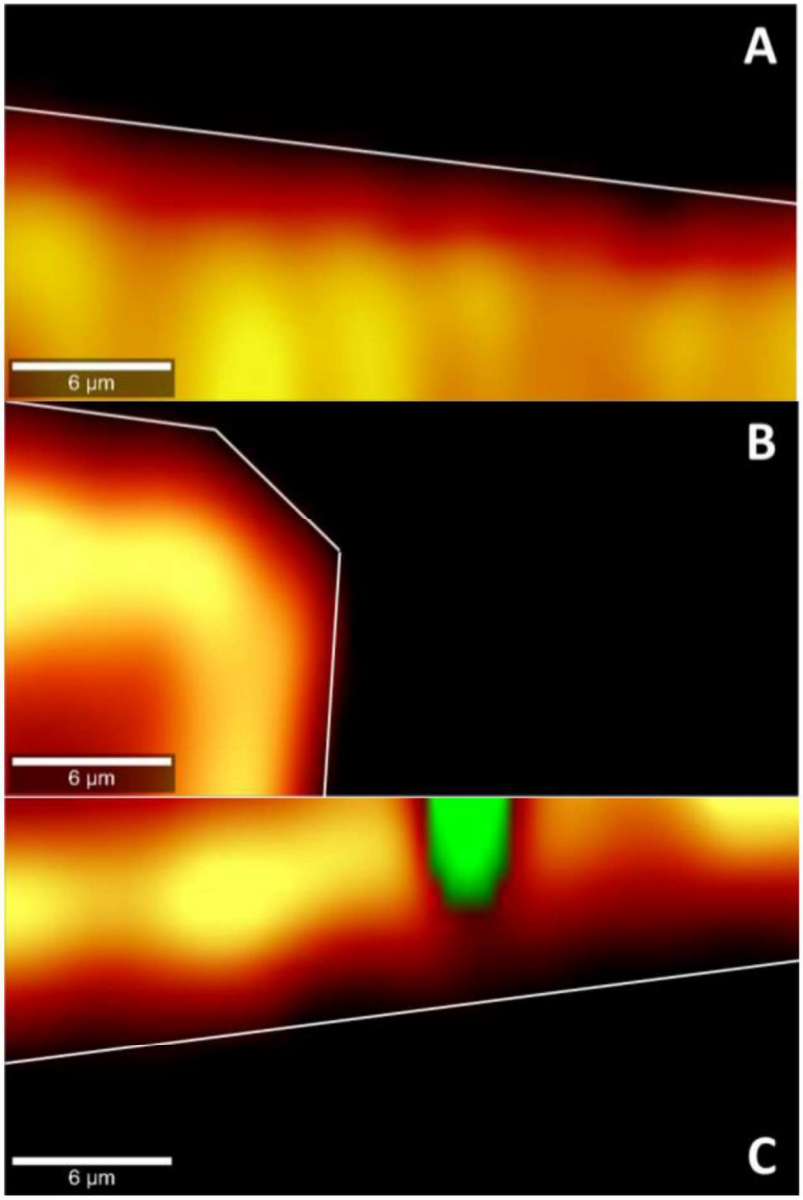

Figure 3.16. Cross-section heat map of epalrestat concentration in a 30 × 15 µm plane of the bottom of the cornea or the sclera after 6 h permeation of niosomes loaded with epalrestat (**A**): TCD0 cornea, (**B**): TCD10 cornea, (**C**): TCD10 sclera. Scale bar: 6 µm.

The ratio of top-to-bottom peak height was close to 1 for TCD0 cornea, TCD5 cornea, TCD10 cornea, and TCD5 sclera, indicating an equal presence of epalrestat on both sides of the tissue, while it is superior to 1 for FD cornea, FD sclera, and TCD0 sclera, indicating a higher presence of epalrestat on the side of the tissue in contact with the donor chamber than the side of the tissue in contact with the receiving chamber. TCD10 sclera is the outlier with a ratio lower than 1, which indicated a higher presence of epalrestat on the side of the tissue in contact with the receiver chamber. This indicates that permeation was confirmed in all tissues with various degrees.

In the pictures of cross sections of the tissue after permeation for 6 h with different epalrestat-loaded niosomal formulations, the heat map (the more yellow, the higher the concentration) represents the concentration of epalrestat in the tissue, while the green represents laser burning. **Figure 3.16A,B** showed the concentration of epalrestat from formulation TCD0 in the corneal tissue, with **Figure 3.16A** having channels of high concentration of epalrestat from formulation TCD10 in the z-orientation, and **Figure 3.16B** showing a bump in the tissue that got permeated both from the top and from the side. Finally, **Figure 3.16C** depicts the scleral tissue that suffered a burn due to laser exposure, represented in the green dot, which was explained by the higher susceptibility of the sclera to absorb light emitted by the laser and overheat. It, however, also showed less concentration gradient of epalrestat in the depth of the tissue. These findings go in the direction of the top-bottom ratio of samples TCD0 cornea, TCD10 cornea, and TCD10 sclera.

3.4 DISCUSSION

To the best of our knowledge, this study is the first of its kind encapsulating epalrestat in niosomes and characterizing them in depth. Niosomes were designed by first choosing an adapted ratio of cholesterol to Tween 60, then testing the effect of the introduction of DOTMA to change the surface charge and render the niosomes cationic.

Three formulations were chosen, TCD0 as a control (−23 mV), TCD5 with low positive surface charge (+17 mV), and TCD10 as highly cationic (+40 mV). All three formulations exhibited sizes smaller than 100 nm, encapsulation efficiencies above 99%, spherical morphologies, and high stability over two months. When comparing the niosomes to other studies, the size of TCD0 niosomes was 20 nm bigger, and its polydispersity index was bigger than Tween 60/cholesterol prepared with the ethanol injection method [56]. The ethanol injection method is known to give more uniform niosomes [57] but is not appropriate for the encapsulation of all drugs. Two other studies made use of cationic niosomes and reported the size and zeta-potential, one substituting lycopene for cholesterol [33] and one substituting Tween 20 for Tween 60 [58]. In the first study, the size (101 nm) and the PDI (0.44) were bigger, and the zeta-potential (+33.8 mV) was lower than the TCD10 formulation. In the second study, the size (130 nm) was bigger, but the PDI (0.14) was smaller than the TCD10 formulation. Here the difference in non-ionic surfactant and helper lipid accounts for the difference in the physicochemical properties [41], as the preparation method was similar. The high encapsulation efficiency of epalrestat may be explained by the highly hydrophobic nature of epalrestat (water solubility of 0.0467 mg/mL [59]) that would tend to remain in the bilayer of the niosome, which is assembled through hydrophobic interactions. An encapsulating effect

of hydrophobic molecules in the bilayer of the niosome was also seen in Span 80 niosomes with an added ionic surfactant [60], blends of Tween60/Span60 anionic niosomes, or Tween 80/Span80 PEGylated systems [61]. A complementary explanation is the length of the alkyl chains (stearyl C18), which usually leads to higher encapsulation efficiencies of hydrophobic cargo. Longer chains tend to display higher entrapment efficiency, with Tween 60 having a longer carbon tail than the lauryl chains (C12) of Tween 20 or Brij 35, for example [62,63]. With these encapsulation efficiencies, epalrestat concentration in the final niosome dispersion was close to 0.2 mg/mL. Niosome morphology (**Figure 3.9**) was spherical with low aggregation, and the size agreed with the DLS data. These images were in line with TEM images of reports describing niosomes made using the thin film hydration method [59].

The release of epalrestat from the niosomes reached 2.6%, 3.2%, and 4.0% after 12 h for the formulations TCD10, TCD5, and TCD0, respectively, which is around therapeutic levels for a tear film volume of 10 µL [13,14]. When releasing hydrophilic molecules, Tween 80/cholesterol niosomes displayed burst release behavior (90% in 1 h), as is the case with (−)-epigallocatechin gallate [52]. Release of lipophilic molecules also showed to be faster with mixed Span 60/Tween 60 cholesterol niosomes loaded with α-tocopherol (40% in 4 h) [64], as with Tween 60 niosomes containing meloxicam (90% in 7 h) [65]. However, it must be noted that these two examples are not exactly similar to our system as the α-tocopherol was released in a simulated gastric environment, and the niosomes containing meloxicam were micrometer size. Furthermore, the behavior of sustained release clashes with previous findings where epalrestat was incorporated into solid-lipid nanoparticles-laden lenses [21], and that showed a burst release. The epalrestat release looked similar to the sustained release

obtained in lens delivery without nanoparticles after the initial release of adsorbed epalrestat [20].

To screen that the formulations are able to be used in eye drop format, alternatives to in vivo experimentation were used: ocular irritability potential assessment with the HET-CAM model, the effect on blood glucose levels using its variation of the gluc-HET assay, and the toxicity using a zebrafish embryotoxicity assay. In the HET-CAM model, the encapsulation of epalrestat decreased ocular irritability by lowering the irritability score of free epalrestat in solution from 18.6 to 0. This demonstrated the ability of niosomes to protect the eye from the irritability potential of epalrestat. In order to make sure that the introduction of this drug/carrier complex would not have a worsening effect on the blood glucose levels of a diabetic patient, it is important to make sure that the blood glucose levels remain the same when epalrestat-loaded niosomes are incorporated into the body. In our case, the niosomal formulation decreased the blood glucose levels at the same level as the positive control. The gluc-HET assay showed that all components lower the blood glucose levels in a similar regard as the positive control (−8 to −10%) with the exception of formulation TCD5. Formulation TCD5, however, still maintained blood glucose level reduction (−5%). These results point toward a possible increased efficacy in the context of diabetic treatment. However, as the mechanism in which these formulations lower blood glucose levels in the chorioallantoic membrane, further investigation is required before imagining epalrestat-loaded cationic niosomes as a glucose reduction agent. Finally, the encapsulation of epalrestat in niosomes increased the survivability of zebrafish embryos from 57.5% to 96% when exposed to 5 µL of the solution. Together these results support the potential use of formulations TCD0, TCD5, and TCD10 topically. When compared to other nanoparticles, such as zinc phthalocyanine and aluminum

phthalocyanine liposomes, our niosomes performed similarly or better; the liposomes achieved between 100% and 65% or 85% survival rates, respectively [66]. Interestingly the results of zebrafish embryo survival with ionic-gradient liposomes go in the opposite direction, as the survival rate dropped when encapsulating bupivacaine in the liposomes [67]. This can be explained by the difference in the release rate of the drugs when encapsulated in niosomes or ionic-gradient liposomes, as the niosome would release epalrestat slower into the zebrafish larvae (2.5–4% for epalrestat against 65–100% for bupivacaine). Furthermore, a positive correlation between DOTMA percentage and mortality was observed (**Table 3.7**), which was to be expected as cationic nanoparticles are known to cause mortality in zebrafish embryos [68]. Therefore, it was expected that formulations TCD0 and TCD5 would be safer than TCD10.

The permeation of epalrestat from the niosomal formulations through the porcine sclera and the cornea was also monitored, reaching 2.5 μg/cm^2 corneal permeation after 6 h in the case of TCD5. When compared to the study utilizing hydrogel lenses to deliver epalrestat [20], the amount of epalrestat accumulated in the tissues is higher using niosomes. However, it must be noted that our experiment took place on porcine cornea instead of bovine cornea, which is thinner. Also, in the previous study with epalrestat loaded in contact lenses, no drug was detected in the receptor after the 6 h test [20], which can be related to the lower drug concentration in the donor chamber that the contact lenses were able to supply. Indeed, in that previous study, the epalrestat control solution was 40 μg/mL, namely, five times lower than the control solution of free drug tested in our present study (200 μg/mL). That diluted free epalrestat solution facilitated the accumulation of only 10 μg drug in the bovine cornea [20], which is approximately 5 times less than the accumulation achieved in the present study. The results

indicate that there is a therapeutic amount of epalrestat [14] that can be delivered to the cornea and the sclera with formulation TCD0. Further investigation needs to be done to confirm the accumulation of epalrestat in further tissues, but the results of our permeation experiments are positive as to the amounts of epalrestat able to traverse the cornea and sclera. The epalrestat steady-state flux obtained for the niosomal formulations is in the same order of magnitude as those recorded for skin formulations prepared with permeability enhancers [69]. The permeability coefficients recorded for epalrestat in niosomes were also in the range of that recorded for epalrestat solution in the mucosal-to-serosal transport through jejunum [70]. The lower permeability recorded for the most cationic niosomes through the cornea may be related to a higher binding to the cornea surface, which may hinder further diffusion of the niosomes and also of the drug encapsulated inside. Indeed, cationic liposomes have been demonstrated to prolong the retention time on the ocular surface [39]. Therefore, the charge density of niosomes should be the result of a compromise between the extended time of permanence on the ocular surface and efficient delivery of epalrestat to the inner eye tissues. It should also be noted that the niosomes have a certain thickening capability increasing 3 to 4 times the viscosity compared to the aqueous medium.

With the help of IR-Raman spectroscopy, drug permeation through the cornea and sclera was evidenced through the whole cross-sections of these tissues. A ratio of the Raman spectrum intensity taken from the top and bottom of the surface of the tissue equal 1, indicating that the concentration of epalrestat was similar on the tissue in contact with the donor as with the receiver chamber after 6 h of application of the formulation. The high values of the ratios of FD cornea (1.06) and FD sclera (1.09) can be explained by the faster access of unencapsulated epalrestat when it is free in solution. The staining of the tissue with the

typical yellow color of epalrestat was also perceptible by the naked eye. The low value of the ratio for TCD10 sclera (0.92) is unusual but could be explained by interference from gasses liberated during the analysis process if the sample started to burn. Indeed, the peak of epalrestat situated at 1575 cm^{-1} is close to that of carbon (1581 cm^{-1}) [71]. This also would explain the great variance in the results between the four measuring points. The heat maps of the cornea and sclera show the presence of epalrestat inside the tissue, permeating in different channels, adding weight to the results obtained from the Franz cell permeation experiments. While Raman spectroscopy has been used on ocular media for the detection of ganciclovir in ocular media in vivo [72] or for the detection of glutamate in tissues [73], this is, to our knowledge, the first time IR-Raman was used to confirm drug permeation through ocular tissues.

Epalrestat is a highly hydrophobic drug, and we found that it can be efficiently encapsulated in niosomes. The niosomes increase the drug's apparent solubility and stability in water, which makes the preparation of eyedrops possible. Moreover, niosomes protect from the irritancy that a pure drug solution causes on the ocular surface. According to our results, the niosomes do not release epalrestat during storage but only when subjected to a strong dilution in the presence of other surfactant molecules, which may resemble the conditions on the ocular surface. The formulation TCD5 seemed to be the most balanced, as it was cationic, had sustained release of epalrestat over a long period, was safe for the ocular surface, and permeated both the cornea and the sclera. The capability to sustain drug release in vitro means that most part of the drug dose remains in niosomes when topically placed on the eye, and niosomes have been reported to enhance drug permeability in vivo [24]. Some previous reports on drug-loaded niosomes for ocular delivery have also shown in vitro sustained release in the frame of a few

days for hydrophobic drugs such as fluconazole [74] and natamycin [75] or even mid-polarity drugs such as vancomycin [76], doxycycline [77] or naltrexone [78]. In vivo, studies evidenced the success of the niosome approach compared to the free drug solution, indeed probably due to the more sustained release. Niosomes have been shown to remain on the ocular surface longer than the drug solution. Thus, a sustained release may prevent a very rapid washout from the ocular surface while still creating a drug concentration gradient that facilitates the diffusion through eye tissues [24].

3.5 CONCLUSIONS

Our study demonstrated the ability of cationic niosomes to encapsulate epalrestat. Neutral to mild-cationic niosomal formulations showed suitable physicochemical characteristics for topical ocular drug delivery, supported by a low ocular irritability potential, high biocompatibility, sustained release, and permeability through the cornea and scleral tissue. Compared to epalrestat-loaded contact lenses or free drug solutions, niosomes can encapsulate more drugs, increasing apparent solubility, and protect better the drug from premature degradation while promoting the pass towards inner eye tissues. Moreover, as revealed in the HET-CAM and zebrafish embryotoxicity assays, drug encapsulation in niosomes makes the formulation safe. Similar concentrations of epalrestat in solution would be harmful to patients. These findings point out epalrestat-loaded niosomes as suitable for non-invasive drug delivery to inner eye structures.

3.6 REFERENCES

1. International Diabetes Foundation. IDF Diabetes Atlas 2021. Available online: www.diabetesatlas.org (accessed on 10 April 2023).

2. Chung, S.S.M.; Ho, E.C.M.; Lam, K.S.L.; Chung, S.K. Contribution of Polyol Pathway to Diabetes-Induced Oxidative Stress. *J. Am. Soc. Nephrol*. **2003**, 14, 233–236.

3. Stitt, A.W.; Curtis, T.M.; Chen, M.; Medina, R.J.; McKay, G.J.; Jenkins, A.; Gardiner, T.A.; Lyons, T.J.; Hammes, H.-P.; Simó, R.; et al. The Progress in Understanding and Treatment of Diabetic Retinopathy. *Prog. Retin. Eye Res*. **2016**, 51, 156–186.

4. Neubauer, A.S.; Ulbig, M.W. Laser Treatment in Diabetic Retinopathy. *Ophthalmologica* **2007**, 221, 95–102.

5. Ferris, F.L.; Davis, M.D.; Aiello, L.M. Treatment of Diabetic Retinopathy. *N. Engl. J. Med*. **1999**, 341, 667–678.

6. Lorenzi, M. The Polyol Pathway as a Mechanism for Diabetic Retinopathy: Attractive, Elusive, and Resilient. *Exp. Diabetes Res*. **2007**, 2007, 061038.

7. Tang, W.H.; Martin, K.A.; Hwa, J. Aldose Reductase, Oxidative Stress, and Diabetic Mellitus. *Front. Pharmacol*. **2012**, 3, 87.

8. Cheng, H.M.; Xiong, J.; Tanaka, G.; Chang, C.; Asterlin, A.A.; Aguayo, J.B. Analysis of Concurrent Glucose Consumption by the Hexose Monophosphate Shunt,

Glycolysis, and the Polyol Pathway in the Crystalline Lens. *Exp. Eye Res*. **1991**, 53, 363–366.

9. Taylor, R.; Agius, L. The Biochemistry of Diabetes. *J. Biochem*. **1988**, 250, 625–640.

10. Lee, A.Y.W.; Chung, S.S.M. Contributions of Polyol Pathway to Oxidative Stress in Diabetic Cataract. *FASEB J*. **1999**, 13, 23–30.

11. Okayama, N.; Omi, H.; Okouchi, M.; Imaeda, K.; Kato, T.; Akao, M.; Imai, S.; Shimizu, M.; Fukutomi, T.; Itoh, M. Mechanisms of Inhibitory Activity of the Aldose Reductase Inhibitor, Epalrestat, on High Glucose-Mediated Endothelial Injury: Neutrophil-Endothelial Cell Adhesion and Surface Expression of Endothelial Adhesion Molecules. *J. Diabetes Complicat.* **2002**, 16, 321–326.

12. Ramirez, M.A.; Borja, N.L. Epalrestat: An Aldose Reductase Inhibitor for the Treatment of Diabetic Neuropathy. *Pharmacotherapy* **2008**, 28, 646–655.

13. Jagdale, A.D.; Bavkar, L.N.; More, T.A.; Joglekar, M.M.; Arvindekar, A.U. Strong Inhibition of the Polyol Pathway Diverts Glucose Flux to Protein Glycation Leading to Rapid Establishment of Secondary Complications in Diabetes Mellitus. *J. Diabetes Complicat*. **2016**, 30, 398–405.

14. Ao, S.; Kikuchi, C.; Ono, T.; Notsu, Y. Effect of Instillation of Aldose Reductase Inhibitor FR74366 on Diabetic Cataract. *Investig. Ophthalmol. Vis. Sci*. **1991**, 32, 3078–3083.

15. Senthilkumari, S.; Sharmila, R.; Chidambaranathan, G.; Vanniarajan, A. Epalrestat, an Aldose Reductase Inhibitor Prevents Glucose-Induced Toxicity in Human Retinal Pigment Epithelial Cells in Vitro. *J. Ocul. Pharmacol. Ther*. **2017**, 33, 34–41.

16. Maladkar, M.; Rajadhyaksha, G.; Venkataswamy, N.; Hariharan, R.; Lohati, S. Efficacy, Safety, and Tolerability of Epalrestat Compared to Methylcobalamine in Patients with Diabetic Neuropathy. *Int. J. Diabetes Dev. Ctries*. **2009**, 29, 28.

17. Banditelli, S.; Boldrini, E.; Vilardo, P.G.; Cecconi, I.; Cappiello, M.; Dal Monte, M.; Marini, I.; Del Corso, A.; Mura, U. A New Approach Against Sugar Cataract Through Aldose Reductase Inhibitors. *Exp. Eye Res*. **1999**, 69, 533–538.

18. Aukunuru, J.V.; Sunkara, G.; Ayalasomayajula, S.P.; Deruiter, J.; Clark, R.C.; Kompella, U.B. A Biodegradable Injectable Implant Sustains Systemic and Ocular Delivery of an Aldose Reductase Inhibitor and Ameliorates Biochemical Changes in a Galactose-Fed Rat Model for Diabetic Complications. *Pharm. Res*. **2002**, 19, 278–285.

19. Kador, P.F.; Randazzo, J.; Babb, T.; Koushik, K.; Takamura, Y.; Zhu, W.; Blessing, K.; Kompella, U.B. Topical Aldose Reductase Inhibitor Formulations for Effective Lens Drug Delivery in a Rat Model for Sugar Cataracts. *J. Ocul. Pharmacol. Ther*. **2007**, 23, 116–123.

20. Alvarez-Rivera, F.; Concheiro, A.; Alvarez-Lorenzo, C. Epalrestat-Loaded Silicone Hydrogels as Contact Lenses to

Address Diabetic-Eye Complications. *Eur. J. Pharm. Biopharm*. **2018**, 122, 126–136.

21. Zhu, Y.; Sheng, Y. Sustained Delivery of Epalrestat to the Retina Using PEGylated Solid Lipid Nanoparticles Laden Contact Lens. *Int. J. Pharm*. **2020**, 587, 119688.

22. Kattar, A.; Concheiro, A.; Alvarez-Lorenzo, C. Diabetic Eye: Associated Diseases, Drugs in Clinic, and Role of Self-Assembled Carriers in Topical Treatment. *Expert. Opin. Drug. Deliv*. **2021**, 18, 1589–1607.

23. Verma, A.; Tiwari, A.; Saraf, S.; Panda, P.K.; Jain, A.; Jain, S.K. Emerging Potential of Niosomes in Ocular Delivery. *Expert. Opin. Drug. Deliv*. **2021**, 18, 55–71.

24. Durak, S.; Rad, M.E.; Yetisgin, A.A.; Sutova, H.E.; Kutlu, O.; Cetinel, S.; Zarrabi, A. Niosomal Drug Delivery Systems for Ocular Disease—Recent Advances and Future Prospects. *Nanomaterials* **2020**, 10, 1191.

25. Xu, Y.; Li, Q.; Li, Z.; Zeng, W.; Ge, S.; Lu, H.; Wu, C.; Ge, L.; Liang, D. Proniosome-Derived Niosomes for Tacrolimus Topical Ocular Delivery: In Vitro Cornea Permeation, Ocular Irritation, and in Vivo Anti-Allograft Rejection. *Eur. J. Pharm. Sci*. **2014**, 62, 115–123.

26. Wu, T.; Zhu, C.; Wang, X.; Kong, Q.; Guo, T.; He, Z.; He, Y.; Ruan, S.; Ruan, H.; Pei, L.; et al. Cholesterol and Phospholipid-Free Multilamellar Niosomes Regulate Transdermal Permeation of a Hydrophobic Agent Potentially Administrated for Treating Diseases in Deep Hair Follicles. *J. Pharm. Sci*. **2022**, 111, 1785–1797.

27. Zhang, Y.; Jing, Q.; Hu, H.; He, Z.; Wu, T.; Guo, T.; Feng, N. Sodium Dodecyl Sulfate Improved Stability and Transdermal Delivery of Salidroside-Encapsulated Niosomes via Effects on Zeta Potential. *Int. J. Pharm*. **2020**, 580, 119183.

28. Kalweit, S.; Besoke, R.; Gerner, I.; Spielmann, H. A National Validation Project of Alternative Methods to the Draize Rabbit *Eye Test. Toxicol. Vitr*. **1990**, 4, 702–706.

29. Haselgrübler, R.; Stübl, F.; Essl, K.; Iken, M.; Schröder, K.; Weghuber, J. Gluc-HET, a Complementary Chick Embryo Model for the Characterization of Antidiabetic Compounds. *PLoS ONE* **2017**, 12, e0182788.

30. Pereira, A.C.; Gomes, T.; Ferreira Machado, M.R.; Rocha, T.L. The Zebrafish Embryotoxicity Test (ZET) for Nanotoxicity Assessment: From Morphological to Molecular *Approach. Environ. Pollut*. **2019**, 252, 1841–1853.

31. Shen, C.; Zuo, Z. Zebrafish (Danio Rerio) as an Excellent Vertebrate Model for the Development, Reproductive, Cardiovascular, and Neural and Ocular Development Toxicity Study of Hazardous Chemicals. *Environ. Sci. Pollut. Res*. **2020**, 27, 43599–43614.

32. Sipes, N.S.; Padilla, S.; Knudsen, T.B. Zebrafish-As an Integrative Model for Twenty-First Century Toxicity Testing. Birth Defects *Res. Part. C Embryo Today Rev*. **2011**, 93, 256–267.

33. Mashal, M.; Attia, N.; Puras, G.; Martínez-Navarrete, G.; Fernández, E.; Pedraz, J.L. Retinal Gene Delivery Enhancement by Lycopene Incorporation into Cationic

Niosomes Based on DOTMA and Polysorbate 60. *J. Control. Release* **2017**, 254, 55–64.

34. Seleci, D.A.; Seleci, M.; Jochums, A.; Walter, J.G.; Stahl, F.; Scheper, T. Aptamer Mediated Niosomal Drug Delivery. *RSC Adv*. **2016**, 6, 87910–87918.

35. Kamboj, S.; Saini, V.; Bala, S. Formulation and Characterization of Drug Loaded Nonionic Surfactant Vesicles (Niosomes) for Oral Bioavailability Enhancement. *Sci. World J*. **2014**, 2014, 959741.

36. Wu, W.; Wang, Y.; Que, L. Enhanced Bioavailability of Silymarin by Self-Microemulsifying Drug Delivery System. *Eur. J. Pharm. Biopharm*. **2006**, 63, 288–294.

37. Wang, J.; Zhao, F.; Liu, R.; Chen, J.; Zhang, Q.; Lao, R.; Wang, Z.; Jin, X.; Liu, C. Novel Cationic Lipid Nanoparticles as an Ophthalmic Delivery System for Multicomponent Drugs: Development, Characterization, in Vitro Permeation, in Vivo Pharmacokinetic, and Molecular Dynamics Studies. *Int. J. Nanomed*. **2017**, 12, 8115–8127.

38. Grijalvo, S.; Puras, G.; Zárate, J.; Sainz-Ramos, M.; Qtaish, N.A.L.; López, T.; Mashal, M.; Attia, N.; Díaz, D.; Pons, R.; et al. Cationic Niosomes as Non-Viral Vehicles for Nucleic Acids: Challenges and Opportunities in Gene Delivery. *Pharmaceutics* **2019**, 11, 50.

39. Chen, X.; Wu, J.; Lin, X.; Wu, X.; Yu, X.; Wang, B.; Xu, W. Tacrolimus Loaded Cationic Liposomes for Dry Eye Treatment. *Front. Pharmacol*. **2022**, 13, 157.

40. Romero, G.B.; Keck, C.M.; Müller, R.H.; Bou-Chacra, N.A. Development of Cationic Nanocrystals for Ocular Delivery. *Eur. J. Pharm. Biopharm*. **2016**, 107, 215–222.

41. Nowroozi, F.; Almasi, A.; Javidi, J.; Haeri, A.; Dadashzadeh, S. Effect of Surfactant Type, Cholesterol Content and Various Downsizing Methods on the Particle Size of Niosomes. *Iran. J. Pharm. Res*. **2018**, 17, 1–11.

42. Bartelds, R.; Nematollahi, M.H.; Pols, T.; Stuart, M.C.A.; Pardakhty, A.; Asadikaram, G.; Poolman, B. Niosomes, an Alternative for Liposomal Delivery. *PLoS ONE* **2018**, 13, e0194179.

43. Fernández-Pérez, E.J.; Sepúlveda, F.J.; Peters, C.; Bascuñán, D.; Riffo-Lepe, N.O.; González-Sanmiguel, J.; Sánchez, S.A.; Peoples, R.W.; Vicente, B.; Aguayo, L.G. Effect of Cholesterol on Membrane Fluidity and Association of Aβ Oligomers and Subsequent Neuronal Damage: A Double-Edged Sword. *Front. Aging Neurosci*. **2018**, 10, 226.

44. Zhang, Y.; Zhang, J.; Li, Q.; Wu, Y.; Wang, D.; Xu, L.; Zhang, Y.; Wang, S.; Wang, T.; Liu, F.; et al. Cholesterol Content in Cell Membrane Maintains Surface Levels of ErbB2 and Confers a Therapeutic Vulnerability in ErbB2-Positive Breast Cancer. *Cell. Commun. Signal*. **2019**, 17, 15.

45. de Oliveira Andrade, L. Understanding the Role of Cholesterol in Cellular Biomechanics and Regulation of Vesicular Trafficking: The Power of Imaging. *Biomed. Spectrosc. Imaging* **2016**, 5, S101–S117.

46. Maulucci, G.; De Spirito, M.; Arcovito, G.; Boffi, F.; Castellano, A.C.; Briganti, G. Particle Size Distribution in DMPC Vesicles Solutions Undergoing Different Sonication Times. *Biophys. J.* **2005**, 88, 3545–3550.

47. Alenaizi, R.; Radiman, S.; Mohamed, F.; Rahman, I.A. Dynamic Light Scattering Study on Vesicles of Netaine-Cholesterol System. In Proceedings of the AIP Conference Proceedings; American Institute of Physics: College Park, MD, USA, 2014; Volume 1614, pp. 99–103.

48. Pencer, J.; White, G.F.; Hallett, F.R. Osmotically Induced Shape Changes of Large Unilamellar Vesicles Measured by Dynamic Light Scattering. *Biophys. J.* **2001**, 81, 2716–2728.

49. Sainz-Ramos, M.; Villate-Beitia, I.; Gallego, I.; Al Qtaish, N.; Menéndez, M.; Lagartera, L.; Grijalvo, S.; Eritja, R.; Puras, G.; Pedraz, J.L. Correlation between Biophysical Properties of Niosomes Elaborated with Chloroquine and Different Tensioactives and Their Transfection Efficiency. *Pharmaceutics* **2021**, 13, 1787.

50. Manca, M.L.; Manconi, M.; Nacher, A.; Carbone, C.; Valenti, D.; MacCioni, A.M.; Sinico, C.; Fadda, A.M. Development of Novel Diolein-Niosomes for Cutaneous Delivery of Tretinoin: Influence of Formulation and in Vitro Assessment. *Int. J. Pharm*. **2014**, 477, 176–186.

51. Li, Z.; Zhang, Y.; Ma, J.; Meng, Q.; Fan, J. Modeling Interactions between Liposomes and Hydrophobic Nanosheets. *Small* **2019**, 15, 1804992.

52. Charoensit, P.; Pompimon, W.; Khorana, N.; Sungthongjeen, S. Effect of Amide Linkage of PEG-Lipid Conjugates on the Stability and Cytotoxic Activity of Goniodiol Loaded in PEGylated Liposomes. *J. Drug. Deliv. Sci. Technol*. **2019**, 50, 1–8.

53. European Union. Directive 2010/63/EU of the European Parliament and of the Council of 22 September 2010 on the Protection of Animals Used for Scientific Purposes; European Union: Brussels, Belgium, 2010; pp. 1–47.

54. Dix, D.J.; Houck, K.A.; Martin, M.T.; Richard, A.M.; Setzer, R.W.; Kavlock, R.J. The ToxCast Program for Prioritizing Toxicity Testing of Environmental Chemicals. *Toxicol. Sci.* **2007**, 95, 5–12.

55. Al-Ghabeish, M.; Xu, X.; Krishnaiah, Y.S.R.; Rahman, Z.; Yang, Y.; Khan, M.A. Influence of Drug Loading and Type of Ointment Base on the in Vitro Performance of Acyclovir Ophthalmic Ointment. *Int. J. Pharm.* **2015**, 495, 783–791.

56. Liang, R.; Chen, L.; Yokoyama, W.; Williams, P.A.; Zhong, F. Niosomes Consisting of Tween-60 and Cholesterol Improve the Chemical Stability and Antioxidant Activity of (−)-Epigallocatechin Gallate under Intestinal Tract Conditions. *J. Agric. Food Chem.* **2016**, 64, 9180–9188.

57. Estupiñan, O.R.; Garcia-Manrique, P.; Blanco-Lopez, M.d.C.; Matos, M.; Gutiérrez, G. Vitamin D3 Loaded Niosomes and Transfersomes Produced by Ethanol Injection Method: Identification of the Critical Preparation Step for Size Control. *Foods* **2020**, 9, 1367.

58. Villate-Beitia, I.; Gallego, I.; Martínez-Navarrete, G.; Zárate, J.; López-Méndez, T.; Soto-Sánchez, C.; Santos-Vizcaíno, E.; Puras, G.; Fernández, E.; Pedraz, J.L. Polysorbate 20 Non-Ionic Surfactant Enhances Retinal Gene Delivery Efficiency of Cationic Niosomes after Intravitreal and Subretinal Administration. *Int. J. Pharm*. **2018**, 550, 388–397.

59. Jagtap, S.; Magdum, C. Influence of Water-Soluble Polymers on Epalrestat Ternary Complexation by Kneading. *Res. J. Pharm. Technol*. **2019**, 12, 3602.

60. Damera, D.P.; Venuganti, V.V.K.; Nag, A. Deciphering the Role of Bilayer of a Niosome towards Controlling the Entrapment and Release of Dyes. *ChemistrySelect* **2018**, 3, 3930–3938.

61. Liu, T.; Guo, R. Preparation of a Highly Stable Niosome and Its Hydrotrope-Solubilization Action to Drugs. *Langmuir* **2005**, 21, 11034–11039.

62. Hao, Y.; Zhao, F.; Li, N.; Yang, Y.; Li, K. Studies on a High Encapsulation of Colchicine by a Niosome System. *Int. J. Pharm.* **2002**, 244, 73–80.

63. Abdelbary, G.; El-gendy, N. Niosome-Encapsulated Gentamicin for Ophthalmic Controlled Delivery. *AAPS PharmSciTech* **2008**, 9, 740–747.

64. Basiri, L.; Rajabzadeh, G.; Bostan, A. Physicochemical Properties and Release Behavior of Span 60/Tween 60 Niosomes as Vehicle for α-Tocopherol Delivery. *Lwt* **2017**, 84, 471–478.

65. Srikanth, K.; Nappinnai, M.; Gupta, V.R.M.; Suribabu, J. Niosomes: A Prominent Tool for Transdermal Drug Delivery. *Res. J. Pharm. Biol. Chem. Sci*. **2010**, 1, 308–316.

66. Dias, L.M.; de Keijzer, M.J.; Ernst, D.; Sharifi, F.; de Klerk, D.J.; Kleijn, T.G.; Desclos, E.; Kochan, J.A.; de Haan, L.R.; Franchi, L.P.; et al. Metallated Phthalocyanines and Their Hydrophilic Derivatives for Multi-Targeted Oncological Photodynamic Therapy. *J. Photochem. Photobiol. B Biol.* **2022**, 234, 112500.

67. Freitas de Lima, F.; da Silva, B.B.; Oliveira, J.D.; de Moura, L.D.; Rodrigues da Silva, G.H.; Fernandes, P.C.L.; Souza, R.I.C.; dos Santos, A.C.; de Paula, E. Prolonged Anesthesia and Decreased Toxicity of Enantiomeric-Excess Bupivacaine Loaded in Ionic Gradient Liposomes. *Int. J. Pharm*. **2021**, 606, 120944.

68. Harper, S.L.; Carriere, J.L.; Miller, J.M.; Hutchison, J.E.; Maddux, B.L.S.; Tanguay, R.L. Systematic Evaluation of Nanomaterial Toxicity: Utility of Standardized Materials and Rapid Assays. *ACS Nano* **2011**, 5, 4688–4697.

69. Furuishi, T.; Takahashi, S.; Ogawa, N.; Gunji, M.; Nagase, H.; Suzuki, T.; Endo, T.; Ueda, H.; Yonemochi, E.; Tomono, K. Enhanced Dissolution and Skin Permeation Profiles of Epalrestat with β-Cyclodextrin Derivatives Using a Cogrinding Method. *Eur. J. Pharm. Sci*. **2017**, 106, 79–86.

70. Šturm, K.; Levstik, L.; Demopoulos, V.J.; Kristl, A. Permeability Characteristics of Novel Aldose Reductase

Inhibitors Using Rat Jejunum in Vitro. *Eur. J. Pharm. Sci*. **2006**, 28, 128–133.

71. Sandler, J.; Shaffer, M.S.P.; Windle, A.H.; Halsall, M.P.; Montes-Morán, M.A.; Cooper, C.A.; Young, R.J. Variations in the Raman Peak Shift as a Function of Hydrostatic Pressure for Various Carbon Nanostructures: A Simple Geometric Effect. *Phys. Rev. B* **2003**, 67, 035417.

72. Hosseini, K.; March, W.; Jongsma, F.H.M.; Hendrikse, F.; Motamedi, M. Noninvasive Detection of Ganciclovir in Ocular Tissue by Raman Spectroscopy: Implication for Monitoring of Drug Release. *J. Ocul. Pharmacol. Ther.* **2002**, 18, 277–285.

73. Katz, A.; Kruger, E.F.; Minko, G.; Liu, C.H.; Rosen, R.B.; Alfano, R.R. Detection of Glutamate in the Eye by Raman Spectroscopy. *J. Biomed. Opt*. **2003**, 8, 167.

74. Elmotasem, H.; Awad, G.E.A. A Stepwise Optimization Strategy to Formulate in Situ Gelling Formulations Comprising Fluconazole-Hydroxypropyl-Beta-Cyclodextrin Complex Loaded Niosomal Vesicles and Eudragit Nanoparticles for Enhanced Antifungal Activity and Prolonged Ocular Delivery. *Asian J. Pharm. Sci*. **2020**, 15, 617–636.

75. Paradkar, M.U.; Parmar, M. Formulation Development and Evaluation of Natamycin Niosomal In-Situ Gel for Ophthalmic Drug Delivery. *J. Drug Deliv. Sci. Technol*. **2017**, 39, 113–122.

76. Allam, A.; El-Mokhtar, M.A.; Elsabahy, M. Vancomycin-Loaded Niosomes Integrated within PH-Sensitive in-Situ Forming Gel for Treatment of Ocular Infections While Minimizing Drug Irritation. *J. Pharm. Pharmacol*. **2019**, 71, 1209–1221.

77. Gugleva, V.; Titeva, S.; Rangelov, S.; Momekova, D. Design and in Vitro Evaluation of Doxycycline Hyclate Niosomes as a Potential Ocular Delivery System. *Int. J. Pharm*. **2019**, 567, 118431.

78. Abdelkader, H.; Ismail, S.; Kamal, A.; Alany, R.G. Design and Evaluation of Controlled-Release Niosomes and Discomes for Naltrexone Hydrochloride Ocular Delivery. *J. Pharm. Sci.* **2011**, 100, 1833–1846.

79. IUPAC Commission on Spectrochemical and Other Optical Procedures for Analysis. Nomenclature, Symbols, Units and Their Usage in Spectrochemical Analysis—II. Data Interpretation. Spectrochim Acta **1978**, 33, 241–24

4. STABILITY OF NIOSOMES FOR OPHTALMIC ADMINISTRATION THROUGH LANGMUIR MONOLAYER STUDIES OF NON-IONIC SURFACTANTS AND DOTMA

4.1 INTRODUCTION

Ocular diseases are a big part of the decreasing quality of life of patients suffering from illnesses that affect the eye. A common example is diabetic retinopathy that occurs in a third of type 1 diabetic patients in Poland [1], 56% of type 1 diabetic patients and 30% of type 2 diabetic patients in the United Kingdom [2] and a study investigating the global prevalence of diabetic retinopathy put the fraction of the diabetic population suffering from diabetic retinopathy at 34.6% [3]. In particular, pathological processes affecting the posterior segment of the eye prove especially hard to treat, as the number and characteristics of physiological barriers drugs need to go through make it a difficult task to get the active ingredients to the therapeutic target in reasonable time and sufficient quantity. Consequently, the need for new drug delivery systems increasing their cargo's bioavailability to treat diseases in the posterior segment of the eye is increasing. The available delivery routes are topical, oral, intracameral, subconjunctival, intravitreal, retrobulbar, peribulbar and posterior juxta scleral [4]. With the exception of the topical and oral drug delivery, all routes involve the injection of the drug into their respective tissue. While this allows for the circumvention of different ocular barriers, it also brings a deal of challenges with it, such as patient discomfort and the need for medical professionals for the administration of the treatment, among others. Therefore, to locally administer ocular drugs, the topical route is privileged in the research

for new drug delivery methods. The challenges encountered by drugs to permeate the different ocular tissues to reach the therapeutic site have directed the design and formulation of drug carriers. In this context, nanocarriers have recently gained a significant amount of interest, due to their versatility.

Polymeric micelles [5] and vesicles such as liposomes [6] and niosomes [7] are all self-assembled structures capable of encapsulating a range of molecules to carry and deliver their payload in various ocular sites. They are made by allowing amphiphilic molecules to arrange inside an aqueous medium, either encapsulating hydrophobic drugs in the micelle core or vesicle bilayer, or encapsulating hydrophilic drugs in the vesicle core. These structures, and niosomes in particular, have been recently studied by our research group in terms of particle characterization, drug encapsulation and tissue permeation [8].

However, there are still gaps in the understanding of the physical chemistry of the aggregation and interaction between the molecules that make up the nanocarrier. Gathering this information is key to fully comprehend their behavior and optimize their composition, so as to improve the efficiency of the nanocarrier and hence the therapeutic action of the drug inside.

The aim of this chapter of the Thesis is to understand the interactions of the different molecules present in the niosome formulation prepared in chapter 3 of the Thesis. The main hypothesis is that DOTMA, the only charged surfactant in the system under the set conditions, plays a key role in the cohesion of the niosome. This has special relevance considering the possibility of cholesterol-mediated interactions with the voluminous hydrophilic group of Tween 60, the majority component. For pharmaceutical use and storage purposes, the effect of the ionic strength of the subphase and temperature on a

monolayer made with the molar fractions of a previously characterized niosomal system [8] was studied. The monolayers are made from polysorbate 60 (Tween 60), cholesterol and 1,2-di-O-octadecenyl-3-trimethylammonium propane (DOTMA) (**Figure 4.1**), as this is the composition of the niosomes described in chapter 3 of this Thesis.

Surfactant monolayers spread at the air/water interface (Langmuir monolayers) were used to model the arrangement different molecules find themselves in when put together and interact with each other within the aggregate. Langmuir monolayers are widely used to study the behavior of surfactants at the interface between a gas and a liquid, with applications of pharmaceutical interest in cell membrane-related studies [9], biosurfactants [10] or stability of colloidal drug carriers, such as vesicles or micelles [11–13] In the context of niosome stability, monolayer studies were used here to evaluate the physical and physicochemical properties of non-ionic surfactants, helper lipids and charge modifiers as they interact on an aqueous solution.

Depositing surfactant on an air-water interface reduces surface tension by positioning amphiphilic molecules with hydrophilic heads in the water phase and hydrophobic tails in the air phase. Surface tension measurements help assess the free energy of the water surface, and the difference between clean water and surfactant-covered water provides the surface pressure, leading to π-A isotherms that reveal molecular arrangements and mechanical properties at the interface.

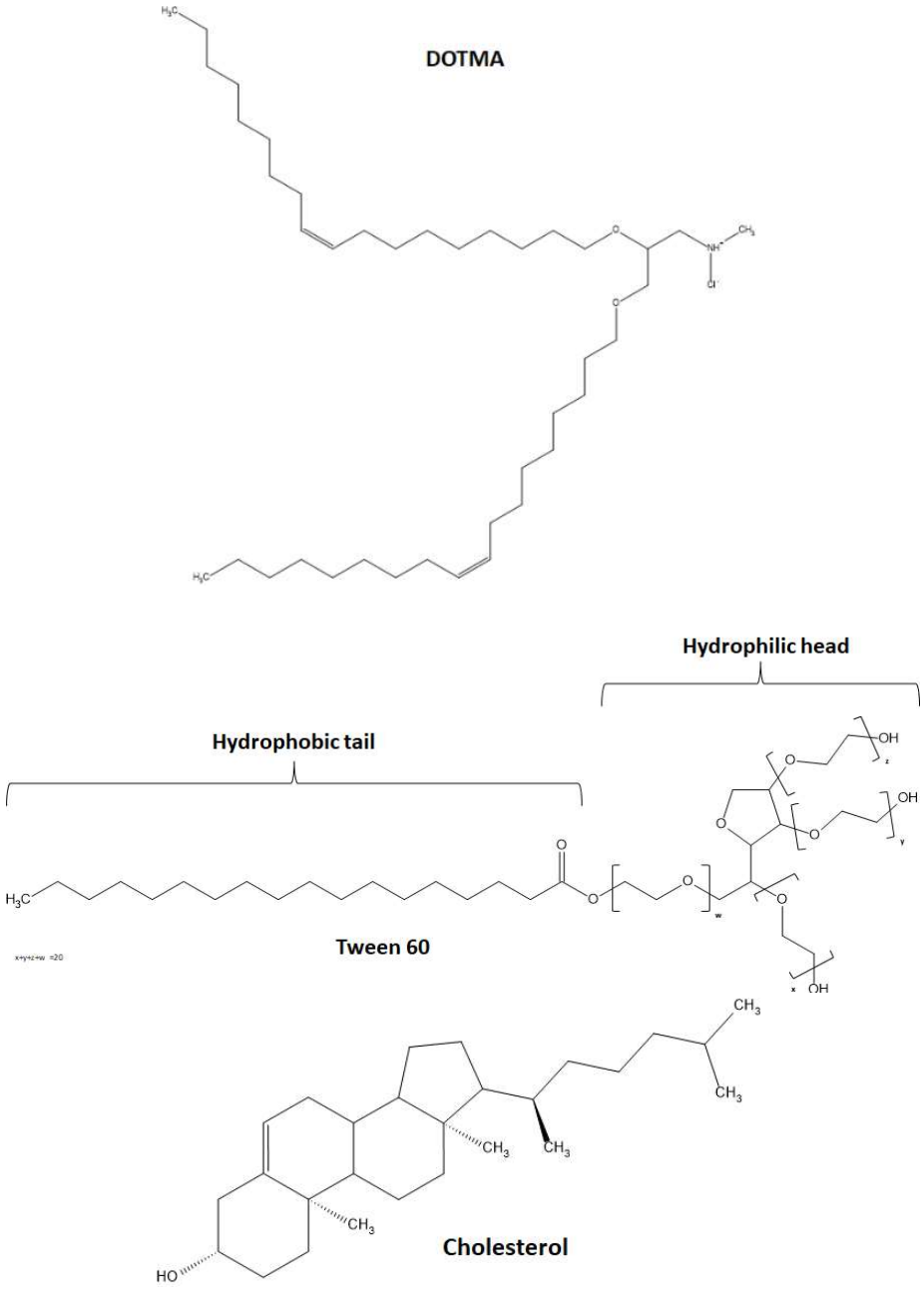

Figure 4.1. Structures of Tween 60, DOTMA and cholesterol

4.2 MATERIALS AND METHODS

4.2.1 Materials

Polysorbate 60 MW 1311.7 g/mol (Tween 60, HLB 14.9, Sigma Aldrich, Buchs, Switzerland), 1,2-di-O-octadecenyl-3-trimethylammonium propane (chloride salt) (DOTMA, 670.58 g/mol) (Avanti, Alabaster, AL, USA), cholesterol (386.7 g/mol) (Chemtrec, Madrid, Spain), dichloromethane (Fischer Scientific, Waltham, MA USA), sodium chloride (Labkem, Barcelona, Spain), potassium chloride (Panreac, Castellar del Vallès, Spain), sodium bicarbonate (Merck, St Louis, MO, USA), calcium dihydrochloride (Merck, Darmstadt, Germany). Ultrapure water (resistivity > 18.2 MΩ cm) was obtained by reverse osmosis (Milli-Q®, Millipore Ibérica, Madrid, Spain). Simulated lacrimal fluid (SLF) was made with 0.68g sodium chloride (Labkem, Barcelona, Spain), 0.22g sodium bicarbonate (Merck, St Louis, MO, USA), 0.008g calcium chloride dihydrate (Merck, Darmstadt, Germany) and 0.14g potassium chloride (Panreac, Castellar del Vallès, Spain) in 100mL distilled water.

4.2.2 Monolayer preparation

Prior to the beginning of the study, the trough was thoroughly cleaned with chloroform, and then with ethanol, along with both barriers, and before each experiment, trough and barriers were cleaned with ethanol and rinsed twice with water. The surfactant solutions of Tween 60 and cholesterol at a fixed 100/42 mol/mol proportion, and DOTMA present at 5% and 10% the amount of Tween 60, were spread with a Hamilton microsyringe (Hamilton, USA) from dichloromethane solutions 0.2 to 0.4 mg/mL in 50 to 200 µL. Film compression began

after leaving 10 minutes for solvent evaporation, and was then registered plotting surface pressure values, measured with a platinum Wilhelmy plate (Biolin Scientific, Finland), against mean molecular area, rendering the π-A isotherms. Monolayers of different compositions were prepared and named according to the fractions displayed in **Table 4.1**.

Table 4.1. Composition of the different monomolecular films obtained in this work.

Monolayer code	Tween 60	Cholesterol	DOTMA	
	(mol fraction, %)	(mol fraction, %)	(mol fraction, %)	(mol % over Tween 60)
C	-	100	-	-
T	100	-	-	0
TD5	95.2	-	4.8	5.0
TD10	90.9	-	9.1	10.0
TC	70.4	29.6	-	0.0
TCD5	68.0	28.6	3.4	5.0
TCD10	65.8	27.6	6.6	10.0

4.2.3 π-A isotherm measurements

Langmuir monolayers of Tween 60 (polysorbate 60), cholesterol and DOTMA at the air/water interface were obtained on purified water from a Milli-Q® dispenser with a minimum resistivity of 18.2 MΩ cm (Millipore SAS, Merck, France) and PBS buffer made according to the Sigma-Aldrich guidelines. Surface pressure (π)-molecuar area (A) isotherms were registered on a KSV-NIMA KN 1006 (Biolin Scientific, Finland) placed on an antivibrational table, with a working surface area of 783 cm^2 equipped with two barriers of poly(methylene oxide), also known as Delrin®. Surface pressure was measured with an accuracy of ± 0.01 mN/m. The subphase temperature was 20 °C and 30 °C maintained with an accuracy of ± 0.5 °C by a Julabo CD-200F thermostatic bath (Julabo, Germany) circulating water system. In

standard experiments monolayers were compressed at a barriers speed of 10 cm/s. Each experiment was repeated at least three times with a reproducibility between the isotherms of ± 0.2 Å/molecule.

4.2.4 Compressibility study

The compressibility modulus or elasticity of a monolayer is a physical magnitude that informs on the resistance of a film to compression [13]. Since it is the reciprocal of compressibility (Cs), the higher the value of this modulus, the more resistance the film offers to being compressed any further. It is mathematically expressed in **Equation 4.1**:

$$C_s^{-1} = -A\left(\frac{\partial \pi}{\partial \mathrm{A}}\right)_T$$

Equation 4.1. Compressibility modulus formula

where A is the value of mean molecular area for each point of the isotherm, π is the surface pressure at that point and T is the temperature at which the compression of the film took place [14,15]. Its value is known to rise with pressure, usually having a positive slope, since the closer molecules are to one another, the greater the resistance to further decreasing the distance between them will be, due to intermolecular repulsive forces [8]. A drop in its value reflects the existence of room for further compression that increases compressibility, usually standing for the collapse of the monolayer, which implies losing its 2D structure [16].

The compressibility modulus vs surface pressure plots were obtained using the data analysis programme OriginLab 2019b. The raw

plot line was smoothed by adjacent-averaging at every 5 points for noise reduction.

4.2.5 Brewster Angle Microscopy

BAM images on a floating monolayer were obtained using a Brewster Angle Microscope, BAM 2 Plus (NFT, Göttingen, Germany), mounted directly on a computer-controlled NIMA 601BAM Langmuir trough (NIMA, Coventry, UK) equipped with a PTFE (Teflon) barrier, with a subphase volume of 310 mL. The trough and the coupled microscope were placed on an antivibrational table (Halcyonics, Accurion GmbH, Germany) and placed into a safety cabinet to protect against dust and air convection.

The equipment added to the microscope was a 30mW NdYAG laser emitting *p*-polarized light at a wavelength of 532 nm. The incident Brewster angle was set at 53.1 ° to reflect the laser on the air/water interface; this geometry ensures that there is no reflectivity of the *p*-polarized beam (R_p) on a pure water surface. Spreading a monolayer at the interface will change the refractive index of the medium and change the Brewster angle, increasing the reflectivity and thus allowing us to obtain an image from the *p*-polarized light. The reflected beam passes through a focal lens, into an analyzer at a known incident polarization angle and finishes its path into a CCD camera. Instead of the relative intensity (I), this camera measures the gray levels (GL), making up the image from those values.

4.3 RESULTS AND DISCUSSION

4.3.1 Effect of monolayer composition

To obtain and analyse information from increasingly complex systems in terms of their composition, first the influence of cholesterol and DOTMA respectively on Tween 60 monolayers was studied. Then the effect of cholesterol on Tween 60/DOTMA was studied, obtaining ternary systems that mimic the niosome's composition [8]. In all cases, the data provided by compression isotherms and compressibility modulus-surface pressure plots of each monolayer system was interpreted, as well as BAM images for the ternary system. First, for the assessment of the effect of cholesterol on Tween 60 monolayers, π-A isotherms of pure polysorbate 60 (labelled as T) with pure cholesterol (C) was compared with a mixture of both components (TC) in the proportion stated in **Table 4.1**. Surface tension isotherms for pure cholesterol [18] are well described in the literature and Tween 60 [19] surface tension isotherms exist in the literature but are less abundant. Compression isotherms of pure Tween 60 and cholesterol have not been extensively studied, and were therefore obtained as part of our experiments, as shown in **Figure 4.2**. The shape of the surface pressure isotherms of Tween 60 will be studied, as it is the majority component of the niosomes, and thus of the monolayers through which the niosomes are understood.

4.3.1.1 Single component system

The L-shaped isotherm for cholesterol has been vastly studied, and its shape is explained by the two main conformations the molecules have at the air/water interface, and hence the two main surface

aggregation states of the cholesterol monolayer (horizontal and vertical) [20]. As for Tween 60, this polysorbate acquires an expanded conformation when spread on a clean water surface, followed by a progressive aggregation, seen as a curve in the isotherm as surface pressure rises, and culminating in a phase transition or conformational change, as also seen for Tween 80 [21]. From a molecular point of view, the branched polar headgroups get closer to each other upon compression, and end up dehydrating if packed too tightly together [19], which might account for the slope change at the end of compression.

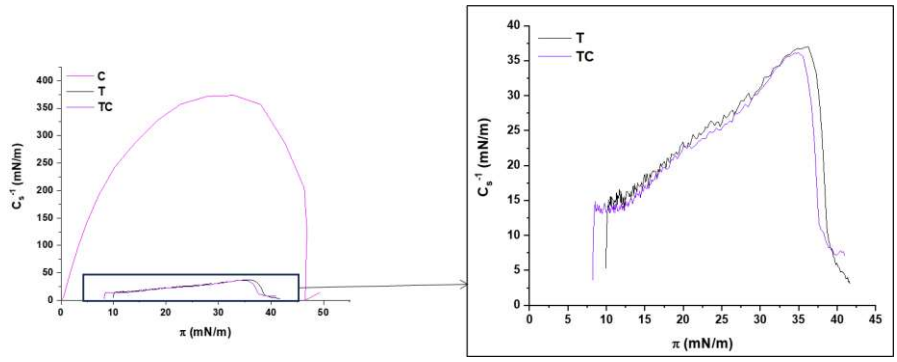

Figure 4.2. Comparison of the compressibility modulus of pure cholesterol and pure Tween 60 monolayers and Tween 60/cholesterol mixture, with zoom in of the monolayers containing Tween 60.

Regarding the compressibility modulus (C_s^{-1}), its high values in the case of cholesterol (max. at 373 mN/m) indicate a very condensed, rigid monolayer, mostly in a solid state (S) of surface aggregation, and its parabole-like shape (**Figure 4.2**) accounts for the change of conformation cholesterol molecules perpendicular to the interface undergo upon compression [20]. Tween 60, on the contrary, forms an expanded, much more compressible monolayer (max. C_s^{-1} at 37 mN/m, 10 times less than the value for cholesterol) in a liquid-expanded (LE)

aggregation state. It shows a steady rise in its compressibility modulus as the monolayer is compressed, only to drop dramatically at a surface pressure of 36.2 mN/m to then reach levels around or below those at the beginning of compression, tending to zero. This indicates the collapse of the monolayer, setting a limit of mean molecular area for Tween 60 molecules occupying a monolayer before a different molecular arrangement needs to be found.

4.3.1.2 Binary systems

To study the interaction between both components, mixed monolayers at a fixed composition (**Table 4.1**) were spread and compressed. The π-A isotherm registered from this process (labelled as TC) indicates there exists an interaction, since the presence of cholesterol in the Tween 60 monolayer in the chosen proportion causes both a change in the slope of the second region of the isotherm appearing at high pressure (in the interval 37-40 mN/m, in which the C_s^{-1} vs π plot proves the film is collapsing) and a minor change in the shape of the isotherm below that point.

As for the compressibility modulus, the addition of cholesterol to the polysorbate 60 film yields lower values for the compressibility modulus, which means cholesterol enhances compressibility of Tween 60. However, this effect seems to be weak, as the curve for the polysorbate/cholesterol mixture is in close vicinity of that for pure Tween 60, revealing the influence of cholesterol on the mechanical properties of the polysorbate film to be small under these conditions.

Looking at the difference in key values of certain properties, as well as at what can happen at the molecular level at the air/water

interface allows for further analysis of the interaction between both components. First, the interaction between the hydrophobic moieties of both Tween 60 and cholesterol molecules was studied. In the case of Tween 60, the non-polar group is a stearoyl chain, identical to that of stearic acid (SA). Therefore, comparing values such as collapse surface pressure (π_{col}) in SA/cholesterol mixed monolayers with those from Tween 60/cholesterol films may provide some evidence related to the importance of these interactions. This quantitative approach provides helpful insight regarding the extent of the effect of cholesterol on Tween 60 in Langmuir monolayers.

Table 4.2. Values from **Figure 4.2** and stearic acid and its mixture with cholesterol at SA/chol. 70/30 % mol/mol [12].

*These values are accurate but approximate as they were obtained directly from graphics (see references). They must also be interpreted with caution, given SA and cholesterol do not mix at the air/water interface.

System	π_{col} (mN/m)	C_s^{-1} (mN/m)
Tween 60 (T)	36.26	37.03
Tween 60/chol (TC)	34.99	36.13
SA	53.0*	699.4
SA/chol	42.6*	550.7

Cholesterol slightly decreases film rigidity (given by the compressibility modulus) in polysorbate 60 monolayers (**Table 4.2**), as it does in stearic acid films [22]. Furthermore, by decreasing the collapse pressure of the monolayer, it also decreases the pressure needed to break the film' cohesion, as expected from a less rigid film.

A possible explanation for this behaviour lies in molecular interactions. Even though SA and cholesterol do not form miscible monolayers, thus showing different π_{col} values without a linear correlation to cholesterol content [23], Tween 60 and cholesterol do mix

at the air/water interface, as can be deduced from the fact there is a single collapse for the Tween 60/cholesterol mixture. Even in this situation, cholesterol polycyclic structure and stearoyl fatty chains may interact if both components are miscible, with cholesterol's polycyclic ring condensate intercalating among acyl chains [23,24].

Their maximum C_s^{-1} value also retains its comparative value: SA/cholesterol (70/30 mol%) monolayers, where both components form solid monolayers at high surface pressures, show a max. C_s^{-1} value far greater than that of Tween 60/cholesterol films at the same proportion, which yield a value in the range 15-50 mN/m, indicative of a LE aggregation state [25]. This significant gap of an order of magnitude is necessarily caused by the different structure of the hydrophilic moieties of SA (a carboxyl group) and much more voluminous polysorbate 60, with an ester group followed by a poly(ethylene oxide) (PEO) group leading to a branched tetrahydrofuran ring with more PEO chains. This bulky headgroup gives Tween 60 its greater compressibility compared to fatty acids with the same structure in their non-polar region.

Otherwise, regarding the interaction between polar headgroups, the hydroxyl group of cholesterol, which lies close to the interface, can interact with the C=O bond in the ester group from polysorbate molecules' stearoyl chain, or the ester O atom in alpha position to the carbonyl bond of the same group. This interaction may occur through H-bonds between cholesterol hydroxyl H atom and the electron-rich O atom in the carbonyl bond and/or the aforementioned alpha O atom, as modelled through molecular dynamics [26]. This intermolecular interaction between polar moieties of both surfactants may increase lateral cohesion, leading to an improvement of shell stabilisation in the niosomes [27].

Another proof of interaction given by the C_s^{-1} plot is how the final stage of decay of the modulus curve shows a different pattern than the one seen for pure polysorbate films (coded as TC and T in **Figure 4.2**, respectively). The existence of cholesterol among Tween 60 molecules and their possible interactions, as discussed above, may stabilise the monolayer at the last stage of collapse, changing the rate at which the film loses its monomolecular arrangement.

All considered, both graphs and all analysed parameters confirm that cholesterol, at the given mole fraction as used for the formation of niosomes described in the previous chapter [8], while not having a particularly large effect in terms of mechanical changes to Langmuir films, gives rise to interactions with polysorbate 60 at the monolayer which influences the stability of the film.

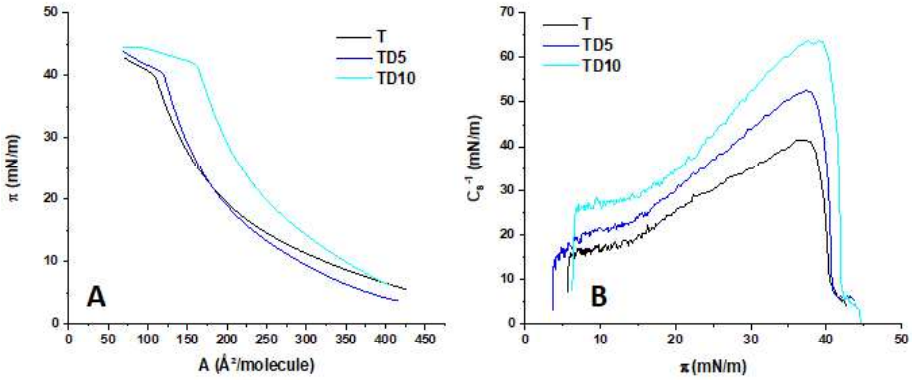

Figure 4.3. π-A isotherms (A) and compressibility moduli (B) of Tween 60 monolayers incorporating 0%, 5% or 10% of DOTMA

Secondly, the effect of DOTMA on Tween 60 monolayers was assessed. The compression isotherm graph (**Figure 4.3**) shows isotherms for Tween 60 and Tween 60/DOTMA binary mixtures where DOTMA is present at 5% or 10% the amount of polysorbate (see **Table**

4.1 for composition), making it the minority component of the system in all cases.

The π-A isotherms for Tween 60 both pure (labelled as T) and mixed with DOTMA at different ratios (TD5, TD10 for 5% and 10%, respectively) provide a picture of the interaction between these two substances at the air/water interface. Early stages of compression show initial pressures below 7 mN/m, which render values of compressibility modulus well below 12 mN/m (**Figure 4.3**) compatible with a gas (G) surface state of aggregation [28]. As surface pressure rises, the monolayer shifts to a mostly liquid-expanded or LE state for the rest of the isotherm, according to the values of the compressibility modulus (ca. 7-29 mN/m) [29,30].

The inclusion of DOTMA in polysorbate 60 monolayers changes both the slope of the isotherm, particularly in the LE state and the interaction of both components changes the arrangement of molecules at the interface before compression, leading to different values of initial surface pressure (**Figure 4.3**).

The decrease in surface area in TD5 vs T -that is, when 4.8% of the polysorbate molecules are replaced by DOTMA molecules at any given pressure below their intersection indicates a significant decrease in surface activity of the monolayer as a whole. This decrease is due to the behaviour of DOTMA molecules in the monolayer, and cannot be ascribed to there being fewer Tween 60 molecule for two reasons: one, DOTMA molecules feature two hydrophobic C18:1 oleic chains that make it surface active, in spite of having a net charge (a trimethylammonium group) in its polar headgroup [18,31,32]; and two, further substitution of Tween 60 molecules by DOTMA, as is the case of TD10, where 9.1% of the polysorbate molecules in the T curve are replaced, does not yield a greater decrease in surface pressure. On the

contrary, it becomes clear that an increase in DOTMA proportion in the monolayer leads to higher surface pressure, not just in the LE surface state but throughout the whole isotherm.

Interestingly, there is a correlation between the amount of DOTMA in the monolayer (0/5/10 mol%) and two important pressure values: the pressure at which the slope of the isotherm changes, probably due to a molecular rearrangement and/or a conformational change of the molecules at the interface (π_{trans}), and the collapse pressure (π_{coll}), plotted for both sets of isotherms in **Figure 4.3**. The slope change is also present in pure Tween 60 monolayers and similar molecules like Tween 80 [33], so it is likely it is this component, also the one in the largest proportion, that governs said conformational change at the interface.

At surface pressure values higher than 22.3 mN/m, the introduction of DOTMA causes an expansion of the polysorbate monolayer, rendering higher values of area per molecule. This is consistent with the intercalation of unsaturated hydrocarbon chains, in this case in an amount proportional to DOTMA concentration, among saturated, single-chain stearic residues of polysorbate molecules. The expanding effect of oleic chains has been reported in the literature for oleic acid/stearic acid [34] and saturated/unsaturated chain phospholipid interactions [35].

The presence of an interaction between both components is further evidenced by the concentration-dependent increase in the C_s^{-1} value with the proportion of DOTMA in the film at all π values. The surface pressure at which the peak of compressibility modulus takes place, which is equivalent to say the point at which compressibility is the lowest throughout compression and the monolayer is most rigid,

changes slightly with DOTMA proportion, but it shows not nearly as dramatic a shift as that in the compressibility modulus (**Table 4.3**).

Along with these differences, the value of the compressibility modulus in the three compared systems indicates the monolayer shows greater resistance to compression the greater the amount of DOTMA in it. This increase in rigidity, apparently contrary to what is known about the aforementioned effect of hydrocarbon chain saturation, can be ascribed to the attractive interaction between DOTMA and Tween 60 polar headgroups. The presence of a positive charge on DOTMA's quaternary ammonium (trimethylammonium) group (**Figure 4.1**) is relevant as to the intermolecular forces at play when in contact with other surfactants, as is the case of Tween 60. We suggest the net charge in DOTMA can establish non-covalent electrostatic bonds with the more densely charged parts of the polysorbate branched headgroup, the O atoms in the ester bond, in the adjacent ethylene oxide moiety and/or in the tetrahydrofuran ring being the ones most likely to participate in such interaction. The existence of these ion-dipole bonds, orders of magnitude times stronger than London interactions taking place between non-polar chains [36], is a possible explanation for their compensation, resulting in a condensing, rigidifying effect as translated into the compressibility modulus values of the three mixtures.

Table 4.3. Maximum values of compressibility modulus for Tween 60 and Tween 60/DOTMA systems, with their corresponding values of surface pressure. All values are expressed in mN/m.

System composition	Low concentration		High concentration	
	$\pi(C_s^{-1}max)$	$C_s^{-1}max$	$\pi(C_s^{-1}max)$	$C_s^{-1}max$
T	36.58	41.59	36.26	37.02
TD5	37.35	52.57	40.18	44.51
TD10	37.62 (38.99)	63.85	41.96	80.96

Table 4.4. Difference between maximum values of compressibility modulus for Tween 60 and Tween 60/DOTMA systems, with the difference in their corresponding values of surface pressure. All values are expressed in mN/m.

Comparison against pure Tween 60 (T)	$\Delta\pi(C_s^{-1}{}_{max})$	$\Delta C_s^{-1}{}_{max}$
TD5	0.77	10.98
TD10	1.04 (2.41)	22.26

4.3.1.3 Tertiary systems

Finally, once the effect of both cholesterol and DOTMA as individual components on polysorbate 60 has been assessed, the influence of cholesterol on Tween 60/DOTMA monolayers became the focus, adding a third component to the last binary system studied.

Monolayers made of three components were obtained and studied in two different concentrations, named low and high, where films spread from the higher concentration contain twice as many molecules as the ones from the lower concentration. This duplicity of experiments for the ternary system, whose composition was set after that of the niosomes made by our group [7], was necessary in order to investigate

the molecular arrangement of these surfactants at a very wide range of surface pressure by obtaining isotherms as representative as possible.

π-A isotherms from films spread in both diluted (a) and concentrated (b) regimes, with regions corresponding to compressibility stages are shown in **Figure 4.4**. The reason the two sets don't overlap resides in the influence of the number of molecules spread onto the air/water interface before compression, which determines the surface area available for molecules to arrange within the film at the beginning of compression [37].

The isotherms from the diluted regime begin with a gas-liquid expanded (G/LE) state [38,39] and molecules moving mostly freely at the interface, up to ca. 550 $Å^2$/molecule, when the interaction between molecules starts raising surface pressure significantly. At as low a pressure value as 3 mN/m, the isotherm corresponding to TCD5 begins to rise above TC and TCD10 and yielding a higher surface pressure (21.6 mN/m, versus 19.5 mN/m with 10% DOTMA and 18.0 mN/m without any) at the end.

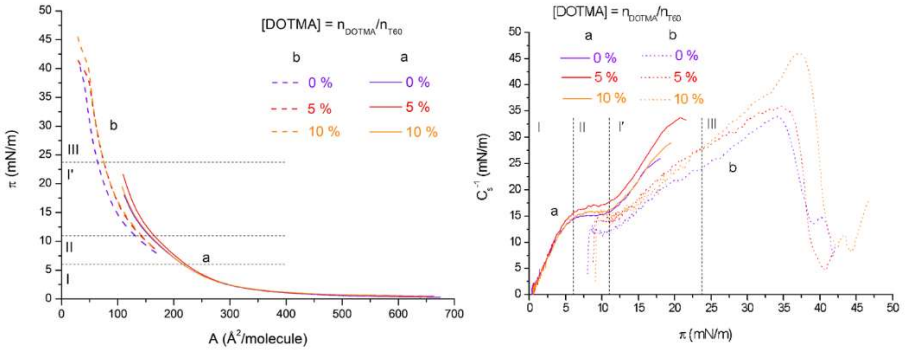

Figure 4.4. π-A isotherms (A) and compressibility moduli (B) of formulations TC, TCD5 and TCD10 at diluted and concentrated regimes.

From the compressibility modulus for the diluted regime (**Figure 4.4Ba**), one can see more clearly the distinct behavior for TCD5 monolayers, as the increased pressure shown by the isotherms comes with an increased modulus, which means films of this composition are more resistant to compression due to a higher packing arrangement.

By taking a closer look at this graph a sigmoid shape can be seen in the compressibility modulus vs surface pressure plot, which features a typical positive slope for the first part of compression (region I**, Figure 4.4**), then gives rise to a plateau in compressibility in the range of 6-11 mN/m for all compositions (region II), only to continue rising at higher pressures. This is a confirmation of the plateau hinted in **Figure 4.2** for the simplest system, Tween 60/cholesterol (TC curve for π=10-15 mN/m). Taking into account the ca. 29% of cholesterol present in the mixture and the surface behavior of both surfactants, the most logical conclusion is that the forces that make molecules repel each other upon compression are cancelled out by the attractive forces that rise when cholesterol molecules shift conformation from parallel to the interface ('lying down' on it) to perpendicular to it ('standing up') [20]. This attractive pull takes place via London dispersion interactions between the cholesterol planar, hydrophobic steroidal structure and non-polar stearyl chains belonging to Tween 60, as happens with stearic acid and cholesterol [40,41]. As soon as all cholesterol has changed conformation, compression continues without any other new interactions, making the plot resume its positive slope (region I' in **Figure 4.4**).

As for the difference in compressibility between systems of all compositions regarding DOTMA presence and concentration, there are two main points to focus on. First, as shown in **Figure 4.4**, the presence of DOTMA raises monolayer rigidity (given by C_s^{-1} values) for all

concentrations studied, although significantly more at 5 mol% than 10 mol% (**Figure 4.4a**), with certain exceptions for the concentrated regime (**Figure 4.4b**).

Second, the effect of DOTMA concentration is different to the findings presented above, which, given the novelty of the introduction of cholesterol in the Tween 60/DOTMA film, hints at a possible cholesterol/DOTMA interaction and points at a predominance of the expanding effect of oleic chains, which are more numerous with greater DOTMA concentration, given the relatively large distance between polar headgroups for a proper interaction.

In the concentrated regime, the trend established for the diluted regime continues (region I', **Figure 4.4**) until the monolayer reaches π = 23.7 mN/m, point at which the TCD10 film becomes less compressible than the TCD5 film (transition from region I' to III in **Figure 4.4**). We ascribe this change to the fact that, if prior to this point the polar headgroups were not close enough to one another for the attractive electrostatic interactions to manifest themselves, hence leaving the system governed by the expanding effect of the oleic chains from DOTMA. At pressures higher than this the interaction between the surfactants in the monolayer is now governed by the polar headgroups, thus making the film more rigid.

Furthermore, Tween 60 has a voluminous, branched headgroup that makes the surfactant moderately hydrophilic (solubility ca. 100 g/L). In this context, it is reasonable to assume the three polyether chains in this polar region of the surfactant, all in the subphase, are highly hydrated and have a certain distance between each other, but we hypothesize that, upon compression beyond 24 mN/m, they start getting closer to each other, decreasing its overall effective volume and progressively dehydrating [42] and facilitating the interactions of

DOTMA's trimethylammonium group, particularly with cholesterol. It is our understanding that this new interaction takes place between the positive charge on the nitrogen atom of the quaternary ammonium group in DOTMA and the electron-rich oxygen atom in cholesterol's hydroxyl group. Thanks to the attractive forces that arise through this interaction, as well as the discussed Tween 60/DOTMA interaction, also ion-dipole in nature, the monolayer adopts a tighter, more stable packing arrangement, becoming more resistant to compression, thus yielding higher C_s^{-1} values. This also leads to the conclusion that both cholesterol and DOTMA play a part in stabilizing the T60/DOTMA/chol monolayer, and therefore the niosomes, making both components necessary at the same time.

The other important feature in region III seen in **Figure 4.4** is that, immediately after rising to a maximum compressibility, there is a dramatic, sudden fall in this property of the film. This is also observed as an evident change of slope in the pressure-area isotherms (**Figure 4.4A**), and it can be ascribed to a conformational change that leads to the collapse of the monolayer.

Collapse implies the loss of the monolayer's structure, after which molecules at the interface are left in a loosely packed arrangement, with plenty of free surface area, that allows further compression and approximation of the molecules to each other. The mechanism through which this phenomenon takes place can follow one out of these two routes: either the formation of a volume phase (multilayer formation), as seen in many lipids such as fatty acids [43], or surfactant desorption into the subphase. It is tempting to rule out the first option by the absence of a similar drop, in this case in surface pressure, in the compression isotherms [15]. An analysis of the structure and solubility of the different chemical species present in the monolayer, as well of

the interactions between them, could point at Tween 60, the most abundant and hydrophilic of the three and the one with the largest polar headgroup, abandoning the interface by solubilising into the subphase. Should this path be followed, one possible scenario involves the surface aggregation of Tween 60 into segregated microdomains within the film, related to its surface miscibility [16,18], which by the great size difference between its hydrophobic chain and its polar headgroup, is likely to use these surface aggregates as a previous step into solubilization, possibly even preserving some degree of aggregation in the bulk [44].

Whatever the mechanism, the collapse pressure, given by the drop in C_s^{-1}, takes place at higher values for the TCD10 monolayer (at 37.2 mN/m) than for TCD5 and TC monolayers (at 34.6 and 34.3 mN/m respectively), further accounting for the tighter packing of the film the higher the concentration of DOTMA for π values above ca. 24 mN/m, at which the vesicles are thought to be [27]. This is compatible with the data published by our group [8] on the stability of niosomes with this exact composition after two months.

From the perspective of the effect of cholesterol, results show that, in spite of these well-established interactions and the stability of both the monolayers and the vesicles, the presence of cholesterol dampens the effect of DOTMA on Tween 60. This further indicates the existence of the cholesterol-DOTMA interactions. In term of mechanism, it is rather likely that the intercalation of cholesterol's polycyclic structure amongst hydrocarbon chains of Tween 60 and DOTMA is responsible for this effect, similarly to what was hypothesised above for T60/cholesterol interactions. In fact, the drop in the maximum C_s^{-1} value for the same T60/DOTMA proportion due to cholesterol is greater

the more DOTMA there is in the monolayer (24.47 mN/m for TCD10 16.04 mN/m for TCD5; 0.90 mN/m for TC).

Cholesterol therefore prevents monolayer packing in Tween 60/DOTMA systems proportionately to the amount of DOTMA, which gives more grounds to the probability of an interaction between DOTMA's oleic chains and cholesterol.

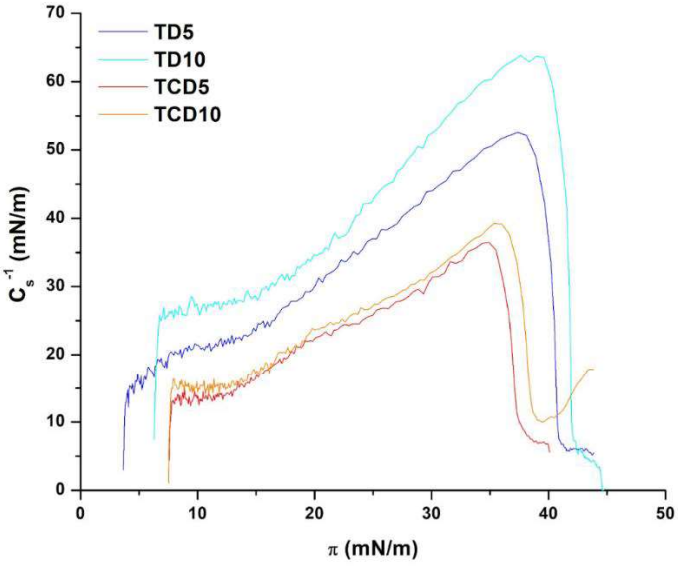

Figure 4.5. Compressibility modulus of Tween 60 monolayers at 5% and 10% DOTMA with and without cholesterol

The introduction of cholesterol in a T60/DOTMA system at a fixed proportion makes niosome-mimicking monolayers more compressible (**Figure 4.5**). It is the same effect it has on pure T60, only to a much greater degree.

4.3.2 Effect of temperature

Isotherms from the compression of films with the three different DOTMA concentrations at the concentrated regime obtained at 20 ºC and 30 ºC (maximum temperature allowed at the interface for technical reasons related to the mechanical properties of the PTFE of the Langmuir trough) were compared in order to study whether the behavior of the monolayer at the air/water interface shown at room temperature is extensive to temperatures closer to that of the human eye [44] (35ºC), at which niosomes are intended to act.

The compression isotherms of these films at 20 ºC (a) and 30 ºC (b) described in **Figure 4.6** show that the shape of the isotherms is the same at both temperatures, but that the behavior shown by the films with different amounts of DOTMA upon compression is completely different.

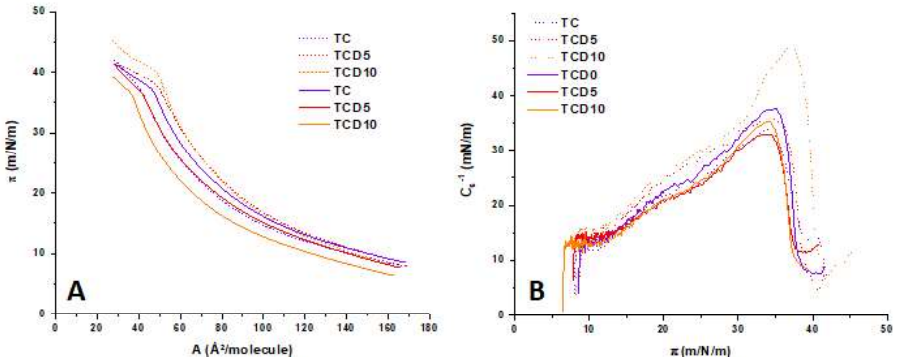

Figure 4.6. π-A isotherms (A) and compressibility moduli (B) of Tween 60/cholesterol/DOTMA monolayers at 20°C and 30°C. The dashed lines represent the monolayers at 20°C and the solid lines represent the monolayers at 30°C.

A quick view of the pressure-area curves manifests an opposite trend on how DOTMA proportion affects the surface activity of the film. At 20 ºC (**Figure 4.6a**), the presence of DOTMA raises surface

pressure throughout the whole compression and doubling the amount of DOTMA in the film implies greater surface pressure, if only at areas below ca. 60 $Å^2$/molecule. Along with the analysis of the elasticity of the monolayer, this reveals that the addition of DOTMA in the proportion range studied here raises the pressure at which the maximum compressibility (C_s^{-1}) is reached, from 34.6 mN/m at 5% to 37.2 mN/m at 10% the amount of Tween 60, indicating an increased stability of the film, but remaining independent on DOTMA concentration at looser packing arrangements typical of greater values of molecular area.

At 30 ºC, however, both the presence and increasing concentration of DOTMA in the monolayer cause a visible decrease in surface pressure at any value of mean molecular area. To explore a quantitative approach to the influence of temperature in these films, the value for surface pressure yielded at the beginning of the compression of the film was analyzed, at an arbitrary value before the maximum elasticity point of the film for all systems, and right at the end of compression.

Table 4.5. Surface pressure difference at given points of the isotherms of the same composition obtained at different temperatures. $\Delta\pi = \pi(30\ ºC) - \pi(20\ ºC)$ at that point.

% DOTMA (over T60)	$\Delta\pi_{init}$ (mN/m)	$\Delta\pi_{60\ Å^2/molec.}$ (mN/m)	$\Delta\pi_{max}$ (mN/m)
0	0.6	2.8	-0.5
5	-1.0	-2.2	-0.4
10	-2.6	-9.1	-7.4

4.3.3 Effect of the subphase

The ionic strength of the subphase has an effect on the monolayer, all the while being less marked than the effect of temperature. (**Figure 4.7**)

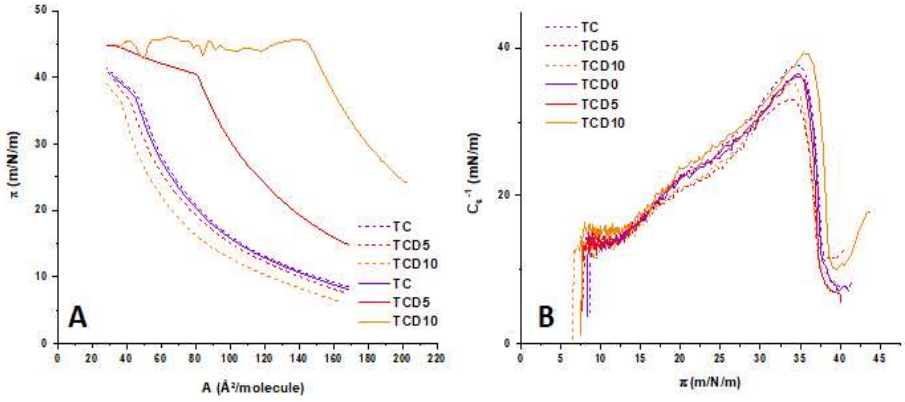

Figure 4.7. π-A isotherms (A) and compressibility moduli (B) of Tween 60/cholesterol/DOTMA monolayers at 30 °C on water and PBS. The dashed lines represent the monolayers deposited onto pure water and the solid lines represent the monolayers deposited onto PBS

While the binary system of Tween 60 and cholesterol seems to have slightly lower modulus with increasing ionic strength of the subphase, the ternary systems have higher modulus with increasing ionic strength of the subphase. This effect is expected as the ternary systems include the charged DOTMA, and goes in the same direction as the published data [45,46]. The ions present in the subphase interacting with the polar headgroup of DOTMA can lead to a salting out effect [48], increasing the presence of DOTMA at the interface. The concentration of salts of the PBS subphase as well as the cationic charge on the DOTMA are the main driving factors in the electrostatic effect.

4.3.4 Brewster Angle Microscopy

The BAM images were obtained by compressing a monolayer of TCD5 on a water surface. The images were taken at regular intervals, and while the available equipment did not permit taking video footage, the movement of the monolayer was clear starting at 80 $Å^2$/molecule.

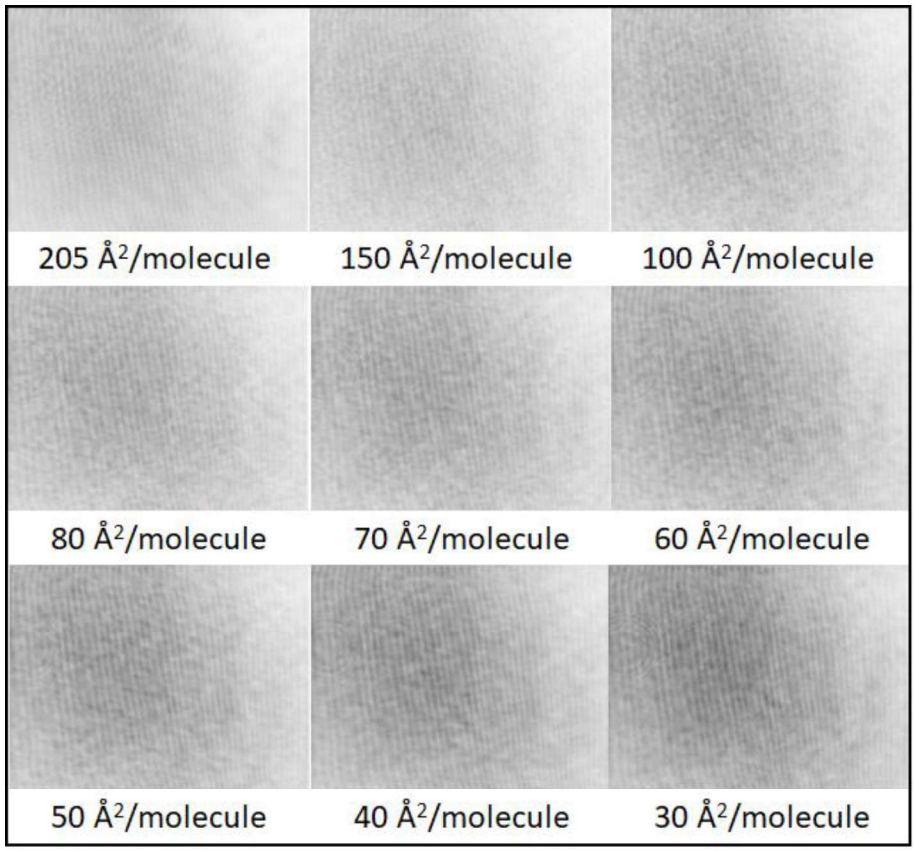

Figure 4.8. BAM images of the compression of the TCD5 monolayer on PBS at 20 °C

The BAM images in **Figure 4.8** show no presence of microdomains [48]. When compression happens and the spatial restrictions on the molecules increases, the only noticeable feature is a

darkening of the image attributed to more reflection of the polarized light by the monolayer. This indicates an increase in density of the monolayer when compressed, and supports the previous compressibility study findings and the comparison with previously published data [49].

4.4 CONCLUSION

Through experiments with Langmuir monolayers and the analysis of their mechanical properties, with all systems having virtually the same cholesterol concentration (0.286 ± 0.01 mg/mL), an increase in compressibility was established in all studied systems in a DOTMA-concentration dependent way, and therefore hinders undesired tightly packing arrangements which might negatively affect drug delivery in the eye. A positive correlation between DOTMA concentration in the studied range and the degree of packing and stability of Tween 60/cholesterol/DOTMA films was found, which is expected to be analogous to that in the vesicle bilayer.

Additionally, the change in niosomes from storage conditions (water formulation, 20 ºC) to administration conditions in the eye (electrolytic medium, closer to 30 ºC) in terms of temperature and ionic strength as studied at the air/water interface indicates that the addition of DOTMA to the binary Tween 60/cholesterol system increases its compression modulus at 30 °C and its pressure at higher surface area available per molecule tremendously in SLF.

4.5 REFERENCES

1. Datta, A.; Chakma, A.K.; Datta, D. Prevalence of Diabetic Retinopathy in Type-2 Diabetes Mellitus Patients in Tripura. *J. Evol. Med. Dent. Sci.* **2014**, *3*, 136–146, doi:10.14260/jemds/1802.

2. Thomas, R.L.; Dunstan, F.D.; Luzio, S.D.; Chowdhury, S.R.; North, R. V.; Hale, S.L.; Gibbins, R.L.; Owens, D.R. Prevalence of Diabetic Retinopathy within a National Diabetic Retinopathy Screening Service. *Br. J. Ophthalmol.* **2015**, *99*, 64–68, doi:10.1136/bjophthalmol-2013-304017.

3. Yau, J.W.Y.; Rogers, S.L.; Kawasaki, R.; Lamoureux, E.L.; Kowalski, J.W.; Bek, T.; Chen, S.J.; Dekker, J.M.; Fletcher, A.; Grauslund, J.; et al. Global Prevalence and Major Risk Factors of Diabetic Retinopathy. *Diabetes Care* **2012**, *35*, 556–564, doi:10.2337/dc11-1909.

4. Kattar, A.; Concheiro, A.; Alvarez-Lorenzo, C. Diabetic Eye: Associated Diseases, Drugs in Clinic, and Role of Self-Assembled Carriers in Topical Treatment. *Expert Opin. Drug Deliv.* **2021**, *18*, 1589–1607, doi:10.1080/17425247.2021.1953466.

5. Alvarez-Rivera, F.; Fernández-Villanueva, D.; Concheiro, A.; Alvarez-Lorenzo, C. α-Lipoic Acid in Soluplus ® Polymeric Nanomicelles for Ocular Treatment of Diabetes-Associated Corneal Diseases. *J. Pharm. Sci.* **2016**, *105*, 2855–2863, doi:10.1016/j.xphs.2016.03.006.

6. Chen, X.; Wu, J.; Lin, X.; Wu, X.; Yu, X.; Wang, B.; Xu, W. Tacrolimus Loaded Cationic Liposomes for Dry Eye Treatment. *Front. Pharmacol.* **2022**, *13*, 1–16, doi:10.3389/fphar.2022.838168.

7. Jain, N.; Verma, A.; Jain, N. Formulation and Investigation of Pilocarpine Hydrochloride Niosomal Gels for the Treatment of

Glaucoma: Intraocular Pressure Measurement in White Albino Rabbits. *Drug Deliv.* **2020**, *27*, 888–899, doi:10.1080/10717544.2020.1775726.

8. Kattar, A.; Quelle-Regaldie, A.; Sánchez, L.; Concheiro, A.; Alvarez-Lorenzo, C. Formulation and Characterization of Epalrestat-Loaded Polysorbate 60 Cationic Niosomes for Ocular Delivery. *Pharmaceutics* **2023**, *15*, 1247, doi:10.3390/pharmaceutics15041247.

9. Nobre, T.M.; Pavinatto, F.J.; Caseli, L.; Barros-Timmons, A.; Dynarowicz-Łatka, P.; Oliveira, O.N. Interactions of Bioactive Molecules & Nanomaterials with Langmuir Monolayers as Cell Membrane Models. *Thin Solid Films* **2015**, *593*, 158–188, doi:10.1016/j.tsf.2015.09.047.

10. Rojewska, M.; Smułek, W.; Grzywaczyk, A.; Kaczorek, E.; Prochaska, K. Study of Interactions between Saponin Biosurfactant and Model Biological Membranes: Phospholipid Monolayers and Liposomes. *Molecules* **2023**, *28*, doi:10.3390/molecules28041965.

11. Bahadur, A.; Cabana-Montenegro, S.; Aswal, V.K.; Lage, E. V.; Sandez-Macho, I.; Concheiro, A.; Alvarez-Lorenzo, C.; Bahadur, P. NaCl-Triggered Self-Assembly of Hydrophilic Poloxamine Block Copolymers. *Int. J. Pharm.* **2015**, *494*, 453–462, doi:10.1016/j.ijpharm.2015.08.058.

12. Seoane, R.; Dynarowicz-tstka, P.; Miñones J., J.; Rey-Gómez-Serranillos, I. Mixed Langmuir Monolayers of Cholesterol and “essential” Fatty Acids. *Colloid Polym. Sci.* **2001**, *279*, 562–570, doi:10.1007/s003960000453.

13. Moghaddam, B.; Ali, M.H.; Wilkhu, J.; Kirby, D.J.; Mohammed, A.R.; Zheng, Q.; Perrie, Y. The Application of Monolayer Studies in the Understanding of Liposomal Formulations. *Int. J. Pharm.* **2011**, *417*, 235–244, doi:10.1016/j.ijpharm.2011.01.020.

14. Cerro, R.L. Moving Contact Lines and Langmuir–Blodgett Film Deposition. *J. Colloid Interface Sci.* **2003**, *257*, 276–283, doi:10.1016/S0021-9797(02)00009-7.

15. Przykaza, K.; Woźniak, K.; Jurak, M.; Wiącek, A.E.; Mroczka, R. Properties of the Langmuir and Langmuir–Blodgett Monolayers of Cholesterol-Cyclosporine A on Water and Polymer Support. *Adsorption* **2019**, *25*, 923–936, doi:10.1007/s10450-019-00117-2.

16. Nagle, J.F. Area Compressibility Moduli of the Monolayer Leaflets of Asymmetric Bilayers from Simulations. *Biophys. J.* **2019**, *117*, 1051–1056, doi:10.1016/j.bpj.2019.08.016.

17. Fidalgo Rodriguez, J.L.; Caseli, L.; Torres Rodrigues, R.; Miñones Conde, J.; Dynarowicz-Latka, P. Phase Transition beyond the Monolayer Collapse – The Case of Stearic Acid Spread at the Air/Water Interface. *Colloids Surfaces A Physicochem. Eng. Asp.* **2021**, *623*, 126781, doi:10.1016/j.colsurfa.2021.126781.

18. Hao, C.; Liu, Q.; Li, Q.; Zhang, J.; Sun, R. Thermodynamic and Structural Studies of DMPC and DSPC with DOTAP Mixed Monolayers at the Air–Water Interface. *Russ. J. Phys. Chem. A* **2016**, *90*, 214–219, doi:10.1134/S0036024415120079.

19. Szymczyk, K.; Zdziennicka, A.; Jańczuk, B. Adsorption and Aggregation Properties of Some Polysorbates at Different Temperatures. *J. Solution Chem.* **2018**, *47*, 1824–1840, doi:10.1007/s10953-018-0823-z.

20. Fidalgo Rodriguez, J.L.; Caseli, L.; Minones Conde, J.; Dynarowicz-Latka, P. New Look for an Old Molecule – Solid/Solid Phase Transition in Cholesterol Monolayers. *Chem. Phys. Lipids* **2019**, *225*, 104819, doi:10.1016/j.chemphyslip.2019.104819.

21. Singhal, S.; Moser, C.C.; Wheatley, M.A. Surfactant-Stabilized

Microbubbles as Ultrasound Contrast Agents: Stability Study of Span 60 and Tween 80 Mixtures Using a Langmuir Trough. *Langmuir* **1993**, *9*, 2426–2429, doi:10.1021/la00033a027.

22. Katarzyna, H.; Wydro, P. The Influence of Fatty Acids on Model Cholesterol / Phospholipid Membranes. **2007**, *150*, 66–81, doi:10.1016/j.chemphyslip.2007.06.213.

23. Seoane, R.; Miñones, J.; Conde, O.; Miñones, J.; Casas, M.; Iribarnegaray, E. Thermodynamic and Brewster Angle Microscopy Studies of Fatty Acid/Cholesterol Mixtures at the Air/Water Interface. *J. Phys. Chem. B* **2000**, *104*, 7735–7744, doi:10.1021/jp001133+.

24. Fantini, J.; Barrantes, F.J. How Cholesterol Interacts with Membrane Proteins : An Exploration of Cholesterol-Binding Sites Including CRAC, CARC, and Tilted Domains. **2013**, *4*, 1–9, doi:10.3389/fphys.2013.00031.

25. Miñones Trillo, J. *La Interfase Aire / Agua : Monocapas de Extension*; **2002**; Real Academia de Farmacia Sección Galicia, 1-204

26. Ritwiset, A.; Krongsuk, S.; Johns, J.R. Molecular Structure and Dynamical Properties of Niosome Bilayers with and without Cholesterol Incorporation: A Molecular Dynamics Simulation Study. *Appl. Surf. Sci.* **2016**, *380*, 23–31, doi:10.1016/j.apsusc.2016.02.092.

27. Arslanov, V. V.; Ermakova, E. V.; Krylov, D.I.; Popova, O.O. On the Relationship between the Properties of Planar Structures of Non-Ionic Surfactants and Their Vesicular Analogues – Niosomes. *J. Colloid Interface Sci.* **2023**, *640*, 281–295, doi:10.1016/j.jcis.2023.02.110.

28. Toimil, P.; Prieto, G.; Miñones, J.; Sarmiento, F. A Comparative Study of F-DPPC/DPPC Mixed Monolayers. Influence of Subphase Temperature on F-DPPC and DPPC

Monolayers. *Phys. Chem. Chem. Phys.* **2010**, *12*, 13323–13332, doi:10.1039/c0cp00506a.

29. Davies, J.T.; Rideal, E.K.. *Interfacial Phenomena*; 2nd ed.; 1963; ISBN 9780323161664.

30. Anwander, A.E.; Grant, R.P.J.S.; Letcher, T.M. Interfacial Phenomena. *J. Chem. Educ.* **1988**, *65*, 608, doi:10.1021/ed065p608.

31. Ren, T.; Song, Y.K.; Zhang, G.; Liu, D. Structural Basis of DOTMA for Its High Intravenous Transfection Activity in Mouse. *Gene Ther.* **2000**, *7*, 764–768, doi:10.1038/sj.gt.3301153.

32. Yang, J.; Hao, C.; Sun, R. Effect of Laminaria Japonica Polysaccharides on Lipids Monolayers at the Air-Water Surface. *Colloids Surfaces B Biointerfaces* **2018**, *161*, 614–619, doi:10.1016/j.colsurfb.2017.11.041.

33. Lu, D.; Rhodes, D.G. Mixed Composition Films of Spans and Tween 80 at the Air-Water Interface. *Langmuir* **2000**, *16*, 8107–8112, doi:10.1021/la000396s.

34. Torrent-Burgués, J. Thermodynamic Behaviour of Mixed Films of an Unsaturated and a Saturated Polar Lipid. (Oleic Acid-Stearic Acid and Popc-Dppc). *Colloids and Interfaces* **2018**, *2*, doi:10.3390/colloids2020017.

35. Wydro, P.; Witkowska, K. The Interactions between Phosphatidylglycerol and Phosphatidylethanolamines in Model Bacterial Membranes. The Effect of the Acyl Chain Length and Saturation. *Colloids Surfaces B Biointerfaces* **2009**, *72*, 32–39, doi:10.1016/j.colsurfb.2009.03.011.

36. Steed, J.W.; Atwood, J.L. *Supramolecular Chemistry*; 2nd ed.; Wiley, 2009; ISBN 9780470512333.

37. Francis, R.; Louche, G.; Duran, R.S. Effect of Close Packing of

Octadecyltriethoxysilane Molecules on Monolayer Morphology at the Air/Water Interface. *Thin Solid Films* **2006**, *513*, 347–355, doi:10.1016/j.tsf.2006.01.065.

38. Harkins, W.D.; Young, T.F.; Boyd, E. The Thermodynamics of Films: Energy and Entropy of Extension and Spreading of Insoluble Monolayers. *J. Chem. Phys.* **1940**, *8*, 954–965, doi:10.1063/1.1750610.

39. Dervichian, D.G. Changes of Phase and Transformations of Higher Order in Monolayers. *J. Chem. Phys.* **1939**, *7*, 931–948, doi:10.1063/1.1750347.

40. Wnętrzak, A.; Chachaj-Brekiesz, A.; Janikowska-Sagan, M.; Fidalgo Rodriguez, J.L.; Miñones Conde, J.; Dynarowicz-Latka, P. Crucial Role of the Hydroxyl Group Orientation in Langmuir Monolayers Organization–The Case of 7-Hydroxycholesterol Epimers. *Colloids Surfaces A Physicochem. Eng. Asp.* **2019**, *563*, 330–339, doi:10.1016/j.colsurfa.2018.12.025.

41. Grimme, S.; Antony, J.; Ehrlich, S.; Krieg, H. A Consistent and Accurate Ab Initio Parametrization of Density Functional Dispersion Correction (DFT-D) for the 94 Elements H-Pu. *J. Chem. Phys.* **2010**, *132*, 154104, doi:10.1063/1.3382344.

42. Fidalgo Rodríguez, J.L.; Dynarowicz-Latka, P.; Miñones Conde, J. Structure of Unsaturated Fatty Acids in 2D System. *Colloids Surfaces B Biointerfaces* **2017**, *158*, 634–642, doi:10.1016/j.colsurfb.2017.07.016.

43. McFate, C.; Ward, D.; Olmsted, J. Organized Collapse of Fatty Acid Monolayers. *Langmuir* **1993**, *9*, 1036–1039, doi:10.1021/la00028a026.

44. Lipp, M.M.; Lee, K.Y.C.; Takamoto, D.Y.; Zasadzinski, J.A.; Waring, A.J. Coexistence of Buckled and Flat Monolayers. *Phys. Rev. Lett.* **1998**, *81*, 1650–1653,

doi:10.1103/PhysRevLett.81.1650.

45. Scott, J.A. The Computation of Temperature Rises in the Human Eye Induced by Infrared Radiation. *Phys. Med. Biol.* **1988**, *33*, 243–257, doi:10.1088/0031-9155/33/2/004.

46. Wang, Y.; Wen, G.; Pispas, S.; Yang, S.; You, K. Effects of Subphase PH, Temperature and Ionic Strength on the Aggregation Behavior of PnBA-b-PAA at the Air/Water Interface. *J. Colloid Interface Sci.* **2018**, *512*, 862–870, doi:10.1016/j.jcis.2017.11.002.

47. Sacré, M.M.; El Mashak, E.M.; Tocanne, J.F. A Monolayer (π,ΔV) Study of the Ionic Properties of Alanylphosphatidylglycerol: Effects of PH and Ions. *Chem. Phys. Lipids* **1977**, *20*, 305–318, doi:10.1016/0009-3084(77)90071-8.

48. Yang, J.X.; He, W.N.; Xu, J.T.; Du, B.Y.; Fan, Z.Q. Influence of Different Inorganic Salts on Crystallization-Driven Morphological Transformation of PCL-b-PEO Micelles in Aqueous Solutions. *Chinese J. Polym. Sci. (English Ed.* **2014**, *32*, 1128–1138, doi:10.1007/s10118-014-1512-z.

49. Teixeira, A.C.T.; Fernandes, A.C.; Garcia, A.R.; Ilharco, L.M.; Brogueira, P.; Gonçalves da Silva, A.M.P.S. Microdomains in Mixed Monolayers of Oleanolic and Stearic Acids: Thermodynamic Study and BAM Observation at the Air-Water Interface and AFM and FTIR Analysis of LB Monolayers. *Chem. Phys. Lipids* **2007**, *149*, 1–13, doi:10.1016/j.chemphyslip.2007.05.004.

50. Nieto-Suárez, M.; Vila-Romeu, N.; Dynarowicz-Latka, P.; Prieto, I. The Influence of Inorganic Ions on the Properties of Nonionic Langmuir Monolayers. *Colloids Surfaces A Physicochem. Eng. Asp.* **2004**, *249*, 11–14, doi:10.1016/j.colsurfa.2004.08.040.

5. FORMULATION AND CHARACTERIZATION OF OLEOGELS FOR TOPICAL ADMINISTRATION OF EPALRESTAT

5.1 INTRODUCTION

A huge increase in eye care and treatment is expected to take place over the next years due to the prevalence of diabetes in an ageing population [1,2]. To treat patients suffering from diabetic ocular diseases an efficient ophthalmic drug delivery method is required as the eye is a difficult target due to its numerous barriers [3].

Devices such as adapted contact lenses [4], nanoparticles like liposomes [5], niosomes [6], cyclodextrins aggregates [7] or microemulsions [8] are being investigated as carriers able to transport drugs to a therapeutic site. Topical administration is commonly accepted as the most convenient delivery method as it does not require the assistance of any medical personnel, putting the patient in charge of their own treatment. Of the topical treatments, eye drops are the most common but have a severe drawback when it comes to bioavailability due to tear clearance [9]. To overcome tear clearance different ways have been explored, such as intraocular injections [10] or implanted hydrogels [11], but these solutions have brought their own challenges. Hydrogels are highly dependent on hydration [12], which can cause swelling and alter the release rate of drugs. Intraocular injections, on the other hand, are invasive and can cause pain, discomfort, and ocular

trauma. They are also associated with a high risk of infection and require skilled administration [13].

Oleogels, on the other hand, have several advantages over hydrogels as topical drug delivery systems. They are made out from a gelator and an oil, which after being melted together solidify at room temperature and are able to be extruded through needles of different sizes [14].They are solid at room temperature, but they become fluid when they come into contact with warm body temperatures, making them ideal for ocular drug delivery [15]. Oleogels are as biocompatible as hydrogels, minimizing the risk of ocular irritation and inflammation [16]. They can be designed to have a low viscosity, making them easier to administer compared to hydrogels [17]. This is particularly important for patients with limited dexterity or who have difficulty instilling eye drops. Another advantage of oleogels is that they have a longer duration of action compared to hydrogels or intraocular injections due to their ability to form a protective film on the ocular surface, reducing the rate of drug clearance. Furthermore, oleogels are able to retain a wide range of drugs, including hydrophobic and hydrophilic compounds [15,18].

In the context of diabetic patients their blood glucose levels can be high enough to activate an uncommon glucose conversion pathway: the polyol pathway [19]. This pathway can be blocked by epalrestat. Epalrestat is a drug that acts as an aldose reductase inhibitor, stopping the conversion of glucose to sorbitol in high glucose environments. This is important as sorbitol accumulation in the cells leads to oxidative and osmotic stress [20,21], cellular death [22], and ultimately loss of vision in the patients.

Research on oleogels for ocular drug delivery is gathering momentum [16,18,23–25] and this study aims to develop oleogels capable of releasing epalrestat in a sustained manner to the eye, by

forming a coat of loaded gel on the ocular surface, demonstrating the viability of the drug delivery platform in the context of diabetic ocular diseases.

5.2 MATERIALS AND METHODS

5.2.1 Materials.

Soybean oil (ThermoScientific, Kandel, Germany), ethyl cellulose (63 mPa.s, 5% in Toluene/EtOH 80:20, 25 °C, 100 s^{-1}, 48.7% w/w ethoxyl content)(Sigma-Aldrich, Louisville, KY, USA), beeswax (Vabneer, Heibei, China), cocoa butter (BambooStory, Peru), epalrestat (319.4 g/mol) (TCI, Tokyo, Japan), Tween 80 (Polyoxyethylene (20) sorbitan monooleate) MW 1310 g/mol, HLB 15 (Sigma Aldrich, Switzerland), phosphate buffered saline (Life Tecnologies Co., Carlsbad, CA, USA), ethanol (VWR Chemicals, Briare, France). Simulated lacrimal fluid (SLF) was made with 0.68 g sodium chloride (Labkem, Barcelona, Spain), 0.22 g sodium bicarbonate (Merck, St Louis, MO, USA), 0.008 g calcium chloride dihydrate (Merck, Darmstadt, Germany) and 0.14 g potassium chloride (Panreac, Castellar del Vallès, Spain) [26] in 100 mL distilled water.

5.2.2 Oleogel formulation.

Soybean oil was chosen as a carrier due to its biocompatibility and high smoke point, allowing for the heating to higher temperatures to melt gelators. Three gelators of different type were chosen: ethyl cellulose as a polymeric gelator, beeswax as a non-lipid based gelator and cocoa butter as a lipid-based gelator [14]. The oleogels were composed of either soybean oil and 5% w/w single gelator at or 10% w/w combined dual gelators (**Table 5.1**).

Table 5.1. Oleogel formulation gelator composition

Oleogel code	Ethyl cellulose % (w/w)	Beeswax % (w/w)	Cocoa butter % (w/w)
B	0	5	0
C	0	0	5
E	5	0	0
EB	5	5	0
EC	5	0	5
BC	0	5	5

The oleogels were formed by melting the gelators according to the compositions in **Table 5.1** and adding different amounts (5/10/30% w/w) of epalrestat in 1 mL soybean oil at 60 °C or 170 °C and 100 rpm magnetic stirring. The temperature of 170 °C was used only when ethyl cellulose was involved. Once the components have melted and the resulting mixture was homogenous it was loaded into a 3 mL syringe and cooled. The syringe was cooled to room temperature and 0.1 mL was extruded through a 22-gauge needle onto the surface of an aqueous medium to form an oleorod. Oleogel EB was chosen to be the oleogel loaded with 5% (46 mg), 10% (92 mg) and 30% (276 mg) w/w epalrestat as it was stable for longer at room temperature when kept in a syringe and allowed for more representative microscopy images.

5.2.3 Oleogel characterization.

Morphological analysis and drug dispersion in the oleogels were verified by imaging under 4x magnification using an Olympus CKX53 microscope equipped with an Olympus EP50 digital camera (Shinjuku, Tokyo, Japan).

Rotational rheology was performed on an AR1000-N Rheometer Rheolys (TA Instruments, Surrey, United Kingdom). The geometry used was a 4 cm cone solvent trap with 1.58 degree angle and a 50 μm

gap. The experiments were conducted at 20 °C. The viscosity and the shear stress were recorded at a controlled shear rate ramp of 0.05 to 1000 s^{-1}, recording 100 sampling points.

5.2.4 Epalrestat release.

Oleorods (0.1 mL) were deposited on top of 10 mL release medium inside a closed off vial. Three media were tested: distilled (DI) water, 1% v/v Tween 80 in water, and simulated lacrimal fluid (SLF). Release was tested at 20 °C and at 37 °C as it mimics both the temperatures of storage and application conditions. Pictures were taken at predetermined timepoints to follow morphological changes in oleorods over time. 1 mL of release medium was drawn at predefined timepoints, analyzed with UV-VIS spectroscopy at 295 nm (Genesis 150 UV-Visible Spectrophotometer, ThermoScientific), and then returned to the vial. Each experiment was repeated in triplicate. Each UV-Vis spectrum was compared with a calibration curve to quantify the epalrestat released. The calibration curve was prepared with concentrations ranging from 10 to 100 µg/mL with an increment step of 10 µg, and from 100 µg/mL 1000 µg/mL with an increment step of 100 µg.

Quantitative analysis of epalrestat with concentrations lower than 10 µg/mL was performed on a Waters 717 plus Autosampler HPLC with a 4.6x250 mm C18 Symmetry column (Waters, Ireland) with 5 µm pores. The mobile phase was acetonitrile:elution buffer 45:55 (v/v). The elution buffer was composed of 25 mM potassium dihydrogen phosphate and 25 mM disodium hydrogen phosphate dihydrate in ultrapure water adjusted to pH 6.5 with phosphoric acid. The flow rate was 0.85 mL/min, the detection wavelength 295 nm, the temperature was maintained at 25˚C, and the injection volume was 40 µL. The calibration curve was prepared with concentrations ranging from 1 to

10 µg/mL with an increment step of 1 µg/mL. The retention time of epalrestat was 4.5 min.

5.2.5 HET-CAM.

For the Hen's Egg Test on Chorioallantoic Membrane (HET-CAM) assay, fertilized eggs (15) were supplied by Coren (Ourense, Spain) and cleaned before incubation in an CCRS 0150 incubator (Ineltec, Spain) for 9 days at 37˚C and 60% relative humidity. On the day of the experiment the shell over the air chamber of the eggs was pared off with a needle and tweezers. The untouched inner membrane was moistened with a 0.9% NaCl solution and the eggs were placed back in the incubator for 30 min. The 0.9% NaCl solution was subsequently removed as well as the inner membrane while being careful not to damage the blood vessels of the CAM underneath. Any non-viable egg was discarded. NaOH 0.1M was used as the positive control and 0.9% NaCl was used as the negative control. Oleogel EB, EC and BC loaded with 5% w/w epalrestat (100 µL) were added to the eggs and the effect on the blood vessels regarding hemorrhage, lysis and coagulation were recorded. The ocular irritability potential score was calculated with the **Equation 5.1** [27]:

$$EE\% = 1 - \frac{amount\ of\ drug\ out\ of\ the\ dyalisis\ membrane}{total\ amount\ of\ drug} * 100,$$

Equation 5.1. Encapsulation efficiency of epalrestat in niosomes.

5.2.6 Corneal and scleral permeation.

Porcine eyes were supplied by a slaughterhouse and transported to the laboratory in diluted PBS solution at 4 ˚C in an ice bath. The corneas were dissected with 2-3 mm of surrounding tissue and washed with 0.9% NaCl to remove any attached tissue. The corneas were mounted in Franz diffusion cells with the outer part of the cornea facing up. In

the case of scleral permeability, the sclera was dissected, the choroid removed and mounted in Franz diffusion cells with the outer part facing up. The area available for permeation was 0.785 cm^2. The receiving chamber was filled with 6 mL of SLF while making sure no bubbles were formed and then agitated with a magnetic stirring rod at 400 rpm. The donor chamber was filled with 2 mL of SLF and closed off with parafilm to prevent evaporation. The system was then left to equilibrate for 1 h at 37 °C. Once the system was balanced, 2 mL of fresh SLF was added and 0.1 mL of oleogel was deposited in the donor chamber. After 30 min, at 1 h and then every hour, 1 mL of the solution in the receiving chamber was removed and replaced with 1 mL of fresh SLF. After 6 h the last sample was taken, and the corneas and scleras were weighed and incubated in ethanol at 37 ˚C for 24 h. They were then sonicated at 37 ˚C in an ultrasonic bath for 90 min. The resulting mixture was centrifuged at 1,000 rpm at 25 ˚C for 5 min and the supernatant was centrifuged at 14,000 rpm at 25 ˚C for 20 min. After filtration through 0.22 µm pore syringe filters (Scharlab, Barcelona, Spain) all the samples from the receptor chamber as well as the supernatant from the tissue incubation were analyzed with HPLC according to the protocol described above. All experiments were carried out in triplicate.

5.2.7 IR-RAMAN spectroscopy.

Porcine cornea and sclera were mounted in Franz cells and left for 6 hours in the same conditions as the corneal permeation experiment described above. The IR-Raman study was performed by taking a minimum of 3 points and a maximum of 6 points per cornea and measuring the Raman scattering of the surface. The excitation wavelength was 532.188 nm, the sample was kept at a temperature of 8 °C for the duration of the experiment with a cooling plate, the laser power was 3 mW, and each point was measured with 60 accumulations,

with an integration time of 0.3 s and an objective of x50 (Zeiss LD EC Epiplan-Neofluar Dic 50x /0.55). The measurement was done on the top and bottom part of the tissue, and the absolute height of the peak (CCD cts) after smoothing and baseline correction was compared between the top and bottom of the cornea.

5.3 RESULTS

5.3.1 Oleogel characterization

Oleogels were prepared choosing soybean oil as main component due to its high smoke point and biocompatibility. Ethyl cellulose, beeswax and cocoa butter were chosen as gelators, mixed based on **Table 5.1** to prepare oleogels that could be extruded into oleorods. It was found that combining two types of gelators for a total amount of 10% w/w gelator resulted in solid oleogels at room temperature different than liquid oleogels using a single type of gelator at 5% w/w. The liquid oleogels can be administered through eye drop form, while the solid oleogels can be extruded into oleorods through 22G needles.

Six oleogel formulations were finally prepared (**Table 5.1**). All oleogels were uniform at the macroscopic level. Only the 10% w/w gelator ratio oleogels were loaded with different amounts of epalrestat. Oleogel EB was loaded with three different epalrestat loading amounts, 5%, 10% and 30% and all loading amounts resulted in an oleorod at room temperature that did not break up. When formulation EC and BC were loaded with 30% epalrestat, the resulting oleorod deposited on water broke up within one hour at 20 °C. This left pools of oil on top of the water phase.

Oleogel EC was able to load 5% w/w (46 mg) and 10% w/w (92 mg) epalrestat, while oleogel BC was only able to load 5% (46 mg) epalrestat.

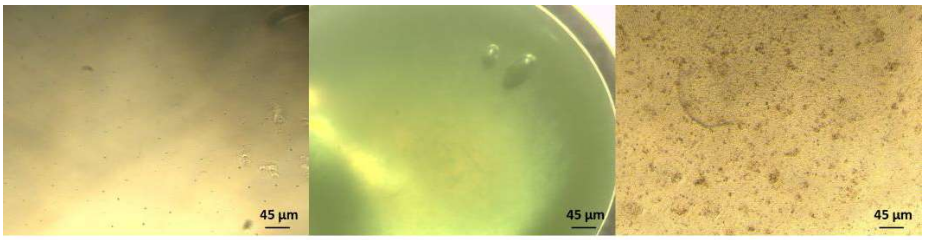

Figure 5.1. Microscope images of oleogels B, C and E (5% beeswax, 5% cocoa butter and 5% ethyl cellulose) loaded with 5% w/w epalrestat in soybean oil under x4 magnification.

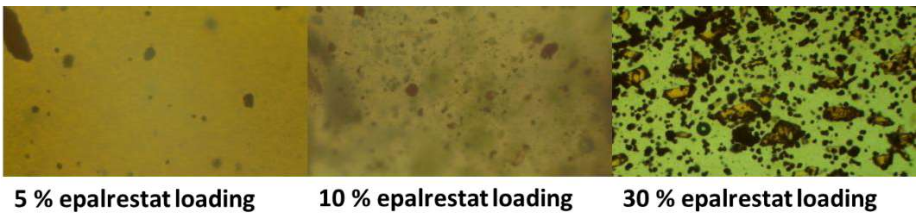

Figure 5.2. Microscope images of oleorod EB (5% ethyl cellulose 5% beeswax) in soybean oil under x4 magnification.

The homogeneousness of the oleogels with a single gelator at 5% w/w ratio can be seen in **Figure 5.1**. Oleogel B made with 5% w/w beeswax was the roughest when looked at 4x magnification. Oleogel C made with 5% w/w cocoa butter was the most homogenous and kept this aspect even at 40x magnification.

The incorporation of different amounts of epalrestat into oleogels allowed for different levels of solubilization of the drug in the oil phase. The presence of crystals in the EB oleords prepared with 30% epalrestat (**Figure 5.2**) demonstrated that at 30% epalrestat was not able to fully dissolve within the oleogel oil phase. In subsequent experiments, 5% epalrestat loading was chosen as it would be enough to reach therapeutic concentrations of epalrestat [27]. Nevertheless, higher amounts of hydrophobic drug could be loaded in oleorods if needed.

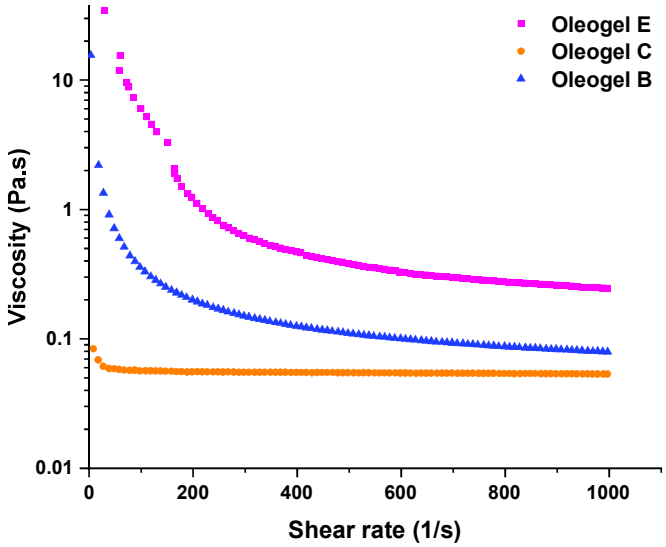

Figure 5.3. Effect of shear rate on the viscosity for oleogels comprised of 5% w/w gelator at 20 °C.

The dynamic viscosity of the single gelator oleogels at different shear rates is displayed in **Figure 5.3**. There was a steep decrease of viscosity as shear rates increased for oleogels B and E while the viscosity of oleogel C remained constant over the range of shear rates. Oleogel C behaved as a Newtonian fluid, with the dynamic viscosity constant over the range of shear rates, while oleogel B and oleogel E showed shear thinning behavior typical of pseudoplastic fluids [28].

Table 5.2. Viscosity of the oleogel formulation at 100 and 1000 s^{-1} at 20 °C

	E	B	C	EB	EC	BC	Soybean oil
100 s^{-1}	6.013	0.359	0.0566	17.10	51.2	-	0.612
1000 s^{-1}	0.245	0.079	0.0535	0.0031	-	-	0.056

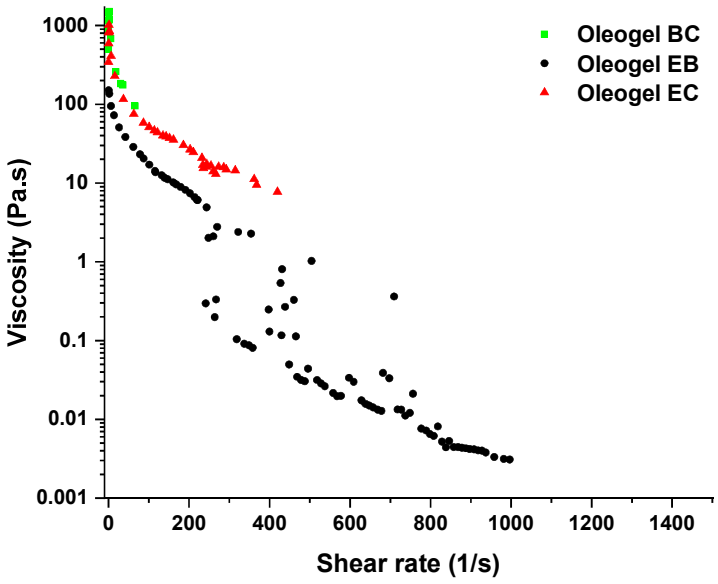

Figure 5.4. Effect of shear rate of the viscosity for oleogels comprised of 10% w/w combined gelators at 20 °C.

When 10% w/w gelator was used, the resulting oleogels showed shear thinning behavior (**Figure 5.4**). However it must be noted that oleogel BC and oleogel EC did not reach the same shear rates as oleogel EB at 20 °C, and this was due to the extreme shear stresses endured by the rheometer at higher shear rates. The viscosity values of each formulation are especially important to consider at two specific shear rates, 100 and 1000 s^{-1}, which are considered to be the shear rates of the progress of the blinking movement [29] (**Table 5.2**). The viscosity of oleogel C corresponds closely to the viscosity of soybean oil at the upper shear rate of the blinking process. Of the double gelator formulations, only oleogel EB reaches low viscosity values, due to the high shear thinning behavior displayed. However, it is important to notice that oleogels E, EB, EC and BC have viscosities at 100 s^{-1} that could be uncomfortable in the context of topical administration.

5.3.2 Epalrestat release

Oleorods were made by extruding 0.1 mL of oleogel through a 22G needle. The resulting oleorods were directly deposited on top of an aqueous subphase. The release of oleorods was carried out over different time periods going from a couple of hours to multiple days, in DI water, SLF and 1% v/v Tween 80 aqueous solution. The release on simulated lacrimal fluid was performed to mimic the conditions in which the oleogel applied topically would have to release epalrestat. The release on a 1% v/v Tween 80 aqueous solution phase was done to simulate conditions with high solubility of epalrestat in aqueous solution. The release was also tested at 20 °C and at 37 °C.

The oleorod displayed in **Figure 5.5** showed a change in the morphology of the rod structure over 4 days. The release of epalrestat was made evident by the color gradient of the oleorod, shifting to a less saturated color with time. The rod sectioned itself off into multiple smaller rods with time, increasing surface area further.

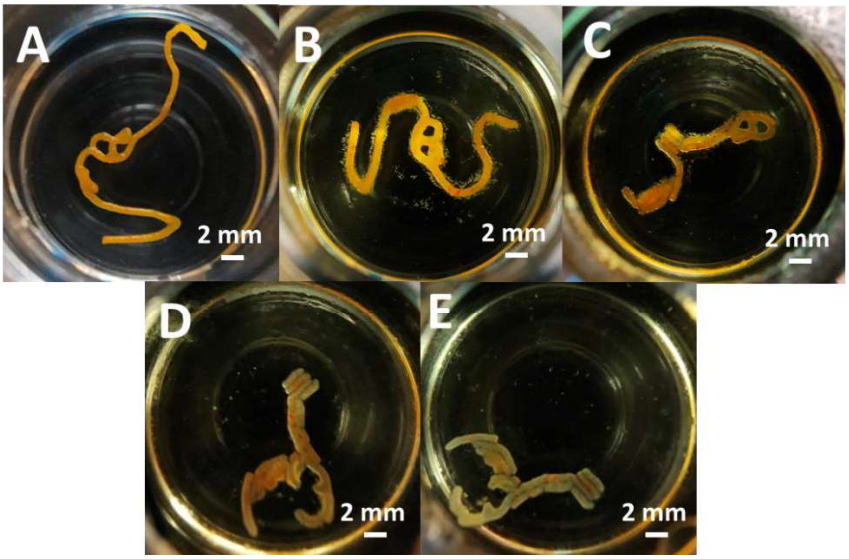

Figure 5.5. Oleorod EB loaded with 10% w/w epalrestat releasing the drug on DI water at 20 °C. The images were taken at timepoints: A: t =0; B = 1h; C = 6h; D = 1 day; E = 4 days at equivalent distance from the surface of the water.

First the release of epalrestat from oleorods was tested at 20 °C in DI water, SLF and 1% Tween 80 v/v aqueous solution for 2 hours. The volume of the oleorods was 0.1 mL, meaning the total amount of epalrestat available for release per oleorod was 4.6 mg.

Epalrestat got released from the oleorods at 20 °C into distilled water at a higher rate from the start of the experiment to 45 minutes for oleorods EC and BC, then plateaued at 1.3 µg/mg (3.0% of total epalrestat loading) and 1.9 µg/mg (4.4% of total epalrestat loading) respectively. This was also the behavior of oleorod EB (3.8% of total epalrestat loading released at 2 h), with the exception of the plateau where it instead had a linear release profile as can be seen in **Figure 5.6**. The release of epalrestat from oleorods at 37 °C was a linear for all three formulations. The increase of the release of epalrestat at 37 °C (EB: 6.7%; EC: 8.3%; BC: 8.7% of total epalrestat loading) is likely

due to the increased solubility of epalrestat in water at higher temperatures.

The release of epalrestat in SLF followed a burst release pattern with the exception of oleorod EC at 20 °C (**Figure 5.7**). The plateau of epalrestat released was the same (3.90 µg/mg; 9% of total epalrestat loading) for oleogels EB at 37 °C and oleorod BC at both temperatures, reached after 10 minutes. Oleorod EB at 20 °C released rapidly until 20 minutes and then slower but at constant rate until plateauing from one hour on. Epalrestat got released from oleorod EC at 37 °C rapidly in 10 minutes and then linearly until 45 minutes, reaching the same plateau as oleorods EB and BC at 37 °C.

Epalrestat release from oleorods into 1% Tween 80 v/v aqueous solution was faster in the case of 37 °C than in the case of 20 °C (**Figure 5.8**). The release of epalrestat into 1% Tween 80 v/v aqueous solution was rapid until 30 minutes, where the release rate diminished. The amounts of epalrestat released after 2 h where at best 3.4 µg/mg and 3.5 µg/mg (7.8% and 8.0% of total epalrestat loading respectively) corresponding to oleorods EC and BC at 37 °C. This is surprising as the expectation was that the total release of epalrestat in 1% v/v Tween 80 aqueous solution would be significantly higher than in DI water or SLF.

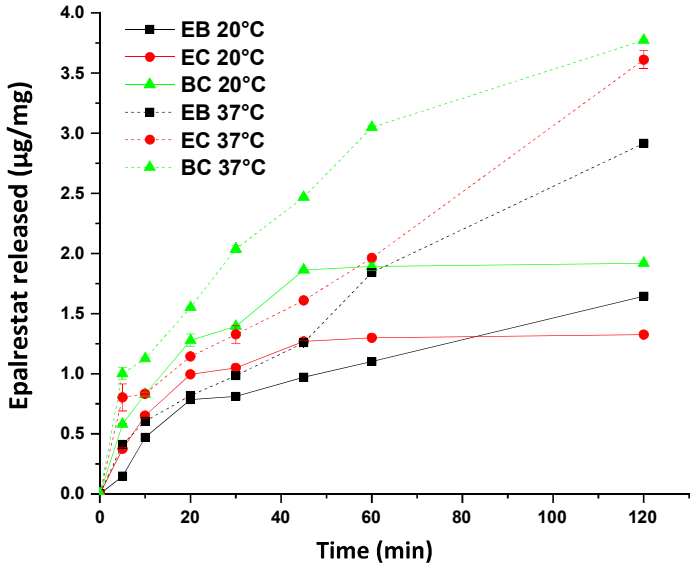

Figure 5.6. Drug released from oleorods loaded with 5% w/w epalrestat at 20 °C and 37 °C deposited on top DI water for 2 h.

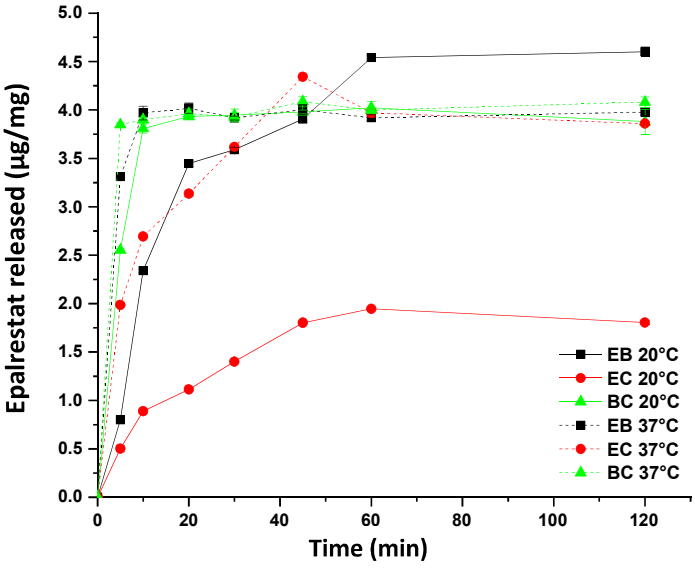

Figure 5.7. Drug released from oleorods loaded with 5% w/w epalrestat at 20 °C and 37 °C deposited on top of SLF for 2 h.

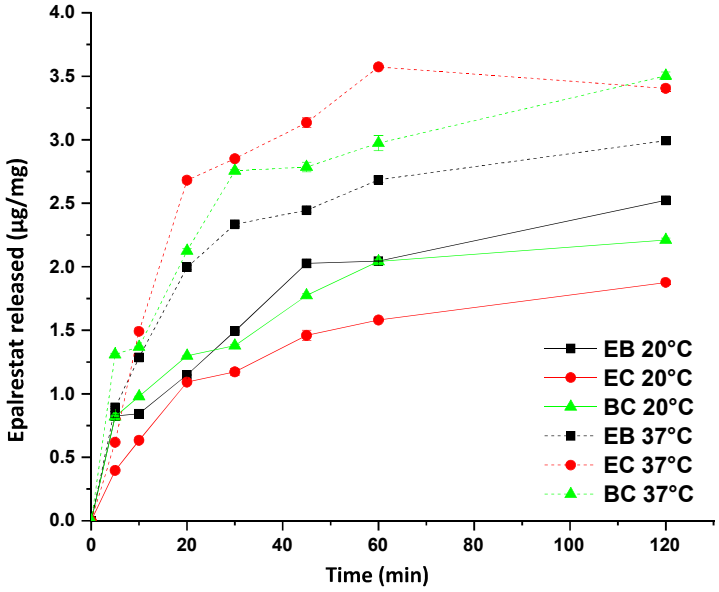

Figure 5.8. Drug released from oleorods loaded with 5% w/w epalrestat at 20 °C and 37 °C deposited on top of 1% Tween 80 v/v aqueous solution for 2 h.

The release of epalrestat in SLF from EC oleorods plateaued after 10 hours for both 5% and 10% epalrestat loaded oleorods (**Figure 5.9**). As expected, the oleorod loaded with 10% epalrestat released about twice the amount of the oleorod loaded with 5%. The final amount of epalrestat released in the case of 5% epalrestat loaded oleorod (1.5 µg/mg) correspond to the amount displayed in **Figure 5.7** after 2 hours.

When the oleorods were made with ethyl cellulose/beeswax instead of ethyl cellulose/cocoa butter as the gelling agent, the release duration increased to 24 h before plateauing (**Figure 5.10**). In this situation the oleorod loaded with 10% epalrestat did not manage to release twice the amount of epalrestat of the 5% loaded oleorod. Furthermore, the release profile and final amount of epalrestat released (2.0 µg/mg) was nearly twice as low as the expected value (4.5 µg/mg) found at the plateau of the precious release.

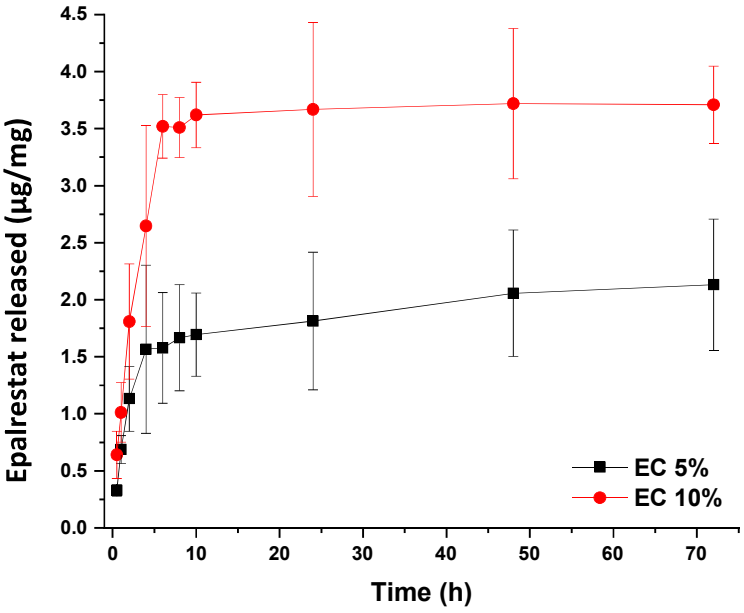

Figure 5.9. Epalrestat release from oleorod EC at 20 °C in SLF over 3 days.

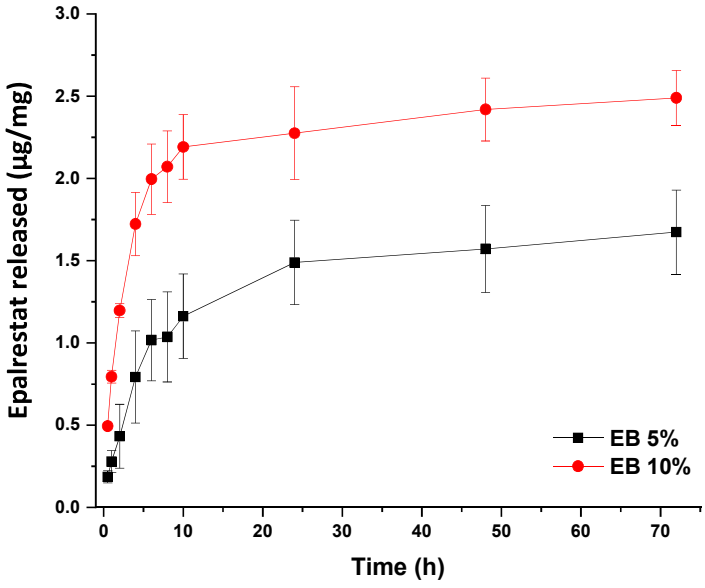

Figure 5.10. Epalrestat release from oleorod EB at 20 °C in SLF over 3 days.

While measuring the release profile of epalrestat from oleorods in 10 mL is important to understand the limitations of drug release, such a release volume is not realistic, as the tear film volume passing on the ocular surface is at most 1 mL in 6 hours [30,31]. Furthermore, during topical administration of oleogels, the deposition of the formulation is likely to be in drop format, restricting the extrusion of oleogels to volumes closer to 50 µL. Due to the high cost of epalrestat and the release limit of the drug in these conditions 5% w/w epalrestat loading was chosen for the following experiments.

5.3.3 HET-CAM

The HET-CAM assay was performed to obtain ocular irritability potential values for the three oleorods, EC, EB and BC. This assay was chosen as it is not considered an animal experiment under Directive 2010/63/EU [32], and gives an accurate idea of the safety of the formulations. The positive control (0.1 M NaOH) and the negative control (0.9% NaCl) displayed ocular irritability potentials of 19.5 ± 0.26 and 0, respectively. In the images of **Figure 5.11** the oleorods are seen as oleogel drops as they do not retain their shape 10 seconds after being brought in contact with the CAM at 37 °C. All three oleorods did not show any noticeable sign of hemorrhage, lysis or coagulation and obtained an ocular irritability potential score of 0. These results suggest that the oleorod formulations are safe for topical administration to the eye.

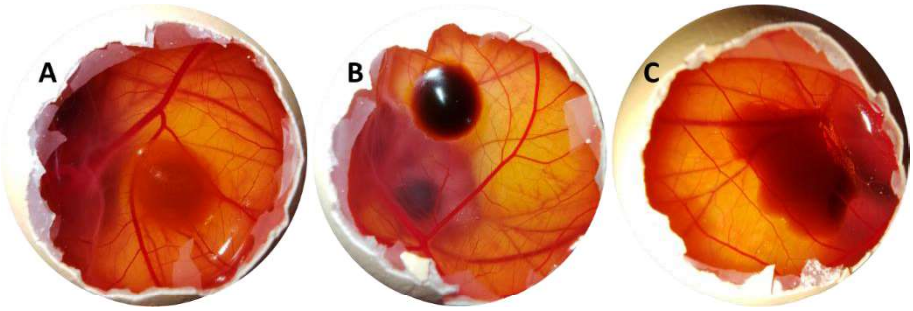

Figure 5.11. Pictures of the chorioallantoic membrane after 300 s. A: oleogel EB, B: oleogel EC, C: oleogel BC, all loaded with 5% w/w epalrestat.

5.3.4 Corneal and scleral permeation

The corneal permeation of epalrestat from oleogels only started after 4 h of contact as can be seen in **Figure 5.12**. Oleorod BC outperformed oleorods EB and EC by permeating about 8 times more by 6 h. For scleral permeation epalrestat started to permeate from 30 min on, with all three formulations permeating linearly. Again, oleorod BC outperformed oleogels EB and EC at 6 h, but by a smaller margin than for corneal permeation.

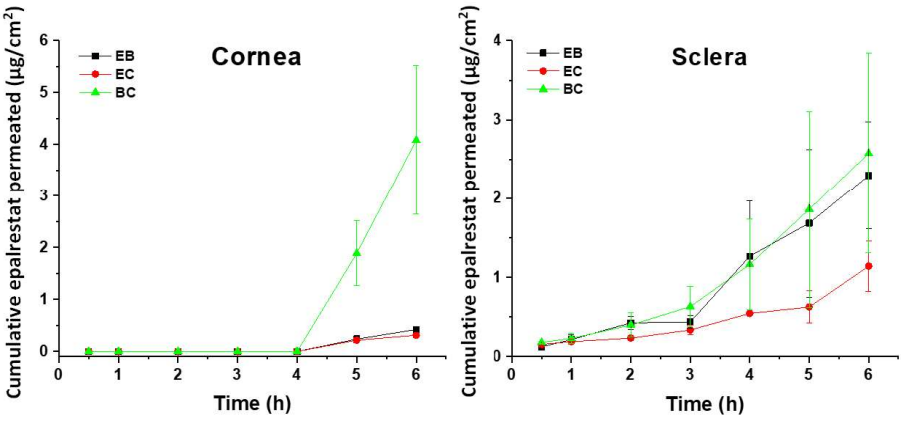

Figure 5.12. Amounts of epalrestat permeated through cornea (left) and sclera (right) after 6 h permeation experiment in Franz's diffusion cells.

The amount of epalrestat remaining in the tissue after 6 h of permeation was quantified by HPLC (**Figure 5.13**). In both corneal and scleral permeation oleorod BC (93 µg/g and 36 µg/g) left more epalrestat in the tissue than oleogels EC (20 µg/g and 31 µg/g) and EB 3 µg/g and 6 µg/g), which is in line with the permeation data. However, the fact that more epalrestat was retained in the tissue in the case of oleorod EC compared to oleorod EB when looking at scleral permeation was surprising as the permeation values showed oleorod EB allowing for better epalrestat scleral permeation than oleorod EC. The permeability coefficients of epalrestat delivered through each tissue by each oleorod are summarized in **Table 5.3**.

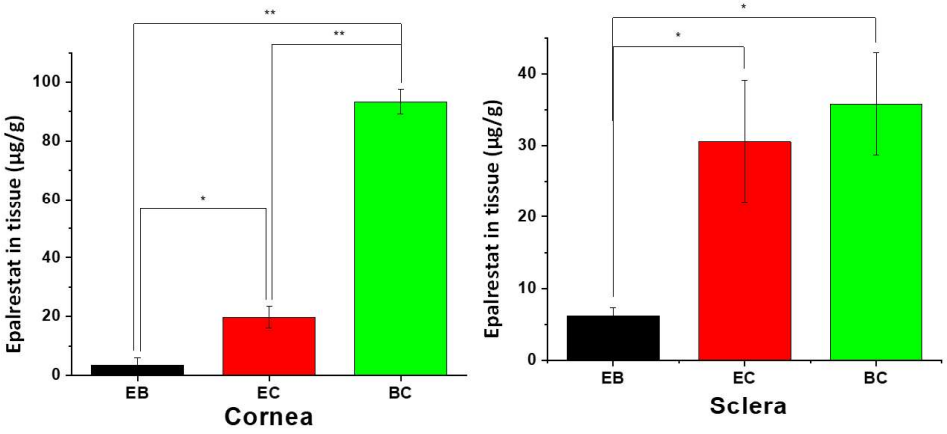

Figure 5.13. Epalrestat retained in corneal (left) and scleral (right) tissue after 6 h permeation experiment in Franz's diffusion cells. * statistically significant higher concentrations in the tissue ($p<0.05$) , ** statistically significant higher concentration in the tissue ($p<0.01$).

Table 5.3. Steady state flux, lag time and permeability coefficient of different tissues and oleorods.

Sample		Steady State Flux (µg/cm^2 × h)	Lag Time (min)	Permeability Coefficient (×10^6 cm/s)
Cornea	EB	1.307 ± 0.912	402.4 ± 246.3	2.520 ± 0.481
	EC	0.573 ± 0.0934	161.0 ± 40.2	0.796 ± 0.130
	BC	13.19 ± 5.931	246.1 ± 15.3	18.31 ± 8.238
Sclera	EB	2.196 ± 1.547	61.90 ± 25.8	3.050 ± 2.100
	EC	0.949 ± 0.254	20.70 ± 4.99	1.318 ± 0.350
	BC	2.571 ± 1.809	35.60 ± 17.5	3.571 ± 2.500

5.3.5 IR-RAMAN

IR-RAMAN spectroscopy was used to assess the presence of epalrestat at the top and bottom of the tissue, to confirm the permeation results displayed in the previous section (**Figure 5.14**). Oleorod EB showed a ratio of top to bottom close to one, confirming permeation of epalrestat through the cornea, with equal epalrestat presence on both

sides of the tissue. The top to bottom ratio of oleorods EC and BC was positive, meaning that there was more epalrestat present on the donor chamber side of the tissue compared to that of the receiver chamber side of the tissue.

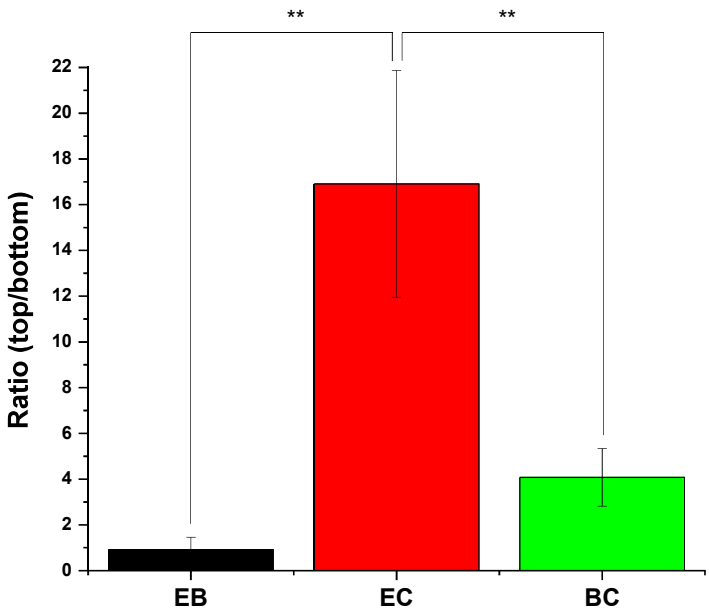

Figure 5.14. Ratio of the top to bottom intensity of Raman peaks indicating the presence of epalrestat in the cornea's outside layer. ** statistically significant higher top to bottom ratio (p<0.01).

5.4 DISCUSSION

Oleogels are being investigated as drug delivery platforms, but few articles are exploring their potential as a platform for ocular drug delivery [15,23–25]. To the best of our knowledge this is the first study incorporating epalrestat into oleogels for ocular delivery.

Six different oleogel formulations were prepared with different gelator combinations, and different epalrestat loading. The oil chosen was soybean oil for all oleogels, while the gelators chosen were ethyl cellulose, cocoa butter and beeswax. These gelators were chosen as they represent three categories of gelating agents: polymeric gelators (ethyl cellulose), lipid-based gelators (cocoa butter), and non-lipid based gelators (beeswax). The oleogels were able to homogeneously incorporate epalrestat up to 10% w/w, as confirmed with microscopy images. The morphology of the oleorods changed over the course of the release study, where it sectioned itself off over time. According to Macoon et al. [18] oleogel inserts made from 10% w/w β-sitosterol /lecithin (8:2), and 15% w/w sorbitan monostearate dissolve over time, reaching full dissolution after 2 and 5 months respectively. This is different than the oleorods made from 5% w/w beeswax, that kept their structure even after 110 days. The overall size of the oleogel inserts (2-4 μL) being smaller compared to the ones extruded in this study (0.1 mL) could account for the lack of sectioning as each section in image E of **Figure 5.5** was approximatively the size of the oleorod extruded in the study of Macoon et al. To keep precorneal residence, the viscosity of the oleogels need to be above 0.01 Pa.s [33,34], which all oleogels achieve in the range of blinking shear rates. While the maximum shear rate of blinking can reach values as high as 20,000 s^{-1} [35], measuring the viscosity at such high shear rates is redundant as the Newtonian plateau had been reached [36]. Commercial artificial tear solutions commonly have viscosities between 1 and 10 Pa.s when behaving as Newtonian fluids and between 8 and 100 Pa.s in the 100 s^{-1} to 1000 s^{-1} shear rate range when exhibiting shear thinning behavior [36]. A positive correlation has been established between higher viscosity and longer precorneal retention both in rabbit and humans [33,37]. The optimal eye drop is therefore viscous enough to increase its precorneal

retention time while simultaneously still being able to be administered in drop form.

The release of epalrestat was higher at 37 °C than at 20 °C in each release medium, as expected, due to the higher solubility of epalrestat at higher temperatures (2.956 mg/L at 25 °C [38] and 4.467 at 37 °C [39]). The most remarkable result was the change in release behavior when the oleogels were deposited on top of a SLF solution, where the epalrestat was able to release extremely rapidly from the oleorod. The behavior of release of an hydrophobic molecule into an ionic medium is in accordance with the results of Buyukozturk et al. [40] where naproxen would also release from soybean oil emulsions into PBS at 37 °C at a fast rate. The content of epalrestat in the oleogels being 4.6 mg per oleogel, the amounts that are released over two hours are always under 10%. The release of hydrophobic drugs from oleogels typically takes time, with the release of diclofenac from paraffin oleogels reaching 7.34% after one hour [41], or the release of ciprofloxacin reaching 10% from Span 60/mustard oil oleogels [42]. Oleorods prepared by Macoon et al. intended for intraocular injection displayed release times of 125 days to release 85% of the dexamethasone loaded in the device [16]. For topical administration, the burst release pattern shown by oleorod EB and BC when releasing epalrestat in SLF is favorable as ocular clearance will remove the formulation from the ocular surface even when deposited into the conjunctival sac.

The deposition of all three 5% w/w epalrestat loaded oleorods on the chorioallantoic membrane resulted in an ocular irritability potential score of 0, indicating the compatibility of the formulation with the eye. This also indicates that the oleorod protects the membrane from the damaging effects of epalrestat when in its free form [6], as epalrestat was previously reported to have an ocular irritability score of 18.58 at

0.2 mg/mL concentration. When compared to the results of HET-CAM assays of epalrestat in niosomes, this indicates that oleogels are able to protect the CAM to the same extent as niosomes [6].

Permeation of epalrestat through corneal and scleral tissue was successful. The scleral route seems to be the privileged route for permeation as epalrestat was detected in the receiving chamber from one hour on, and with the exception of oleorod BC, had higher permeability coefficients than permeation through corneal tissue. In both cornea and scleral tissue, the permeability coefficients indicated an efficiency of BC>EB>EC. The permeability coefficients of the corneal permeation are very different for each oleorod, which can be explained by the long time needed for the drug to start being detected in the receptor chamber of the Franz cell. The permeability coefficients are therefore calculated with linear regressions relying on less data points than the coefficients obtained for scleral permeation. When comparing the scleral permeability coefficients of epalrestat from oleogels to epalrestat from niosomal formulations, the range is in the same order of magnitude. The final cumulative amounts of epalrestat permeated through the tissues is also similar, however it needs to be pointed out that the 5% w/w loading of the oleogels represent 4.6 mg total epalrestat per oleorod, while the niosomes concentration and volume amounted to 0.4 mg total encapsulated epalrestat. This represents an 11.5 times increase of available epalrestat in the oleogel formulation. When relativized in regards to the amount of epalrestat loaded per formulation and compared to the permeability of epalrestat encapsulated in niosomes [6] the oleogels were less effective by a factor 10^4. This points to a relevant hypothesis; that while the absolute amounts of epalrestat permeated and recovered from the tissues are higher in the case of oleogels, owing to the higher loading potential of oleogels, the niosomes are able to help with permeation in a way that

oleogels cannot. This would mean that the permeation of epalrestat through corneal and scleral tissues follow Fickian diffusion kinetics and are affected by saturation effects in the donor chamber. This hypothesis is further supported by the results of *ex vivo* corneal permeation of ciprofloxacin from graphene oxide reinforced nanocomposite oleogels that managed to reach cumulative permeation percentages between 0.6% and 1.0%, with cumulative drug releases between 0.7% and 1.2% [23]. The Fickian diffusion of the drug was also the determining factor for the corneal permeation of voriconazole from palmitic acid and safflower oil oleogels, even though the drug molecule is hydrophilic than epalrestat or ciprofloxacin and was able to reach cumulative drug permeations values as high as 35% [25].

Interestingly, both in the recovery of epalrestat from permeated tissue and IR-RAMAN data, oleorod EC displayed higher values than oleorod EB. Oleorod EB having only a little amount of epalrestat remaining in the corneal and scleral tissue in comparison to the other two oleogels. The higher amounts of permeation from oleorod BC was further supported by the amounts of epalrestat recovered from the tissues after 6 hours of permeation. The trend of niosomes increasing permeation by a factor 10^4 was also found in the amounts of epalrestat recovered from the tissues [6], giving more weight to the hypothesis of Fickian diffusion governing permeability kinetics. The top to bottom ratios of the different oleogels indicate differences in the amounts of epalrestat in the first few microns of the cornea in contact with each of the chambers of the Franz cell. The ratio close to 1 of oleogel EB is logical seen as the epalrestat recovered from the tissue (3.45 µg/g) was significantly smaller than the epalrestat recovered from oleogels EC and BC (19.79 µg/g and 93.37 µg/g respectively). The high corneal permeation of epalrestat in the case of oleogel BC is corroborated by the high amount of epalrestat recovered in the corneal tissue and further

supported by the ratio of 4 between the epalrestat concentration on top and on the bottom of the cornea, pointing to an epalrestat gradient in the tissue. However, the permeation behavior of oleogel EC is less evident, as it was the oleogel with the highest top to bottom ratio (17) but a recovery of 19.37 µg/g epalrestat in the cornea and 0.31 µg/cm^2 cumulative permeated epalrestat after 6 hours. A possible explanation is that the oleogel at 37 °C would start to dissolve [43] and that parts of the oleogel matrix get deposited on the corneal tissue, creating a barrier to permeation which would explain the poor permeability results and the high ratio of top to bottom epalrestat concentration.

The most promising oleorod seems to be formulated with soybean oil, beeswax and cocoa butter. This was supported by its high release profile, and scleral permeation outperforming that of the other two oleogel formulations. Assuming a loading of 5% w/w of epalrestat, a volume of 100 µL equivalating to 2 to 3 eye drops, a human patient can expect to have 2.5 µg/cm^2 of epalrestat permeating through their sclera. This is enough to have a therapeutically significant amount of epalrestat cross the sclera [44,45].

5.5 CONCLUSION

This study shows the successful preparation of oleogels dissolving epalrestat. Compared to niosomes [6] and contact lenses [4] the potential loading of epalrestat is significantly higher, and the release of the drug in simulated lacrimal fluid is sufficient for the drug to saturate the tear film during a retention time close to 20 minutes. The loaded oleogels are non-irritating, and therefore comparable to other ocular formulations protecting the surface of the eye against the irritating effects of epalrestat in solution. The permeation of the epalrestat is

similar to the permeation of epalrestat encapsulated into niosomes and higher than the permeation of epalrestat eluting from contact lenses. This first incorporation of epalrestat in oleogels for topical administration represents a technologically sound way deliver epalrestat to the ocular tissues in a non-invasive way.

5.6 REFERENCES

1. European Commission *The 2021 Aeging Report*; **2021**; https://ec.europa.eu/info/publications/2021-ageing-report-economic-and-budgetary-projections-eu-member-states-2019-2070_en;

2. Laiteerapong, N.; Huang, E.S. *Diabetes in America; Chapter 16 Diabetes in Older Adults*; 3rd ed.; NIDDK, **2018**;

3. Kattar, A.; Concheiro, A.; Alvarez-Lorenzo, C. Diabetic Eye: Associated Diseases, Drugs in Clinic, and Role of Self-Assembled Carriers in Topical Treatment. *Expert Opin. Drug Deliv.* **2021**, *18*, 1589–1607, doi:10.1080/17425247.2021.1953466.

4. Alvarez-Rivera, F.; Concheiro, A.; Alvarez-Lorenzo, C. Epalrestat-Loaded Silicone Hydrogels as Contact Lenses to Address Diabetic-Eye Complications. *Eur. J. Pharm. Biopharm.* **2018**, *122*, 126–136, doi:10.1016/j.ejpb.2017.10.016.

5. Chen, X.; Wu, J.; Lin, X.; Wu, X.; Yu, X.; Wang, B.; Xu, W. Tacrolimus Loaded Cationic Liposomes for Dry Eye Treatment. *Front. Pharmacol.* **2022**, *13*, 1–16, doi:10.3389/fphar.2022.838168.

6. Kattar, A.; Quelle-Regaldie, A.; Sánchez, L.; Concheiro, A.; Alvarez-Lorenzo, C. Formulation and Characterization of

Epalrestat-Loaded Polysorbate 60 Cationic Niosomes for Ocular Delivery. *Pharmaceutics* **2023**, *15*, 1247, doi:10.3390/pharmaceutics15041247.

7. Elmotasem, H.; Awad, G.E.A. A Stepwise Optimization Strategy to Formulate in Situ Gelling Formulations Comprising Fluconazole-Hydroxypropyl-Beta-Cyclodextrin Complex Loaded Niosomal Vesicles and Eudragit Nanoparticles for Enhanced Antifungal Activity and Prolonged Ocular Delivery. *Asian J. Pharm. Sci.* **2020**, *15*, 617–636, doi:10.1016/j.ajps.2019.09.003.

8. Li, C.C.; Abrahamson, M.; Kapoor, Y.; Chauhan, A. Timolol Transport from Microemulsions Trapped in HEMA Gels. *J. Colloid Interface Sci.* **2007**, *315*, 297–306, doi:10.1016/j.jcis.2007.06.054.

9. Akhter, M.H.; Ahmad, I.; Alshahrani, M.Y.; Al-Harbi, A.I.; Khalilullah, H.; Afzal, O.; Altamimi, A.S.A.; Najib Ullah, S.N.M.; Ojha, A.; Karim, S. Drug Delivery Challenges and Current Progess in Nanocarrier-Based Ocular Therapeutic System. *Gels* **2022**, *8*, 82, doi:10.3390/gels8020082.

10. Rimpelä, A.-K.; Kiiski, I.; Deng, F.; Kidron, H.; Urtti, A. Pharmacokinetic Simulations of Intravitreal Biologicals: Aspects of Drug Delivery to the Posterior and Anterior Segments. *Pharmaceutics* **2018**, *11*, 9, doi:10.3390/pharmaceutics11010009.

11. Xeroudaki, M.; Thangavelu, M.; Lennikov, A.; Ratnayake, A.; Bisevac, J.; Petrovski, G.; Fagerholm, P.; Rafat, M.; Lagali, N. A Porous Collagen-Based Hydrogel and Implantation Method for Corneal Stromal Regeneration and Sustained Local Drug Delivery. *Sci. Rep.* **2020**, *10*, 16936, doi:10.1038/s41598-020-73730-9.

12. Kim, S.W.; Bae, Y.H.; Okano, T. Hydrogels: Swelling, Drug Loading, and Release. *Pharm. Res.* **1992**, *9*, 283–290,

doi:10.1023/a:1015887213431.

13. de Vries, V.A.; Bassil, F.L.; Ramdas, W.D. The Effects of Intravitreal Injections on Intraocular Pressure and Retinal Nerve Fiber Layer: A Systematic Review and Meta-Analysis. *Sci. Rep.* **2020**, *10*, 13248, doi:10.1038/s41598-020-70269-7.

14. Sagiri, S.S.; Rao, K.J. Natural and Bioderived Molecular Gelator–Based Oleogels and Their Applications. In *Biopolymer-Based Formulations*; Elsevier, **2020**; Vol. 1, pp. 513–559 ISBN 9780128168981.

15. Macoon, R.; Chauhan, A. Ophthalmic Delivery of Hydrophilic Drugs through Drug-Loaded Oleogels. *Eur. J. Pharm. Sci.* **2021**, *158*, 105634, doi:10.1016/j.ejps.2020.105634.

16. Macoon, R.; Guerriero, T.; Chauhan, A. Extended Release of Dexamethasone from Oleogel Based Rods. *J. Colloid Interface Sci.* **2019**, *555*, 331–341, doi:10.1016/j.jcis.2019.07.082.

17. Sahu, S.; Ghosh, M.; Bhattacharyya, D.K. Utilization of Unsaponifiable Matter from Rice Bran Oil Fatty Acid Distillate for Preparing an Antioxidant-Rich Oleogel and Evaluation of Its Properties. *Grasas y Aceites* **2020**, *71*, 336, doi:10.3989/gya.0938182.

18. Macoon, R.; Robey, M.; Chauhan, A. In Vitro Release of Hydrophobic Drugs by Oleogel Rods with Biocompatible Gelators. *Eur. J. Pharm. Sci.* **2020**, *152*, 105413, doi:10.1016/j.ejps.2020.105413.

19. Lorenzi, M. The Polyol Pathway as a Mechanism for Diabetic Retinopathy: Attractive, Elusive, and Resilient. *Exp. Diabetes Res.* **2007**, *2007*, 1–10, doi:10.1155/2007/61038.

20. Tang, W.H.; Martin, K.A.; Hwa, J. Aldose Reductase, Oxidative Stress, and Diabetic Mellitus. *Front. Pharmacol.* **2012**, *3*, 1–8, doi:10.3389/fphar.2012.00087.

21. Taylor, R.; Agius, L. The Biochemistry of Diabetes. *J. Biochem.* **1988**, *250*, 625–640.

22. Kang, Q.; Yang, C. Oxidative Stress and Diabetic Retinopathy: Molecular Mechanisms, Pathogenetic Role and Therapeutic Implications. *Redox Biol.* **2020**, *37*, 101799, doi:10.1016/j.redox.2020.101799.

23. Hasda, A.M.; Vuppaladadium, S.S.R.; Qureshi, D.; Prasad, G.; Mohanty, B.; Banerjee, I.; Shaikh, H.; Anis, A.; Sarkar, P.; Pal, K. Graphene Oxide Reinforced Nanocomposite Oleogels Improves Corneal Permeation of Drugs. *J. Drug Deliv. Sci. Technol.* **2020**, *60*, 102024, doi:10.1016/j.jddst.2020.102024.

24. Dhal, S.; Qureshi, D.; Mohanty, B.; Maji, S.; Anis, A.; Kim, D.; Sarkar, P.; Pal, K. Kokum Butter and Rice Bran Oil-Based Oleogels as Novel Ocular Drug Delivery Systems. In *Advances and Challenges in Pharmaceutical Technology*; Elsevier, **2021**; pp. 147–179.

25. Mohanty, B.; Pal, K.; Quereshi, D.; Nayak, S.K.; Rathnam, V.S.S.; Banerjee, I.; Anis, A.; Barik, C.S.; Sarkar, P.; Rout, S.K. Oleogels Based on Palmitic Acid and Safflower Oil: Novel Formulations for Ocular Drug Delivery of Voriconazole. *Eur. J. Lipid Sci. Technol.* **2020**, *122*, 1–15, doi:10.1002/ejlt.201900288.

26. Liu, Y.; Liu, J.; Zhang, X.; Zhang, R.; Huang, Y.; Wu, C. In Situ Gelling Gelrite/Alginate Formulations as Vehicles for Ophthalmic Drug Delivery. *AAPS PharmSciTech* **2010**, *11*, 610–620, doi:10.1208/s12249-010-9413-0.

27. Kalweit, S.; Besoke, R.; Gerner, I.; Spielmann, H. A National Validation Project of Alternative Methods to the Draize Rabbit Eye Test. *Toxicol. Vitr.* **1990**, *4*, 702–706, doi:10.1016/0887-2333(90)90147-L.

28. Maraghechi, S.; Dupont, A.-L.; Cardinaels, R.; Paris-Lacombe,

S.; Hoefnagels, J.P.M.; Suiker, A.S.J.; Bosco, E. Assessing Rheometry for Measuring the Viscosity-Average Degree of Polymerisation of Cellulose in Paper Degradation Studies. *Herit. Sci.* **2023**, *11*, 15, doi:10.1186/s40494-022-00855-7.

29. A. Arshinoff, S.; Hofmann, I.; Nae, H. Role of Rheology in Tears and Artificial Tears. *J. Cataract Refract. Surg.* **2021**, *47*, 655–661, doi:10.1097/j.jcrs.0000000000000508.

30. Dartt, D.A.; Willcox, M.D.P. Complexity of the Tear Film: Importance in Homeostasis and Dysfunction during Disease. *Exp. Eye Res.* **2013**, *117*, 1–3, doi:10.1016/j.exer.2013.10.008.

31. Van Haeringen, N.J. Clinical Biochemistry of Tears. *Surv. Ophthalmol.* **1981**, *26*, 84–96, doi:10.1016/0039-6257(81)90145-4.

32. European Union *DIRECTIVE 2010/63/EU OF THE EUROPEAN PARLIAMENT AND OF THE COUNCIL of 22 September 2010 on the Protection of Animals Used for Scientific Purposes*; **2010**; pp. 1–47;.

33. Zaki, I.; Fitzgerald, P.; Hardy, J.G.; Wilson, C.G. A Comparison of the Effect of Viscosity on the Precorneal Residence of Solutions in Rabbit and Man. *J. Pharm. Pharmacol.* **2011**, *38*, 463–466, doi:10.1111/j.2042-7158.1986.tb04611.x.

34. Rahman, M.Q.; Chuah, K.S.; MacDonald, E.C.A.; Trusler, J.P.M.; Ramaesh, K. The Effect of PH, Dilution, and Temperature on the Viscosity of Ocular Lubricants-Shift in Rheological Parameters and Potential Clinical Significance. *Eye* **2012**, *26*, 1579–1584, doi:10.1038/eye.2012.211.

35. Tiffany, J.M. The Viscosity of Human Tears. *Int. Ophthalmol.* **1991**, *15*, 371–376, doi:10.1007/BF00137947.

36. Arshinoff, S.; Hofmann, I.; Nae, H. Rheological Behavior of Commercial Artificial Tear Solutions. *J. Cataract Refract.*

Surg. **2021**, *47*, 649–654, doi:10.1097/j.jcrs.0000000000000507.

37. Guillaumie, F.; Furrer, P.; Felt-Baeyens, O.; Fuhlendorff, B.L.; Nymand, S.; Westh, P.; Gurny, R.; Schwach-Abdellaoui, K. Comparative Studies of Various Hyaluronic Acids Produced by Microbial Fermentation for Potential Topical Ophthalmic Applications. *J. Biomed. Mater. Res. Part A* **2010**, *92A*, 1421–1430, doi:10.1002/jbm.a.32481.

38. Putra, O.D.; Umeda, D.; Nugraha, Y.P.; Furuishi, T.; Nagase, H.; Fukuzawa, K.; Uekusa, H.; Yonemochi, E. Solubility Improvement of Epalrestat by Layered Structure Formation via Cocrystallization. *CrystEngComm* **2017**, *19*, 2614–2622, doi:10.1039/C7CE00284J.

39. Furuishi, T.; Takahashi, S.; Ogawa, N.; Gunji, M.; Nagase, H.; Suzuki, T.; Endo, T.; Ueda, H.; Yonemochi, E.; Tomono, K. Enhanced Dissolution and Skin Permeation Profiles of Epalrestat with β-Cyclodextrin Derivatives Using a Cogrinding Method. *Eur. J. Pharm. Sci.* **2017**, *106*, 79–86, doi:10.1016/j.ejps.2017.05.047.

40. Buyukozturk, F.; Benneyan, J.C.; Carrier, R.L. Impact of Emulsion-Based Drug Delivery Systems on Intestinal Permeability and Drug Release Kinetics. *J. Control. Release* **2010**, *142*, 22–30, doi:10.1016/j.jconrel.2009.10.005.

41. Vilimi, Z.; Hajdú, M.; Kállai-Szabó, N.; Antal, I. Study on Drug Release from Oleogel Carriers. *Acta Pharm. Hung.* **2021**, *91*, 328–329, doi:10.33892/aph.2021.91.328-329.

42. Sagiri, S.S.; Kasiviswanathan, U.; Shaw, G.S.; Singh, M.; Anis, A.; Pal, K. Effect of Sorbitan Monostearate Concentration on the Thermal, Mechanical and Drug Release Properties of Oleogels. *Korean J. Chem. Eng.* **2016**, *33*, 1720–1727, doi:10.1007/s11814-015-0295-4.

43. Qureshi, D.; Choudhary, B.; Mohanty, B.; Sarkar, P.; Anis, A.; Cerqueira, M.A.; Banerjee, I.; Maji, S.; Pal, K. Graphene Oxide Increases Corneal Permeation of Ciprofloxacin Hydrochloride from Oleogels: A Study with Cocoa Butter-Based Oleogels. *Gels* **2020**, *6*, 43, doi:10.3390/gels6040043.

44. Jagdale, A.D.; Bavkar, L.N.; More, T.A.; Joglekar, M.M.; Arvindekar, A.U. Strong Inhibition of the Polyol Pathway Diverts Glucose Flux to Protein Glycation Leading to Rapid Establishment of Secondary Complications in Diabetes Mellitus. *J. Diabetes Complications* **2016**, *30*, 398–405, doi:10.1016/j.jdiacomp.2016.01.001.

45. Ao, S.; Kikuchi, C.; Ono, T.; Notsu, Y. Effect of Instillation of Aldose Reductase Inhibitor FR74366 on Diabetic Cataract. *Investig. Ophthalmol. Vis. Sci.* **1991**, *32*, 3078–3083.

6. COMPARISON OF IN VIVO EPALRESTAT OCULAR DISTRIBUTION FROM NIOSOMES, MICELLES AND OLEOGELS

6.1 INTRODUCTION

Diabetic eye diseases have a big impact on the quality of life of the patients affected. They are illnesses affecting patients with diabetes and include cataracts, glaucoma, macular edema and diabetic retinopathy They often cause loss of vision and in the worst cases lead to blindness. The current standard of care for diabetic retinopathy involve intraocular anti-VEGF injections, laser treatment and eye surgery [1–3]. These procedures require specialized medical attention and entail significant risks for the patient. Intraocular injections and eye surgery can lead to retinal detachment, intraocular inflammation, ocular hypertension, intraocular hemorrhage, cataract or hypotony [4–6]. Development of diabetic retinopathy can be prevented using aldose reductase inhibitors such as epalrestat that prevent the accumulation of sorbitol in the retina in hyperglycemic conditions. When a patient suffers from hyperglycemia, the normal glycolysis pathway becomes saturated and the polyol pathway becomes active to transform glucose into sorbitol, and then sorbitol into fructose. The first reaction is the rate limiting step, and as sorbitol does not permeate cell membranes it leads to osmotic stress [7]. This step also consumes NADPH, leading to oxidative stress [8].

Epalrestat is a hydrophobic molecule and its topical administration demands the development of a drug carrier capable of delivering the drug to the therapeutic site. The safety of epalrestat has been studied *in*

vitro on retinal pigment epithelial cells [9] and *in vivo* on albino rabbits [10]. Further *in vivo* studies have looked at the pharmacokinetics of epalrestat in rabbits [11] and the effect of epalrestat on pulmonary fibrosis in rats [12]. In chapter 3 and 5 of this Thesis, two formulations were developed and characterized that showed promise in the encapsulation and ocular permeation of epalrestat. They had to comply with certain requirements, such as low viscosity to be able to be topically administered, to hold 0.2 mg/mL of epalrestat, and to minimize the possible side effects while keeping the initial concentration of the drug high enough for therapeutic concentrations to reach the retina. Furthermore, they were non-irritating in HET-CAM assays, and displayed effective corneal and scleral permeation in *ex vivo* assays. Cationic niosomes were prepared and showed therapeutic levels of epalrestat delivery across the sclera and the cornea in *ex vivo* experiments, and demonstrated their safety in both the HET-CAM model and the zebrafish embryotoxicity model (chapter 3). Oleogels made from cocoa butter and soybean oil and loaded with epalrestat also showed suitable characteristics for *in vivo* application (chapter 5). The administration of epalrestat dissolved in a medium without any encapsulation is highly irritating. Therefore, micelles were developed with the objective of encapsulating epalrestat in their core to act as a control.

Micelles were added as a formulation to compare each respective *in vivo* permeation and distribution efficiency. Micelles are well studied and have previously been used in animal experiments involving drug delivery to rabbits' eyes [13–15]. The micelles chosen to fill this comparative role were Pluronic® F127 micelles previously developed and characterized within our research group for the efficient ocular delivery of resveratrol [13]. We hypothesized that micelles can host epalrestat in the hydrophobic core [16]. Pluronic® F127 is a polymer

of poly (ethylene oxide)-poly(propylene oxide)-poly(ethylene oxide) (PEO- PPO-PEO) regarded as safe [17], and has already been used in *in vivo* ocular drug delivery experiments on rabbit models [18,19]. *In vivo* experiments are an essential step in the bench to bedside process of drug formulation development. While the experiments on *ex vivo* tissues and the toxicity tests are very valuable to reduce the number of potential formulations fit for human testing, *ex vixo* and *in ovo* experiments are not yet able to encompass all the variable influencing the absorption and transport of drugs in the eye, thus rendering animal experiments unavoidable.

Rabbit models have been used to assess drug clearance and safety of drugs as their pharmacokinetics are similar to that of humans [20,21]. New Zealand Albino rabbits have been used in ocular drug delivery research to determine the distribution of drugs after topical administration [22]. The main differences lay in the tear flow of rabbits (0.7 µL/min) when compared to humans (3 µL/min), the presence of a nictitating membrane, the presence of a sole lacrimal puncta and a lower corneal thickness (0.4 mm) but bigger corneal surface area ($1.5 - 2$ cm^2) than human cornea (0.53 mm and 1.04 cm^2) [23]. The ratio of conjunctival surface to corneal surface is about double in humans compared to rabbits [24]. Despite these differences the rabbit model is considered to be the most appropriate as relevant pharmacokinetic parameters such as clearance rate and distribution are similar to the human eye [25–29]. The evidence provided by experiments on rabbit models balance the reliability of the data gathered and translation to humans while complying with ethical guidelines and cost requirements.

The experiments described in this chapter had a threefold objective; (I) determining the safety and tolerance of the three formulations by rabbits, (II) measuring the outflow of epalrestat from

the eye due to lacrimal activity, and (III) measuring the accumulation of epalrestat in the different tissues of the eye.

The objectives of these animal experiments were prepared in accordance with the 3R's principles (Replace, Reduce, Refine): looking for alternatives to the use of animals, minimizing the amount of experiments and amounts of animals used while keeping result credibility and performing the experiments in a way as to avoid distress in the animals while the experiment is unfolding.

6.2 MATERIALS AND METHODS

6.2.1 Materials

Polysorbate 60 MW 1311.7 g/mol (Tween 60, HLB 14.9, Sigma Aldrich, Buchs, Switzerland), 1,2-di-O-octadecenyl-3-trimethylammonium propane (chloride salt) (DOTMA, 670.58 g/mol) (Avanti, Alabaster, AL, USA), epalrestat (319.4 g/mol) (TCI, Tokyo, Japan), cholesterol (386.7 g/mol) (Chemtrec, Madrid, Spain), ethanol (VWR Chemicals, Briare, France), methanol (Fisher Scientific Loughborough, UK), sodium chloride (Labkem, Barcelona, Spain), potassium chloride (Panreac, Castellar del Vallès, Spain), sodium bicarbonate (Merck, St Louis, MO, USA), calcium dihydrochloride (Merck, Darmstadt, Germany), Soybean oil (ThermoScientific, Bremen, Germany), cocoa butter (BambooStory, Lima, Peru), Kolliphor® P 407 (Pluronic® F127) (BASF ChemTrade GmbH, Burgbernheim, Germany), Propofol Lipuro® 10mg/mL (B. Braun vetcare, Tuttlingen, Germany), pentobarbital sodium Euthasol (Dechra, Barcelona, Spain)

6.2.2 Experimental design

The animal experiments were all performed in accordance with the Association for Research in Vision and Ophthalmology Statement for the Use of Animals in Ophthalmic and Vision Research [30] and with European Directive 2010/63/EU [31]. The protocols were approved the committee of animal experimentation ethics (CEEA) of University of Santiago de Compostela (registration number: ES150780292901). and the Consellería de Medio Rural of Xunta de Galicia. The study was supported by the European Union's Horizon 2020 research and innovation programme under the Marie Skłodowska-Curie Actions grant agreement N◦ 813440 (ORBITAL–Ocular Research by Integrated Training And Learning).

The *in vivo* experiments were performed on twelve healthy male New Zealand white rabbits (age approx. 3 months weighing 3.06 ± 0.20 kg). The animals were in a light-controlled room (12 h light/ 12 h dark cycles) at 18 °C in individual cages with unlimited access to food and water. Rabbits with unusual low weight or corneal disruptions were not included in the study. During the experiments and sampling, the rabbits were placed in restrainers with continuous monitoring to ensure there was no removal of the formulations deposited in the conjunctival sac.

To minimize the effects of subjective bias, the experiments were carried out in three days and the rabbits were randomly divided into three groups, i.e., the niosome group (n = 4), micelle group (n = 4) and oleogel group (n = 4). Each rabbit received an instillation of a drop of their respective formulation (50 μL; 0.2 mg/mL epalrestat). Samples of lacrimal fluid were gathered at predetermined timepoints, and images of the animals eyes were taken. The rabbits were subsequently euthanized after 6 hours and the eyes enucleated. All experiments started at 9 a.m. On the first day, the four rabbits of the niosome group

were assayed. On the second day, the four rabbits of the micelle group were assayed. On the third day, the four rabbits of the oleogel group were assayed.

6.2.3 Formulations preparation

Niosomes TCD5 and oleogel C were prepared as described in chapter 4 and chapter 5 respectively, with the only difference being the use of sterile PBS as the dispersion medium for niosomes. Niosomes TCD5 were prepared using 67 mg of Tween 60, 8.3 mg of cholesterol and 2.57 mg of DOTMA. Oleogel C was prepared using 1mL of soybean oil and 46 mg cocoa butter. Both the niosomes and the oleogel were loaded with 0.2 mg/mL epalrestat. The micelle formulation was prepared adapting a previously published method from our research group [13] to encapsulate 0.2 mg/mL epalrestat. 10 mM Pluronic® F127 micelles were prepared by mixing 12.6 w/w Pluronic® F127 in sterile PBS at 300 rpm for 5 h in an ice bath to prevent gelling. Once the copolymer was completely dispersed, epalrestat was added and the mixture was left to stir for another 5 h at 300 rpm in an ice bath. The final dispersion was kept at 4 °C until instillation.

Formulations were characterized in terms of size, polydispersity index, viscosity and encapsulation efficiency. The particle size and polydispersity index of the micelles were measured with dynamic light scattering (DLS) using a Zetasizer Nano (Malvern Instruments, Herrenberg, Germany) in ultrapure water at 20 °C with 10 s equilibration time using back scatter. The values taken were measured by number.

6.2.4 Viscosity

Rotational rheology was performed on an AR1000-N Rheometer (TA Instruments, Surrey, UK). The geometry used was a 4 cm cone solvent trap with 1.58 degree angle, and the gap was 50 μm. The experiments were conducted at 35 °C from 0.05 to 1000 s-1, recording 100 sampling points. All three formulations, niosomes TDC5, micelles F127 and oleogel C were tested.

6.2.5 In vivo release

Prior to drug administration the rabbits were weighed and placed into restrainers. Pictures of their eyes were taken to assess any damage or pre-existing ocular conditions. The right eye of the rabbits was used to gently instill 50 μL of the attributed formulation (0.2 mg/mL epalrestat loaded niosomes, micelles or oleogels) into the conjunctival sac with a micropipette. The left eye of each rabbit was kept as a control without treatment. Before and after the treatment instillation, at time points t = 10 min, 20 min, 30 min and ever hour until 6h, tear fluid samples were collected from each eye by placing Schirmer strips in the tarsal conjunctiva of the lower eyelid for 10 seconds with the eye closed. The volume of the tear fluid was recorded as the millimetres of moistened strip.

6.2.5.1 Epalrestat quantification in tear fluid

The Schirmer test strips were placed in 2 mL Eppendorf tubes with 1 mL of methanol:water 70:30 solution for 12 h at 4 °C while shaking at 50 rpm. The strips were removed and the Eppendorf tubes were

centrifuged at 14,000 rpm at 5 °C for 30 minutes. Finally, the supernatants were collected and stored at -80 °C until UPLC analysis. In preliminary tests, this extraction method was shown to reproducibly recover >98% epalrestat present in the strips. The quantification of epalrestat present in the tear fluid after the extraction procedure was adapted from a protocol used by Huang et al. [32]. The chromatographic equipment employed was an Agilent 1290 Infinity II and QQQ G6475 mass spectrometer system. An Agilent ZORBAX Rapid Resolution High Definition (RRHD) Eclipse Plus C18 LC column, with sizes 2.1 * 50 mm, and particle size of 1.8 µm was used at a flow rate of 0.5 mL/min. Water with 5 mM ammonium acetate was used as solvent A and acetonitrile with 5 mM ammonium acetate was used as solvent B. The gradient program used was as follows: 0–0.1 min. 40% B, 0.1-2.0 min. 40–100% B, 2.0-2.5 min. 100% B, 2.5-2.9 min. 100-60% B, and 2.9–3.0 min. 40% B. The mass spectrometer was operated in a negative ESI mode with a capillary voltage of 4400 V, a nozzle voltage of 1700 V, a gas temperature of 280 °C, a gas flow of 12 L/min and a nebulizer at 34 psi. The sheath gas temperature and gas flow were at 270°C and at 12 L/min, respectively. The compound of interest was monitored in multiple reaction monitoring (MRM) mode. 318.0 > 273.9 m/z transition was quantified.

6.2.5.2 Epalrestat quantification in the tissues

All the rabbits were euthanized by intravenous administration of 7.5 mg/Kg of propofol for anaesthesia and 200 mg/Kg of pentobarbital sodium (Euthasol). Following euthanization, aqueous humour was directly extracted from the anterior chamber using a needle and stored at -80 °C until UPLC analysis. Then, the eyes were enucleated and immediately dissected, separating and weighing the cornea, sclera,

crystalline lens, vitreous humour, and retina. 1 mL methanol was added to cornea, crystalline, sclera and retina [32]. The tissues were incubated for 12 hours at 4 °C and then centrifuged at 14,000 rpm at 5 °C for 30 minutes. The supernatant was collected and MilliQ water was added to reach 30 vol% and stored at -80 °C until UPLC analysis. The addition of water was done to allow the samples to freeze at -80 °C. The UPLC protocol was the same as for the quantification of epalrestat in the tear fluid.

6.2.6 Statistical analysis

Statistical analysis was performed using Origin 2018. The descriptive data were presented as mean ± standard deviation. One-way analysis of variance (ANOVA). The level of significance was 0.05.

6.3. RESULTS AND DISCUSSION

6.3.1 Characterization of the formulations

The formulations used in the *in vivo* experiments were characterized to ensure the reproducibility of the experiment and the compliance with the protocols of chapter 3 and 5 of this Thesis. The size, polydispersity index and zeta potential of the formulations can be seen in **Table 6.1**.

Table 6.1. Size, polydispersity index, surface charge and drug loading of the three formulations used *in vivo*

Formulation	Size (nm)	PDI	Zeta-potential (mV)	Loading efficiency (%)
Niosomes (TCD5)	79.88	0.51	+15.67 ± 8.53	99.76 ± 0.35
Micelles (F127)	19.3	0.69	+0.79 ± 4.46	98.55 ± 0.64
Oleogel (C)	N/A	N/A	N/A	100

The three formulations had very different physical characteristics, making the comparison between them relevant on a qualitative base. As both niosomes and micelles are self-assembled systems the size comparison is interesting. Niosomes are bigger than micelles due to the structure being a bilayer with the polar heads of the amphiphilic molecules pointing both outward to the aqueous medium and inward the core of the particle that is also composed of aqueous medium. In contrast the micelle has a core composed of the hydrophobic tails and the hydrophilic moieties are all pointing outward to the aqueous medium. Furthermore, only niosomes were charged as the inclusion of 5 mol% DOTMA made sure that the niosomes were cationic and more stable in solution. All three formulations achieved an excess of 98% encapsulation of epalrestat at 0.2 mg/mL loading.

6.3.2 Viscosity

The viscosity of each formulation was assessed over a 0.05 to 1000 s^{-1} shear rate range to mimic the behavior of blinking progression [33]. Furthermore, the temperature was kept at 35 °C to mimic the surface temperature of the eye [34]. As expected the oleogel was more viscous than the suspensions, and itself and the micelles reached a viscosity plateau (at 0.035 and 0.015 Pa.s respectively) around 60 and 200 s^{-1} respectively. In contrast the niosomes displayed more pronounced shear

thinning behavior, but lower viscosity overall, starting at 0.019 Pa.s and reaching a plateau of 0.0013 Pa.s at a shear rate of 450 s^{-1}.

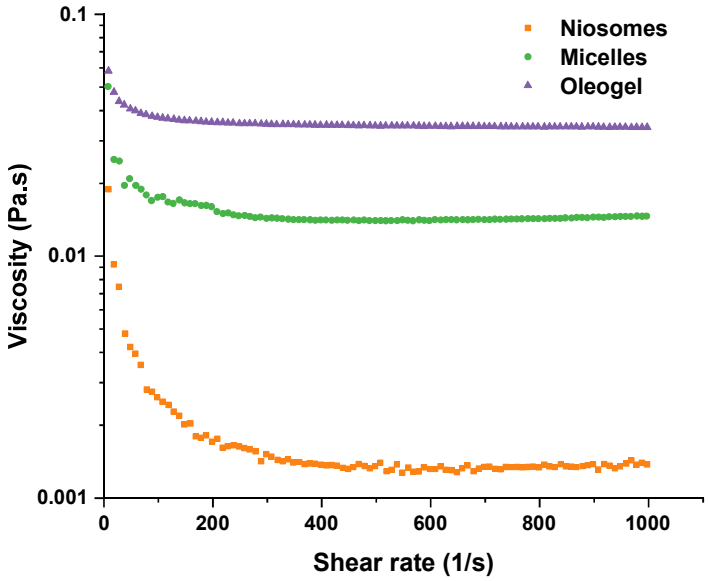

Figure 6.1. Effect of shear rate on the viscosity for TCD5 niosomes, F127 micelles and C oleogel 35 °C.

Niosomes behave as pseudoplastic as the larger vesicle can resist initial flow. This behavior is in accordance with the current literature [35–37]. The micelles were kept at low temperatures during the whole preparation process and storage to ensure that no gel was forming. The sol-gel transition temperature for micelles made from 10 mM Pluronic® F127 is 35 °C [13], which explains the higher viscosity of the micelles when compared to the niosomes. The oleogel C behaved in a near Newtonian way, with a small viscosity decrease past the very low shear rate, that can be attributed to the energy needed to get the gel moving [38].

6.3.3 In vivo experiment

The *in ovo* and zebrafish embryotoxicity experiments of the previous chapters indicated that the formulations developed were capable of efficiently protecting tissues from the irritating effects of epalrestat. Subsequently, an *in vivo* experiment was planned with a threefold objective: (I) confirm the safety of the formulations deposited on the ocular surface of rabbits, (II) quantifying the amounts of epalrestat in the lacrimal fluid over the duration of the experiment and (III) quantifying the accumulation of epalrestat in the different ocular tissues after 6 hours. This information is essential to ensure safety and efficiency of the formulations in the next steps of development, trending towards clinical trials. The study was funded by the European Union's Horizon 2020 research and innovation program under the Marie Sklodowska-Curie Actions (grant agreement-No 813440). The work was also supported by MCIN/AEI/10.13039/501100011033 [PID 2020-113881RB-I00 to A.C. and C.A.-L., and PID2020-115121GB-I00 to L.S.], Spain, Xunta de Galicia [ED431C 2020/17], and FEDER.

During the experiment the right eye was always the eye receiving the formulation while the left eye was kept as a control. The images displayed in **Table 6.2**, **Table 6.3** and **Table 6.4** show that there was no corneal damage induced by the formulations. The formulation that irritated the rabbits the most was oleogel C as can be seen from the images in **Table 6.4** where the conjunctiva gets progressively more red over the course of the experiment. According to the European Communities guidelines for the use of *in vivo* rabbit eye test [39] and the European Union Dangerous Substances Directive (EU DSD) [40] the presence of minimal or reversible irritancy does not eliminate a formulations from eligibility for clinical evaluation, but quantitative data would need to be gathered to assess the severity of the irritancy in

the case of oleogels. The lacrimal concentration data from two rabbits (Rb2 and Rb3) in the niosomes group as well as the lacrimal concentration data from one rabbit (Rb7) were not used as the values were not reasonably believable and probably came from contamination of the samples. The data from the aqueous humor from the right eye of one niosome group rabbit (Rb 1) and from the aqueous humor of the left eye of one oleogel group rabbit (Rb 11) were not as the values were not reasonably believable and probably came from contamination of the samples

Table 6.2. Images of the eyes of the rabbits taken at t = 0, 1,4, 6h after administration of TCD5 niosomes loaded with 0.2 mg/mL epalrestat to the right eye

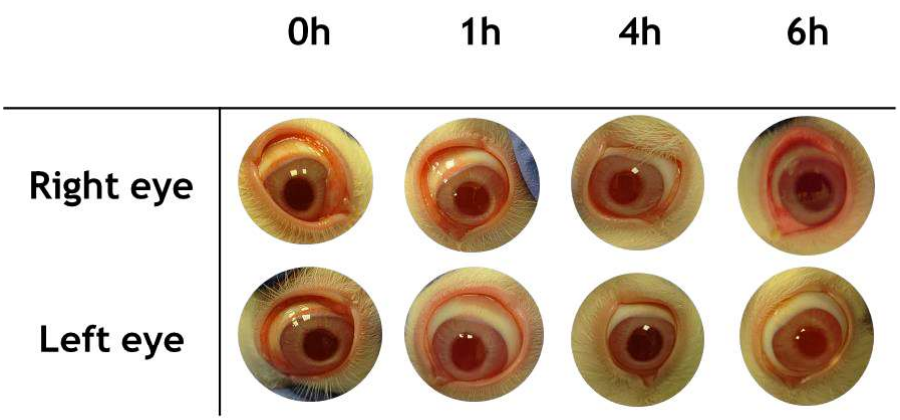

Table 6.3. Images of the eyes of the rabbits taken at t = 0, 1,4, 6h after administration of F127 micelles loaded with 0.2 mg/mL epalrestat to the right eye

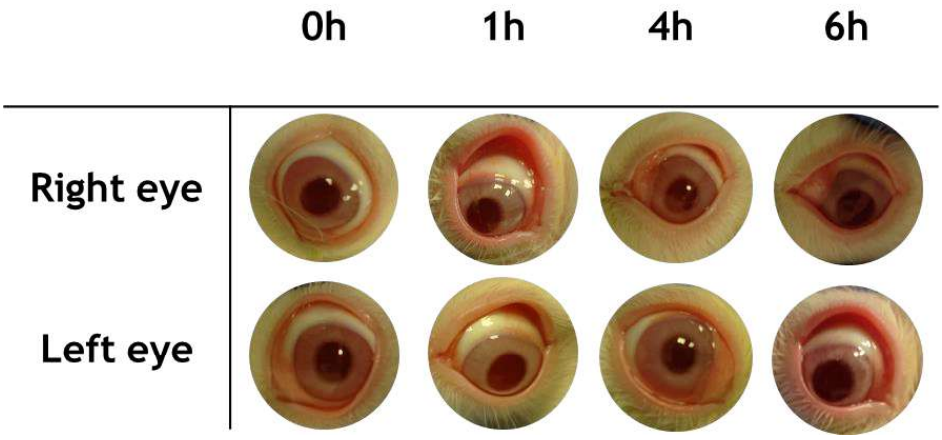

Table 6.4. Images of the eyes of the rabbits taken at t = 0, 1,4, 6h after administration of oleogel C loaded with 0.2 mg/mL epalrestat to the right eye

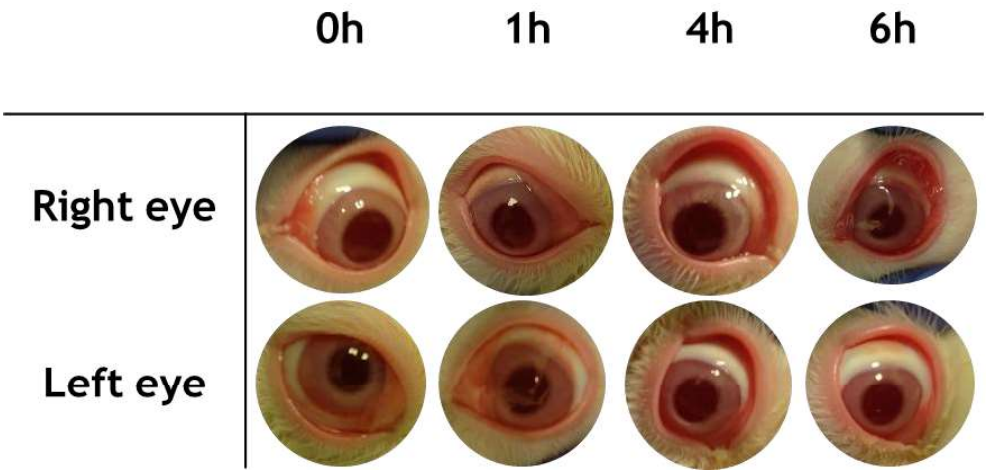

6.3.3.1 Epalrestat quantification in the lacrimal fluid

Each of the three formulations had their peak epalrestat concentration measured 10 minutes after application of the eye drop (**Figure 6.2**). The micelle formulation reached a higher concentration in the lacrimal fluid (48.3 ± 16.2 ng/µL) than the niosomes (12.3 ± 13.2 ng/µL) and the oleogel (15.8 ± 12.2 ng/µL). The release and duration of release (2 h) of epalrestat was higher for micelles, while the oleogel and the niosomes performed similarly. Interestingly, the values for the lacrimal concentration of epalrestat in the case of oleogel from 3 to 6 hours seemed higher than the one from micelles and oleogels, which trended towards zero, indicating that the oleogel deposited in the conjunctival sac did not completely get cleared by the tear turnover.

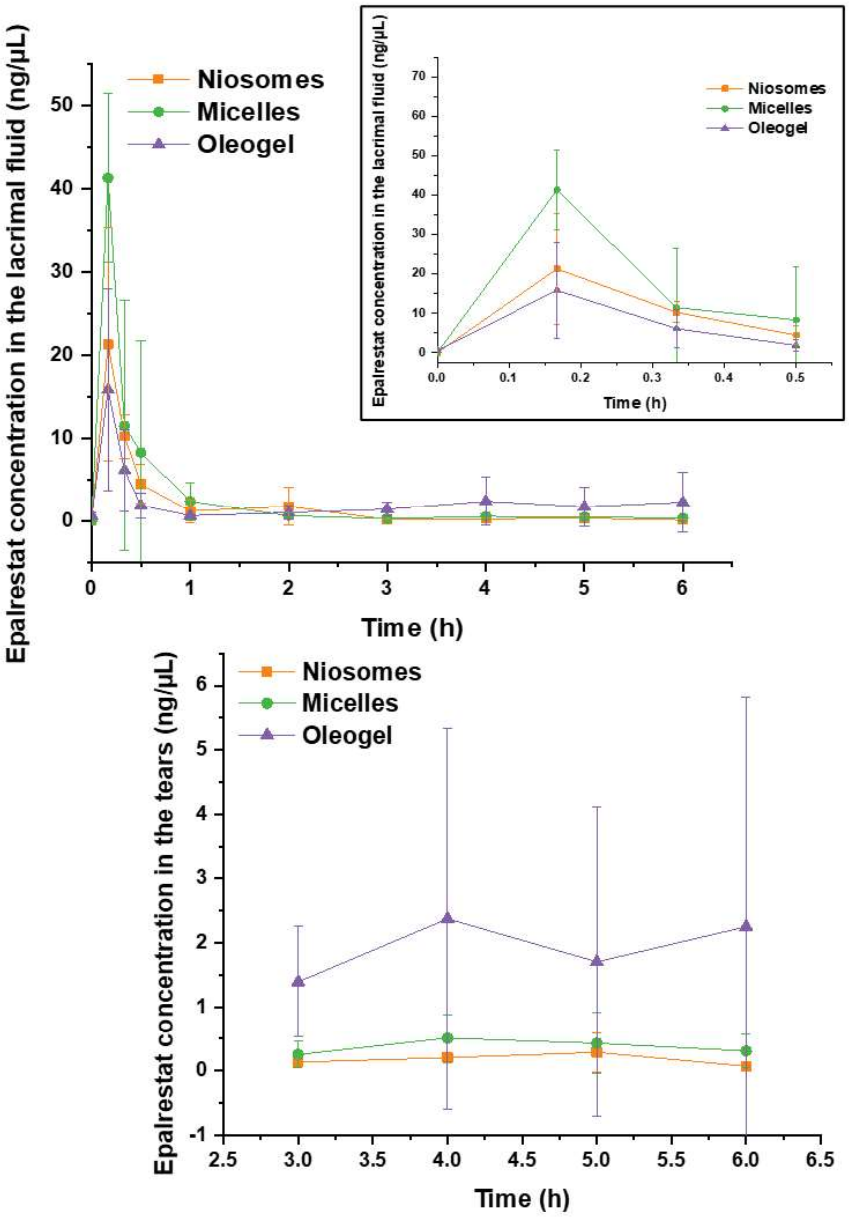

Figure 6.2. Epalrestat concentration in the tear fluid after a single instillation of loaded TCD5 niosomes, F127 micelles and C oleogel (50 µL, 0.2 mg/mL, *n* = 4 for each formulation) (mean values and standard deviations).

There was no significant differences found in the lacrimal concentration of epalrestat during the 6 hours of the experiment. The seemingly higher lacrimal concentration of epalrestat when encapsulated in F127 micelles can be explained by the formation of a gel at 35 °C. The temperature of the eye [34] is approximatively the sol-gel transition temperature of the micellar suspension [13], which would increase its retention time compared to niosomes. For the oleogel, its higher viscosity might have led to longer retention of the gel in the conjunctival sac, creating a depot that would release the drug in the later stages (3-6 h) of the experiment.

6.3.3.2 Epalrestat in the tissues

Biodistribution of epalrestat over the ocular tissues was evaluated 6 hours after eye drop instillation (**Figure 6.3** and **Figure 6.4**). The highest amounts of epalrestat were recovered from the cornea and the aqueous humor of the niosome group. The cornea being in direct contact with the formulation, the high concentration of epalrestat in this tissue indicates that the drug was able to permeate inside the tissue from the tear film. The high amount of epalrestat also found in the aqueous humor indicates that the drug was capable of passing through the cornea, however it was then blocked from travelling further. Indeed, the drug transport pathways are governed by pressure differentials going from the back to the front of the eye [41]. The epalrestat able to cross the cornea does not permeate further than the aqueous humor. This is more pronounced in the case of niosomes than in the case of micelles or of the oleogel. Furthermore, the low amounts of epalrestat found in the vitreous and in the lens suggest that the scleral route was favored for drug delivery to the vitreous. The scleral route was targeted when the topical formulations were designed, and the comparison of

epalrestat found in the retina and in the sclera point to scleral permeation without significant retention.

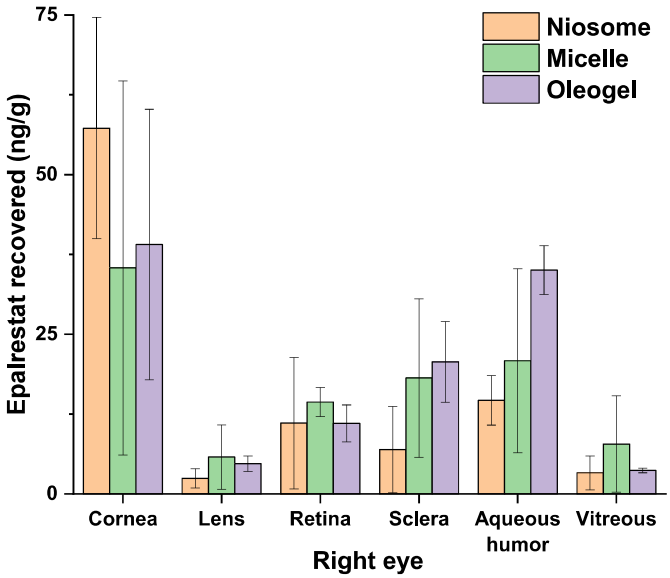

Figure 6.3. Epalrestat accumulated in various ocular tissues of the right eye 6 h after eye drop instillation (*n* = 4).

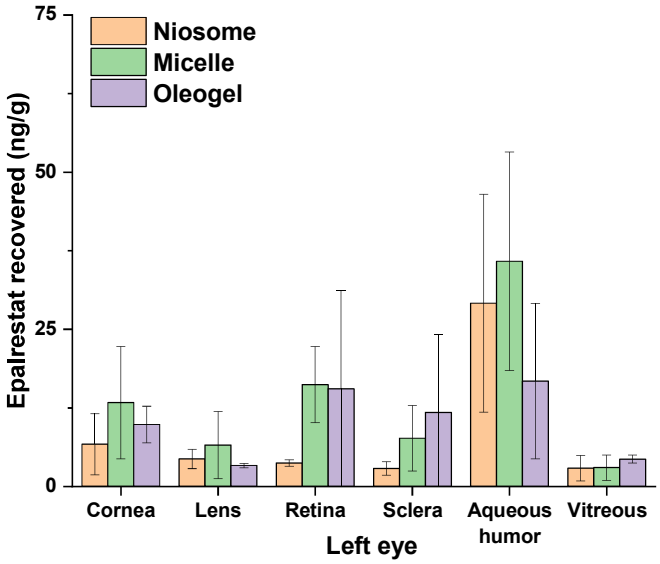

Figure 6.4. Epalrestat accumulated in various ocular tissues of the left eye (control) 6 h after eye drop instillation (*n* = 4).

The values of epalrestat concentration in the control eye are lower than those of the eye where the formulations were administered, with the unexpected exception of the aqueous humor. While the high amounts of epalrestat recovered from the retina of the control eyes can be explained by the high vascularization of the tissue [42] which could receive epalrestat from the bloodstream, the high presence of epalrestat in the aqueous humor of the control eye is less evident. To the best of our knowledge this is the first study that compares the biodistribution of epalrestat from three different formulations: niosomes, micelles and oleogels. In the case of drug suspension of voriconazole the drug concentration in the aqueous humor decreased significantly after only 2 minutes, and even with the use of a proniosomal *in situ* gelling ocular insert, the concentration of drug decreased significantly after 8 minutes [43]. Another proniosomal gel study investigating the distribution of lomefloxacin reported a significantly higher lomefloxacin concentration in aqueous humor, vitreous humor, cornea and conjunctiva when compared to a marketed formula. This is due to the mucoadhesive properties of the proniosomal gel, and the non-ionic surfactants acting as penetration enhancers [44]. The penetration enhancement from non-ionic surfactants would explain the higher corneal concentration of epalrestat in the right eye of the rabbits.

Not a lot of permeation assays *in vivo* have been performed with oleogels. Cao et al. have looked at the cyclosporin A [45] distribution in the cornea, conjunctiva and sclera when an organogel made from stearic acid, soybean oil, and N-methyl-2-pyrrolidinone was deposited in the lacrimal canaliculi to block lacrimal drainage. The concentrations of cyclosporin A at six hours were higher when the organogel was used compared to an ophthalmic solution, and the concentration ranges for the cornea were around 150 ng/g for the cornea and 40 ng/g for the sclera.

6.4 CONCLUSION

The preparation of micelles prepared from Pluronic® F127 were a good comparison for the *in vivo* administration of eye drops containing 0.2 mg/mL epalrestat. The micelles were able to demonstrate high lacrimal concentrations staying present until one hour. All three formulations, TCD5 niosomes, F127 micelles and oleogel C were able to deliver epalrestat to the different tissues of the eye *in vivo* without statistically significant differences. While the corneal route is not likely to provide an efficient route to reach the retina, which is the therapeutic site for diabetic retinopathy, the transscleral route seems to offer a way for epalrestat released from each formulation to arrive in the retina. To ensure the safety of the formulations, quantitative irritation tests will need to be performed with oleogel C.

6.5 REFERENCES

1. Stitt, A.W.; Curtis, T.M.; Chen, M.; Medina, R.J.; McKay, G.J.; Jenkins, A.; Gardiner, T.A.; Lyons, T.J.; Hammes, H.-P.; Simó, R.; et al. The Progress in Understanding and Treatment of Diabetic Retinopathy. *Prog. Retin. Eye Res.* **2016**, *51*, 156–186, doi:10.1016/j.preteyeres.2015.08.001.

2. Neubauer, A.S.; Ulbig, M.W. Laser Treatment in Diabetic Retinopathy. *Ophthalmologica* **2007**, *221*, 95–102, doi:10.1159/000098254.

3. Ferris, F.L.; Davis, M.D.; Aiello, L.M. Treatment of Diabetic Retinopathy. *N. Engl. J. Med.* **1999**, *341*, 667–678, doi:10.1056/NEJM199908263410907.

4. Jager, R.D.; Aiello, L.P.; Patel, S.C.; Cunningham, E.T. Risks of Intravitreous Injection: A Comprehensive Review. *Retina* **2004**, *24*, 676–698, doi:10.1097/00006982-200410000-00002.

5. Arevalo, J.F.; Garcia-Amaris, R.A. The Role of Vitreo-Retinal Surgery in Children With Uveitis. *Int. Ophthalmol. Clin.* **2008**, *48*, 153–172, doi:10.1097/IIO.0b013e31817d7fc1.

6. Nicolai, M.; Lassandro, N.; Franceschi, A.; Rosati, A.; De Turris, S.; Pelliccioni, P.; Pirani, V.; Mariotti, C. Intraocular Pressure Rise Linked to Silicone Oil in Retinal Surgery: A Review. *Vis.* **2020**, *4*, 1–18, doi:10.3390/vision4030036.

7. Galvez, A.S.; Ulloa, J.A.; Chiong, M.; Criollo, A.; Eisner, V.; Barros, L.F.; Lavandero, S. Aldose Reductase Induced by Hyperosmotic Stress Mediates Cardiomyocyte Apoptosis. *J.*

Biol. Chem. **2003**, *278*, 38484–38494, doi:10.1074/jbc.M211824200.

8. Lee, A.Y.W.; Chung, S.S.M. Contributions of Polyol Pathway to Oxidative Stress in Diabetic Cataract. *FASEB J.* **1999**, *13*, 23–30, doi:10.1096/fasebj.13.1.23.

9. Senthilkumari, S.; Sharmila, R.; Chidambaranathan, G.; Vanniarajan, A. Epalrestat, an Aldose Reductase Inhibitor Prevents Glucose-Induced Toxicity in Human Retinal Pigment Epithelial Cells in Vitro. *J. Ocul. Pharmacol. Ther.* **2017**, *33*, 34–41, doi:10.1089/jop.2016.0103.

10. Alvi, Z.; Akhtar, M.; Rahman, N.U.; Hosny, K.M.; Sindi, A.M.; Khan, B.A.; Nazir, I.; Sadaquat, H. Utilization of Gelling Polymer to Formulate Nanoparticles Loaded with Epalrestat-Cyclodextrin Inclusion Complex: Formulation, Characterization, In-Silico Modelling and In-Vivo Toxicity Evaluation. *Polymers (Basel).* **2021**, *13*, 4350, doi:10.3390/polym13244350.

11. Alvi, Z.; Akhtar, M.; Mahmood, A.; Ur-Rahman, N.; Nazir, I.; Sadaquat, H.; Ijaz, M.; Syed, S.K.; Waqas, M.K.; Wang, Y. Enhanced Oral Bioavailability of Epalrestat SBE7-β-CD Complex Loaded Chitosan Nanoparticles: Preparation, Characterization and in-Vivo Pharmacokinetic Evaluation. *Int. J. Nanomedicine* **2021**, *16*, 8353–8373, doi:10.2147/IJN.S339857.

12. Li, X.; Shen, Y.; Lu, Y.; Yang, J. Amelioration of Bleomycin-Induced Pulmonary Fibrosis of Rats by an Aldose Reductase

Inhibitor, Epalrestat. *Korean J. Physiol. Pharmacol.* **2015**, *19*, 401, doi:10.4196/kjpp.2015.19.5.401.

13. Vivero-Lopez, M.; Sparacino, C.; Quelle-Regaldie, A.; Sánchez, L.; Candal, E.; Barreiro-Iglesias, A.; Huete-Toral, F.; Carracedo, G.; Otero, A.; Concheiro, A.; et al. Pluronic®/Casein Micelles for Ophthalmic Delivery of Resveratrol: In Vitro, Ex Vivo, and in Vivo Tests. *Int. J. Pharm.* **2022**, *628*, doi:10.1016/j.ijpharm.2022.122281.

14. Sun, F.; Zheng, Z.; Lan, J.; Li, X.; Li, M.; Song, K.; Wu, X. New Micelle Myricetin Formulation for Ocular Delivery: Improved Stability, Solubility, and Ocular Anti-Inflammatory Treatment. *Drug Deliv.* **2019**, *26*, 575–585, doi:10.1080/10717544.2019.1622608.

15. Zhou, T.; Zhu, L.; Xia, H.; He, J.; Liu, S.; He, S.; Wang, L.; Zhang, J. Micelle Carriers Based on Macrogol 15 Hydroxystearate for Ocular Delivery of Terbinafine Hydrochloride: In Vitro Characterization and in Vivo Permeation. *Eur. J. Pharm. Sci.* **2017**, *109*, 288–296, doi:10.1016/j.ejps.2017.08.020.

16. Menger, F.M.; Doll, D.W. On the Structure of Micelles. *J. Am. Chem. Soc.* **1984**, *106*, 1109–1113, doi:10.1021/ja00316a050.

17. Brown, L.R. Ophthalmic Composition Comprising Polyoxyethylene-Polyoxypropylene Polymers WO1997021441A1.

18. El-Kamel, A.. In Vitro and in Vivo Evaluation of Pluronic F127-Based Ocular Delivery System for Timolol Maleate. *Int.*

J. Pharm. **2002**, *241*, 47–55, doi:10.1016/S0378-5173(02)00234-X.

19. Taha, E.I.; Badran, M.M.; El-Anazi, M.H.; Bayomi, M.A.; El-Bagory, I.M. Role of Pluronic F127 Micelles in Enhancing Ocular Delivery of Ciprofloxacin. *J. Mol. Liq.* **2014**, *199*, 251–256, doi:10.1016/j.molliq.2014.09.021.

20. Fauser, S.; Kalbacher, H.; Alteheld, N.; Koizumi, K.; Krohne, T.U.; Joussen, A.M. Pharmacokinetics and Safety of Intravitreally Delivered Etanercept. *Graefe's Arch. Clin. Exp. Ophthalmol.* **2004**, *242*, 582–586, doi:10.1007/s00417-004-0895-x.

21. Iyer, M.N.; He, F.; Wensel, T.G.; Mieler, W.F.; Benz, M.S.; Holz, E.R. Intravitreal Clearance of Moxifloxacin. *Trans. Am. Ophthalmol. Soc.* **2005**, *103*, 76–81; discussion 81-3.

22. Owen, G.R.; Brooks, A.C.; James, O.; Robertson, S.M. A Novel in Vivo Rabbit Model That Mimics Human Dosing to Determine the Distribution of Antibiotics in Ocular Tissues. *J. Ocul. Pharmacol. Ther.* **2007**, *23*, 335–342, doi:10.1089/jop.2006.0123.

23. Agrahari, V.V.V.; Mandal, A.; Agrahari, V.V.V.; Trinh, H.M.; Joseph, M.; Ray, A.; Hadji, H.; Mitra, R.; Pal, D.; Mitra, A.K. A Comprehensive Insight on Ocular Pharmacokinetics. *Drug Deliv Transl Res.* **2016**, *6*, 735–754, doi:10.1016/j.physbeh.2017.03.040.

24. Worakul, N.; Robinson, J.R. Ocular Pharmacokinetics/Pharmacodynamics. *Eur. J. Pharm.*

Biopharm. **1997**, *44*, 71–83, doi:10.1016/S0939-6411(97)00064-7.

25. del Amo, E.M.; Urtti, A. Rabbit as an Animal Model for Intravitreal Pharmacokinetics: Clinical Predictability and Quality of the Published Data. *Exp. Eye Res.* **2015**, *137*, 111–124, doi:10.1016/j.exer.2015.05.003.

26. Djebli, N.; Khier, S.; Griguer, F.; Coutant, A.-L.; Tavernier, A.; Fabre, G.; Leriche, C.; Fabre, D. Ocular Drug Distribution After Topical Administration: Population Pharmacokinetic Model in Rabbits. *Eur. J. Drug Metab. Pharmacokinet.* **2017**, *42*, 59–68, doi:10.1007/s13318-016-0319-4.

27. Gupta, S.; Fink, M.K.; Martin, L.M.; Sinha, P.R.; Rodier, J.T.; Sinha, N.R.; Hesemann, N.P.; Chaurasia, S.S.; Mohan, R.R. A Rabbit Model for Evaluating Ocular Damage from Acrolein Toxicity in Vivo. *Ann. N. Y. Acad. Sci.* **2020**, *1480*, 233–245, doi:10.1111/nyas.14514.

28. Saleh, M.; Jehl, F.; Dory, A.; Lefevre, S.; Prevost, G.; Gaucher, D.; Sauer, A.; Speeg-Schatz, C.; Bourcier, T. Ocular Penetration of Topically Applied Linezolid in a Rabbit Model. *J. Cataract Refract. Surg.* **2010**, *36*, 488–492, doi:10.1016/j.jcrs.2009.09.036.

29. Robinson, M.R.; Lee, S.S.; Kim, H.; Kim, S.; Lutz, R.J.; Galban, C.; Bungay, P.M.; Yuan, P.; Wang, N.S.; Kim, J.; et al. A Rabbit Model for Assessing the Ocular Barriers to the Transscleral Delivery of Triamcinolone Acetonide. *Exp. Eye Res.* **2006**, *82*, 479–487, doi:10.1016/j.exer.2005.08.007.

30. ARVO *Statement for the Use of Animals in Ophthalmic and Visual Research*; **2013**; p. 1;.

31. European Union *DIRECTIVE 2010/63/EU OF THE EUROPEAN PARLIAMENT AND OF THE COUNCIL of 22 September 2010 on the Protection of Animals Used for Scientific Purposes*; **2010**; pp. 1–47;.

32. Huang, J.; Sun, R.; Feng, S.; He, J.; Fei, F.; Gao, H.; Zhao, Y.; Zhang, Y.; Gu, H.; Aa, J.; et al. Sensitive Analysis and Pharmacokinetic Study of Epalrestat in C57BL/6J Mice. *J. Chromatogr. B* **2017**, *1055–1056*, 98–103, doi:10.1016/j.jchromb.2017.03.040.

33. A. Arshinoff, S.; Hofmann, I.; Nae, H. Role of Rheology in Tears and Artificial Tears. *J. Cataract Refract. Surg.* **2021**, *47*, 655–661, doi:10.1097/j.jcrs.0000000000000508.

34. Scott, J.A. The Computation of Temperature Rises in the Human Eye Induced by Infrared Radiation. *Phys. Med. Biol.* **1988**, *33*, 243–257, doi:10.1088/0031-9155/33/2/004.

35. Kattar, A.; Quelle-Regaldie, A.; Sánchez, L.; Concheiro, A.; Alvarez-Lorenzo, C. Formulation and Characterization of Epalrestat-Loaded Polysorbate 60 Cationic Niosomes for Ocular Delivery. *Pharmaceutics* **2023**, *15*, 1247, doi:10.3390/pharmaceutics15041247.

36. Manca, M.L.; Manconi, M.; Nacher, A.; Carbone, C.; Valenti, D.; MacCioni, A.M.; Sinico, C.; Fadda, A.M. Development of Novel Diolein-Niosomes for Cutaneous Delivery of Tretinoin: Influence of Formulation and in Vitro Assessment. *Int. J.*

Pharm. **2014**, *477*, 176–186, doi:10.1016/j.ijpharm.2014.10.031.

37. Sainz-Ramos, M.; Villate-Beitia, I.; Gallego, I.; AL Qtaish, N.; Menéndez, M.; Lagartera, L.; Grijalvo, S.; Eritja, R.; Puras, G.; Pedraz, J.L. Correlation between Biophysical Properties of Niosomes Elaborated with Chloroquine and Different Tensioactives and Their Transfection Efficiency. *Pharmaceutics* **2021**, *13*, 1787, doi:10.3390/pharmaceutics13111787.

38. Dolores Alvarez, M.; Cofrades, S.; Espert, M.; Salvador, A.; Sanz, T. Rheological Studies on Cocoa Butter with Hydroxypropil Methylcellulose-Based Oleogel as a Substitute. *Adv. Food Sci.* **2021**, 1–38.

39. Wilhelmus, K.R. The Draize Eye Test. *Surv. Ophthalmol.* **2001**, *45*, 493–515, doi:10.1016/S0039-6257(01)00211-9.

40. EEC *Council Directive 67/548/EEC of 27 June 1967 on the Approximation of Laws, Regulations and Administrative Provisions Relating to the Classification, Packaging and Labelling of Dangerous Substances.*; **1967**; Vol. 80, pp. 234–256;.

41. Toffoletto, N.; Saramago, B.; Serro, A.P.; Chauhan, A. A Physiology-Based Mathematical Model to Understand Drug Delivery from Contact Lenses to the Back of the Eye. *Pharm. Res.* **2023**, *40*, 1939–1951, doi:10.1007/s11095-023-03560-7.

42. Chase, J. The Evolution of Retinal Vascularization in Mammals. *Ophthalmology* **1982**, *89*, 1518–1525, doi:10.1016/S0161-6420(82)34608-4.

43. Shukr, M.H. Novel in Situ Gelling Ocular Inserts for Voriconazole-Loaded Niosomes: Design, in Vitro Characterisation and in Vivo Evaluation of the Ocular Irritation and Drug Pharmacokinetics. *J. Microencapsul.* **2016**, *33*, 71–79, doi:10.3109/02652048.2015.1128489.

44. Abdelbary, A.; Salem, H.F.; Khallaf, R.A.; Ali, A.M.A. Mucoadhesive Niosomal in Situ Gel for Ocular Tissue Targeting: In Vitro and in Vivo Evaluation of Lomefloxacin Hydrochloride. *Pharm. Dev. Technol.* **2017**, *22*, 409–417, doi:10.1080/10837450.2016.1219916.

45. Cao, Z.; Chen, Y.; Bai, S.; Zheng, Z.; Liu, Y.; Gui, S.; Shan, S.; Wu, J.; He, N. In Situ Formation of Injectable Organogels for Punctal Occlusion and Sustained Release of Therapeutics: Design, Preparation, in Vitro and in Vivo Evaluation. *Int. J. Pharm.* **2023**, *638*, 122933, doi:10.1016/j.ijpharm.2023.122933.

CONCLUSIONS

7. CONCLUSIONS

According to the aims of this Thesis, formulations carrying and delivering epalrestat to the posterior segment of the eye have been developed, characterized and evaluated. Three different carriers were explored; niosomes, micelles and oleogels.

The investigation was carried out in four steps and the conclusions which arise from each chapter are summarized in the following paragraphs.

1. Cationic niosomes were successfully designed with the intent of encapsulating epalrestat. The prepared nanoparticles displayed favorable physicochemical properties for delivering drugs to the ocular surface. These formulations have a low potential for causing eye irritation, are highly biocompatible, offer sustained drug release, and possess the ability to permeate the cornea and scleral tissue. They also provide superior protection against premature drug degradation while facilitating its passage into the inner eye tissues. Furthermore, our research has indicated the safety of drug encapsulation in niosomes, as demonstrated in HET-CAM and zebrafish embryotoxicity assays. In contrast, similar concentrations of epalrestat in solution could be harmful to patients. These findings underscore the suitability of epalrestat-loaded niosomes for non-invasive drug delivery to the inner eye structures.

2. Through experiments involving Langmuir monolayers and the analysis of their mechanical properties, the niosomal arrangement in the bilayer was studied. The results revealed that there was a DOTMA dependent increase in compressibility in all the systems examined. This effect served to impede the formation of tightly packed arrangements, which could have adverse effects on drug loading in the niosomal bilayer. Furthermore, a positive correlation between the concentration of DOTMA and the degree of packing or stability in the films composed of Tween 60, cholesterol, and DOTMA was found. This relationship is expected to mirror what occurs in the bilayer of vesicles. In addition to these findings, the change in niosomes as they transitioned from storage conditions (a water-based formulation at 20°C) to conditions resembling those encountered in the eye during administration (an electrolytic medium at a temperature closer to 30°C) was explored. This chapter showed that the inclusion of DOTMA in the binary system of Tween 60 and cholesterol significantly increased the compression modulus at 30°C and the pressure at higher surface area per molecule, particularly in the air/water interface suggesting that cholesterol holds an important role in the stability of the niosomal bilayer.

3. Successful preparation of olegels capable of incorporating epalrestat was achieved. These oleogels exhibit a significantly greater capacity for loading epalrestat compared to niosomes and contact lenses. Moreover, the release of the drug in simulated lacrimal fluid is ample to saturate the tear film within 20 minutes. Importantly, the loaded oleogels are non-irritating, making them comparable to other ocular formulations that shield the eye's surface from the potential irritations caused by epalrestat in solution. Furthermore, the permeation of epalrestat through the cornea and sclera is akin to the permeation observed when epalrestat is encapsulated in niosomes, and it surpasses the permeation rate seen with epalrestat released from contact lenses.

This novel use of oleogels to administer epalrestat topically represents a technologically robust method for delivering the drug to ocular tissues in a non-invasive manner.

4. Micelles formulated from Pluronic® F127 serve as a valuable point of comparison for the in vivo administration of eye drops containing 0.2 mg/mL epalrestat. These micelles outperformed niosomes TCD5 and oleogel C in terms of lacrimal and retinal concentrations. Notably, the micelles maintained high lacrimal concentrations for up to two hours. It is worth mentioning that all three formulations, including TCD5 niosomes, F127 micelles, and oleogel C, effectively delivered epalrestat to various eye tissues in vivo. However, the corneal route may not be the most efficient path to reach the retina, which is the therapeutic target for diabetic retinopathy. On the other hand, the transscleral route appears to offer a viable means for epalrestat, released from each of these formulations, to reach the retina.

As a uniform overview of the conclusions put forth in this Doctoral Thesis, the possibilities for topical delivery of epalrestat for the treatment of diabetic retinopathy have been extended. Three drug carriers have been developed from the chemical assembly of the system to the *in vivo* distribution when applied to a rabbit model. The results obtained during this investigation may pave the way towards less invasive forms of administration for patients suffering from diabetic retinopathy.

ANNEXES

ANNEXES

DECLARACIÓNS, CONFLITO DE INTERESES E RELACIÓN DE PUBLICACIÓNS QUE ACHEGAN CONTIDOS

CONFLITO DE INTERESE

O doutorando declara non ter ningún conflito de interese en relación coa Tese de Doutoramento.

RELACIÓN DE PUBLICACIÓNS QUE ACHEGAN CONTIDOS

Capítulo 1:

Autores (p.o. de firma): A. Kattar, A Concheiro, C. Alvarez-Lorenzo

Título: Diabetic eye: associated diseases, drugs in clinic, and role of self-assembled carriers in topical treatment

Revista: *Expert Opinion on Drug Delivery* 18(11), 1589-1607, 2021.

Factor de impacto: 8.129 (2021); Q1

Contribución do doutorando: Pesquisa bibliográfica e participación na redacción do texto da revisión.

Capítulo 3:

Autores (p.o. de firma): A. Kattar, A. Quelle-Regaldie, L. Sànchez, A. Concheiro, C. Alvarez-Lorenzo.

Título: Formulation and Characterization of Epalrestat-Loaded Polysorbate 60 Cationic Niosomes for Ocular Delivery

Revista: *Pharmaceutics* 15(4), 1247, 2023.

Factor de impacto: 6.525 (2023). JCR (Q1, Pharmacology & Pharmacy); CiteScore (Q1, Pharmaceutical Science). ISSN: 1999-4923.

Contribución do doutorando: Pesquisa bibliográfica, colaboración no deseño dos experimentos, realización da experimentación, análise dos resultados, redacción do borrador do traballo e participación na preparación do texto definitivo.

PERMISOS DE REPRODUCIÓN TOTAL OU PARCIAL DE TRABALLOS PUBLICADOS POLO DOUTORANDO

Chapter 1. Diabetic eye: associated diseases, drugs in clinic, and role of self-assembled carriers in topical treatment

The work described in this chapter was published in **Diabetic eye: associated diseases, drugs in clinic, and role of self-assembled carriers in topical treatment**, *Expert Opinion on Drug Delivery* 18(11), 1589-1607, 2021, authored by

Axel Kattar, Angel Concheiro, and Carmen Alvarez-Lorenzo

Departamento de Farmacología, Farmacia y Tecnología Farmacéutica, I+D Farma Group (GI-1645), Facultad de Farmacia, Instituto de Materiales (iMATUS) and Health Research Institute of Santiago de Compostela (IDIS), Universidade de Santiago de Compostela, 15782 Santiago de Compostela, Spain.

Author contribution: Bibliographic research and participation in the writing of the review text.

Expert Opinion on Drug Delivery

ISSN: 1744-7593

Journal Impact Factor: 6.6 (2022)

JCR Category: Pharmaceutical Science

Category Quartile: Q1

Reproduction permission: The article was published in open access

Chapter 3. Formulation and Characterization of Epalrestat-Loaded Polysorbate 60 Cationic Niosomes for Ocular Delivery

The work described in this chapter was published in **Formulation and Characterization of Epalrestat-Loaded Polysorbate 60 Cationic Niosomes for Ocular Delivery**, *Pharmaceutics* 15(4), 606, 2021, authored by:

Ana F. Pereira-da-Mota[a], María Vivero-Lopez[a], Ana Topete[b], Ana Paula Serro[b], Angel Concheiro[a] and Carmen Alvarez-Lorenzo[a]

[a]Departamento de Farmacología, Farmacia y Tecnología Farmacéutica, I+D Farma (GI-1645), Facultad de Farmacia and Health Research Institute of Santiago de Compostela (IDIS), Universidade de Santiago de Compostela, 15782 Santiago de Compostela, Spain.

[b]Centro de Química Estrutural, Departamento de Engenharia Química, Instituto Superior Técnico, Universidade de Lisboa, Av. Rovisco Pais, 1049-001 Lisbon, Portugal.

Author contribution: Bibliographic research, collaboration in the design of the experiments, data collection and processing, participation in the elaboration of the final text.

***Pharmaceutics*, 1247, 2023.**

ISSN: 1999-4923

Journal Impact Factor: 6.525 (2023)

JCR Category: Pharmacology & Pharmacy

Category Quartile: (Q1, Pharmacology & Pharmacy); **CiteScore** (Q1, Pharmaceutical Science).

Reproduction permission: The article was published in Open Access**.**

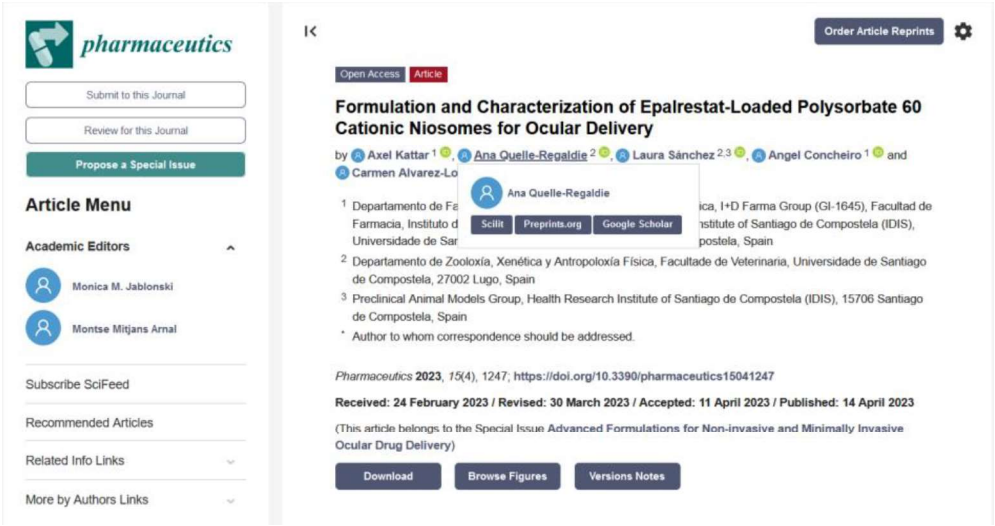

ETHICAL PERMISSIONs FOR ANIMAL EXPERIMENTS

VICERREITORÍA DE POLÍTICA CIENTÍFICA
Oficina de Investigación e Tecnoloxía
Edificio CACTUS – Campus Terra
27002 Lugo
Enderezo electrónico: comite.bioetica@usc.es

JOSÉ MANUEL CIFUENTES MARTÍNEZ, PRESIDENTE DO COMITÉ DE BIOÉTICA DA UNIVERSIDADE DE SANTIAGO DE COMPOSTELA, cuxa Sección de Experimentación animal ten sido designada como Órgano Habilitado para a avaliación de proxectos de experimentación animal por resolución da Xunta de Galicia, con data 11 de novembro de 2013, de acordo co esixido por o RD 53/2013 de 1 de febreiro, por o que se establecen as normas básicas aplicables para a protección dos animalas utilizados en experimentación e outros fins científicos, incluíndo a docencia,

INFORMA:

Que o proxecto de investigación titulado: **"Estudo *in vivo* da liberación de atropina a partir de novos sistemas de administración tópica ocular de fármacos"** do que é investigadora responsable **Dona Carmen Álvarez Lorenzo,** ten sido examinado por o Comité de Bioética desta Universidade, Sección de Experimentación Animal, chegando as seguintes conclusións:

Con respecto a súa finalidade, trátase de un proxecto cuxa finalidade principal do é realizar investigación fundamental e translacional sobre lentes de contacto preparadas con polímeros biocompatibles e colirios a base de nanotransportadores para o tratamento de patoloxías tanto a nivel do segmento anterior coma posterior do ollo.

- Con respecto a os requisitos das 3Rs,
  - Non cabe la posibilidade de reemprazo xa que non se atoparon métodos ou estratexias de ensaio que permitan levar a cabo os experimentos propostos neste traballo.
  - A experimentación realizarse nun centro rexistrado como usuario de animais de experimentación por o que a manipulación, manexo e supervisión dos animais durante todo o proxecto será levada a cabo por persoas capacitadas. O grupo investigador compóñeno persoas con capacitacións a, b, c, d; o que asegura a súa preparación para garantir o benestar animal durante todos os procedementos (requisito de refinamento).
  - Finalmente, con respecto ao requisito de redución, considera que el número de animais a utilizar axústase para a obtención dos resultados fiables.

- A clasificación dos procedementos en función do seu grao de severidade é de "moderado" para o procedemento 1 e "leve" no caso do procedemento 2.

- Con respecto ao balance dos danos e os beneficios, os procedementos efectúanse baixo anestesia e analxesia por o que se minimiza a dor, angustia e sufrimento. Os métodos de

VICERREITORÍA DE POLÍTICA CIENTÍFICA
Oficina de Investigación e Tecnoloxía
Edificio CACTUS – Campus Terra
27002 Lugo
Enderezo electrónico: comite.bioetica@usc.es

sacrificio descritos (sobredose de anestésico) atópanse entre os indicados por o propio RD 53/2013.

- Téñense examinado as situacións y excepcións previstas no punto e) do artigo 34. 2 atopando que ningunha delas é aplicable neste proxecto.

- O proxecto clasificase como tipo II e por o tanto non precisa ser sometido a avaliación retrospectiva.

Por todas estas razóns, este Comité acordou emitir un **INFORME FAVORABLE.**

Na avaliación deste proxecto NO TEN EXISTIDO CONFLICTO DE INTERESES.

Lugo, 19 de maio de 2023

VICERREITORADO DE INVESTIGACIÓN
E INNOVACIÓN
Oficina de Investigación e Tecnoloxía

Edificio CACTUS – Campus universitario sur
15782 Santiago de Compostela
Tel. 981 547 040 - Fax 981 547 077
Correo electrónico: citinfo@usc.es
http://maisd.usc.es

Informe del Comité de Ética de Experimentación Animal (CEEA) de los centros usuarios de animales de experimentación de la USC en el Campus de Santiago

El CEEA de los centros usuarios de animales de experimentación de la USC en el Campus de Santiago, tras evaluar el Proyecto titulado "Estudo in vivo da liberación de atropina a partir de novos sistemas de administración tópica ocular de fármacos." del que es Investigadora Responsable Dña. Carmen Álvarez Lorenzo, acordó con fecha 10 de mayo de 2023 emitir

INFORME FAVORABLE

para la realización de dicho proyecto, así como los procedimientos que incluye, en las instalaciones del establecimiento usuario Centro de Biomedicina Experimental (CEBEGA), con número de registro ES150780292901, siempre que en cumplimiento del RD 53/2013 se obtenga la correspondiente autorización.

El presidente del comité,

Firmado digitalmente por VIDAL FIGUEROA ANXO - 36097751X
Nombre de reconocimiento (DN): c=ES, serialNumber=IDCES-36097751X, givenName=ANXO, sn=VIDAL FIGUEROA, cn=VIDAL FIGUEROA ANXO - 36097751X
Fecha: 2023.05.10 19:40:48 +02'00'

CHECKLIST FOR THESIS THAT INCLUDE EXPERIMENTAL ANIMALS.
EXPERIMENTAL ANIMALS ARRIVE

Yes/No/NA		page
	Title	
Yes	Provide as accurate and concise a description of the content of the article as possible.	221
	Abstract	
Yes	Provide an accurate summary of the background, research objectives, including details of the species or strain of animal used, key methods, principal findings and conclusions of the study.	10-12
	Background	
Yes	Provide an accurate summary of the background, research objectives, including details of the species or strain of animal used, key methods, principal findings and conclusions of the study.	221-249
Yes	Explain how and why the animal species and model being used can address the scientific objectives and, where appropriate, the study's relevance to human biology.	231-240
	Objectives	
Yes	Clearly describe the primary and any secondary objectives of the study, or specific hypotheses being tested.	220-223
	Methods	
	Ethical statement	
Yes	Indicate the nature of the ethical review permissions, relevant licenses, and national or institutional guidelines for the care and use of animals, that cover the research.	232
	Study design	

Yes	Number of experimental and control groups	232
Yes	Steps taken to minimize the effects of subjective bias when allocating animals to treatment (e.g. randomization procedure) and when assessing results (e.g. if done, describe who was blinded and when).	232
Yes	The experimental unit (e.g. a single animal, group or cage of animals). A time-line diagram or flow chart can be useful to illustrate how complex study designs were carried out.	232
	Experimental procedures	
Yes	How (e.g. drug formulation and dose, site and route of administration, anesthesia and analgesia used [including monitoring], surgical procedure, method of euthanasia). Provide details of any specialist equipment used, including supplier(s).	232
Yes	When (e.g. time of day).	232
Yes	Where (e.g. home cage, laboratory, water maze).	232
Yes	Why (e.g. rationale for choice of specific anesthetic, route of administration, drug dose used).	232
	Experimental animals	
Yes	Provide details of the animals used, including species, strain, sex, developmental stage (e.g. mean or median age plus age range) and weight (e.g. mean or median weight plus weight range).	232
Yes	Provide further relevant information such as the source of animals, international strain nomenclature, genetic modification status (e.g. knock-out or transgenic), genotype, health/immune status, drug or test naïve, previous procedures, etc.	232
	Housing and husbandry	
Yes	Housing (type of facility e.g. specific pathogen free [SPF]; type of cage or housing; bedding	232

	material; number of cage companions; tank shape and material etc. for fish).	
Yes	Husbandry conditions (e.g. breeding program, light/dark cycle, temperature, quality of water etc for fish, type of food, access to food and water, environmental enrichment).	232
Yes	Welfare-related assessments and interventions that were carried out prior to, during, or after the experiment.	232
	Sample size	
Yes	Specify the total number of animals used in each experiment, and the number of animals in each experimental group.	232
Yes	Explain how the number of animals was arrived at. Provide details of any sample size calculation used.	232
Yes	Indicate the number of independent replications of each experiment, if relevant.	232
	Allocating animals to experimental groups	
Yes	Indicate the number of independent replications of each experiment, if relevant.	232
Yes	Describe the order in which the animals in the different experimental groups were treated and assessed.	232
	Experimental outcomes	
Yes	Clearly define the primary and secondary experimental outcomes assessed (e.g. cell death, molecular markers, behavioral changes).	233-240
	Statistical methods	
Yes	Provide details of the statistical methods used for each analysis.	229
Yes	Specify the unit of analysis for each dataset (e.g. single animal, group of animals, single neuron).	227-229; 232

Yes	Describe any methods used to assess whether the data met the assumptions of the statistical approach.	229; 236-240
	Results and discussion	
	Basal data	
Yes	For each experimental group, report relevant characteristics and health status of animals (e.g. weight, microbiological status, and drug or test naïve) prior to treatment or testing (this information can often be tabulated).	232
	Numbers analyzed	
Yes	Report the number of animals in each group included in each analysis. Report absolute numbers (e.g. 10/20, not 50%).	232
Yes	If any animals or data were not included in the analysis, explain why.	233
	Outcomes and estimation	
Yes	Report the results for each analysis carried out, with a measure of precision (e.g. standard error or confidence interval).	232-240
	Adverse events	
NA	Give details of all important adverse events in each experimental group.	
Yes	Describe any modifications to the experimental protocols made to reduce adverse events.	232
	Interpretation/scientific implications	
Yes	Interpret the results, taking into account the study objectives and hypotheses, current theory and other relevant studies in the literature.	232-240
Yes	Comment on the study limitations including any potential sources of bias, any limitations of the animal model, and the imprecision associated with the results.	232
NA	Describe any implications of your experimental methods or findings for the replacement,	

	refinement or reduction (the 3Rs) of the use of animals in research.	
	Generalizability/translation	
Yes	Comment on whether, and how, the findings of this study are likely to translate to other species or systems, including any relevance to human biology.	232-240
	Funding	
Yes	List all funding sources (including grant number) and the role of the funder(s) in the study.	232

Based on The ARRIVE guidelines: Animal Research: Reporting of In Vivo Experiments.

PhD Student signature

Kattar Axel

Digitally signed by Kattar Axel
Date: 2023.11.06 16:31:50 +01'00'

The eye is a crucial organ that allows us to experience the world visually, and the loss of vision is a fear for many. One significant threat to eye health is diabetic retinopathy, which can result in consequences as severe as blindness if left untreated. Current treatments for diabetic retinopathy involve injections and laser exposure, but they only slow down the degeneration of the retina. Therefore, there exists a need for preventive treatments to protect patients' vision. One potential solution is the use of a small molecule called epalrestat, which can block a metabolic pathway involved in the development of diabetic retinopathy. To enhance the delivery of epalrestat to the eye, drug carriers have been investigated. Niosomes and oleogels were formulated, characterized, and tested in various models including ex vivo, in ovo, and in vivo assays. The self-assembly process of the niosomes was investigated with the help of a monolayer model. These carriers provided a safe and efficient way to help with the transport of epalrestat across the various ocular barriers.